



UNIVERSITY OF
LIVERPOOL

Quantifying the impacts of uncertainties in coastal hazard modelling

Thesis submitted in accordance with the requirements of the University of Liverpool for the degree of
Doctor in Philosophy

by

Charlotte Lyddon

School of Environmental Science

Department of Geography and Planning

June 2020

Declaration

This thesis is the result of my own work and includes nothing which is the outcome of work done in collaboration except where specifically indicated in the text. It has not been previously submitted, in part or whole, to any university or institution for any degree, diploma, or other qualification.

In accordance with The University of Liverpool guidelines, this thesis does not exceed 100,000 words.

Signed: C. Lyddon

Date: 19.06.2020

Abstract

This thesis applies coupled regional models to address coastal flood risk management needs in hyper-tidal estuaries. The project aims to understand how tide-surge-wind-waves combine to increase flood and wave hazard at the coast, using the Severn Estuary, southwest England as an extreme example. Little previous research has considered the impact of tide-surge-wind-wave interaction on total water level in a hyper-tidal estuary.

Numerical modelling tools can be used to predict the individual contributions of physical factors to total water levels and forms a key component of flood hazard assessment. However uncertainty can be introduced into model predictions due to inaccurate boundary forcing or representation of the physical processes which control the volume and rate water moves through a model domain. Uncertainties in model predictions lead to a wide spread of results within which exposure or impacts could occur. Similarly, a range of possible values exist for a single parameter which may cause errors in the definition of critical thresholds or presents challenges to emergency response planners. Sources of uncertainty in flood hazard assessments should be identified and quantified as sustainable coastal management requires confidence in the knowledge of any possible future changes to flood and wave hazard.

The thesis utilises wave, ocean and meteorological observation and model hindcast data to simulate total water level and significant wave height using the Delft3D-FLOW-WAVE modelling package. The validated Severn Estuary model domain is used to investigate the sensitivity of extreme water levels to changes in event severity, timing of the peak of a storm surge relative to tidal high water and the temporal distribution of the storm surge component, and wave heights to changes in wind-wave direction, model coupling and forcing processes. Model outputs from Delft3D-FLOW-WAVE are viewed in the context of the source-pathway-receptor-consequence model to better understand the influence of coastal hazard uncertainty on flood and wave hazard. Event severity is the most important control on flood hazard, and concurrence of the sources of flood hazard generate greatest water levels along the coastline of the estuary. Estuarine morphology acts as a pathway for flood hazard, as funnelling effects control the spatial variability of flood hazard and amplify surge magnitude up to 255% up-estuary. Surge predictions from forecasting systems at tide gauge locations could under-predict the magnitude and duration of surge contribution to up-estuary water levels. Wave height and wave period controls the response of wave generation and propagation to other factors. Wind speed generates greatest wave hazard, and uncertainty in wind and wave direction generate a large spread of results. Stronger, opposing winds steepen high amplitude, low period waves in the outer estuary and stronger, following winds enhance propagation of low amplitude high period waves up-estuary. The inclusion of locally generated winds is most important in regional models to continue to add momentum to the estuarine system, and model coupling processes (the representation of interaction between wave and currents) improve accuracy of flood and wave hazard predictions. Exclusion of locally generated

winds can generate up to 1.45 m error in high water significant wave heights in the outer estuary, and 1.13 m error in the upper estuary.

Coastal hazard uncertainty due to model coupling and forcing processes is propagated through the modelling chain to the two-dimensional inundation model LISFLOOD-FP to understand how changes in boundary condition and boundary position influences depth, extent and volume of inundation over a storm event. The exclusion of local atmospheric forcing increases coastal hazard uncertainty in the boundary forcing and under-predicts damage by up to £26.2 M at Oldbury-on-Severn. Once the threshold for flooding is exceeded, a few centimetres increase in coastal hazard conditions increases both the inundation and consequent damage costs for suburbia and arable land.

The results of this thesis identify optimum model setups for simulating coastal flood hazard, which includes incorporating local atmospheric forcing and representing two-way interaction between waves and currents. Coastal hazard uncertainty can cause large variability in simulated total water level and wave heights, which has implications for flood damage assessments, shoreline management plans and emergency response plans. The research findings can aid long-term coastal defence and management strategies for improved public safety, and improve the timing and accuracy of early warning systems. Key sources of coastal hazard uncertainty have been identified here, e.g. the importance of storm surge timing relative to tidal high water and sensitivity of wave propagation to winds speeds, and these can be accounted for in future management plans. Utilising optimal model setups when predicting water level and wave height under current and future climate conditions can also help to increase confidence in results. Further to this, if the key sources of uncertainty which contribute to a large spread of results are known, e.g. exclusion of local atmospheric forcing, then this can be resolved in predictions which are used to inform early warning systems. The spread of model results can therefore be minimised to more accurately know who or what is in a flood or wave hazard zone.

Acknowledgements

I would like to thank my supervisors for the help, guidance and feedback that they have provided during this work. Many thanks to Dr Jennifer Brown, Dr Nicoletta Leonardi and Prof Andrew Plater who have provided endless support and enthusiasm and have been fantastic mentors and role models.

This PhD had no associated research, travel and subsistence fund, therefore I am hugely grateful to Prof Andy Plater for providing funding from the Engineering and Physical Science Research Council (EPSRC) funded Adaptation and Resilience of Coastal Energy Supply (ARCoES) research project (EPSRC EP/I035390/1) and National Environmental Research Council (NERC) funded highlight topic “Physical and biological dynamic coastal processes and their role in coastal recovery” as part of the BLUEcoast project (NE/N015614/1) to allow me to attend and present my research at conferences. I would also like to thank the Environmental Change Research Group which has also provided funding to allow me to present my research at conferences.

Acknowledgement must also be made to the National Oceanography Centre for the provision of research facilities and resources throughout this project.

Thanks are also due to friends and colleagues across the institutions and departments, who have supported and encouraged me.

Finally, my greatest acknowledgement goes to my family and better half. I am immensely grateful and lucky to have them; this work is dedicated to them.

Table of Contents

1. Background & rationale	1
1.1. Drivers of coastal flood hazard	1
1.1.1. Implications of flooding	2
1.2. Combined flood hazard events in estuaries	3
1.2.1. River influence in estuaries	4
1.2.2. Tide dominance in estuaries	5
1.2.2.1. Hyper-tidal estuaries	5
1.3. Flood hazard assessment	6
1.4. Numerical modelling tools for flood hazard assessment	7
1.5. Numerical modelling uncertainties	8
1.6. Thesis aim and research questions	9
1.7. Severn Estuary model setup	10
1.7.1. Delft-3D FLOW	10
1.7.1.1. Development of model grid and bathymetry	10
1.7.1.2. Boundary conditions	12
1.7.1.3. Model parameters	12
1.7.1.4. Calibration and validation	13
1.7.2. Delft3D-WAVE	14
1.7.3. LISFLOOD-FP	15
1.7.3.1. Digital Elevation Model	15
1.7.3.2. Model inputs	15
1.8. Thesis structure	17
2. Flood hazard assessment for a hyper-tidal estuary as a function of tide-surge-morphology interaction	24
2.1. Abstract	25
2.2. Introduction	25
2.3. Methods	28
2.3.1. Delft3D	28
2.3.2. Model domain	28
2.3.3. Boundary conditions	30
2.3.4. Timing of surge occurrence	34
2.4. Model validation	34
2.4.1. Funnelling effect vs frictional effect	37
2.5. Results	39
2.5.1. Water level variations along estuary	39

2.5.2. Changes in flood hazard proxy with surge timing	43
2.6. Discussion	50
2.6.1. Physical drivers and sources of flood hazard in the Severn Estuary model domain	50
2.6.2. Implications for local management needs in the Severn Estuary and worldwide	55
2.7. Conclusion	56
2.8. Acknowledgements and Data	57
3 Uncertainty in estuarine extreme water level predictions due to surge-tide interaction	58
3.1. Abstract	59
3.2. Introduction	59
3.3. Methods	62
3.3.1. Delft3D and model domain	62
3.3.2. Long-term tide gauge records	63
3.3.3. Tested tide-surge configurations	63
3.3.4. Model validation	64
3.4. Results	66
3.4.1. Surge elevation on 3 January 2014	66
3.4.2. Surge elevation along thalweg	69
3.5. Discussion	72
3.6. Conclusion	75
3.7. Acknowledgements and Data	75
4 Increased coastal wave hazard generated by differential wind and wave direction in hyper-tidal estuaries	76
4.1. Abstract	77
4.2. Introduction	77
4.2.1. Wave hazard impacts	77
4.2.2. Wave hazard in hyper-tidal estuaries	79
4.2.3. Case study	81
4.3. Methods	83
4.3.1. Delft3D-WAVE	83
4.3.2. Boundary conditions	83
4.3.3. Model validation and scenarios	87
4.4. Results	88
4.4.1. High amplitude waves	88
4.4.2. Low amplitude waves	91
4.5. Discussion	93
4.5.1. Younger, rougher seas show more sensitivity to wind direction.	93

4.5.2. Long period, low amplitude waves amplified due to strong winds	94
4.5.3. Waves impact on flood hazard and economic activities	95
4.5.4. Changing future storm tracks and climate	96
4.6. Conclusion	97
4.7. Acknowledgements and Data	98
5 Quantification of the uncertainty in coastal storm hazard predictions due to wave-current interaction and wind forcing	99
5.1. Abstract	100
5.2. Introduction	100
5.2.1. Case Study	101
5.2.2. Outline of the paper	102
5.3. Method	102
5.3.1. Delft3D hindcast of select historic events	102
5.3.2. Model validation and scenario test	104
5.4. Results	106
5.4.1. Uncertainty in High Water Level (HWL)	111
5.4.2. Uncertainty in High Water Significant Wave Height (HWHs)	113
5.4.3. Uncertainty in High Water Hazard Proxy (HWHP)	115
5.4.4. Spatial variability of hazard	115
5.5. Discussion	116
5.6. Conclusion	117
5.7. Acknowledgments and Data	118
6 Uncertainty propagation in flood hazard assessments	119
6.1. Abstract	120
6.2. Introduction	120
6.2.1. Case study	122
6.3. Method	125
6.3.1. Input data	125
6.3.2. Inundation model boundary conditions	126
6.3.3. Flood inundation scenarios	128
6.3.4. Depth damage curves	129
6.4. Results	129
6.4.1. Depth and extent of inundation	129
6.4.2. Flood hazard rating at operational sites	138
6.4.3. Volume of inundation in the model domain	140
6.4.4. Quantification of flood hazard due to coastal hazard uncertainty	141

6.4.5. Economic cost of inundation for arable and suburban land uses	143
6.5. Discussion	145
6.6. Conclusion	148
6.7. Acknowledgments and Data	150
7 Conclusions and Implications	151
7.1. Uncertainty in sources and pathways of flood and wave hazard	151
7.1.1. Extra-model uncertainties	151
7.1.2. Intra-model uncertainties	154
7.2. Impacts of coastal hazard uncertainty on receptors and consequences of flood and wave hazard	156
7.3. Applicability of results to other estuaries	157
7.4. Practical application of thesis results	159
7.5. Coastal hazard uncertainty: implications for long-term planning (up to 2105) with sea level rise	161
7.5.1. Resilience and flexibility in long-term management plans	162
7.6. Coastal hazard uncertainty: implications for early warning systems	163
8 References	165
Appendix 1 – Delft3D User Guide	195
Appendix 2 – LISFLOOD User Guide	235

Table of Figures

Figure 2.1: Severn Estuary model domain extending from Ilfracome (51°12.668'N, 4°6.743'W) and The Mumbles (51°34.203'N, 3°58.534'W) in the west, to Gloucester (52° 89.3020'N, -2°2. 6361'W) in the east. The bathymetry is relative to chart datum (CD).	29
Figure 2.2: Long-term tide gauge record at The Mumbles, Bristol Channel, U.K showing tide gauge time series, points in the time series representing high water peaks and events to be modelled. The panels on the right illustrate the three selected events representing the 95th (i, 14th December 2012), 90th (ii, 18 December 2013) and 99th (iii, 3 January 2014) water level percentile values.	30
Figure 2.3: Long-term tide gauge record at Ilfracombe, Bristol Channel, U.K showing tide gauge time series, points in the time series representing high water peaks and events to be modelled. The panel on the right illustrates one selected event representing the 95th (i.e. 5 May 2015) water level percentile values.	31
Figure 2.4: Normalised filtered surge shape component with time, characterised by historical event severity and skewness (measure of asymmetry).	33
Figure 2.5: Validation down-estuary, Hinkley Point tide gauge.	35
Figure 2.6: Validation up-estuary, Sharpness river gauge. As above.	36
Figure 2.7: Water level along the deepest channel in the Severn Estuary, 3 January 2014, under varying Manning friction values (99th percentile); the shading represents the range in results for each filtered surge time shift scenario. Subpanels show the tidal response of i) hypersynchronous and ii) hyposynchronous estuary to changing frictional effects.	38
Figure 2.8: Maximum water level along the thalweg of the Severn Estuary; a) 99th water level percentile event (3 January 2014); b) 95th water level percentile event (14 December 2012); c) 90th water level percentile event (18 December 2013); d) 95th water level percentile event (5 May 2015).	41
Figure 2.9: Range of water level values for time shift configurations along deepest channel of the Severn Estuary when overall maximum water level occurs. For each event, in the legend the first value represents the percentile of the event and the second value is the skewness.	42
Figure 2.10: 3 January 2014. Flood hazard proxy calculated at each tide gauge location. a) percent change in maximum water level; b) percent change in maximum total surge elevation; c) percent change in duration exceeding MHWS; d) percent change in area exceeding MHWS. All data is displayed as percentage change, compared with the tide only	44

model scenario, apart from total surge elevation which is compared with the model run when the peak of the surge and high water coincide.

Figure 2.11: 14 December 2012. Flood hazard proxy, as in Figure 2.10.	46
Figure 2.12: 5 May 2015. Flood hazard proxy, as in Figure 2.10.	48
Figure 2.13: 18 December 2013. Flood hazard proxy as in Figure 2.10.	49
Figure 2.14: Duration and area of storm tide peak exceeding MHWS at Sharpness.	50
Figure 3.1: Severn Estuary model domain extending from Ilfracome (51°12.668'N, 4°6.743'W) and The Mumbles (51°34.203'N, 3°58.534'W) in the west, to Gloucester (52° 89.3020'N, -2°2. 6361'W) in the east. The bathymetry is relative to chart datum (CD).	63
Figure 3.2: Model output validation for realistic timing of total water level and tide only model runs compared to observational data at Hinkley Point tide gauge, Severn Estuary, southwest England.	65
Figure 3.3: Model output validation for realistic timing of total water level and tide only model runs compared to observational data at Sharpness tide gauge, Severn Estuary, southwest England.	66
Figure 3.4: Modelled tidal time series (black); modelled surge elevation for the realistic surge timing (red line); range of surge elevations for time shifted configurations shaded (blue band); observed filtered surge (orange line) at a) Hinkley; b) Newport; c) Portbury; d) Oldbury; e) Sharpness for the 3rd January 2014 event.	68
Figure 3.5: a) Tidal range; b) Surge elevation range for observed event timing; c) Variability in surge values; d) Variability in skew surge values for time shift configurations along thalweg of the Severn Estuary.	71
Figure 4.1: 5 years of observational wave buoy data taken from Scarweather (located in Figure 4.2), Severn Estuary, UK showing a) wave direction (deg) and significant wave height (m), b) average wave direction and wave period (s) and c) 5 years of observational wind data taken from Chivenor, Devon (located in Figure 4.2).	82
Figure 4.2: Delft3D-WAVE model grid. The bathymetry is relative to chart datum (CD).	83
Figure 4.3: Model schematic for the coupled Delft3D hydrodynamic (FLOW) and wave (SWAN) model with forcing data sources.	84
Figure 4.4: Wave selection for Hs and Tz. 25th percentile Tz (blue line) and 75th percentile Tz (red line), color coordinated based on wave direction.	85

Figure 4.5: Delft3D-WAVE model validation comparing model simulations to 5 years observational data at Scarweather wave buoy. Symbols representing directions over a range of 45 degrees. 87

Figure 4.6: Normalized significant wave height (model scenario – no wind baseline scenario) for representative high amplitude, short period waves along the shoreline of Severn Estuary, starting at Swansea to Gloucester and thence down-estuary towards Hinkley Point. 89

Figure 4.7: Normalized significant wave height (model scenario – no wind baseline scenario) for representative low amplitude, longer period waves along the shoreline of Severn Estuary, starting at Swansea to Gloucester and thence down-estuary towards Hinkley Point. 92

Figure 5.1: a) Delft3D-FLOW-WAVE model domain. Bathymetry relative to CD. Average bias and RMSE (m) of WL and Hs model results for four events to tide gauge and wave buoy observations are shown in brackets; (b) six year Hs record from Scarweather wave buoy; (c) Long-term tide gauge record taken from Ilfracombe, with HWHP grouped based on wind direction at the time of the event. HWL, HWHs, and wind speed (WS) at the time of the events are shown. Horizontal black lines indicate maximum, 90th, 50th and 10th percentile HP thresholds. 103

Figure 5.2: Simulated a) HWL; b) HWHs; c) HWHP along the coastline of Severn Estuary starting at Swansea to Gloucester and thence down-estuary towards Woolacombe for maximum event (3 January 2014 07:00); d-f) % difference between each run and run 8. The divide between north and south coastlines (dashed black vertical line) and wave limit where $H_s < 10$ cm (dashed grey vertical line) is shown. Solid black vertical lines indicate locations of critical infrastructure and coastal towns. 108

Figure 5.3: Absolute difference for a) HWL; b) HWHs; c) HWHP between each run and run 8 along the coastline of Severn Estuary starting at Swansea to Gloucester and thence down-estuary towards Hinkley Point for maximum event (3 January 2014 07:00). The divide between north and south coastlines (dashed black vertical line) and wave limit where $H_s < 10$ cm (dashed grey vertical line) is shown. Solid black vertical lines indicate locations of critical infrastructure and towns along the coastline. 111

Figure 5.4: For the a) north (left panels) and b) south (right panels) coastlines the alongshore maximum, mean and median percentage difference in i) HWL; ii) HWHs; iii) HWHP between model simulations is calculated for the four events with hazard potential calculated using the HP parameter. 111

Figure 5.5: For the a) north (left panels) and b) south (right panels) coastlines the alongshore maximum, mean and median absolute difference in i) HWL; ii) HWHs; iii) HWHP between model simulations is calculated for the four events with hazard potential calculated using the HP parameter. 112

Figure 5.6: % difference across the Severn Estuary model domain in HWHs for the 50th percentile event between a) run 8 (two-way + wind) – 7 (two-way); b) run 8 (two-way + wind) – 6 (one-way + wind); and c) % difference depth average velocity run 8 (two-way + wind) – 6 (one-way + wind) Limits are scaled to show the main differences, but the values may exceed these in isolated areas at the coastline. 114

Figure 6.1: a) Oldbury model domain, including the location of Delft3D outputs (coloured dots) used to force the HP and WR boundary approach (coloured lines); boundary midpoint to calculate change in coastal hazard uncertainty (black cross); sites of critical infrastructure (yellow star and triangle); and b) Delft3D-FLOW-WAVE model domain with extent of the up-estuary Oldbury model domain shown. 123

Figure 6.2: Model inputs and the process followed to propagate and quantify uncertainty in flood hazard assessments, and results that are presented in section 3. 125

Figure 6.3: a) Coastal hazard uncertainty time series from Delft3D-FLOW-WAVE used to force LISFLOOD-FP, for Jan 14 event using the HP approach, shown here as an example; b) zoom of peak of the Jan 14 event to show coastal hazard uncertainty. 127

Figure 6.4: Depth and extent of flooding at Oldbury-on-Severn for HP approach to forcing the model boundary where maps 1-8 represent coastal hazard uncertainty (see Table 6.1) for Jan 14. 131

Figure 6.5: Depth and extent of flooding at Oldbury-on-Severn for WR approach to forcing the model boundary where maps 1-8 represent coastal hazard uncertainty (see Table 6.1) for Jan 14. 133

Figure 6.6: Depth and extent of flooding at Oldbury-on-Severn for HP approach to forcing the model boundary where maps 1-8 represent coastal hazard uncertainty (see Table 6.1) for Dec 12. 135

Figure 6.7: Depth and extent of flooding at Oldbury-on-Severn for WR approach to forcing the model boundary where maps 1-8 represent coastal hazard uncertainty (see Table 6.1) for Dec 12. 137

Figure 6.8: Flood hazard rating during the Jan 14 event at a) road junction; b) pylon; and during Dec 12 event at c) road junction; and d) pylon using the HP (dashed black line) and 139

WR approach (solid black line). Modelled tidal signal at the boundary midpoint (vertical dotted black line) and extreme (red, horizontal dotted line), significant (amber, horizontal dotted line) and moderate (green, horizontal dotted line) thresholds for hazard to people (DEFRA 2003).

Figure 6.9: Change in volume of inundation (Mm³) in the Oldbury model domain for Jan 14 forced by a) HP and c) WR; and Dec 12 forced by c) HP and d) WR. Modelled high tide from low water to low water is also shown (dashed line). 140

Figure 6.10: Absolute difference in HP at the boundary midpoint (shown in Figure 6.1a) against absolute difference in time-integrated volume for a) all runs compared to baseline run 8; and b) zoomed into run 1, 2, 5, and 7. 141

Figure 6.11: Absolute difference in HP at the boundary midpoint (shown in Figure 6.1a) against absolute difference in a) arable land costs and b) suburban land cost for runs 1,2,5,6 and 7 compared to baseline run 8. 144

Table of Tables

Table 2.1: Scenarios modelled in Delft3D for each historical extreme water level event.	34
Table 2.2: Statistical validation down-estuary, Hinkley tide gauge. The filtered surge is applied at a realistic time relative to tidal high water for validation purposes.	35
Table 2.3: Statistical validation up-estuary, Sharpness river gauge	36
Table 3.1: Contribution of surge to total water level at the time of maximum surge (total water level – predicted tidal level), tidal low water and tidal high water.	69
Table 4.1: Representative wind wave conditions close to the estuary mouth based on 5 years of observational data from Scarweather Waverider buoy.	86
Table 4.2: Representative wind speeds based on 5 years of observational data from Chivenor in Devon (England) and Pembrey Sands in Dyfed (Wales) UK Met Office MIDAS land station data.	86
Table 5.1: Eight model simulations completed in Delft3D-FLOW-WAVE for each historic storm event.	105
Table 5.2: Overall maximum, mean and median percentage difference in HWL, HWHs and HWHP in the lower/mid estuary (to wave limit) and the entire estuary coastline.	115
Table 6.1: Eight model simulations completed in Delft3D-FLOW-WAVE for each historic storm event, and outputs used to force the boundary of the Oldbury model domain in LISFLOOD-FP from the low water mark and defence crest.	126
Table 6.2: Simulated economic cost of inundation for arable land cover	143
Table 6.3: Simulated economic cost of inundation for suburban land cover	143

1. Background & rationale

1.1. Drivers of coastal flood hazard

Coastal communities and infrastructure are increasingly vulnerable to the combined effect of astronomical tides, storm surges, wind, waves and rivers, as floodplain development becomes increasingly connected and interdependent (Aerts et al., 2014; Blackburn et al., 2019). Violent storms and hurricanes can cause short-term, local variations in sea level due to the combined effect of i) reduced atmospheric pressure (inverse barometer effect) (Proctor and Flather 1989); ii) strong winds, leading to build up of water in shallow areas (wind setup) (Hoeke et al., 2015); iii) short-term rise in sea level due to wave breaking (wave setup) (Brown et al., 2013); iv) cumulative effect of instantaneous uprush of individual waves (wave runup) (Senechal et al., 2011); v) high river discharge in estuaries and deltas (Bricheno et al., 2016). Total water level at the coast is highly sensitive to other external forces including changes in near-shore coastal bathymetry due to sediment transport processes (Pollard et al., 2019), and inter-annual and seasonal variability in sea level (Amiruddin et al., 2015; Dangendorf et al., 2013). The combined effect of these coastal hazard parameters can elevate observed water levels above the predicted level, generating extreme water levels (Marcos et al., 2019). Tide-surge and wave-current interaction has also been shown to influence The timing and magnitude of extreme water levels at the coast can also be influenced by tide-surge interaction, which is largely a function of surge magnitude and enhances current velocities during storms, or wave-current interaction which can generate larger waves at high water (Horsburgh and Wilson, 2007; Idier et al., 2012; Lewis et al., 2019). These high frequency variations in sea level occur on an event, or weather, timescale with storms typically effecting sea level in the UK for 3.5 days (Haigh et al., 2016), and can be superimposed onto longer term, low frequency variations. Spring tidal cycles and nodal cycles are phase locked, which can make extreme water levels more predictable (Boon, 2004). Inter-annual and decadal variability in sea level and storminess can be observed because of changes in climate such as El Niño Southern Oscillation (ENSO), North Atlantic Oscillation (NAO) or Pacific Decadal Oscillation (PDO) (Barnard et al., 2017; Idier et al., 2019). For example, positive NAO can shift storm tracks up to 180 km north, lower pressure to generate storm surges and increase wind speeds. This has implications for the coastline response to wind speed, direction, sea level and waves for communities on the North West European shelf (Phillips et al., 2013). This may also have implications for river hydrograph shapes, generating greater flow magnitude and increasing water levels in up-estuary locations (Robins et al., 2018). Thermal expansion and contribution of melting ice caps under future, long term climate change will continue to elevate mean sea level and the baseline on which storms are generated in the UK (Lowe and Gregory 2005) and worldwide (Nicholls et al., 2014; Shepard et al., 2012). There is a need to understand the temporal changes in drivers for flooding, notably high frequency variations which can elevate coastal water levels. The impact of extreme water levels on developed, interconnected floodplains is particularly

critical in heavily populated and industrialised estuaries, where low-lying floodplains are increasingly used for critical infrastructure, that provide essential services to communities (Ruckert et al., 2019). Industrialised estuaries and deltas support transport and energy infrastructure, water supply and access (i.e. ports & harbours), and 21 of the world's 30 largest cities are located next to estuaries (Ashworth et al., 2015). It is of critical, international importance that we fully understand the drivers of flood hazard on the shores of estuaries for accurate hazard assessments in long-term management plans.

Coastal communities and critical infrastructure are often protected against the effect of extreme water levels, due to the combined effect of coastal hazard parameters (i.e. tide, surge, wind, wave, river), by sea walls or coastal defences. These defences are designed and built to a critical threshold height ($h_{threshold}$) which should offer protection from extreme water levels. Natural barriers, such as gravel forelands or shingle barriers, also offer a degree of protection from extreme water levels but also face erosion hazard during extreme events (Brown et al., 2016). If the combined effect of coastal hazard parameters is below a critical threshold then no adverse effects at the coast are experienced. As soon as the combined effect of these coastal hazard parameters causes highest water levels or waves to exceed critical threshold height then a coastal community is considered vulnerable to the flood hazard, as higher water levels represent an agent for potential damage or harm (Idier et al., 2013). Substantial impacts can be expected at the coast once an extreme water level exceeds critical threshold, and damaging coastal flooding can occur under present-day sea-level conditions, at a specific location (x) at a specific time (t) as soon as:

$$h_{threshold}(x, t) < h_{pred}(x, t) + \xi_{bar}(x, t) + \xi_{wind}(x, t) + \xi_{waves}(x, t) + \xi_{river}(x, t)$$

where h_{pred} is the water level corresponding to the predicted tide and ξ_{bar} , ξ_{wind} , ξ_{wave} and ξ_{river} are the additional water levels resulting from barometric and wind effects and the wave set-up (adapted from Le Cozannet et al., 2015). The combined effect of coastal hazard parameters can elevate water levels and exceed critical thresholds, which poses a hazard to coastal communities. Research has previously considered the probability of events occurring, including joint probability studies (e.g. Prime et al., 2016) and the dependence or independence of coastal hazard parameters (e.g. Williams et al., 2016). Here we focus on hazards only, no account is being made of risk, and how physical processes combine to elevate water level and wave height at the coast.

1.1.1. Implications of flooding

The combined effect of tide, surge, wind, waves, and rivers represents a significant flood hazard, and critical thresholds may be exceeded to cause flooding. Flooding can have wide implications for people and cause significant economic and environmental damage in estuarine and coastal zones (Wolf 2009). 12% of all deaths from natural disasters in the 1990s were due to flooding, which claimed over 90,000 lives across the world (Defra, 2006). Over 300 million people live in low-lying coastal zones and are

directly vulnerable to the effects of flooding (Hinkel et al., 2014), which can cause damages in the order of tens of billions of US\$ per year (Kron 2013). Several recent extreme meteorological events have caused catastrophic human and economic losses in coastal areas (Brown et al., 2014), such as Cyclone Nargis (Myanmar, 2008), Hurricane Sandy (eastern United States, Canada and Caribbean, 2012) and Typhoon Haiyan (Philippines, 2013). Flash floods, due to heavy and persistent precipitation, have caused fatalities and damages in coastal towns including Lynmouth, Devon (1952) and significant damage in Boscastle, Cornwall (2004) (Archer and Fowler 2018). Floods not only directly and immediately cause loss of human life, damage to property and environmental damage due to erosion, but can also impact livelihoods due to destruction of crops, loss of livestock, and disruption to communication links and infrastructure (such as power plants, roads, bridges and railways) e.g. Dawlish railway, Devon (Dawson et al., 2016), which can cause economic standstill. Floods can increase the transport and delivery of untreated sewage, toxic substances (i.e. heavy metals), pathogens, and pollutants which can enter the food chain or water supply and cause deterioration of health conditions, due to contamination and waterborne diseases (Robins et al., 2018). Impacts can be experienced long after flood waters have receded, as saltwater intrusion can cause deterioration of water quality and influence nutrient levels, hydration and growth of plants and crops (Williams 2009; Gimeno et al., 2012; Tully et al., 2019) which can take years to recover from, and displacement from homes and businesses can cause emotional distress. These impacts will be site specific, and the severity will depend on when and where they occur, the preparedness of a community and emergency response plans that are in place. Estuaries worldwide have high socio-economic value, are ecologically rich and have dense, growing populations, therefore it is valuable to understand how physical processes combine to cause flooding, as these events can have significant and long-term consequences.

1.2. Combined flood hazard events in estuaries

Estuarine environments are particularly at risk from the combined effect of coastal hazard parameters due to their exposure to both storm tides from the ocean side and riverine discharges from the terrestrial side (Monbaliu et al., 2014; Olbert et al., 2017). When these parameters interact, floods can be more severe than when they occur in isolation and the impacts disproportionately large and adverse; this is called ‘compound flooding’ (Hendry et al., 2019). The relative contribution of each coastal hazard parameter to an extreme water level varies in estuaries dependent on differentiation at: i) a global scale including latitude, oceanic basins and large landmasses; ii) regional variation in estuary hydrodynamic processes, controlled by estuary basin geometry, and river and oceanic forcing; and iii) local catchment processes due to local geology and land cover (Hume et al., 2007; Olbert et al., 2013). The geometry of an estuary (i.e. size and shape) and the dominant drivers of flood hazard are one of the strongest controls on flood hazard, and closely interlinked. River, tide, or wave dominance in an estuarine system can shape the local morphology but can also be a function of local morphology.

1.2.1. River influence in estuaries

Rivers can be an important drivers of water levels and flooding in upper estuaries and lower catchments, due to hydrological and atmospheric processes. Increased local rainfall intensities alone can increase river discharges and enhance river levels to exceed critical thresholds, and cause flooding (Barker et al., 2016). There is also a compound flood hazard when increased river discharges transport river runoff to estuaries near-simultaneously with the peak of storm surge, which often both originate from the same storm (Prime et al., 2015; Khanal et al., 2019). The river is not able to discharge its water at the outlet, as high seawaters block the estuary, and river water levels rise (Van Den Hurk et al., 2015). There is a recognised global statistical dependence between storm surge and precipitation/river floods (Svensson and Jones 2002; Zheng et al., 2013), and the simultaneous occurrence of high discharge and sea-levels is important for designing flood protection infrastructure (Ward et al., 2018). However, variation in prevailing storm conditions catchment characteristics at a regional scale strongly influences the dominance of rivers in estuarine systems. Spatial variability in storm characteristics between the east and west of the UK influences the joint occurrence of high skew surges and high river discharges, indicating that storms which generate both are more likely to occur on the west coast (Hendry et al., 2019). Temporal variability in river contribution to coastal water levels is highlighted in the Scheldt Estuary, Belgium, as rainfall intensity and subsequent magnitude of river discharge has a strong control on tidal amplification and tidal range in the whole river (Wang et al., 2019). The characteristics of river catchments has a strong control on the rate of transport of river discharges to estuaries, and the subsequent likelihood and severity of compound events occurring. Estuaries with steeper catchments are more prone to combined storm tide and riverine flooding, due to the rapid transport of abundant rainfall through the system to the coast (Svensson and Jones, 2002). Rapid-response systems, such as the Conwy River, Wales have smaller catchment areas and are sensitive to sub-daily river flow variability which may influence representation of water quality modelling studies, whereas slow response systems, such as the Humber Estuary, UK, have larger catchments with shallower slopes and are less sensitive to high frequency variations in river flow (Robins et al., 2018). The lagged occurrence between elevated river and coastal water levels can also influence flood hazard; clear correlation between storm surge and increased river discharge was found in the Rhine catchment, but only when a substantial time lag of 6 days was considered, which is the timescale for excess precipitation to reach the estuary (Klerk et al., 2015). The occurrence of peak river flow several days after the storm surge has also been noted in catchments with larger areas and shallow elevation gradient in the UK, such as the Severn Estuary, therefore reducing the hazard from river flooding (Hendry et al., 2019). Rivers can be important drivers of flooding, alone or in combination with storm surges but the relative contribution of rivers to coastal flood hazard is site specific and primarily dependent on storm and catchment characteristics.

1.2.2. Tide dominance in estuaries

Tide-dominated estuaries largely occur on coastlines with a strong M2 semi-diurnal tide, and the shape and size of an estuary can also influence the tidal characteristics of a system (Pye and Blott, 2014). Analytical solutions for a range of estuarine shapes and sizes indicate how by length, bed friction and river flow influence the varying tidal characteristics (Prandle 1985). As tides, which are generated in the deep ocean basins, propagate into estuaries they can be amplified due to the geometrical shape (bathymetry and topography) of long, shallow, narrow funnel-shaped estuaries, causing large tidal ranges in their head region and potentially a bore (e.g. Qiantang River, China). Tides may also be rapidly diminished if an estuary is constricted by geology, such as open to the ocean via a narrow inlet or constricted by a bar (e.g. Kochi Inlet, India) (De Ruiter et al., 2017). Estuaries can be classified based on their shape or origin e.g. coastal plain (funnel-shaped), bar-built, fjords or tectonic (Prandle 2009), which can then influence the tidal characteristics of an estuary (Davies 1964). Classifications based on tidal characteristics and range are as follows; micro-tidal (tidal range < 2 m, e.g. Curonian Lagoon, Baltic Sea), meso-tidal (2 m < tidal range < 4 m, e.g. Colombia River, USA), macro-tidal (4 m < tidal range < 6 m, e.g. Gomso Bay, South Korea), and hyper-tidal (tidal range > 6 m, e.g. Bay of Fundy, Canada). Each estuary will respond differently to drivers of flood hazard depending primarily on its shape and size and studying the response of individual estuaries can provide useful case studies of the dominant drivers of flood hazard.

1.2.2.1. Hyper-tidal estuaries

Hyper-tidal estuaries display some of the most extreme tidal ranges worldwide. The Bay of Fundy, Canada has a mean spring tidal range up to 13.5 m at Noel Bay (Marmer, 1922) and the Severn Estuary, which borders south-west England and south Wales has a mean spring tidal range up to 12.2 m at Avonmouth (Uncles, 2010). These estuaries both display resonance with the M2 tide, which causes enhancement of the tide (Godin, 1993; Liang et al., 2014). The extreme tidal range has been shown to be a result of the overall shape and length of the estuary, as a pronounced 'funnel shape' and channel convergence amplifies the tidal wave up-estuary (Prandle 1985; Davies and Woodroffe 2010; Dronkers 2017). The shape and length-scale makes a hyper-tidal estuary more susceptible to the effects of combined hazards, and the impacts of a hazard could be amplified when all parameters occur concurrently. Small changes in water level due to the combined effect of coastal hazard parameters, can influence fetch, wave propagation, refraction and breaking and wetting and drying, to substantially alter flood hazard. Coincidence of the Groundhog Day storm in 1976 with sustained winds up to 102 mph generating large waves, along with the 18.03 year tidal modulation in the Bay of Fundy, Canada, caused up to 1.6 m flooding and substantial damage (Desplanque and Mossman 2004). The 3 January 2014 storms in southwest England and Wales saw record water levels exceeded, as a low pressure system, with central pressure 989 mbar, coincided with a perigee new moon spring tide (Sibley et al., 2015).

Different combinations of high tidal levels, notably due to equinoctial spring tides or the nodal cycle (Haigh et al., 2011), and storm surge can generate higher peak storm tides with longer duration to increase flood hazard at specific times (Menéndez and Woodworth 2010). These examples show how coastal hazards can combine to elevate flood hazard in hyper-tidal estuaries, however it should be noted that increased river discharge did not contribute to flood hazard during these events. Hyper-tidal estuaries are largely tide-dominated, and river flow has little influence on tidal dynamics (Prandle and Lane, 2015). That is not to say that high river discharge could not coincide with a storm surge and elevate flood hazard, but the large catchment area and additional time-take for increased fluvial discharge to travel through these systems, sometimes up to 6 days (Hendry et al., 2019), means that flood hazard is largely driven by forcing from the ocean side (tide, surge, wind, waves) and may not be so important here. Further to this, there is nothing to stop any combination of drivers of flood hazard occurring in a hyper-tidal estuary and the impacts may be amplified when they occur concurrently, maybe more so that in a micro-tidal or bar-built estuary. Therefore, hyper-tidal estuaries present a unique and extreme case study to understand the interactions between coastal flood hazard parameters during high-frequency storm event, and their impacts at a regional scale to support adaptation and mitigation planning. The extreme tidal range could also contribute to large uncertainties in predictions of tide, storm surge and waves at locations away from tide gauges and observation stations, which should be considered in flood hazard assessments.

1.3. Flood hazard assessment

The accurate prediction of each coastal hazard parameter and its contribution to peak storm tide along a coastline forms a key component of flood hazard assessment (Perini et al., 2016). These assessments ultimately aim to understand the susceptibility of coastlines to flooding and potential implications of floods (Carrasco et al., 2012). This involves developing a thorough understanding of the characteristics of a particular flood event due to combined effect of coastal hazard parameters, combined with an understanding of the assets that would be exposed to the particular hazard and subsequent damage (de Moel and Aerts 2011). Flood hazard can be represented in the form of maximum water level and wave heights that occur along the coastline which could lead to the exceedance of critical thresholds, or hazard maps to show subsequent impacts of exceedance including flood characteristics, such as inundation depth, flow velocity and inundation duration (Merz et al., 2010). This information can be used to define high risk areas where additional mitigation measures should be focused, inform cost-benefit analysis of intervention schemes and aid the development of long-term management plans (Barnard et al., 2019). Flood hazard assessments aim to minimise the negative effects of combined coastal hazards, not only to reduce economic impacts but also to protect public safety and environmental integrity.

1.4. Numerical modelling tools for flood hazard assessment

One key aspect of flood hazard assessment is the accurate prediction and likely projection of extreme water levels to understand the duration and intensity of a hazard for forecasts, alerts, flood warnings at an event scale (Lewis et al., 2013) and the design of suitable, site-specific defence measures based on potential consequences (Wadey et al., 2015). Further to this, combining predictions of coastal hazard parameters with flood damage assessment can inform and support long-term, sustainable flood resilience and adaptation strategies for communities at risk of flooding (Roebeling et al., 2011), notably shoreline management plans up to 2105 (Environment Agency 2010). Process-based, numerical modelling tools can be applied to a range of environments and can be forced with observation or model data to generate extreme water level scenarios, and also simulate the impacts of individual coastal hazard events. Hydrodynamic numerical models, e.g. Delft3D (Lesser et al., 2000), MIKE21 (Warren and Bach 1992) or Telemac (Galland et al., 1991), are based on finite differences which solve unsteady shallow water equations in two (depth-averaged) or three dimensions. These models are forced at an open boundary with water level to simulate tide and surge propagation based on the horizontal momentum equations, the continuity equation, the transport equation, and a turbulence closure model, the details of which are provided in each model handbook e.g. Deltares, 2011. Simulating WAVes Nearshore (SWAN) is a 3rd generation spectral wave model to simulate nearshore waves (Booij et al., 1999), which can be coupled with hydrodynamic models to simulate peak storm tide heights along a coastlines length (including wave effects and natural variability) and when critical thresholds may be exceeded. Shoreline response models, e.g. LISFLOOD (Bates et al., 2005) and X-Beach (Roelvink et al., 2009) can help to link information on total water level components (i.e. tide, surge, runup) with coastal impacts, by inferring likely flood extents, erosion risk and potential losses from specific events. Bathtub flood maps are a 1D option for simulating the effects of extreme water levels, but have been shown to underperform compared to 2D models (Didier et al., 2018). Numerical modelling tools can provide useful assessments of the drivers of extreme water levels and their impacts to facilitate the management and emergency response of coastal resources, improve the design of sea defences, and inform the public and decision makers to minimise loss of life from extreme events. The prediction of coastal hazard parameters is not only important for predicting when water level and wave heights will exceed critical thresholds, but also in designing appropriate thresholds in the first place, for cost-effective coastal protection strategies (Del R o et al., 2012). Finally, a thorough understanding of the combined effect of coastal hazard parameters can aid long-term inundation assessments to understand how estuarine and coastal zones may response to future changes in sea level and storm tracks (Pasquier et al., 2019; Robins et al., 2016). However, uncertainty is inevitably introduced into model predictions due to inaccurate representation of baseline / initial conditions, inaccurate boundary forcing, or the inability of a model to accurately represent physical processes which control the volume and rate water enters a model domain, and subsequent distribution across the domain (Quinn et al., 2014). Therefore

there is a need to identify sources of uncertainty in flood hazard assessments, and account for them when used by coastal asset managers, forecasters or planners.

1.5. Numerical modelling uncertainties

Uncertainties in coastal hazard parameters, particularly close to the time of tidal high water when exceedance of critical thresholds is more likely, can impact predictions of inundation duration, extent and depth, or erosion. Uncertainty in model predictions results in a wide, future window within which exposure or impacts could occur, and a range of possible values exist for a single parameter (Stephens et al., 2017). A lack of sureness in data which is used to support decisions can lead to error, delay or confusion (Fischhoff and Davis 2014). Sources of uncertainty can be categorised as i) aleatory, which arise due to the natural randomness of a process and inherent variation in a system; and ii) epistemic, which arises due to limited data or knowledge about a physical process (Beven, 2016; Zhang and Achari, 2010). Aleatory uncertainty can be mathematically modelled; random variables are assigned a probability density function to understand when certain events e.g. large storm surge, energetic waves, or high rainfall, may occur simultaneously (e.g. Hawkes et al., 2002; Unnikrishnan and Sundar, 2004; Moftakhari et al., 2017). Analysis of epistemic uncertainty focuses on ranges of possible outcomes, achieved through repeated experiments such as sensitivity testing (Gouldby et al., 2010). Sensitivity analysis in numerical modelling studies enables the influence of individual uncertainties on the output to be isolated (Sayers et al., 2003; Quinn et al., 2014; Garzon and Ferreira, 2016). These individual uncertainties can arise due to i) lack of knowledge of interaction or feedbacks within a system (knowledge uncertainty; ii) inability of a numerical model to simulate a physical processes (model uncertainty); and iii) measurement errors which are non-representative of real-life phenomena due to the temporal or spatial resolution of a dataset (data uncertainty) (Sayers et al., 2003). Epistemic uncertainty can occur in predictions of coastal hazard parameters due to inaccurate boundary forcing and model setup; theoretical wind and pressure field have been shown to cause uncertainty in modelled storm surge and wave heights along the US North Atlantic coastline (Bastidas et al., 2016). Coastal hazard uncertainty can cause errors in the definition of critical storm thresholds, operational forecasts or analysis into the exposure of assets to storm events. Variability in the time series of peak water levels has been shown to influence overflow volumes at tide gauge locations around the UK; this has subsequent implications for defence failure which is increasingly likely the longer a peak water level occurs for (Quinn et al., 2014). Inundation has shown greater sensitivity to the representation of coastal water levels and defence failures, rather than model setup including resolution of model grid and terrain, and bottom friction (e.g. Brown, et al., 2007). This highlights the need for accurate tide-surge-wind-wave-river predictions to act as boundary conditions to predict coastal events and change (e.g. flooding, erosion, sediment transport) (Teng et al., 2017) to minimise the impacts of storm events on communities, property and infrastructure. There is a need to understand and reduce epistemic uncertainty in predictions of coastal hazard parameters that contribute to long-term hazard assessments,

as sustainable coastal management requires confidence in the knowledge of any possible future changes to flood and wave hazard (Ranasinghe 2020).

1.6. Thesis aim and research questions

The overall goal of this work is to utilise numerical modelling tools to identify and quantify sources of uncertainty in coastal hazard prediction, and quantify the impacts of coastal hazard uncertainty on coastal communities to support the development of effective coastal hazard mitigation strategies and builds resilience to future change.

This research uses the Severn Estuary, which borders southwest England and south Wales as an extreme test case of how coastal hazard parameters can combine and influence flood hazard in an estuary. The estuary has a mean spring tidal range up to 12.2 m at Avonmouth, which occurs due to the estuaries long-length scale and shape, which causes a funnelling effect to amplify tidal propagation up-estuary (Uncles 2010). Near resonance with the M2 tidal component (the back and forth movement of water from head to mouth of the estuary occurs at the same frequency as the M2 tide) also amplifies the tidal range (Liang et al., 2014). The orientation of the estuary to the Atlantic Oceans means that the fetch is large, and it is exposed to prevailing wind, wave and storm conditions. Flood hazard is largely attributable to tidal water sources. The contribution of river flow to flood hazard increases east towards the tidal limit of the estuary at Gloucester (Atkins, 2013), however a time-lag up to 6 days between occurrence of a storm surge and peak river flow occurring from the same storm means that river level rarely contributes to coastal flood hazard (Hendry et al., 2019). Therefore, sensitivity of coastal flood hazard to fluvial contribution is not considered in this study but could be considered in the future. 50,000 hectares of land, over 250,000 homes and £14 billion infrastructure, including the decommissioned Oldbury Nuclear Power Station, are located between Hinkley Point, Somerset and Gloucester on the south coastline of the estuary, and tidal floodplains extend up to 5 km inland (Environment Agency, 2011). Major Welsh cities, including Swansea, Cardiff, and Newport are located on the north coastline of the estuary which are important centres for port operations, cargo and steel handling.

The Severn Estuary is a suitable location to assess and quantify coastal hazard uncertainty and subsequent impacts because of its hyper-tidal regime, which is an extreme test case of how a large tidal range can influence tide-surge-wave propagation, local fetch, wetting and drying impacts on hazard. Many businesses, communities and hugely critical infrastructure rely on accurate flood assessments in the Severn Estuary, and the results presented here can help to inform future adaptation, resilience and mitigation strategies in this estuary, and other similar shaped, hyper-tidal estuaries worldwide.

This thesis will apply coupled regional models to coastal flood hazard management needs in the Severn Estuary to answer the following research questions;

- i. Which key sources of coastal hazard uncertainty should be considered when predicting coastal flood and wave hazard?
- ii. What is the relative importance of each source of uncertainty in coastal flood hazard assessments?
- iii. How does coastal hazard uncertainty influence the physical and economic impacts of flooding?

1.7. Severn Estuary model setup

Process-based numerical modelling tools are based on detailed knowledge of the physical processes and phenomena that describe hydrodynamic and sediment transport characteristics and feedback using basic physical principles (Dissanayake et al., 2015). Delft3D is used here as a process-based model to simulate coastal hazard parameters in the Severn Estuary, and LISFLOOD-FP is used to transform offshore boundary forcing from Delft3D into the nearshore area. The following section describes these models in more detail, and a user guide for each is provided in Appendix 1 and 2.

1.7.1. Delft3D-FLOW

Delft3D is an integrated flow and transport modelling system which is widely used to simulate flows, sediment transport, waves and morphological developments in coastal, river and estuarine areas (Lesser et al., 2004; Condon and Veeramony, 2012; George et al., 2012; Borsje et al., 2013). The FLOW module of the model can simulate two-dimensional (2DH, depth-averaged) or three-dimensional (3D) unsteady flow resulting from tidal and/or meteorological forcing (Deltares 2011). Delft3D-FLOW solves the unsteady shallow water equations, derived from Navier-Stokes, which describes the flow below a surface in an incompressible fluid over time (Dastgheib et al., 2008). The momentum and continuity equations propagate the variables through curvilinear, rectilinear or flexible mesh grid based on the principles that i) mass is conserved and ii) Newton's second law ($Mass \times acceleration = force$) (Roelvink and Van Banning, 1994; Lesser et al., 2004). Water is driven through the model domain by gravity and water level gradients induced by tides, wind and river, and simulates wetting and drying processes. Density and salinity changes can be important in generating residual currents or when considering sediment transport processes in 3D. Momentum can be dissipated within the modelled area by bottom friction, waves, bedforms and turbulence. Delft3D-FLOW can be setup and calibrated to include mathematical formulations of numerous physical phenomena including Coriolis force, tidal forcing, shear stress, wind driven flows and atmospheric pressure. The flexibility of the model and range of setup options available makes Delft3D a suitable choice for simulating complex coastal environments.

1.7.1.1. Development of model grid and bathymetry

The development of the model grid and bathymetry is described here systematically however in reality it is a trial and error process, which utilises sensitivity testing. A grid is developed, tested, improved on and then tested again. Numerous iterations of the grid and bathymetry were developed to ensure optimal resolution, computational efficiency, improve the Courant number (which denotes time step) and ensure the model ran error free.

The outline of the model domain was selected in ArcMap from the Coastline feature within the Ordnance Survey Strategi digital vector dataset, which represents the coastline at mean high water level (Ordnance Survey, 2013). The land boundary outline was loaded into the grid generation module of Delft3D, RGFGRID, and a series of splines specified by hand to create a curvilinear grid. It was ensured that grid cell orientation follows direction of flow from the mouth to the head of the estuary. Grid cell resolution is coarser near the open sea boundary, and becomes increasingly finer up-estuary to improve computational efficiency.

The position of the open sea boundary (shown in Figure 2.1) was set as a straight line across the mouth of the Bristol Channel between Woolacombe, Devon and Rhossili, Swansea for the reasons listed below:

1. This position of the open sea boundary allows the model to be forced by open source, observation data. Tide gauge data, with a high temporal resolution of 15 minutes and available from the National Tidal and Sea Level Facility, is taken from gauges in Ilfracombe, Devon and The Mumbles, Swansea. The results can be used as evidence of how numerical models can be successfully forced with observation data, which represents a unique and valuable resource.
2. The model can also be forced by hindcast model data, such as the Met Office Unified Model, as the grid nodes of this coarser model domain lie across the boundary. The position of the open sea boundary follows the approach of the national surge forecasting system, with a high resolution, nested model of the Bristol Channel and Severn Estuary forced at the mouth of the estuary with offshore data. This ensures that offshore conditions can be transformed to impacts at the coast, such as flooding or overwashing.
3. Deep water conditions are captured within the boundary conditions. Tide gauge and wave buoy data will capture tide-surge interaction and the hindcast model data, from the Met Office Unified Model will capture deep water wave effects.
4. The points of main interest within the research, e.g. sites of critical nuclear infrastructure (Oldbury), and ports and harbours (Portbury, Cardiff) are located far up-estuary and will not be subject to boundary effects.
5. The up-estuary boundary was set at Gloucester, Gloucestershire which is the tidal extent of the Severn Estuary.

Once the model grid had been created, gridded bathymetry at a resolution of 1 ArcSecond was downloaded from Edina Digimap and cropped to the land boundary and model domain extent within ArcMap. Fortunately, data could be used from this one source, and there no need to interpolate between disparate datasets. A vertical datum correction was applied to the bathymetry in ArcMap, and then exported as an .xyz file. The .xyz file was loaded into Delft QUICKIN, which is used for the generation and manipulation of grid-related parameters such as bathymetry, initial conditions, and roughness (Deltares, 2014a). Where bathymetry data was a finer resolution than the model grid, then ‘grid cell averaging’ was used to apply bathymetry data onto the model grid. In locations of the model grid where bathymetry was a coarser resolution than the grid cell, then ‘triangular interpolation’ was used to interpolate the bathymetry onto the grid. The availability of bathymetry data in the upper estuary was low, therefore uniform depth values were applied up-estuary of Minsterworth, Gloucestershire which become increasingly shallow towards Gloucester. Gaps in bathymetry along the coastline were filled using the ‘internal diffusion’ function. Flat Holm Island and Steep Holm island were smoothed out of the model domain due to the coarser grid resolution near the open sea boundary.

1.7.1.2. Boundary conditions

The position of the open sea boundary allows for the model to be forced by observation (NTSLF, 2016) and model hindcast data (CS3X / Met Office Unified Model) (Saulter et al., 2016; Siddorn et al., 2016), which are utilised to force the open sea boundary. The model domains used by CS3X and the Met Office Unified Model have a resolution of 1.5 km and include the Severn Estuary so resonance effects will also be captured in the boundary forcing. The boundary conditions become increasingly complex through the course of the research, guided by the aims of each chapter. Chapter 2 – 4 utilise tide and wave observation data from gauges and buoys located within the estuary, with a time-varying, but spatially uniform open sea boundary. Tide and wave data are downloaded from online sources in .txt or .ascii formats and processed in Matlab to create boundary condition files for Delft3D. The open sea boundary is developed in chapter 5, so that it is time- and space-varying; 5 points along the open sea boundary represent grid cell nodes in the Met Office Unified Model, and Delft3D linearly interpolates between these equally spaced boundary points.

1.7.1.3. Model parameters

The model parameters are described here systematically but as with the grid and bathymetry development, the setup of the model is not a linear process. Each parameter is decided upon based on trial and error, and sensitivity testing.

The bottom roughness is a key parameter within Delft3D which determines the frictional energy loss at the ocean bed boundary condition and has an impact on the long-wavelength wave propagation (Sraj et al., 2014; Bastidas et al., 2016). A range of Manning friction coefficients were applied, based on values

used in similar studies and tabulated records in the literature (Chow 1959; Arcement Jr and Schneider, 1989; Bastidas et al., 2016). The sensitivity of the model to Manning friction coefficient was tested, with some results presented here in section 2.4.1). Values were selected for a range of natural environments which represent hydraulic resistance in natural stream channels (0.02), straight river channels (0.03), and muddy channels (0.05) (Chow, 1959). A uniform Manning friction parameter was applied to the model domain because this is a common approach in coastal and estuarine studies (e.g. Condon and Veeramony, 2012) and because there was limited data available to design a spatially-varying Manning parameter.

The computational time step describes the rate at which information is transported through the model grid, based on the wave speed of a system. A 0.1 time step denotes that water should not move more than 1 grid cell in a single time step. The time step is based on the Courant number, which can be inspected within QUICKIN (Deltares, 2011). Exceeding the appropriate time step for the grid resolution of the model domain can cause instability within the model. As the model domain used here has a variable grid resolution, a different time step is appropriate for different parts of the grid. Therefore sensitivity tests were completed to define the most appropriate time step for the grid, which also ensures computational efficiency and maintains stability.

The model is used here in barotropic depth-averaged (2D-horizontal mode), which simplifies 3D flow into 2D flow so that vertical velocities are very small, and the model runs with one horizontal layer. This model setup is appropriate for wave and water level simulations to assess flood hazard. The tide is the main driver of pressure changes within the Severn Estuary, and flood hazard primarily occurs due to the vertical movement (up/down) of water. Running the model in 3D model would capture density gradients due to temperature and salinity from the open boundary, river boundary and atmospheric forcing if boundary conditions are provided, which are important for transport processes in the Severn Estuary (Uncles, 2010), and their exclusion could cause some uncertainty in total water levels. Some 3D processes are important when considering flood hazard, such as wave-current interaction which can influence variability in long-shore and cross-shore currents and bed shear stress, ultimately controlling whether waves and tidal high water coincide (Lewis et al., 2019). Wave-current interaction in depth-averaged mode, is represented using the radiation stress approach to take into account the mean flow induced by wave motion and is introduced in current solvers as a barotropic forcing (Lalli et al., 2016). A lack of high-resolution directional wave data can also limit model setups to 2D.

1.7.1.4. Calibration and validation

Model calibration is the process by which parameters and boundary conditions are adjusted to obtain representative model outputs of the physical processes of interest (Williams and Esteves, 2017). Water level outputs from Delft3D simulations are calibrated to tide gauge data through the estuary for the most extreme event on record (3 January 2014), to ensure that extreme water levels can be simulated with

confidence. The most extreme event on record is calculated for the tide gauge record from 1991, when the temporal resolution of observation data improved from hourly to every 15 minutes. Model calibration is initially for tide and storm surge forcing only (chapter 2). Model outputs are compared to observational tide gauge data at Hinkley Point, Newport, Portbury, Oldbury, and Sharpness graphically and statistically using error metrics (R^2 , RMSE, Willmott Index of Agreement (Willmott, 1981; Willmott et al., 2012), Bias of the maximum value)). If there is a poor agreement between the model outputs and observation data, then a model parameter is adjusted (e.g. Manning friction coefficient) and the simulation is re-run. Error metrics confirm if the model can reproduce observational tide gauge data and assess the error introduced by the methodology used. When there is good agreement between the model output and observation data, then the same model setup is applied to simulate three less severe storm events, and the model is validated using error metrics. If the model is not able to represent certain physical processes and cannot be validated, then the calibration process can help to identify model parameters which contribute to uncertainty. The accuracy, or uncertainty, in model outputs should be communicated to the end user to show it is fit for purpose.

The same process of calibration and validation is used in chapter 5, where the tide-surge-wind-wave-river model is first calibrated to the most extreme event on record, and then validated to three less severe events on record. The ability to calibrate and validate a model to observation data is largely dependent on data availability. In this study the events that were selected to be simulated were based on whether data was available within the estuary for validation at the start of the modelling process.

1.7.2. Delft3D-WAVE

The Delft3D-WAVE module is used in chapter 4 and 5, which is based on SWAN (Simulation WAVes Nearshore), a third generation, spectral wave model (Booij et al., 1999). Third generation refers to the model's ability to simulate a 2D wave spectrum freely, without restriction (rather than individual waves), so it is appropriate to use in larger regions. Waves are described with the 2D wave action density spectrum, based on frequency and direction, and includes the interaction of wave fields with currents and bathymetry (Booij et al., 1999). The model represents nonlinear wave-wave interaction, refraction, shoaling, whitecapping, and depth-induced breaking (Deltares, 2011), and predicts directional spectra (angle of wave direction relative to the wind).

The model is used here in chapter 4 and 5, and significant wave height outputs are calibrated to the most extreme event on record. The process of calibration helped to identify the importance of forcing the model with a time- and space-varying wind and atmospheric pressure field, to continue to add momentum to the wave field up-estuary. Model hindcast data from CS3X is used to represent the wind and atmospheric pressure field. Calibration also helped to identify that a time- and space-varying open wave boundary is required, to represent spatial-variability in wave characteristics at the mouth of the estuary. Model hindcast data from Met Office WAVEWATCH III hindcast (Saulter et al., 2016;

Siddorn et al., 2016) is used to force the open wave boundary. Significant wave height outputs were then validated for three less severe storm events (as described in section 5.3.2).

1.7.3. LISFLOOD-FP

LISFLOOD-FP, used in chapter 5, is a 2D hydrodynamic model that simulates the propagation of flood waves across floodplains and along channels (Bates et al., 2013). The model uses a storage cell approach, and is based on the simplified shallow water equations (momentum and continuity equations) (Sosa et al., 2020). The momentum equation is implemented at the four interfaces of the neighbouring cell, and describes flow rate between two cells controlled by gravity and the prescribed Manning friction coefficient (Bates et al., 2013). The continuity equation denotes that volume remains the same. The model calculates inundation based on volumetric flow rate, cross-sectional area of flow, water depth, bed elevation, friction and time. Different solvers are available within LISFLOOD, depending on the aims of the research, physical characteristics of the area to be modelled and available data. All solvers are based on the simplified shallow water equations, but place significance on individual components i.e. the routing solver is the simplest and assumes all shallow water terms to be negligible, whereas the flow limited solver assumes local and convective acceleration to be negligible (Bates et al., 2013). The acceleration solver is used in this study, which assumes only the convective acceleration term is negligible and implements adaptive time steps.

1.7.3.1. Digital Elevation Model

A key component of a LISFLOOD-FP model setup is a raster Digital Elevation Model (DEM), which is typically based on airborne laser altimetry surveys (LiDAR). The DEM is a raster dataset, which has a user-defined, uniform cell size. LiDAR data was downloaded from Edina Digimap (Environment Agency Geomatics, 2019) in .ascii format, and converted to a raster dataset in ArcMap. The LiDAR is downloaded at 2 m resolution but resampled to 5 m for computational efficiency. This resampling technique means that some key features in the coastal zone are smoothed out e.g. sea defences, dykes, seawalls, therefore these are digitised by hand back into the DEM with a representative elevation. The DEM is cropped to the required size of the model domain. The inland extent of the model domain is set at 5 km inland, and the offshore boundary is set at the low water mark or the defence crest line depending on the aims of the research. In some cases, disparate LiDAR data requires joins between datasets to be smoothed used interpolation techniques. Additional practical steps to develop a DEM are provided in Appendix 2.

1.7.3.2. Model inputs

LISFLOOD-FP requires a series of input files, describing model parameters (e.g. time steps, Manning friction coefficient, solver), time-varying boundary conditions, and boundary condition type. A uniform Manning friction coefficient can be implemented, or a space-varying coefficient applied if appropriate

data on land use is available. A uniform Manning friction coefficient is used here, and the most appropriate value was selected here following a series of sensitivity tests. Manning friction coefficients from similar studies were tested (e.g. Prime et al., 2015) and small differences were observed between simulations. A value of 0.03 was finally selected. It has been shown that at an event scale, boundary conditions can be more important than model parameters in accurately representing inundation (Wong et al., 2015). Data availability makes calibration and validation of an inundation more challenging than a hydrodynamic model such as Delft3D, and secondary data sources, such as photos, or newspaper articles can be useful to understand where flooding may have occurred (Hall et al., 2005). Observed water levels from satellite images have been successfully used in the past (Mason et al., 2009), however this method is also dependent on data availability. This is a key limitation in inundation modelling, and should be considered when interpreting and communicating results to an end user.

1.8. Thesis structure

The chapters listed below, written in the form of published and submitted manuscripts, utilise wave, ocean and meteorological observation and model hindcast data to simulate extreme water level and significant wave height using the Delft3D-FLOW-WAVE modelling package, and inundation using LISFLOOD-FP. Each chapter that is presented represents an increase in the complexity of the modelling work completed through the course of the research, by utilising different modules of Delft3D and incorporating coupling processes between them, and including more time- and space-varying data to force the model boundaries. The results work towards improving public safety and awareness of coastal hazards in a hyper-tidal estuary.

2. Lyddon, C., Brown, J.M., Leonardi, N. and Plater, A.J., 2018. Flood Hazard Assessment for a Hyper-Tidal Estuary as a Function of Tide-Surge-Morphology Interaction. *Estuaries and Coasts*, 41(6), 1565–1586.

Contributions by authors to manuscript:

C. Lyddon: principal investigator and author, data processing, analysis and plot creation

J.M. Brown: manuscript development, and advice on experimental design, model setup and figure plot creation

N. Leonardi: manuscript development, and advice on experimental design, model setup and figure plot creation

A.J. Plater: manuscript development, and advice on experimental design and figure plot creation

Chapter 2 develops the model grid and bathymetry data, and validates and calibrates Delft3D-FLOW, a numerical hydrodynamic model of the Severn Estuary, which borders south Wales and southwest England. The model is used here in barotropic, two-dimensional horizontal mode, and forced with local tide gauge and river inflow data to simulate tide-surge interaction, which are two key drivers of flood hazard within the estuary. Total water level is validated at five tide gauges within the estuary for the most extreme event on record, to ensure the model accurately simulates tide-surge propagation.

The validated and calibrated model is used to assess key sources of uncertainty in combined flood hazard in the Severn Estuary resulting from astronomical high tides and meteorological storm surges due to i) event severity; ii) timing of the peak of a storm surge relative to tidal high water; and iii) temporal distribution of the storm surge component (termed the surge skewness), and their influence on spatial-temporal variability of flood hazard up-estuary. The influence of uncertainty in combined flood hazard is quantified by presenting percentage change in four flood hazard proxies including: i) total water level, and consequently flood hazard; ii) time-integrated elevation; iii) duration of the peak of the storm tide exceeding mean high water spring tide; and iv) and surge elevation. The results examine the implications of the variability observed in the storm-tide time series at different tide gauge sites and are analysed in the context of the source-pathway-receptor-consequence model (Narayan et al., 2012). The results of this research identify the combined effect of the dominant factors in a hyper-tidal estuary which contribute to extreme water levels for local scale, flood hazard management, and the relative importance of each source of uncertainty when predicting extreme water levels.

3. Lyddon, C., Brown, J.M., Leonardi, N. and Plater, A.J., 2018. Uncertainty in Estuarine Extreme Water Level Predictions Due to Surge-Tide Interaction. *PLoS ONE*, 13(10): e0206200.

Contributions by authors to manuscript:

C. Lyddon: principal investigator and author, data processing, analysis and plot creation

J.M. Brown: manuscript development, and advice on experimental design, model setup and figure plot creation

N. Leonardi: manuscript development, and advice on experimental design, model setup and figure plot creation

A.J. Plater: manuscript development, and advice on experimental design and figure plot creation

Chapter 3 also uses the calibrated and validated tide-surge-river model of the Severn Estuary, southwest England, but focuses solely on how modelled surge residual varies at five tide gauge location within the estuary, and through the thalweg of the estuary. Temporal and spatial variability in the surge residual and tide-surge interaction can cause large uncertainties in total water level predictions, which are used by coastal asset managers for hazard mitigation strategies.

Delft3D-FLOW is used to assess the sensitivity of the surge, including a tide-surge interaction component, to uncertainty in the storm-tide time series. The influence of the key sources of uncertainty, presented in chapter 2, on surge residual alone is quantified by directly comparing: i) tidal range; ii) surge elevation; and iii) variability in skew surge at five tide gauge locations and through the thalweg of the Severn Estuary. Analysis of the residual surge identifies where variability in surge elevation occurs through the tidal cycle, and how this varies spatially to improve understanding of tide-surge propagation in a shallow, narrow estuary. The results show there is a need to capture uncertainties associated with the timing and shape of representative surge curves to minimise uncertainties in forecasting systems used in flood hazard assessments. This is particularly the case at up-estuary locations away from tide gauges, where the funnelling effect and tide-surge interaction amplify the magnitude and duration of surge residuals above predicted levels.

4. Lyddon, C., Brown, J.M., Leonardi, N. and Plater, A.J., 2019. Increased Coastal Wave Hazard Generated by Differential Wind and Wave Direction in Hyper-Tidal Estuaries. *Estuarine, Coastal and Shelf Science*, 220, 131-141.

Contributions by authors to manuscript:

C. Lyddon: principal investigator and author, data processing, analysis and plot creation

J.M. Brown: manuscript development, and advice on experimental design, model setup and figure plot creation

N. Leonardi: manuscript development, and advice on experimental design, model setup and figure plot creation

A.J. Plater: manuscript development, and advice on experimental design and figure plot creation

Delft3D-WAVE, a third-generation spectral wave model based on SWAN, is used in standalone mode in chapter 4 to isolate the contribution of uncertainty in wind and wave characteristics to wave hazard within the Severn Estuary. Isolating the effect of wind and wave characteristics on wave hazard is important in a heavily populated and industrialised estuary, where critical infrastructure must be designed to withstand this hazard.

The model is forced with representative values for total water level, wave period, significant wave height and wind speed based on five years of observational data within the estuary and combined with varying wind and wave direction to simulate wave evolution up-estuary. The research aims to identify key combinations of wind-wave characteristics which contribute to wave hazard throughout the Severn Estuary. Variability in wave hazard due to uncertainty in wind and wave direction is quantified by presenting percentage change in maximum significant wave height along the shoreline of the estuary between scenarios. The model highlights the sensitivity of higher amplitude, shorter period waves to opposing wind direction to increase wave hazard, and the sensitivity of lower amplitude, longer period waves to wave and wave direction to amplify wave hazard further up-estuary. The results highlight uncertainty in wave hazard due to wind-wave characteristics, and the importance of accounting for these processes to ensure accurate prediction of significant wave height to inform sea defence design to withstand overwashing under a range of conditions, minimise operational downtime in ports and harbours due to wave transmission, and to inform long-term coastal management of the potential implications of future climate changes on wave hazard in the estuary.

5. Lyddon, C., Brown, J.M., Leonardi, N., Saulter, A. and Plater, A.J., 2019. Quantification of the Uncertainty in Coastal Hazard Predictions Due to Wave-Current Interaction and Wind Forcing. *Geophysical Research Letters*, 46, 14,576 – 14,585.

Contributions by authors to manuscript:

C. Lyddon: principal investigator and author, data processing, analysis and plot creation

J.M. Brown: manuscript development, and advice on experimental design, model setup and figure plot creation

N. Leonardi: manuscript development, and advice on experimental design, model setup and figure plot creation

A. Saulter: provision of WAVEWATCH III data from Met Office and manuscript editing

A.J. Plater: manuscript development, and advice on experimental design and figure plot creation

The accurate definition of high water level and high water significant wave height is crucial for critical storm threshold identification, however uncertainty in storm surge and wave forecasts due to errors in model setups or boundary forcing may mean that flood events are underestimated or missed. Following on from the modelling work in chapter 2 and 3 (using Delft3D-FLOW) and chapter 4 (that uses Delft3D-WAVE in standalone mode) the complexity of the modelling process is developed further in chapter 4. The hydrodynamic and wave model are coupled together to account for the influence of the circulation on the waves and waves on the circulation (two-way coupling). A space- and time-varying wave, wind and atmospheric pressure is added using data from the Met Office Unified Model to more accurately represent wave generation and propagation. Significant wave height predictions from the two-way coupled Delft3D-FLOW-WAVE simulations are statistically validated at four wave buoys within the estuary.

Delft3D-FLOW-WAVE is then used in a series of standalone, uncoupled and coupled scenarios, with and without local atmospheric forcing, to quantify the uncertainty in forecasting estuarine water levels due to coupling and forcing processes in the Severn Estuary, southwest England. Uncertainty introduced into coastal hazard predictions due to coupling and forcing processes are quantified by presenting % difference in of high water level and high water significant wave height, and hazard proxy (water level + $\frac{1}{2}$ significant wave height, used to understand the severity of a hazard condition) between simulations along the north and south shoreline. The results highlight the importance of the inclusion of atmospheric forcing to continue to add momentum to wave generation up-estuary, and the need for accurate, local boundary conditions when predicting coastal hazard parameters. Aspect and geometry of an estuary is also a crucial control on spatial variability of flood hazard. The results highlight how coastal and estuarine numerical models should be set up to ensure confidence in their results, to ensure timely and accurate flood warnings.

6. Lyddon, C., Brown, J.M., Leonardi, N., and Plater, A.J., 2020. Uncertainty propagation in flood hazard assessments. *Journal of Marine Science and Engineering* (under review).

Contributions by authors to manuscript:

C. Lyddon: principal investigator and author, data processing, analysis and plot creation

J.M. Brown: manuscript development, and advice on experimental design, model setup and figure plot creation

N. Leonardi: manuscript development, and advice on experimental design, model setup and figure plot creation

A.J. Plater: manuscript development, and advice on experimental design and figure plot creation

Uncertainties in coastal hydrodynamic models, such as those identified in chapter 4, can propagate and accumulate through the modelling chain to influence shoreline response models, and the accuracy of their outputs. Chapter 6 aims to quantify the sensitivity of inundation to uncertainty in coastal hazard conditions and method used to force the open boundary of an inundation model, and the impact of uncertainty on specific targets (e.g. people, critical infrastructure, and different land uses). LISFLOOD-FP, a 2D finite difference inundation model based upon the storage cell approach, is used in chapter 5 to quantify uncertainty in inundation at Oldbury-on-Severn, southwest England, due to coastal hazard uncertainty and using different approaches to force the model boundary. Outputs from standalone, coupled and uncoupled scenarios completed in chapter 5 using Delft3D-FLOW-WAVE, which represent coastal hazard uncertainty in water level and significant wave height, are used to force the boundary of LISFLOOD-FP. Two approaches to forcing the open boundary of LISFLOOD-FP are used to represent different pathways of flood hazard. The inundation is forced from the low water mark using hazard proxy (water level + $\frac{1}{2}$ significant wave height) and from the defence crest line using wave runup (Stockdon et al., 2006). The influence of uncertainty in coastal hazard parameters and different approaches to force the model boundary on inundation is quantified by presenting: i) flood inundation maps; ii) hazard to people with “traffic light” ratings at two sites of critical infrastructure; iii) volume of inundation; absolute difference in iv) time-integrated volume of inundation, and v) economic costs to arable and suburban land uses between coupled and uncoupled simulations. The results identify the importance of small changes in total water level at the coast for the exceedance of critical thresholds; the optimum model setup for simulating coastal flood inundation; and how variability in inundation due to coastal hazard uncertainty can substantially alter flood damage assessments, shoreline management plans and emergency response plans. Contributions to uncertainty in inundation models should be considered when developing local scale studies of storm events under present and future sea-level scenarios for coastal hazard mitigation and adaptation or resilience planning.

7. Conclusion and Implications

Chapter 7 summarises the key results and findings of each chapter of this study in the context of the Source-Pathway-Receptor-Consequence model to identify how this research can be applied to improving the accuracy of flood hazard assessments. Finally, the results are discussed to show help they can i) improve prediction of coastal hazards for long-term coastal planning, alongside uncertainty arising from future changes in climate and sea level, and ii) inform early warning systems, including flood alerts, warnings and emergency response. The discussion identifies areas of this research requiring further consideration to support these two applications.

2. Flood hazard assessment for a hyper-tidal estuary as a function of tide-surge-morphology interaction

Chapter 2 quantifies the sensitivity of two key drivers of flood hazard in a hyper-tidal estuary, astronomical tide and meteorological storm surge, to three key sources of uncertainty. There is a need to accurately predict total water levels arising from the combined effect of astronomical tide and meteorological storm surges, which can elevate observed water levels above the predicted level. Delft3D-FLOW is setup and statistically validated to five tide gauges within the Severn Estuary, southwest England, used here as a test case for heavily populated and industrialised hyper-tidal estuaries worldwide. The spatial and temporal variability of extreme water levels are analysed at five tide gauge locations within the estuary, and through the thalweg of the estuary to understand the mechanisms controlling tide-surge propagation and interaction, and its contribution to site specific flood hazard assessment.

2.1. Abstract

Astronomical high tides and meteorological storm surges present a combined flood hazard to communities and infrastructure. There is a need to incorporate the impact of tide-surge interaction and the spatial and temporal variability of the combined flood hazard in flood risk assessments, especially in hyper-tidal estuaries where the consequences of tide and storm surge concurrence can be catastrophic. Delft3D-FLOW is used to assess up-estuary variability in extreme water levels for a range of historical events of different severity within the Severn Estuary, southwest England as an example. The influence of the following on flood hazard is investigated: i) event severity, ii) timing of the peak of a storm surge relative to tidal high water and iii) the temporal distribution of the storm surge component (here in termed the surge skewness). Results show when modelling a local area event severity is most important control on flood hazard. Tide-surge concurrence increases flood hazard throughout the estuary. Positive surge skewness can result in a greater variability of extreme water levels and residual surge component, the effects of which are magnified up-estuary by estuarine geometry to exacerbate flood hazard. The concepts and methodology shown here can be applied to other estuaries worldwide.

2.2. Introduction

Coastal zones worldwide are subject to the impacts of short term, local variations in sea-level, particularly communities and industries developed on estuaries (Pye and Blott 2014). Extreme sea levels, caused by the combination of astronomical high tides and meteorological storm surges, are a major threat to coastal communities and infrastructure (Elliott et al., 2014; Quinn et al., 2014; Webster et al., 2014; Prime et al., 2015). This is of particular significance in hyper-tidal estuaries, where tidal range exceeds 6 m (Davies 1964).

Tidal range can exceed 6 m as tides are amplified through an estuary due to near resonance, shallow bathymetry and channel convergence (Pye and Blott 2014). Surges can also be amplified through hyper-tidal estuaries, due to reduced hydraulic drag caused by greater mean depths, as seen along the Orissa coast of India (Sinha et al., 2008) and narrowing topography and orientation of the coastline, as seen in the Cape Fear River Estuary, North Carolina (Familkhalili and Talke 2016). Maximum water levels and storm surge impacts are not simply linearly related to increased tidal range (Spencer et al., 2015), but the complex interactions seen in hyper-tidal estuaries between tide, surge and landscape changes increases sensitivity to timing of storm events (Desplanque and Mossman 2004), and thus exaggerate water levels. Tidal amplification and extreme surge development in hyper-tidal estuaries means concurrence of a large astronomical tide and extreme surge can be catastrophic, as seen in the Bay of Fundy, Canada (Desplanque and Mossman 1999), Meghna Estuary, Bangladesh (As-Salek and Yasuda 2001) and Severn Estuary, UK (Pye and Blott 2010).

Accurate prediction of extreme water level and its timing is essential for storm hazard mitigation in heavily populated and industrialized, hyper-tidal estuaries (Williams and Horsburgh 2013). Such prediction requires accurate understanding of the tide-surge propagation, how this varies as a function of the timing and shape of the storm surge relative to high water, and how such interaction changes due to estuary morphology and bathymetry.

The Bay of Fundy, between the Canadian provinces of New Brunswick and Nova Scotia, has a maximum mean spring tidal range 16.9 m which is the largest in the world (Greenberg et al., 2012). The tidal range is so large due to near resonance with incoming North Atlantic tides (Desplanque and Mossman 1999) and shallow water depths amplify the tide through the Bay (Marvin and Wilson 2016). Shallow water depths and dimensions of the Bay also amplify extra-tropical storm surges through the bay, therefore, when a surge coincides with an amplified, high astronomical tide the results may be little short of catastrophic. The concurrence of a rapid drop in pressure and a “higher than normal” tide meant that water levels were elevated 2.5 m above predicted level on the Groundhog Day storm, 1976 (Desplanque and Mossman 2004).

The narrow geometry of the Qiantang River, east China, has a maximum tidal range of 7.72 m at Ganpu at its head and produces one of the world’s largest tidal bores which reaches up to 9 m and travels up to 40 km / hr (Pan et al., 2007; Zhang et al., 2012). On the Qiantang River, concurrence of high tide and typhoon-induced storm surges can raise observed water levels up to 10 m above predicted levels (Chen et al, 2014).

Extreme water level events are exaggerated in hyper-tidal estuaries due to the amplified tide-surge propagation, which in turn can increase flood hazard. Flood hazard is defined as the possibility of flood event occurring which could be damaging and harmful to communities and infrastructure (Kron 2009; Shanze 2006). Expansion of the energy and agricultural sector, migration and residential development in the coastal zone can increase the vulnerability of communities to flood hazard in estuaries (Pottier et al., 2005; McGranahan et al., 2007). Shanghai, on the Yangtze River Estuary, is a centre for human population and economic activities, with flood hazard further exacerbated by land subsidence (Wang et al., 2012). Coastal flood hazard analysis aims to understand the processes and dynamics of coastal flooding to assess the potential consequences for people, businesses, the natural and built environment (Monbaliu et al., 2014; Narayan et al., 2012). However the coastal flood system is a dynamic and complex system, with both physical and human elements possibly exacerbating hazard. Decision-makers must therefore employ a variety of system level analysis models and frameworks that account for key elements of the flooding system to understand the hazard (Sayers et al., 2003).

The commonly used Source-Pathway-Receptor-Consequence (SPRC) model identifies key links between the built and natural environment and sources of physical change (Horrillo-Caraballo et al., 2013). This model was adopted by the Environment Agency for local scale, coastal flooding to describe

floodwater propagation from source to floodplains, including physical processes and drivers, infrastructure and strategy (Narayan et al., 2012; Sayers et al., 2003). The first component of the SPRC model are the physical characteristics of flood hazard; sources which may result in flooding events such as intense rainfall, astronomical high tides and storm surges. However quantifying sources in dynamic, interlinked systems can be complex. Spatial & temporal variations in tidal levels, wave setup, and rainfall, interaction between sources, natural variability and combinations of sources are hard to account for (Sayers et al., 2002). Therefore there is a need to better understand variability and combinations of physical processes driving local flood systems to improve flood hazard assessment.

Accurate prediction of the combination of factors driving extreme water levels is a key component of understanding and assessing flood hazard (Pender and Néelz 2007). Numerical models can be used to simulate physical processes and calculate rates of change across time and space that result from different combinations of variables, e.g. meteorological conditions, tidal conditions and coastal defence systems (Lewis et al., 2013; Quinn et al., 2014). Analysis of extreme water levels requires a hydrodynamic model, which is able to simulate the flow and velocity of water, for example FVCOM, POLCOMS, TELEMAC and Delft3D. Two-dimensional, depth-averaged hydrodynamic models have previously been used to successfully simulate the barotropic hydrodynamics in estuaries to help better understand past events, inform decisions concerning flood hazard and the development of energy resources and coastal defence intervention (Xia et al., 2010; Cornett et al., 2013; Maskell et al., 2014). These models rely on accurate bathymetry and boundary conditions when modelling coastal and estuarine areas to limit uncertainties in modelled results. Modelling studies which focus on the physical drivers of coastal flood hazard can aid decision-makers and clarify connections in the system.

This research focuses on the Severn Estuary as an exemplar of hyper-tidal estuaries worldwide, due to its national significance for nuclear energy infrastructure (Ballinger and Stojanovic 2010), and where complex interactions influence extreme water level and subsequent flood hazard. The Bristol Channel and Severn Estuary, south-west England, is an example of a hyper-tidal estuary prone to relatively frequent meteorologically-induced surges generated by North Atlantic low pressure systems (Uncles 2010). For the purposes of this paper the “Severn Estuary” is taken to include the Bristol Channel. These storm surges can be exacerbated by the estuary’s dimensions and characteristics. The tidal range increases from 6.2 m in the outer Bristol Channel to 12.20 m at Avonmouth as a function of geometry (Pye and Blott 2010).

This paper uses the Severn Estuary, south-west England, as an example to describe the assessment of combined flood hazard in the Severn Estuary resulting from astronomical high tides and meteorological storm surges. A sensitivity study is conducted using long term tide gauge data to force the model boundary of Delft3D-FLOW to investigate variability of extreme water levels. The effect of river flow on extreme water levels is not considered here, because the sensitivity of the Severn Estuary to river

flow is not as great as tidal and meteorological drivers. Also the greatest implications of flood hazard upon various nuclear infrastructure will result from tide-surge propagation especially because this is a hyper-tidal estuary. River flow would be an important factor to consider in estuaries with smaller tidal ranges or greater discharge, e.g. Pearl River Delta in China (Leonardi et al., 2015; Hoitink and Jay, 2016). The results show the severity of the combined tide and storm surge event, timing of the peak of the surge relative to tidal high water and the surge skewness are important controls on flood hazard in estuarine environments. This methodology can be applied to other estuaries worldwide, in the context of the SPRC model to help to better understand past extreme events and inform local management needs to minimise future flood hazard.

2.3. Methods

2.3.1. Delft3D

Delft3D-FLOW, an open source, hydrodynamic model which solves depth-averaged unsteady shallow-water equations across a boundary fitted grid (Lesser et al., 2004), is used to simulate barotropic tide-surge-river propagation and interaction in the Severn Estuary. The Delft3D-FLOW module has been used in a number of studies to simulate tide-surge propagation and extreme water levels in a coastal environment (Condon and Veeramony 2012; Irish and Cañizares 2009).

2.3.2. Model domain

The Severn Estuary model domain (Figure 2.1) extends from Woolacombe, Devon and the Rhossili, Gower Peninsula in the West, up to Gloucester in the East, which is the tidal limit of the Bristol Channel. The 2DH curvilinear grid closely follows the coastline of the Severn Estuary. The horizontal model grid cell size varies from 3 km at the seaward boundary in the lower estuary, to less than 10 m in the upper estuary. The model domain has two open boundaries: a sea boundary forced by 15 minute tide gauge water level data to the West, and a river boundary forced by 15 minute river gauge water level data from Sandhurst to the East.

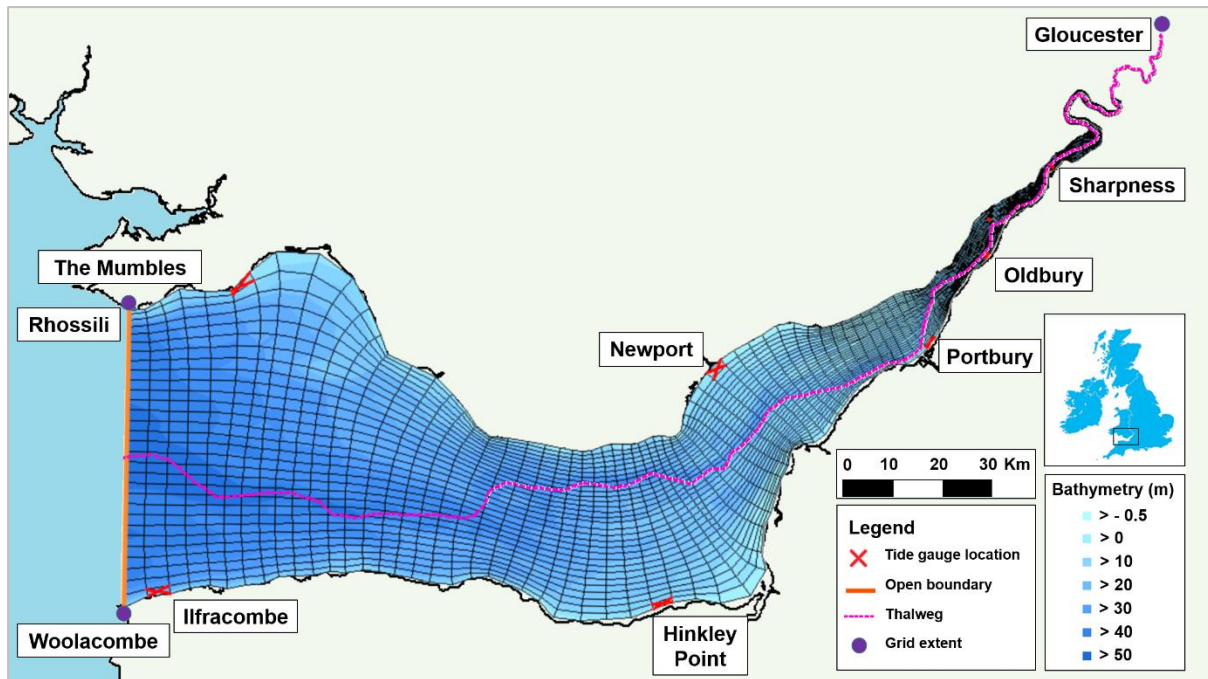


Figure 2.1: Severn Estuary model domain extending from Ilfracombe ($51^{\circ}12.668'N$, $4^{\circ}6.743'W$) and The Mumbles ($51^{\circ}34.203'N$, $3^{\circ}58.534'W$) in the west, to Gloucester ($52^{\circ} 89.3020'N$, $-2^{\circ} 6361'W$) in the east. The bathymetry is relative to chart datum (CD).

Gridded bathymetry data at 50 m resolution (SeaZone Solutions Ltd. 2013) were interpolated onto the model grid. Lack of bathymetric data and poor resolution of data in the upper estuary meant that a uniform value had to be applied north of Epney to the river boundary. The value imposed was 2 m, which represented a more realistic channel depth. Sensitivity analysis has been limited to external barotropic tide-surge forcing and river discharge only and no meteorological or wave forcings have been included in the model. Freshwater has not been considered as it has a lower impact on estuarine circulation and water levels. This is shown by the Richardson number, calculated by Reynolds and West (1988) 0.04 – 0.4 on spring tides, dependent on depth and breadth of the Severn Estuary. This is so impact of tide-surge propagation and external surge timing on extreme water levels up-estuary can be assessed, which is likely to have the greatest impact upon various nuclear energy infrastructure assets within the estuary.

A 0.1 minute time step is used to allow for calculations of the shallow water equations to be solved in the fine resolution grid up-estuary. This is validated against the Courant number for the grid. A uniform 0.025 Manning bottom roughness value is applied to the grid.

Tide gauge locations in Figure 2.1 indicate where long-term water level records are available, with which to compare and validate the model results.

2.3.3. Boundary conditions

2.3.3.1. Long-term tide gauge data

Long-term tide gauge records from The Mumbles (Figure 2.2) and Ilfracombe (Figure 2.3), located close to the western boundary of the model domain, are used to force the total and tidal water levels in different model setups. The long-term tide gauge records collected by the UK Tidal Network (https://www.bodc.ac.uk/data/online_delivery/ntslf/) provide hourly sampled tidal records prior to 1992 and quarter hourly sampled tidal records from 1993 to present day. All high water peaks (astronomical tide + storm surge) in the record from Ilfracombe and The Mumbles were identified and isolated. Sea-level values flagged in the tidal record by BODC as improbable, null or interpolated values were discarded, to ensure only accurate observational data are used to force the model boundary.

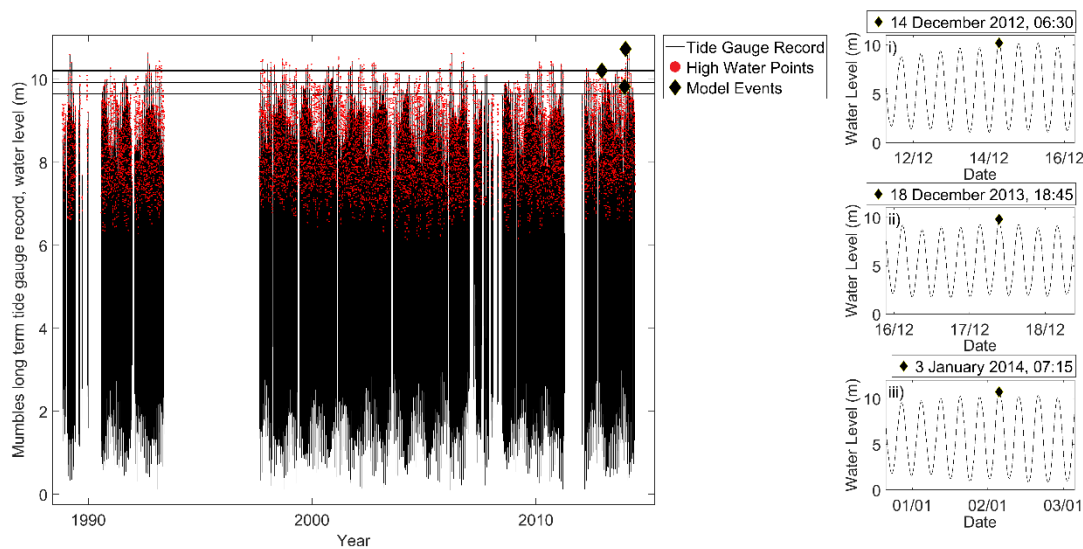


Figure 2.2: Long-term tide gauge record at The Mumbles, Bristol Channel, U.K showing tide gauge time series, points in the time series representing high water peaks and events to be modelled. The panels on the right illustrate the three selected events representing the 95th (i, 14th December 2012), 90th (ii, 18 December 2013) and 99th (iii, 3 January 2014) water level percentile values.

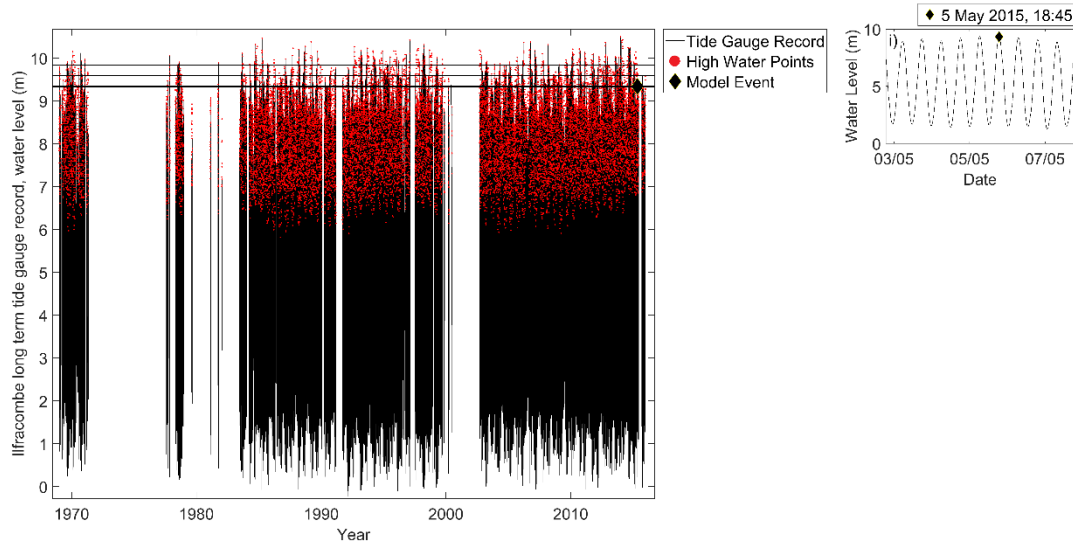


Figure 2.3: Long-term tide gauge record at Ilfracombe, Bristol Channel, U.K showing tide gauge time series, points in the time series representing high water peaks and events to be modelled. The panel on the right illustrates one selected event representing the 95th (i.e. 5 May 2015) water level percentile values.⁵

While joint probability distribution analysis is a common approach to defining event severity (McMillan et al., 2011; Williams et al., 2016), here we use percentile values applied to long-term monitoring data. This is because many tide-surge water level combinations have the same severity, making it hard to choose a single event. Although return period analysis provides a statistically representative event, we use observed events and classify their severity against long-term records by the use of percentile values. To identify extreme events at Ilfracombe and The Mumbles we calculated the 99th, 95th and 90th percentile values of the high water levels and created a set of severity thresholds. Extreme water level events exceeding the 90th, 95th and 99th percentile severity thresholds are identified. Four extreme water level events for which a positive surge occurs and a complete total water level series are available at Ilfracombe or The Mumbles and the tide gauge locations up-estuary (Hinkley, Newport, Portbury, Oldbury, Sharpness, Figure 2.1) for validation purposes are identified. Using the Environment Agency return period for still water, extreme sea level values these events fall within the range between a 1/1 (5.41 m) and 1/100 (6.03 m) year event (McMillan et al., 2011). A historical water level event which falls within the 1/200 year category would be defined as a more severe event. Missing data in the tide gauge records did not allow for data from both Ilfracombe and The Mumbles to be interpolated across the seaward open boundary in the model.

Small differences are present in the tide-gauge records for amplitude and phase between Ilfracombe and The Mumbles. The maximum difference in phase between high water points is 15 minute, with high water occurring later at The Mumbles. Small differences occur in amplitude, with a higher water level occurring at the Mumbles, to the order of tens of centimetres. It is likely that tide and surge effects that

occur over a region could be coherent at neighbouring stations (Proctor and Flather 1989). The differences could also be an artefact of the recording frequency and could potentially be smaller than observed. Therefore differences in phase and amplitude are considered small enough to impose conditions from either location across the sea boundary in a uniform manner

River level data from Sandhurst river gauge station, located just north of Gloucester, is used to force the eastern model boundary. The river level data is converted to chart datum, to match the model datum.

2.3.3.2. Surge characteristics

The extreme water level event is isolated as a storm tide, 6 hours before and 6 hours after the maximum water level. Water level time series are isolated from the tide gauge record from 3 days prior to and 2 days after the storm tide peak; each model run scenario is 5 days long. Following these criteria, it can be seen that only events since 2012 are taken from the tide gauge record. A notably stormy winter in 2013 / 2014 coincided with the peak of the 18.6 year tidal lunar cycle (Gratiot et al., 2008; Haigh et al., 2016).

The surge component time series during the 5 day simulations is separated from the total water level time series. Long-term tide gauge records provide information on both total water level and residual surge. The residual surge is calculated as the total observed water level minus the predicted tide, taken from POLTIPS3 which is available from the National Tide and Sea Level Facility (Prime et al., 2015). This way, any tide-surge interaction remains within this residual surge component. A Chebyshev type II, low pass filter is applied to the residual surge component to separate out the time-varying meteorological residual and the tide-surge interactions (an approach used by Brown et al., 2014). The low pass filter is designed to remove all energy at tidal frequencies, using a stop-band of 26 h and a pass-band of 30 h. A 3 dB passband ripple and 30 dB stopband attenuation was used, to leave only the meteorological residual (low frequency surge component with no tidal energy or tide-surge interaction) in the time series. Tidal energy and tidal interaction is removed, as it has a similar frequency to the tide and leaves only the low-frequency (>30 h, sub-tidal) residual (Brown et al., 2014). The low pass filter approach was validated using the 25 hour running mean of the surge component.

Storm surge features are characterized by the skewness of the residual surge component with time. Skewness is a measure of the asymmetry of the data around the time series mean. The skewness of a distribution is defined as:

$$skewness = \frac{N}{(N-1)(N-2)} \sum \left[\frac{x_i - \bar{x}}{s} \right]^3$$

where N is the number of observations, x_i is the i^{th} observation, \bar{x} is the mean of the observations, and s is the standard deviation of the sample (Gronewald and Meeden 1984). Positive skewness describes

a shorter, steeper rising limb on the surge; negative skewness refers to a shorter, steeper falling limb following the maximum surge.

Two events have a surge component with positive skewness, and 2 with negative skewness. The skewness value of the filtered surge component as defined in this manuscript (asymmetry of the shape of the surge curve) must not be confused with a ‘skew surge’ (the difference between the maximum observed water level and the maximum predicted tidal level, regardless of timing (de Vries et al., 1995)).

To investigate the effects of skewness of the surges on extreme water level, 4 historical events are presented based on the characteristics of the filtered residual surge component with time (Figure 2.4).

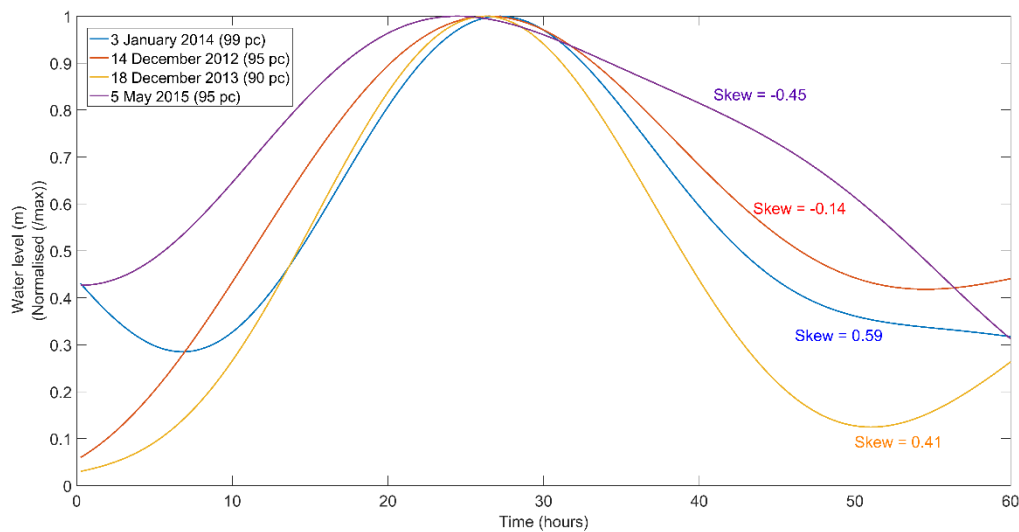


Figure 2.4: Normalised filtered surge shape component with time, characterised by historical event severity and skewness (measure of asymmetry).

Results from the 99th water level percentile event (3 January 2014), the most extreme event on record, shows a high, positive skewness value of 0.59 from the filtered surge data. This indicates the surge has a longer falling limb; the influence of the surge is extended over time after the peak of the surge. The filtered surge component for the 90th water level percentile event (18 December 2013) shows a lower, positive skewness value of 0.41. This is a lower skewness value than the 99th water level percentile event (3 January 2014), but still indicates a longer falling limb of the surge curve.

The filtered surge component for the 95th water level percentile event (5 May 2015) shows a negative skew value of -0.45. This indicates a long rising limb of the surge. The filtered surge component for the 95th water level percentile event (14 December 2012) shows a negative skewness value of -0.14. This value also still indicates the filtered surge component has a longer rising limb; the influence of the surge is extended over time before the peak of the surge.

2.3.4. Timing of surge occurrence

The filtered surge component is recombined with the predicted tide at the tide gauge locations in a range of different time-shifted configurations (McMillan et al., 2011). The peak of the surge changes in time relative to the peak of high water to investigate the influence of the timing of the surge on the total water level throughout the estuary.

The first time series represents the realistic timing of the peak of the surge relative to high water for each extreme water level. An additional 13 time series are created with the peak of the surge changing relative to the peak of high water. Starting from a configuration where the peak of the surge coincides with the peak of high water, the peak is then advanced incrementally to 6 hours before and delayed equally incrementally to 6 hours after high water to cover 1 full tidal cycle.

A total of 16 model runs are thus completed for each historical extreme water level event (Table 1). One validation run is completed for each historical event to ensure the model can reproduce the tide gauge data at stations up-estuary. For this validation model run, the boundary is forced by the total water level time series from Ilfracombe or The Mumbles tide gauge. A ‘tide only’ model run is simulated to provide a baseline, and a number of filtered surge plus tide model runs are simulated to represent the possible timings of the peak of the surge relative to predicted tidal high water.

Table 2.1: Scenarios modelled in Delft3D for each historical extreme water level event.

Model run scenario	Purpose
Total water level	Validation
‘Tide only’	Baseline
Tide + surge	Baseline
Tide + filtered surge at 0 mins	Sensitivity timing study
Tide + filtered surge at +/- 15 mins	
Tide + filtered surge at +/- 30 mins	
Tide + filtered surge at +/- 45 mins	
Tide + filtered surge at +/- 1 hour	
Tide + filtered surge at +/- 3 hours	
Tide + filtered surge at +/- 6 hours	

2.4. Model validation

Water level time series at tide gauge locations in the estuary are isolated from the model outputs. The model is initially validated using the most extreme event on record; with a storm tide peak which occurred at 07:15 on 3 January 2014. The model has been validated at the coast to observation data from tide gauges up-estuary, using data from the UK Tidal Network, Environment Agency and Magnox

at Oldbury. Error metrics (R^2 , RMSE, Willmott Index of Agreement (Wilmott, 1981; Wilmott et al., 2012), Bias of the maximum value)) are calculated at tide gauge locations up-estuary for model runs with realistic timings of the surge peak relative to tidal high water (total water level, filtered surge + tide) and the tide only simulation to provide a baseline. Error metrics confirm if the model can reproduce observational tide gauge data and assess the error introduced by this methodology.

Figure 2.5 illustrates validation runs and observational data for Hinkley Point; there is good graphical and statistical agreement between the model output (dashed lines) and observational data (solid line). The model is able to reproduce the tide gauge data at Hinkley Point well, with an R^2 value of 0.996 (Table 2.2). High water levels are over estimated, as confirmed with a bias value of 0.242, by 15-20 cm. However this represents just 1.5% of the overall tidal range (12.29 m at Hinkley Point).

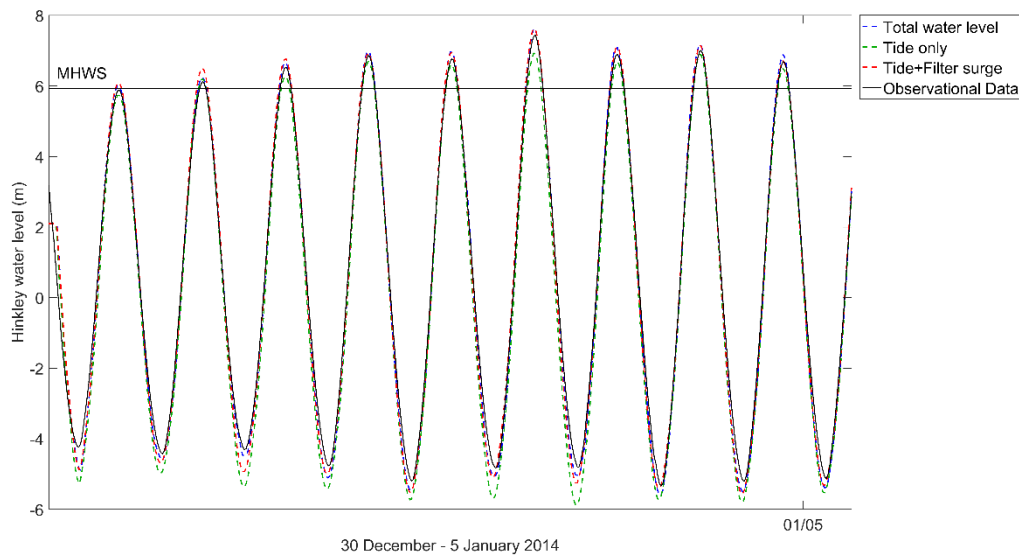


Figure 2.5: Validation down-estuary, Hinkley Point tide gauge.

Table 2.2: Statistical validation down-estuary, Hinkley tide gauge. The filtered surge is applied at a realistic time relative to tidal high water for validation purposes.

	Total water level	'Tide only'	Tide + Filter surge
R^2	0.996	0.909	0.955
RMS Error	0.172	0.255	0.212
Willmott Index of Agreement	0.969	0.913	0.946
Bias of maximum value	0.242	- 0.91	- 0.556

The 'tide only' model provides a baseline which subsequent model runs can be compared with, as there is no meteorological influence. It can be seen the 'tide only' model run is not resolving the high water peaks as there is no meteorological influence, and the low water is underestimated, as shown by the

negative bias value. There is a bias away from the tide gauge data in a negative direction – the values are all lower than the observation data. The tidal phase is successfully reproduced. The tide + filtered surge model run, where there is no change in timing of the surge from the real event, also overestimates low water. The tide + filtered surge model run is very similar to total water level simulation, suggesting that external tide-surge interaction, which has been filtered out of the boundary conditions, has a small contribution.

Figure 2.6 shows how the model has been tested further up-estuary, at Sharpness, using river gauge data from the Environment Agency. The quality of bathymetry and geometry of the long, shallow, narrow channel of the River Severn strongly influence the model results up-estuary. The lower Index of Agreement and R^2 value and higher RMSE and bias (Table 2.3) for the ‘tide only’ model run indicates that surge has a large contribution to total water level in this location up-estuary. There remains good graphical and statistical agreement between model runs (dashed line) and tide gauge data (solid line). Figure 2.6 shows that the model is able to capture tidal asymmetry, which refers to the interaction between tidal wave propagation and shallow water impacts due to changes in width and depth of the channel up-estuary (Uncles 1981; Pye and Blott, 2010).

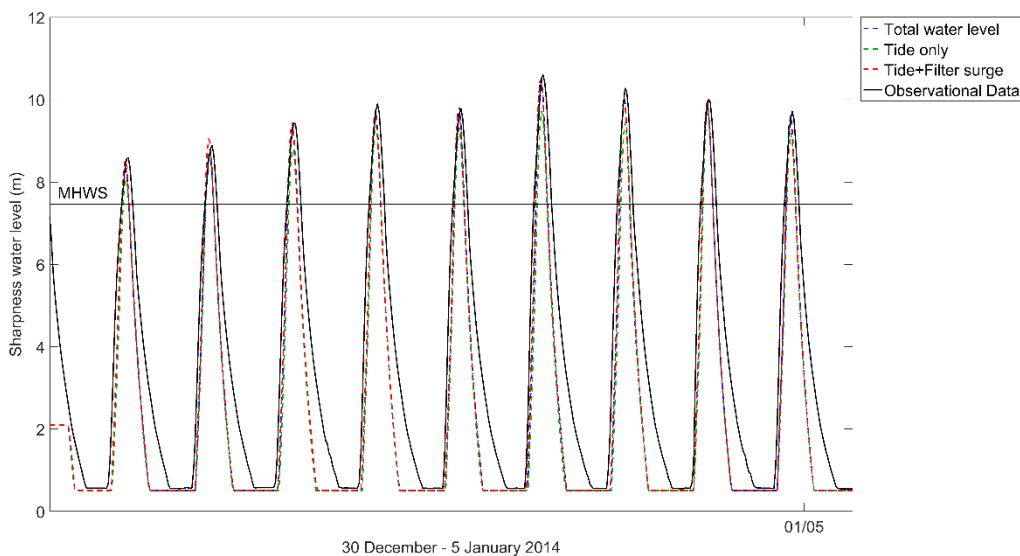


Figure 2.6: Validation up-estuary, Sharpness river gauge. As above.

Table 2.3: Statistical validation up-estuary, Sharpness river gauge

	Total water level	‘Tide only’	Tide + Filter surge
R^2	0.985	0.897	0.937
RMS Error	0.157	0.62	0.206
Wilmott Index of Agreement	0.9856	0.787	0.97
Bias of maximum value	0.634	-0.609	-0.746

The tidal phase is in good agreement however some of the high water points are not achieved, which is likely to be due to error in the low resolution bathymetry influencing the propagation of the tide in the upper estuary; the bathymetric survey will not match the bathymetry at the time of the event. Errors in bathymetry and flushing can explain the poorer simulation of low water than high water at both locations.

The model is in good agreement without the inclusion of meteorological forcing and waves, confirming the approach is adequate to capture spatial variations in extreme water levels.

2.4.1. Funnelling effect vs frictional effect

The greatest maximum water elevation along the thalweg of the estuary is 8.12 m at 108 km up-estuary, beyond Portbury, when the peak of the surge occurs 15 minutes before the peak of high water on 3 January 2014 (99th percentile). It can be seen in Figures 2.7 and Figure 2.8 that the maximum water elevation, along the thalweg of the estuary, during each of the 4 events consistently occurs close to Portbury. After this point, the maximum water elevation begins to fall again.

The tidal amplitude along estuary is determined by competing processes of tidal damping due to friction, and tidal amplification due to funnelling effect and reflection. From the mouth of the estuary up to Portbury, the funnelling effect dominates to amplify the tidal wave as it propagates up the estuary (Dyer 1995). Mean spring tidal range increases up-estuary towards Portbury due to the funnelling effect of coastal topography, the continuously upward slope of the basin and near-resonance of the estuary to the M2 tidal period (Liang et al., 2014; Uncles 1981). Portbury has the second largest mean spring tidal range in the world, approaching 12.2 m (Uncles 2010). Beyond Portbury, the funnelling effect is counteracted by friction. Friction acts to dampen the propagation of the tidal wave (Proudman 1955b). This balance between the funnelling effect and friction determines where overall maximum water level will occur in the estuary.

The sensitivity of the model domain to an applied friction value and the point where the friction and funnelling effect is balanced is investigated.

A higher friction value (Manning = 0.075) and lower friction value (Manning = 0.013) was applied to the model domain for the 99th water level percentile event (3 January 2014) model runs. The range in maximum water elevations along the deepest channel of the estuary for results of the altered friction values are compared to the original model run (Manning = 0.025).

Figure 2.7 shows that a higher friction value dampens the amplitude of the water elevation from the mouth up-estuary; the funnelling effect has little influence here and there is no obvious tipping point between funnelling and friction. A lower friction value means the funnelling effect significantly

amplifies the tidal wave up-estuary, producing water elevations beyond those that would realistically be seen in this estuary. The tipping point between funnelling and friction moves up beyond Oldbury.

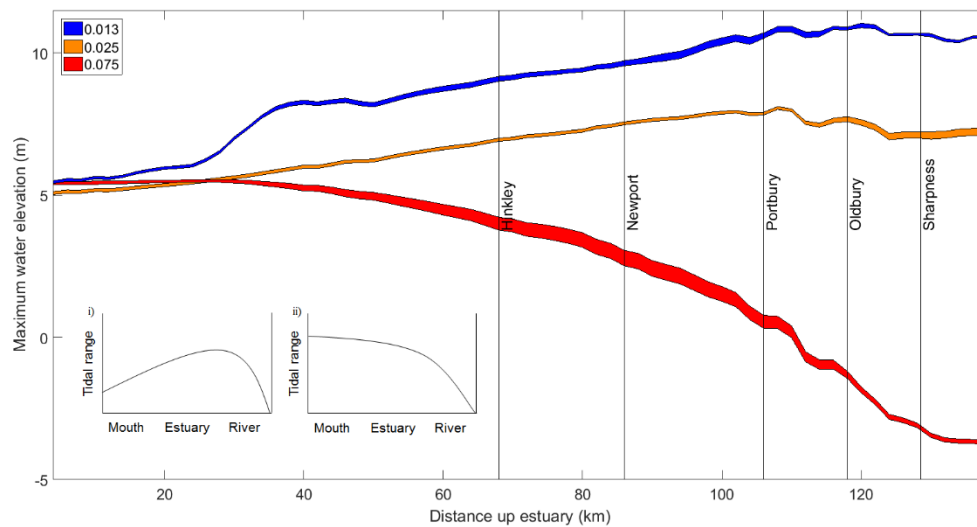


Figure 2.7: Water level along the deepest channel in the Severn Estuary, 3 January 2014, under varying Manning friction values (99th percentile); the shading represents the range in results for each filtered surge time shift scenario. Subpanels show the tidal response of i) hypersynchronous and ii) hyposynchronous estuary to changing frictional effects.

The response of the model to changing friction follows the characteristic of tidal response in estuaries (Dyer 1995). Under a friction value of 0.025, the estuary shows a hypersynchronous response (Figure 2.7i) where funnelling effect exceed frictional effects with increasing tidal range up to a point where friction then dominates, due to the shallow, narrow channel morphology. With a low friction value the estuary responds in a more extreme hypersynchronous manner. Funnelling effects exceed frictional effects throughout the estuary and tidal range continues to increase further up-estuary. Under a high friction value the model responds in a hyposynchronous manner (Figure 2.7ii). Friction dominates and tidal range diminishes through the estuary. The funnelling vs friction effect is likely to be a dominating factor in the hydrodynamics of the Severn Estuary, with a change in friction value in the model domain changing where maximum tidal range occurs. Under future sea levels and saltmarsh extents, the estuary dynamics under extreme could change the spatial variability in extreme water levels.

2.5. Results

Model outputs are analysed to identify how the total water level, and consequently flood hazard, and local interactions change up-estuary, for different timing of surge occurrence, and surge characteristics. Results are presented systematically for the four extreme events previously selected.

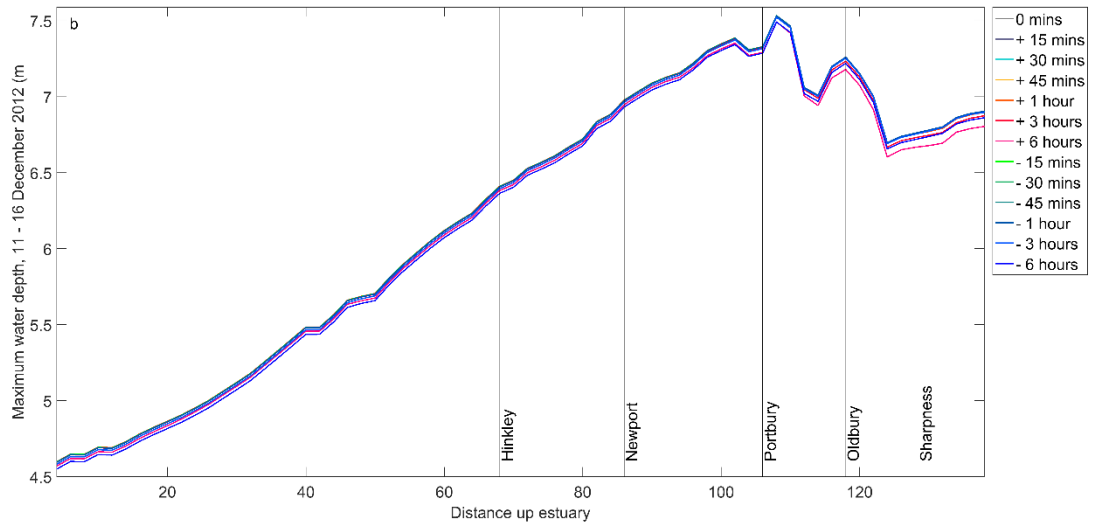
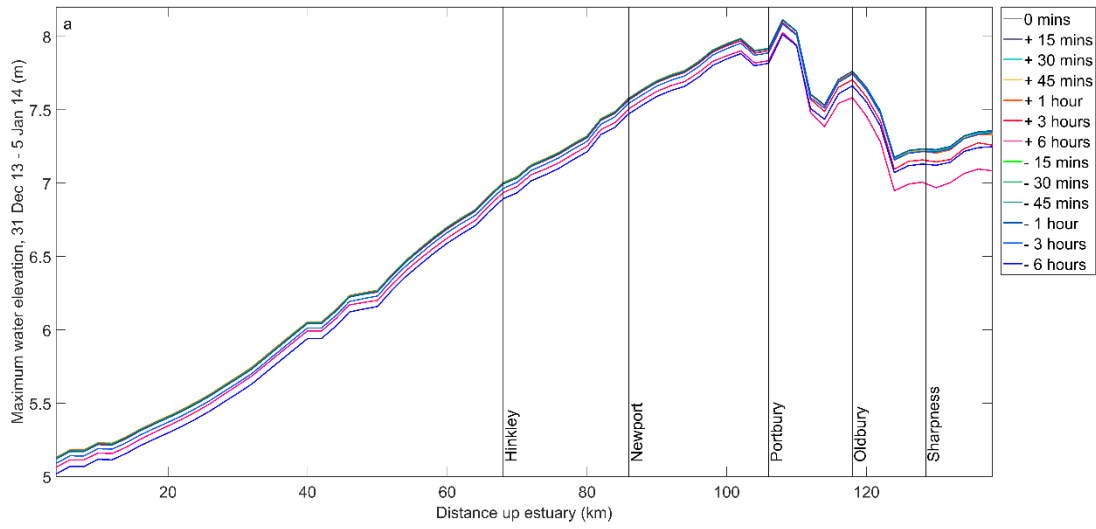
In the first part of the results, variations in maximum water level values along the estuary thalweg, and for different timing of surge occurrence are presented. Changes in water level as a function of surge skewness, and percentile are presented. After that, we will use the following plots as flood hazard proxies at each tide gauge location up-estuary:

- Percentage change in maximum total water level compared with the ‘tide only’ model run is plotted as a function of change in timing of surge at the model boundary;
- Percentage change in the time integrated elevation, i.e. the area (m^2/s) under the curve of the peak of the storm tide event, exceeding Mean High Water Spring (MHWS) compared with the model run when the peak of the surge and high water coincide (0 minutes);
- Percentage change in duration (minutes) of the peak of the storm tide event exceeding MHWS, calculated by interpolating between time steps exceeding the MHWS elevation, compared with the ‘tide only’ model run;
- Percentage change in maximum total surge elevation, compared with the 0 minute model run when the peak of the filtered surge and tide coincide; the total surge is calculated by removing the modelled tidal time series from all total water level model run scenarios, and includes a tide-surge interaction component and a meteorological component. The tide-surge interaction generates harmonics at tidal frequencies, which means that relative contributions cannot be separated.

MHWS is used as the baseline for proxy calculations as this is the reference level for all sea defence designs (McMillan et al., 2011). All calculated water levels, areas, and timings apply to the peak of the storm tide event within the 5 day simulation. The storm tide event is defined as 6 hours before and 6 hours after the maximum peak of high water in the time series peak. Correlation between each flood hazard proxy, skewness of the filtered surge component and severity of the event is analysed.

2.5.1. Water level variations along estuary

Figure 2.8 a-d shows maximum water elevation every 2 km along the thalweg of the main channel of the Severn Estuary (Figure 2.1) over the duration of the simulation, for each shift in the timing of the peak of the surge relative to tidal high water. The plots illustrate how maximum water elevation changes up-estuary.



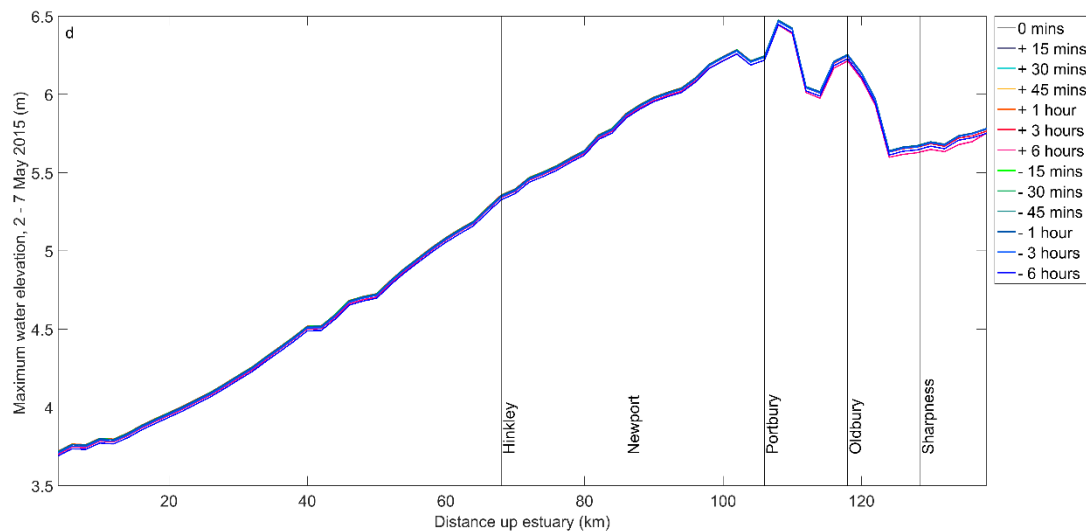
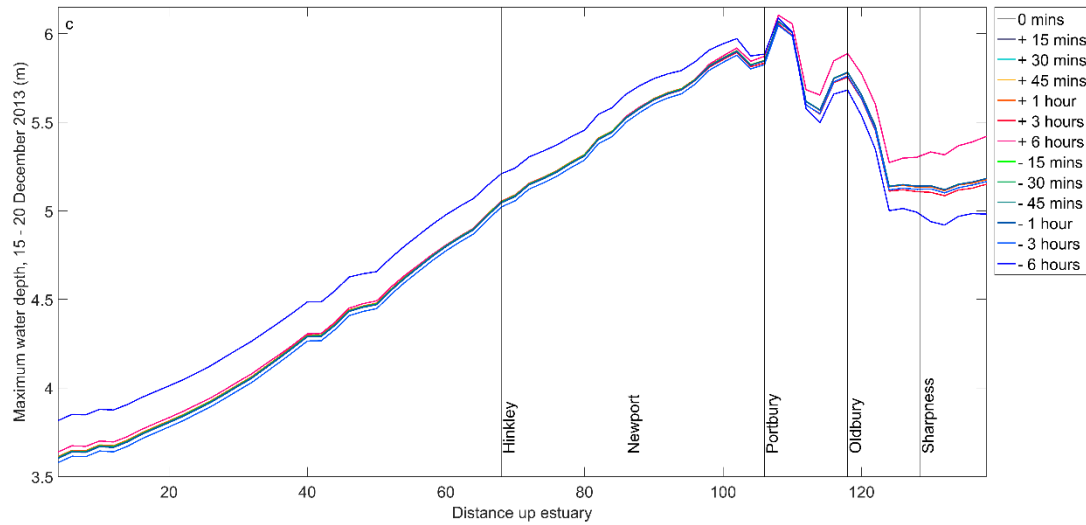


Figure 2.8: Maximum water level along the thalweg of the Severn Estuary; a) 99th water level percentile event (3 January 2014); b) 95th water level percentile event (14 December 2012); c) 90th water level percentile event (18 December 2013); d) 95th water level percentile event (5 May 2015).

It is noticeable from Figures 2.8 a-d that there is sensitivity to the timing of the peak of the surge relative to tidal high water and there are noticeable changes in maximum water elevations along the deepest channel of the estuary for each time shifted configuration. Maximum range in water elevations due to surge timing occurred for the 90th and 99th percentile events.

For the 90th water level percentile event (18 December 2013), the highest water elevation down estuary is seen when the peak of the surge occurs 6 hours before the peak of high water. The maximum water elevation down estuary is consistently 0.2 – 0.25 m higher than the 0 minute scenario when the peak of the surge occurs 6 hours before the tidal peak. There is a change in which scenario results in the highest

water elevation at 106.5 km up-estuary. In the upper estuary, the highest water elevation is seen when the peak of the surge occurs 6 hours after the peak of high water. The water elevation is consistently 0.1 – 0.35 m higher than the 0 minute scenario, when the peak of the surge occurs 6 hours after the tidal peak.

For the 99th water level percentile event (3 January 2014), the highest water elevation down estuary is seen when the peak of the surge occurs 1 hour after the peak of high water. The maximum water elevation down estuary is consistently 0.2 – 0.25 m higher than the 0 minute scenario when the peak of the surge occurs 1 hour after the tidal peak. The minimum water elevation down estuary is 0.1 – 0.15 m lower than the 0 minute scenario when the peak of the surge occurs 6 hours before high water. In the upper portion of the estuary, the highest water elevation consistently occurs 0.01 – 0.05 m higher than the 0 minute scenario when the peak of the surge is 30, 45 or 60 minutes after high water: there is no scenario which consistently results in the maximum water elevation. However the lowest water elevation in the upper portion of the estuary is consistently a result of when the surge peak is 6 hours before the tidal peak, and is up to 0.25 m lower than the 0 minute scenario.

It is noticeable in the Figures 2.8 a-d that change in time of the peak of the surge relative to high water causes little variability in the maximum water elevation in the lower estuary, and greatest variability in water elevation between time shift scenarios beyond Portbury, 106 km up-estuary.

Figure 2.9 shows the range of maximum water elevation every 2 km along the thalweg for all time shift configurations. The range of values are coloured according to the skewness of the surge component with time, and also classified based on the severity of the extreme event.

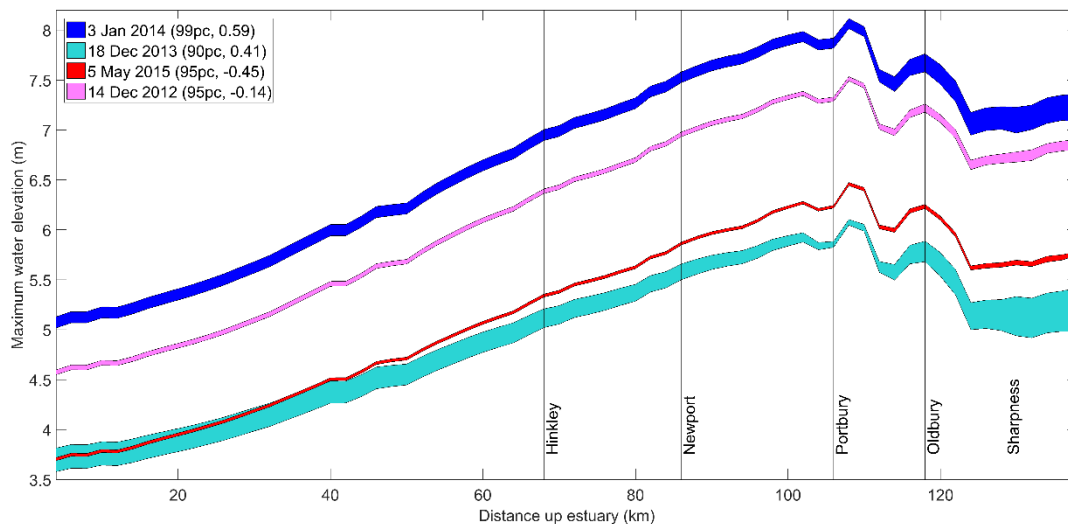


Figure 2.9: Range of water level values for time shift configurations along deepest channel of the Severn Estuary when overall maximum water level occurs. For each event, in the legend the first value represents the percentile of the event and the second value is the skewness.

The greatest range between maximum and minimum water elevation across the surge time shift scenarios is 0.44 m for the 90th water level percentile event (18 December 2013) and 0.27 m for the 99th water level percentile event (3 January 2014). Deviations in water level are not uniform along the estuary, and the 90th water level percentile event shows a positive shift in water level in the lower part, and negative shift in the upper part. The surge component of both of these events have a positive skewness value. The smallest range between maximum and minimum water elevation across the surge time shift scenarios is 0.03 m, for 95th water level percentile event (14 December 2012). This event has a surge component with a negative skewness value.

The surge components which have a positive skewness value, a steeper rising limb and a longer falling limb, show the greatest range of water elevation values along the deepest channel of the estuary. The range of values increases up-estuary, with the greatest range in water level values occurring beyond Portbury. This indicates that location in the upper estuary may be more sensitive to changes in the timing of the peak of a surge which displays a positive skewness. The surge components which have a negative skewness, a longer rising limb and steeper falling limb, show a more constrained range of maximum water elevations and there is less sensitivity throughout the estuary to the timing of the surge peak.

The maximum water elevations are stacked on top of each other according to severity of the event. It can be seen that the 99th water level percentile event (3 January 2014) consistently results in the greatest maximum water elevations along the thalweg of the estuary. The 95th percentile events show less extreme maximum water elevations in the estuary. There is approximately a 1 metre difference between the 95th water level percentile event (14 December 2012) and 95th water level percentile event (5 May 2015). The 95th water level percentile event (5 May 2015) initially shows similar water level values to the 90th water level percentile event (18 December 2013), before increasing beyond this 90th percentile event. As expected, the 90th water level percentile event (18 December 2013) shows the lowest maximum water elevations along the deepest channel of the estuary.

It is also evident in Figure 2.8 and Figure 2.9 that the maximum water elevation for all extreme water level events consistently occurs close to Portbury, the location for maximum observed tidal range in the estuary (Pye and Blott 2014).

2.5.2. Changes in flood hazard proxy with surge timing

Figure 2.10 – 2.13 show changes in flood hazard up-estuary in locations where nuclear assets and / or tide gauges are located, as a function of change in timing of the surge at the model boundary. Each flood hazard proxy (maximum total water level, maximum total surge, time integrated elevation and duration exceeding MHWS) is calculated from the storm tide peak: 6 hours before and 6 hours after high water. All data are displayed as percentage change, compared with the ‘tide only’ model scenario,

apart from maximum total surge which is compared with the model run when the peak of the surge and high tidal water coincide ('0 minutes').

Figure 2.10 shows flood hazard at each tide gauge location for a 99th water level percentile event (3 January 2014), the most extreme event on record.

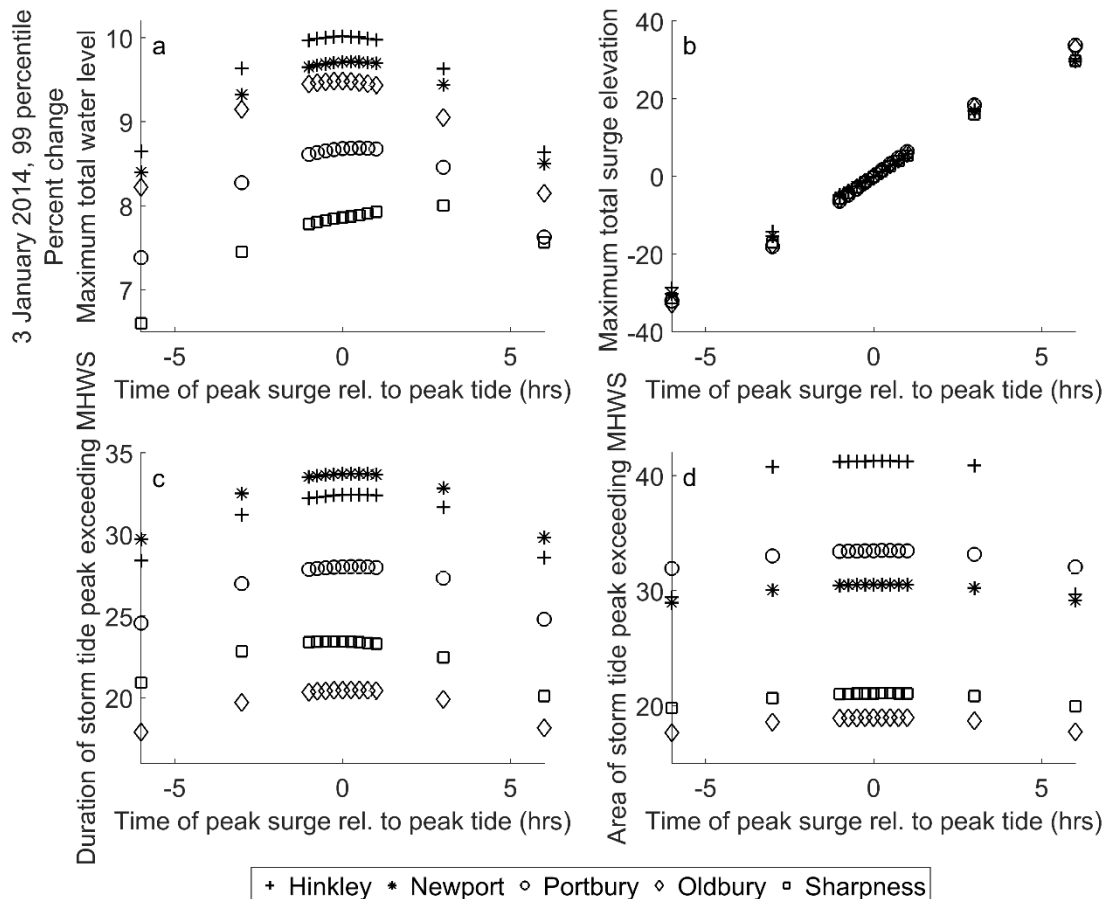


Figure 2.10: 3 January 2014. Flood hazard proxy calculated at each tide gauge location. a) percent change in maximum water level; b) percent change in maximum total surge elevation; c) percent change in duration exceeding MHWS; d) percent change in area exceeding MHWS. All data is displayed as percentage change, compared with the tide only model scenario, apart from total surge elevation which is compared with the model run when the peak of the surge and high water coincide.

The greatest percentage change in maximum total water level between each time shift scenario and the 'tide only' scenario is seen in tide gauge locations down-estuary, notably Hinkley Point and Newport (up to 10.02%). Tide gauge locations down-estuary, Hinkley Point, Portbury and Oldbury show symmetry in the results: the highest maximum water level happens when the surge occurs at the same time as high water. The magnitude of the maximum total water level then reduces when the peak of the surge occurs before or after the peak of high tide.

There is less percentage change in maximum total water level at tide gauge locations further up-estuary. The greatest percentage change in maximum total water level occurs when the peak of the surge happens 3 hours after the peak of high water. This is particularly clear at Sharpness, up to 8%.

There is a noticeable linear trend in the percentage change of maximum total surge value which occurs +/- 6 hours of the storm tide peak, compared with the 0 minute scenario. The greatest positive percentage change in maximum total surge elevation can be seen when peak of the surge occurs after 6 hours after the peak of tidal high water. A similar magnitude of negative percentage change in maximum total surge can be seen when the peak of the surge occurs 6 hours before the peak of tidal high water. There is little sensitivity of maximum total surge elevation to the timing of the surge when the peak occurs around the time of high water, and there is also little spatial variability between the locations. There is increased variability in maximum total surge elevation across the estuary with greater shift away tidal high water. The greatest variability can be seen when the peak of the surge occurs significantly after tidal high water. Portbury shows the greatest positive percentage change in maximum total surge elevation (32.5%) when the peak of the surge occurs 6 hours after tidal high water. This could be linked to the positive skewness of the surge with greater influence after the peak.

The maximum change in duration of peak of the storm tide exceeding MHWS is seen at locations down-estuary, Hinkley Point and Newport. Portbury and Oldbury show greatest change in duration when the peak of the surge occurs 1 – 3 hours after the peak of high water. There is a smaller percentage change in duration of the storm tide peak exceeding MHWS further up-estuary, at Sharpness. These tide gauge locations show asymmetrical results, with the greatest change in duration when the peak of the surge occurs 3 hours before the peak of high water.

The greatest change in time integrated elevation of the peak of the storm tide exceeding MHWS is seen at Hinkley Point, with the greatest area exceeding MHWS when the peak of the surge occurs at the same time relative to the peak of high water. Model results from Portbury and Newport also show over 28% change in time integrated elevation (m²) exceeding MHWS. Locations further up-estuary, Oldbury and Sharpness, consistently show lower percentage change within the range of 17 – 21 %. These results are also symmetrical, with the greatest % change in area when the peak of the surge occurs at the same time as the peak of high water.

Figure 2.11 shows flood hazard at each tide gauge location for a 95th water level percentile event (14 December 2012). The greatest percentage change in maximum total water level between each time shift scenario and the ‘tide only’ model run is seen in tide gauge locations down-estuary, at Hinkley Point and Newport, up to 5%. Oldbury is located further up-estuary, where the channel of the River Severn begins to narrow, but still shows a greater percentage change than Portbury. The change in maximum water level for this event is not to the same extent as the 99th water level percentile event (3 January 2014). Sharpness shows the smallest percentage change in maximum total water level,

compared with the ‘tide only’ model run. All results show a symmetrical shape, with the greatest change in total maximum water level when the peak of the surge coincides with the peak of high water. The smallest percentage change in maximum water level occurs at all locations up-estuary when the peak of the surge occurs 6 hours after the peak of high water.

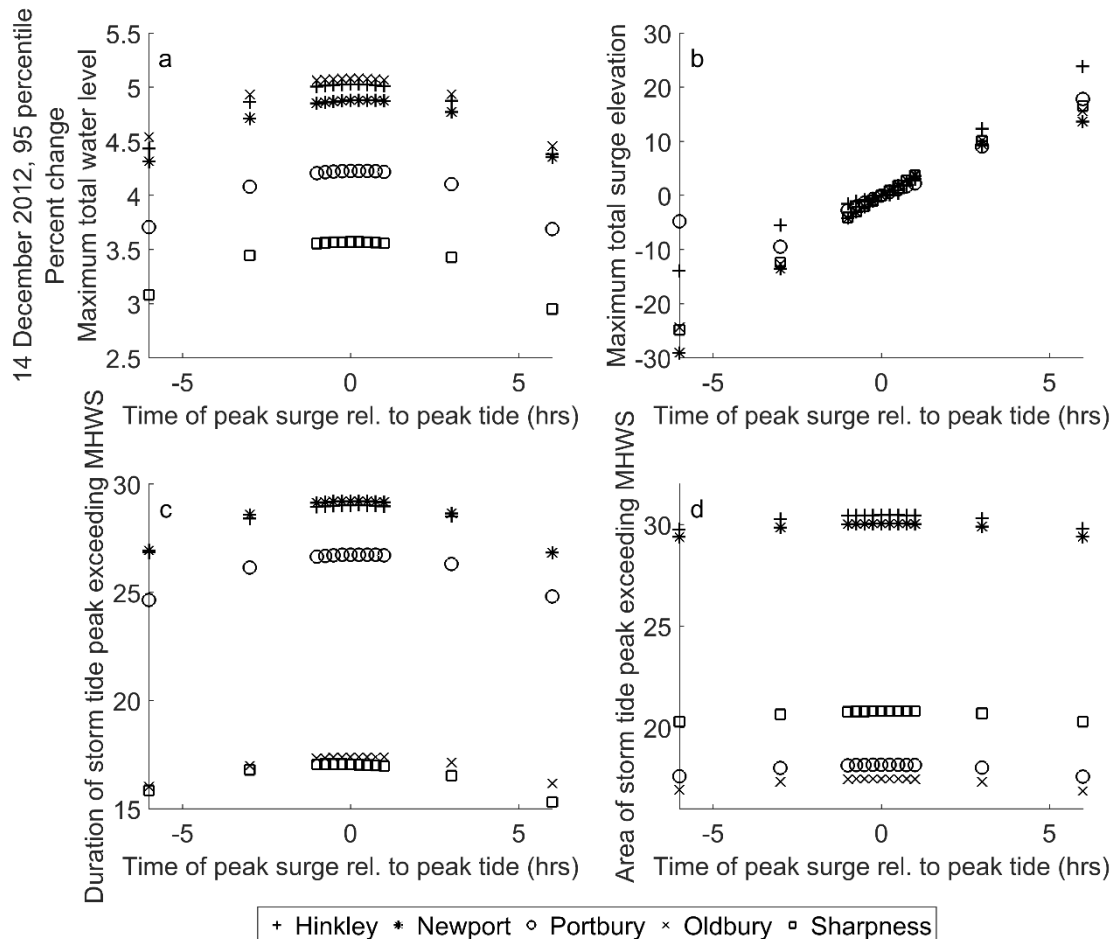


Figure 2.11: 14 December 2012. Flood hazard proxy, as in Figure 2.10.

The linear trend in percentage change of maximum total surge elevation for a 95th water level percentile event (14 December 2012) is similar to 99th water level percentile event (3 January 2014), with the changing time of the peak of the surge relative to tidal high water. The greatest positive percentage change occurs when the peak of the surge occurs significantly after tidal high water, at Hinkley Point (21.2%) and Portbury (17.8%). The greatest variability and magnitude in percentage change of maximum total surge elevation occurs when the surge occurs 6 hours before the peak of tidal high water. This could be linked to the negative surge skewness, with greater influence before the peak of the surge. There is less variability in maximum total surge elevation when the surge occurs 6 hours after tidal water.

The greatest percentage change in duration of the peak of high water exceeding MHWS is in locations down-estuary, notably Hinkley Point and Newport, up to 29.2%. These locations also show a symmetrical trend; the greatest percentage change is when the peak of the surge occurs at the same time as the peak of high water. The locations are stacked on top of each other, which is determined by the location up-estuary. There is a notable gap in percentage change in duration between locations in the lower estuary (Hinkley Point, Newport) and the upper estuary (Sharpness, Oldbury). Greatest duration at Oldbury and Sharpness is when surge occurs 1 hour before high water.

The greatest percentage change in area of the peak of high water exceeding MHWS is in locations down-estuary, notably Hinkley and Newport, up to 30.5%. Locations are stacked on top of each other, as a function of the distance up-estuary. All locations show symmetrical trends as the peak of the surge changes relative to high water; the greatest change in area is when the peak of the surge and tide coincide. In addition to this there is less variation between each time shift, and results at each location appear flatter than changes seen in maximum total water level and duration of peak exceeding MHWS.

Figure 2.12 shows flood hazard at each tide gauge location for a 95th water level percentile event (5 May 2015). The greatest percentage change in maximum total water level, compared with the 'tide only' model run, is seen at Hinkley Point, Newport and Portbury, up to 8.6%. As seen in other figures, the locations are stacked on top of each other based on their distance up-estuary. Epney, for example, shows smallest percentage change. All locations show least percentage change at -6 hours.

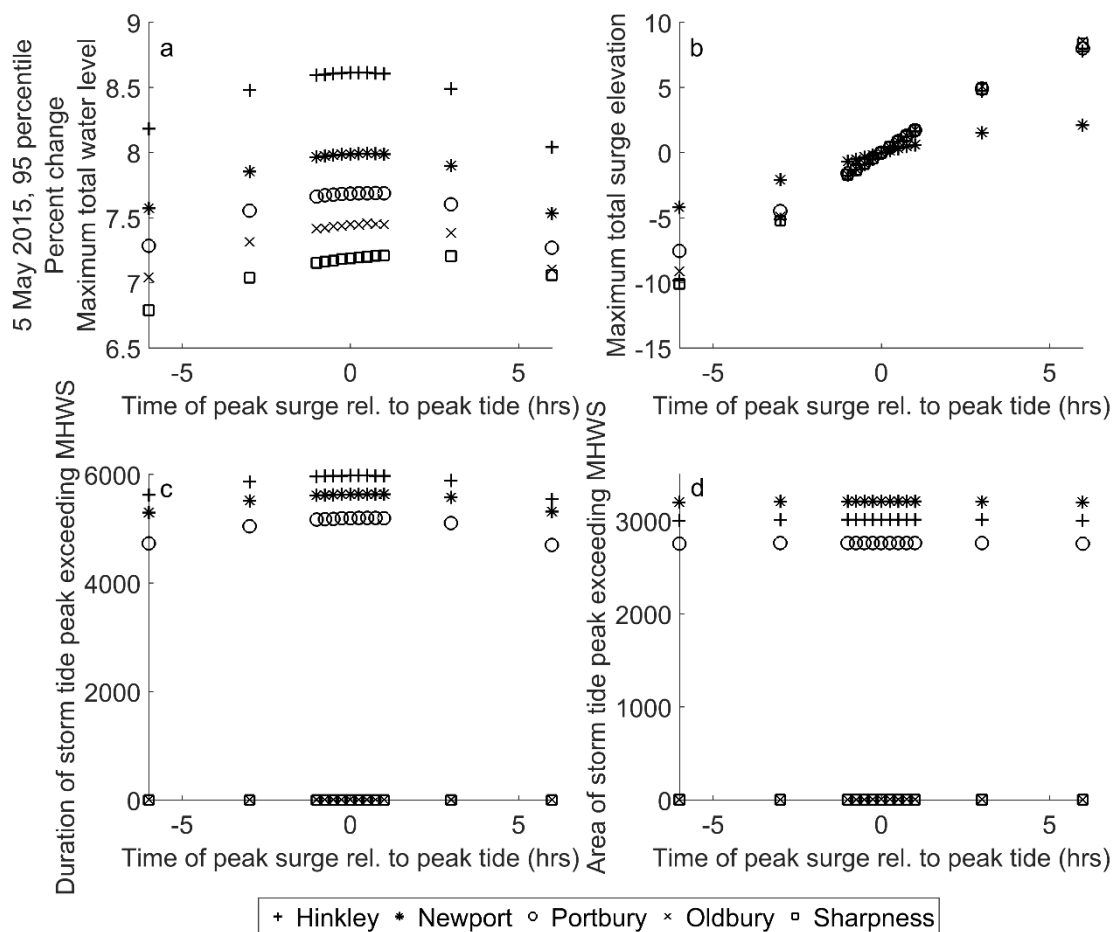


Figure 2.12: 5 May 2015. Flood hazard proxy, as in Figure 2.10.

The linear trend in percentage change of maximum total surge elevation is also noticeable for 5 May 2015. There is a smaller overall magnitude of positive and negative percentage change compared to the other events. Sharpness shows greatest negative percentage change (-10%) and Oldbury shows greatest positive percentage change in maximum total surge elevation (8.6%). Newport shows little sensitivity to the changing time of the peak of the surge relative to high water. There is less variability between locations, excluding Newport, when the peak of the surge occurs significantly before or after tidal high water.

The storm tide peak exceeds MHWS at all locations for a 95th water level percentile event (5 May 2015). Hinkley Point shows the greatest percentage change in duration of the storm tide peak exceeding MHWS, but there are small changes between each time shift scenario.

The greatest change in duration at Portbury occurs at -15 mins (11.725%), followed by 0 mins (11.72%) and -30 mins (11.71%). Small percentage changes occur across all locations (within 0.1% change in duration) when the surge occurs within 1 hour of high water. The lowest percentage change at all locations occurs when the peak of the surge occurs 6 hours after the peak of high water. This could be

due to the influence of the characteristics of the filtered surge that has been modelled for this historical event.

Figure 2.13a shows flood hazard at each tide gauge location for 90th water level percentile event (18 December 2013). Down-estuary locations, at Hinkley Point, Newport, Portbury and Oldbury show a similar percentage change in maximum total water level, up to 7%, compared with the ‘tide only’ model run. The smallest percentage change is seen at Sharpness. All locations show a jump in maximum water level at + 6 and – 6 hours, which could be due to the influence of the shape of the surge, as the other time shifts show a flatter trend.

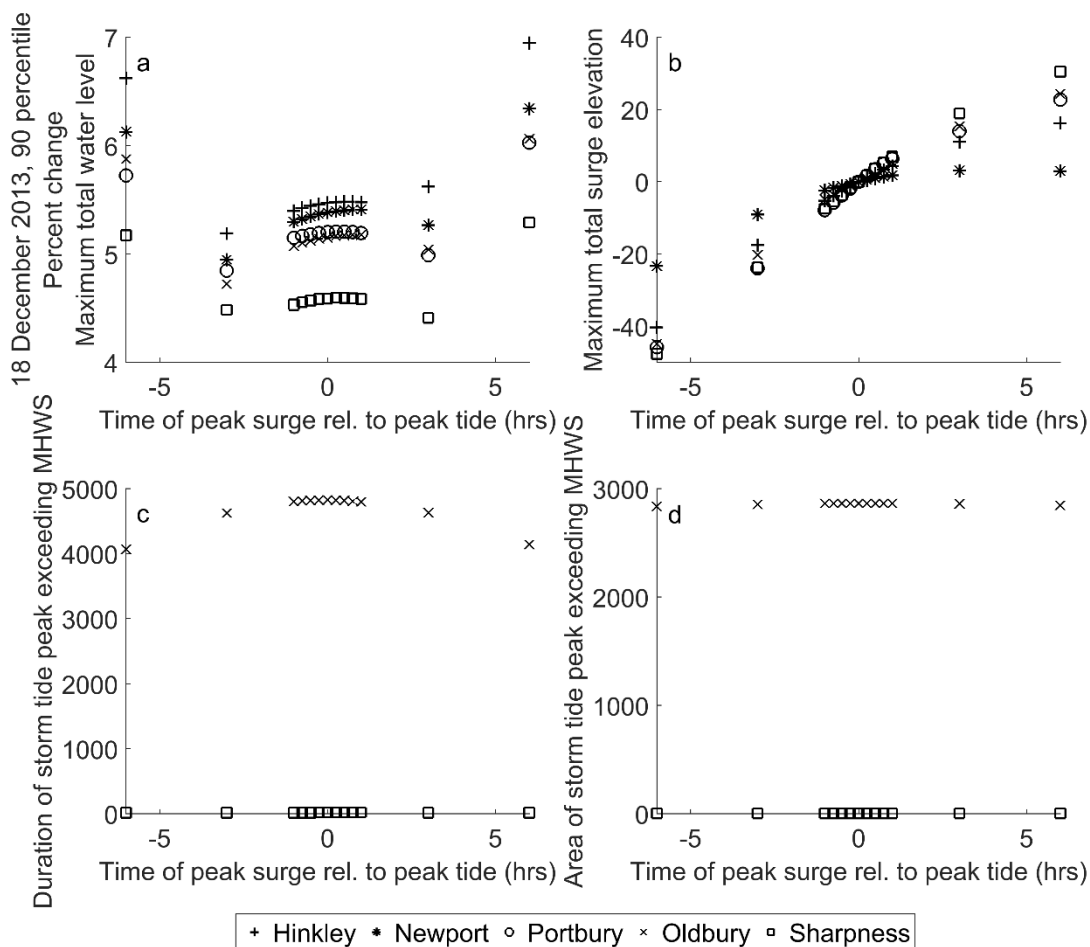


Figure 2.13: 18 December 2013. Flood hazard proxy as in Figure 2.10.

The linear trend in percentage change of maximum total surge elevation in Figure 2.13a is similar to other events. There is greater variability between locations when the peak of the surge occurs 3 or 6 hours before and after tidal high water like the 99th water level percentile event (3 January 2014). This could be linked to surge skewness like the 3 January 2014. The greatest magnitude of percentage change can be seen when the peak of the surge occurs significantly before tidal high water. The greatest positive (29.08%) and negative (-47.57%) percentage change in maximum total surge elevation occurs at

Sharpness. Newport shows less sensitivity to the timing of the peak of the surge relative to high water, with a range of 20.1% and a more symmetrical trend.

The peak of the storm tide only exceeds MHWS at Sharpness and Oldbury when the 18 December 2013 event is simulated, likely to be because it is a 90th percentile event. Oldbury shows a clear percentage change because the ‘tide only’ scenario (6.821 m), which all time shift scenarios are compared with, does not exceed MHWS (7.02 m). The surge is having a noticeable influence on the time the peak of the storm tide exceeds MHWS at these locations. Figure 2.14 shows Sharpness has an asymmetrical trend with the greatest percentage change in duration (19.9%) when the surge occurs 45 minutes after high tide.

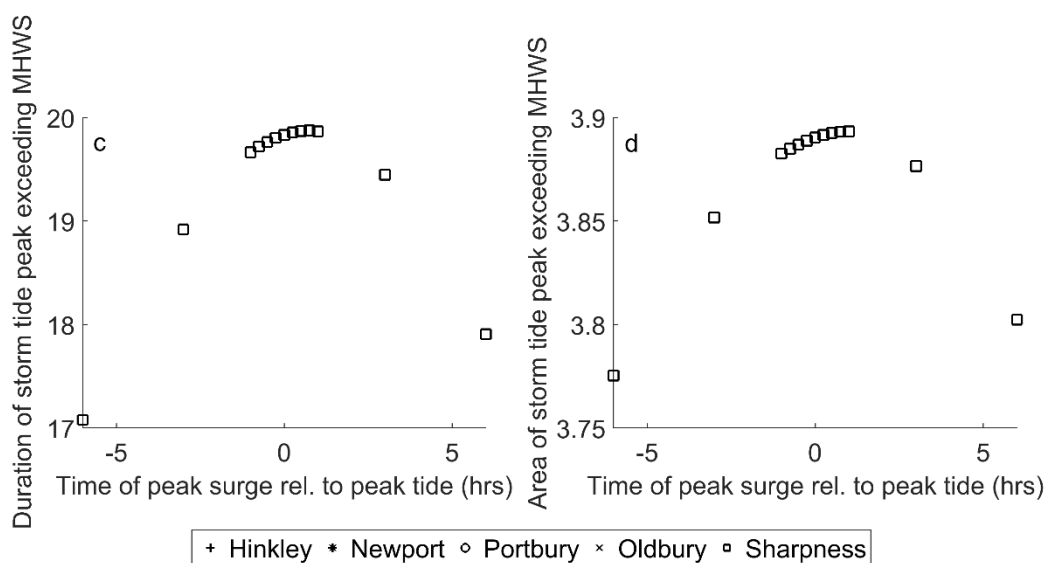


Figure 2.14: Duration and area of storm tide peak exceeding MHWS at Sharpness.

Oldbury also shows a noticeable percentage change for area exceeding MHWS compared with the ‘tide only’ model run, and a very small value for Sharpness (Figure 2.14). Sharpness shows a small range of 0.1% between time-shift scenarios. The greatest change in area (3.9%) when the surge occurs 1 hour after high tide.

2.6. Discussion

2.6.1. Physical drivers and sources of flood hazard in the Severn Estuary model domain

Delft3D-FLOW is used to simulate barotropic tide-surge propagation, river flow and interaction in the Severn Estuary across a 2DH grid. Results from 4 historical events are presented which show the influence of the severity of the storm surge, the influence of the timing of the surge on the total water level, and characteristics of the filtered surge component on the total water level throughout the Severn

estuary. The results presented here can help to identify variability in the sources of an extreme water level event in a hyper-tidal estuary, which can contribute towards flood hazard. These results can help to inform local management needs in a hyper-tidal estuary when viewed in the context of the source – pathway – receptor – consequence (SPRC) conceptual model (Narayan et al., 2012).

2.6.1.1. Influence of storm severity on extreme water levels

The results suggest that severity of the event is an important control on the magnitude of extreme water levels throughout the Severn Estuary. The 99th water level percentile event (3 January 2014) consistently produced greatest water elevations along the deepest channel of the estuary and greatest percentage change in maximum water levels at all sites. A more severe storm surge event, driven by low atmospheric pressure, wind speed, wind direction and storm duration (Woth et al., 2006), increases extreme water levels throughout in the Severn Estuary and is an important driver of flood hazard. Extreme tidal levels are known to be the predominant driver of flooding events in the Severn Estuary, particularly in locations close to the maximum MHWS at Avonmouth (Capita Symonds 2011). A 3.54 m (11.6 ft) surge was recorded at Avonmouth in March 1947 (Heaps 1983), attributed to very low pressure (974 mb, which is 38 mb below normal regional level) and predominantly easterly track of the depression (Lennon et al., 1963), indicating the severity of a storm surge event is a combination of meteorological factors.

99th percentile water level events may be a rare occurrence, and equal consideration should be given to the effect of more frequent, less severe events in the estuary. However much of the UK is defended against high frequency, low magnitude events up to a 1:200 year event, therefore reducing flood hazard. An understanding that a more severe, extreme water level event can increase flood hazard can be used by local coastal planners to manage flood risk and can aid operational flood management (Menéndez and Woodworth 2010). If the severity of an event can be forecast then warnings can be issued to appropriate authorities and the public. Event severity is an important control when modelling to extreme water levels on a local scale.

2.6.1.2. Influence of the timing of the peak of the surge

The timing of the peak of the storm surge relative to tidal high water is another important contribution to the physical drivers of flood hazard at the coast. There is sensitivity to the timing of the peak of the surge throughout the Severn Estuary model domain. This is particularly evident in the upper estuary; when the peak of the surge occurs 2 – 6 hours after high water there is a greater percentage change in maximum water level. Increased water depth at the time of tidal high water could induce surge propagation through the estuary to increase extreme water levels up-estuary. Increased water depths would limit shallow water and quadratic friction effects on the tidal amplitude. However, at these shifts the flood hazard (area and duration of the storm tide peak exceeding MHWS) is lower.

There is less sensitivity to changes in the timing of the surge in the lower estuary, notably Hinkley Point. The greatest percentage change in maximum water level occurs when the peak of the storm surge and tide coincide. The concurrence of high tide and storm surge peak in the Severn Estuary has resulted in extreme water levels in the past (Lennon et al., 1963). The highest recorded water level in the Severn Estuary in a century occurred during the storm 13 December 1981 (Proctor and Flather 1989). A fast moving secondary depression, tracking further south than usual for the time of year, produced strong west to northwesterly gales over the Bristol Channel (Williams et al., 2012). This depression generated a surge peak of 1.5 – 2 m, which occurred close to the time of high water of a large spring tide (Heaps, 1983; Smith et al, 2012). Little warning was given, and the event resulted in severe flooding and damage to property and agricultural land from east of Bideford to Gloucester (Uncles 2010). The timing of the passage of the depression, which was coincident with tidal high water in the Bristol Channel, was a vital contributor to the water levels produced (Proctor and Flather 1989). This event was significant as it highlighted the importance of high-resolution temporal monitoring data during fast moving depressions, and reanalysis atmospheric data for the event has been used to test the accuracy of operational forecasting systems (Williams et al., 2012). A larger storm surge (2.4 m) in the Severn Estuary on 24 December 1977 occurred 3 hours before high water, giving no cause for concern (Proctor and Flather 1989). Surges larger than 2 m rarely occur within 1 hour of tidal high water in the Severn Estuary due to locally generated tide-surge interaction (Horsburgh and Horritt 2006). However there is no mechanism to stop the peak of a spring tide and storm surge coinciding in the Severn Estuary (Pye and Blott 2010).

Flood hazard is also increased in the Bay of Fundy when adverse weather conditions, e.g. a drop in pressure greater than 5 kPa, coincides within one to two hours of high water of large spring tides (Greenberg et al., 2012). Significant low pressure systems have coincided with a very high spring tide on only a few occasions; November 1759, October 1869, during the Saxby Gale, and the 1976 Groundhog Day storm (Desplanque and Mossman 2004). During all events seawalls and wharfs were breached, leading to severe flooding, damage to boats and infrastructure, and lives lost (Desplanque and Mossman 1999). Storms not occurring near high water or on average tides will produce water levels within the ‘normal’ range that are often reached by astronomical tides alone (Desplanque and Mossman 1999). The concurrence of the peak of a storm surge with the peak of spring tidal high water could be rare occurrence, but would cause the greatest impacts on maximum extreme water levels. The timing of surge events is crucial in predicting extreme water levels and assessing flood hazard in estuaries with a large tidal range (Batstone et al., 2013).

2.6.1.3. Influence of the storm surge shape

The shape of the storm surge component with time (surge skewness) influences variability in extreme water levels and total surge in the Severn Estuary model domain. As seen in Figure 2.8, a storm surge

with a positive skewness appears to create a greater range in maximum water elevation at every point along the deepest channel of the estuary. Positive skewness can act to extend the duration of high water, and there increase water volume and surge inflow in the estuary. This could help to amplify the tide further up the estuary (as shallow water effects are reduced) (Proudman 1955b). With distance up-estuary, the surge skewness may become more negative or more positive consistent with the magnitude of the local interaction growing with tide-surge propagation up-estuary. The shape and time profile of each storm surge generated on the continental shelf varies between historical extreme water level events, and skewness of the storm surge component could be just one of many characteristics controlling this driver of flood hazard. If shape of a storm surge can be forecast or detected early then locations in the upper estuary can be warned of consequential amplification of the flood hazard.

Previous studies have highlighted the influence surge shape may have on water levels in the coastal zone (McMillan et al., 2011; Proudman 1955b). The Environment Agency has provided time-integrated duration design surge shapes at tide gauge locations around the UK coastline, from the 15 largest ‘skew surge’ events on record (McMillan et al., 2011). The skewness, i.e. the measure of asymmetry, of the design surge shapes for tide gauge locations in the Severn Estuary were calculated and shown to have a negative skewness over a 60-hour window (Ilfracombe -0.46, The Mumbles, -0.26). These results indicate that storm surges with a negative skewness create a constrained range of extreme water elevations in the Severn Estuary model domain. Therefore it would be diligent to undertake sensitivity testing of surge skewness derived from historic events to understand variability in extreme water levels.

2.6.1.4. Estuarine form as a pathway to increase flood hazard

The severity of the extreme water level event, timing and surge skewness each contribute to the source of a potential flood event. Pathways are the mechanisms that convey floodwaters from physical drivers, to impact receptors (people, businesses and the built environment). These are often considered to be overland flows, flows in river channels and sea defence overtopping (Le Cozannet et al., 2015; Idier et al., 2013). However it is known that estuaries and coastal inlets can affect surge and wave propagation in the coastal zone (Sayers et al., 2003). Therefore the geometry, bathymetry and form of the estuary should be considered a pathway or source in itself, and influence on flood hazard acknowledge.

The geometry of the Severn Estuary has a strong control on tide-surge propagation and total surge contribution to water levels. The greatest percentage change in maximum total surge elevation in the model domain occurs when the peak of the surge occurs significantly before or after tidal high water, in locations further up-estuary e.g. Portbury and Sharpness. As the peak of the surge occurs closer to low water there may be greater effect bottom friction and shallow water effects on tidal dynamics (Proudman 1955a). Flood hazard is reduced when changes in maximum total surge elevation increase. Total surge, including a meteorological component and tide-surge interaction component, does not

appear to contribute to extreme water levels, but appears to create variability in extreme water levels in the upper estuary.

The smallest change in maximum total surge elevation in the model domain can be seen when the peak of the surge occurs within 1 hour of tidal high water. This is a phenomenon often observed along the west coast of Britain: if the peak of a storm surge occurs close to the time of tidal high water then there is very little time for interactions to develop and little effect of bottom friction due to the greater volumetric contribution of the tide and surge (Jones and Davies 2007). Tide-surge interaction may not contribute to extreme water levels in the estuary but the shallow, narrow estuary creates variability which should be considered to potentially increase exposure and consequences of coastal towns in the upper estuary.

The geometry of the estuary has a particularly strong control over the location of maximum tidal range in the estuary, close to Portbury (Figures 2.8 and Figure 2.9). Maximum overall water elevation in the Severn Estuary model domain consistently occurs close to Portbury. This is known to be as a result of the funnelling and friction effect in the estuary (Dyer 1995). Tides and surges are amplified from the deeper part of the estuary, through the increasingly narrow, shallow channel towards Portbury (Pye and Blott 2010). This funnelling effect, due to channel convergence, increases tidal range to a maximum within the estuary at Portbury (Lennon 1963). The cyclic semi-diurnal tide is analogous to the incoming resonance from the west side of the Atlantic Ocean to the east (Gao and Adcock 2016), which further amplifies storm surges up estuary (Liang et al., 2014). Beyond Portbury, frictional effects control the dampening of the tide as energy is lost and the tidal range decreases.

Further to this, human intervention in the estuary itself could influence how the physical drivers of flood hazard ('sources') move through the estuary. The location and design of sea defences, harbours and interventions (e.g. managed realignment schemes at Steart Marshes (Wright et al., 2011)) would also act to influence the magnitude and variability of extreme water levels (Sayers et al., 2003). These interventions would in turn also influence the damage caused and extent of coastal flooding that may be experienced as a result of the event. River discharge is another pathway to consider, and can induce interactions that lead to increases in the non-tidal residual elevation up to 0.35 m in the Severn Estuary (Maskell et al., 2014).

Flood hazard assessment, and application of the SPRC model at a local and regional scale, should consider that the form of a hyper-tidal estuary is a 'source' or 'pathway' in itself, influencing how floodwaters are conveyed through the system.

2.6.2. Implications for local management needs in the Severn Estuary and worldwide

When viewed in an operational context, these results help to identify contributions to the sources of flood hazard and identify the estuarine form as a source and pathway in itself which can act to exacerbate flood hazard. As seen in Figure 2.9, the severity of an event appears to be the most important control on flood hazard in a hyper-tidal estuary. The events are stacked as a function of severity, and the 99th percentile event, 3rd January 2014, consistently produces the maximum water level through the thalweg. The ‘worst case’ combination of variables to result in greatest flood hazard would be a 99th percentile event and concurrence of a storm surge peak with positive skewness and tidal high water. However it should be considered that accurate bathymetry and boundary forcing data is important when testing hypotheses in estuaries. The accuracy of models which aim to link estuarine hydrodynamic processes and form e.g., extreme water levels is dependent on accurate bathymetry. The Severn Estuary model is forced at the tidal boundary with data from one tide gauge, which could act limit how accurately water levels and interactions within the estuary are reproduced. There is a need for clear, accurate information to inform operational flood management, with the aim of reducing the hazard from flood events to the people who are located in flood prone areas which should utilise the best available data.

Freshwater flow can be an important control on tide-surge propagation in some hyper-tidal estuaries (Hoitink and Jay 2016). River discharge and its associated water levels can combine with storm surges driven by the same weather system (Svensson and Jones 2002), to alter the timing and magnitude of water levels within the estuary. Nonlinear interactions between extreme river discharge and storm surges can elevate residual water levels up to 0.35 m in idealised estuaries (Maskell et al., 2014), and have been shown to influence subtidal friction and the timing of high and low water in the River Mahakam, Indonesia (Sassi and Hoitink 2013). Heavy rainfall and spring meltwater, which result in high discharges have been shown to inhibit tide-surge propagation up-estuary in the LaHave Estuary, Nova Scotia (Webster et al., 2014), however dredging activities in the Modaomen Estuary, China, facilitates inland propagation of surges and can alter salinization within an estuary (Cai et al., 2012). Flood hazard and inundation extents are largely controlled by surge elevation, except in the most extreme river discharge events (Maskell et al., 2014). Freshwater flow and tide-surge propagation are not statistically independent (Svensson and Jones 2002), and their combined impact is controlled by the timing of peak river discharge, geometry of the estuary and floodplains and human intervention within the estuary.

Under changing climate and sea-level rise, the methods and results presented here could change due to changes in tidal range, which would alter tide-surge interaction (Robins et al., 2016). Deeper water will change frictional influence, and the tipping point between the effect of funnelling and friction effect is likely to change, which impact the location of maximum tidal range within the estuary and tidal

asymmetry. In addition to this, rising sea level may alter channel depths or alter tidal prism (Leuven et al., 2019; Marcos et al., 2019), therefore fundamentally altering the feedback between estuarine form and water level. In some coastal regions, sea-level rise will increase the magnitude and frequency of extreme storm events, leading to increased flood hazard (Menéndez and Woodworth 2010; Nicholls et al., 2014). Therefore, the need for accurate operational forecasting of extreme storm events will increase under changing climates.

Analysis of barotropic tide-surge propagation in a hyper-tidal estuary has shown sensitivity of coastal flood hazard, generated from the water level boundary conditions, to storm timing, storm surge shape and event severity. This knowledge is of significance to operational modelling for local predictions and flood hazard assessments. However sources of coastal flood hazard are not just limited to the contributions of astronomical tide and storm surges to water level, but also wave run-up and overwashing or overtopping, driven by coincidental sea state (Prime et al., 2016). Locally-generated wind waves and propagating swell waves, generated by an offshore storm, which coincide with an extreme water level can increase flood hazard at the coast (Wolf 2008). Maximum wave height at time of tidal high water can be significant for coastal flooding (Fairley et al., 2014), and runup associated with direct wind setup or breaking offshore waves can influence defence overtopping and breaching (Wadey et al., 2012). Future work to consider the influence of swell and wind waves on water levels and uncertainty in wave forcing has the potential to provide improved understanding of the combined effect of tide-surge-river-waves on water levels in a hyper-tidal estuary. Model outputs from a study into the combined effect of tide-surge-river-waves on water levels can be used to force an inundation model (e.g. Bates and De Roo, 2000), to simulate the area of maximum inundation from extreme water level events. Modelling studies that combine tide-surge-river-wave propagation with depth and extent of inundation can be effective for floodplain development, flood defences and protection for critical infrastructure in the estuary.

2.7. Conclusion

There is a need to understand the combination and variability of physical drivers contributing to flood hazard in hyper-tidal estuaries, due to their dynamic nature and increasing development pressures. Delft3D-FLOW is used to simulate tide-surge propagation in a hyper-tidal estuary to understand the mechanisms controlling extreme water levels, which contribute to flood hazard. Long-term tide gauge records are used to consider the influence of event severity, the timing of the peak of the surge relative to tidal high water and storm surge skewness on spatial variability of historic extreme water level events in the Severn Estuary example. Event severity is the most important control on extreme water levels when modelling tide-surge propagation on a local scale. The shape of the storm surge component with time, classified using surge skewness as a measure of asymmetry, and timing of the storm surge peak relative to tidal high water influence spatial variability of water levels throughout the estuary.

Demonstration of the shallow water effect shows the effect estuarine form can have on the variability of extreme water levels, therefore it is crucial to have accurate bathymetry and boundary conditions to capture these changes throughout the estuary. However maximum total surge elevation does not appear to significantly contribute to flood hazard as the maximum contribution occurs during the rise of an adjacent tide to that of the storm tide. The results can be interpreted in the context of the SPRC model, to identify the combined effect of factors which contribute to extreme water levels for local scale, flood hazard management. The methodology can be applied to understand past extreme water level events, and in turn help to identify future flood hazard in hyper-tidal estuaries worldwide.

2.8. Acknowledgements and Data

The authors thank colleagues at the British Oceanographic Data Centre (BODC) for providing tidal data; Magnox for providing tidal data; Environment Agency for providing tidal data and river gauge data; Gloucester Harbour Trustees for providing tidal data; and EDINA for bathymetric data.

This work was supported by the Engineering and Physical Sciences Research Council as part of the Adaptation and Resilience of Coastal Energy Supply (ARCoES) project, grant number EP/I035390/1.

3. Uncertainty in estuarine extreme water level predictions due to surge-tide interaction

Chapter 3 continues to use the statistically validated and calibrated Delft3D-FLOW modelling system to consider the variability in residual sea level up-estuary due to three key sources of uncertainty identified in chapter 2. Changes in the surge residual, defined as observed sea level minus predicted tide, are quantified at five tide gauge location and through the thalweg of the estuary to show the spatial variability of tide-surge propagation, and the influence on subsequent maximum surge residual. The variability in the surge residual needs to be captured accurately to reduce uncertainty in site specific flood hazard assessment.

3.1. Abstract

Storm surge is often the greatest threat to life and critical infrastructures during hurricanes and violent storms. Millions of people living in low-lying coastal zones and critical infrastructure within this zone rely on accurate storm surge forecast for disaster prevention and flood hazard mitigation. However, variability in residual sea level up-estuary, defined here as observed sea level minus predicted tide, can enhance total water levels; variability in the surge thus needs to be captured accurately to reduce uncertainty in site specific hazard assessment. Delft3D-FLOW is used to investigate surge variability, and the influence of storm surge timing on barotropic tide-surge propagation in a tide-dominant estuary using the Severn Estuary, south-west England, as an example. Model results show maximum surge elevation increases exponentially up-estuary and, for a range of surge timings consistently occurs on the flood tide. In the Severn Estuary, over a distance of 40 km from the most upstream tide gauge at Oldbury, the maximum surge elevation increases by 255 %. Up-estuary locations experience short duration, high magnitude surge elevations and greater variability due to shallow-water effects and channel convergence. The results show that surge predictions from forecasting systems at tide gauge locations could under-predict the magnitude and duration of surge contribution to up-estuary water levels. Due to the large tidal range and dynamic nature of hyper-tidal estuaries, local forecasting systems should consider changes in surge elevation and shape with distance up-estuary from nearby tide gauge sites to minimize uncertainties in flood hazard assessment.

3.2. Introduction

Storm surges occur in coastal zones worldwide and correspond to short-term variations in sea-level driven by winds and atmospheric pressure changes associated with storms, tropical hurricanes and typhoons (Lewis et al., 2011). The concurrence of storm surges and astronomical tides presents a combined flood hazard, elevating observed water levels above the predicted tide, to create an extreme water level at observed high water (Lewis et al., 2013; Prime et al., 2015). It is also documented that interaction between tide and surge can alleviate flood hazard, as storm surge peak does not coincide with tidal high water in some coastal and estuarine areas (Horsburgh and Wilson 2007). Evidence of the damage caused by this combined flood hazard to coastal communities and critical infrastructure is well documented for the UK (Wolf and Flather, 2005; Sibley et al., 2015; Spencer et al., 2015) and worldwide (Kates et al., 2006). Severe storm surge events, such as the 1953 North Sea storm surge (Wolf and Flather 2005) and the 28 foot surge generated by Hurricane Katrina in Mississippi in 2005 (Kates et al., 2006), present a serious threat to coastal communities, with an increased risk of loss of life and damage to property. Severe flood events in recent decades and increasing numbers of assets within the coastal zone (Hallegatte et al., 2013) have led to an increased prevalence of risk-based coastal planning frameworks (Quinn et al., 2014).

Risk-based coastal planning frameworks rely on accurate water level boundary conditions, i.e. input data, to drive model simulations of flood events, which are representative of probabilistic extreme water levels within impact model assessments (Brown et al., 2018). However the accurate representation of total water levels, which form the basis of flood hazard assessments in heavily populated and industrialized coastal zones, can be undermined by the variability in the combined forcing of extreme water levels. This variability can lead to uncertainty in flood hazard assessments, which poses a problem to policy makers and coastal planners as this uncertainty can result in underestimation of the severity and implications of extreme water levels (Prime et al., 2016).

Variability in the combined effect of tide-surge propagation is of particular significance in hyper-tidal estuaries, where the tidal range exceeds 6 m due to bathymetry of the estuary funnelling and amplifying tidal wave propagation (Davies 1964) . Even small changes in the magnitude or timing of a surge will contribute to increased total water levels and can be catastrophic if happening during high tide (Horsburgh and Wilson 2007; Lyddon et al., 2018a). Catastrophic flooding experienced in the Bay of Fundy, Canada during the Groundhog Day Storm of 1976 would have been lessened if the peak of the surge arrived 1 hour before or after tidal high water (Greenberg et al., 2012). The combined forcing of extreme water levels, notably tide and storm surges, can interact with each other in shallow water regions to alter the phase and amplitude of tidal high water (Wolf and Flather 2005), as shown by examples in the English Channel (Idier et al., 2012), Taiwan coast (Liu et al., 2016), and Queensland coast (Tang et al., 1996). Interaction effects are largely a function of storm surge magnitude and can vary spatially across hyper-tidal estuaries, as shown in the Bay of Fundy where interaction effects are most strongly felt in the Northumberland Strait (Bernier and Thompson 2007). Storm surges can also enhance tidal wave propagation in estuaries and shallow coastal waters (Prandle and Wolf 1978), as in the Bay of Bengal where advancement of high water can result in increased flood hazard (Antony and Unnikrishnan 2013). Due to the importance of surge magnitude and timing relative to tidal high water in a hyper-tidal estuary (Lyddon, et al., 2018a), a precise surge prediction is required, in combination with the predicted tide, for estimation of total water levels for flood hazard assessment (Brown et al., 2012). Current methods for storm surge prediction are limited in their accuracy as they may consider tide and surge as independent processes (Bobanović et al., 2006), and rarely consider the important of a coupled tide-surge interaction component or physical processes e.g. funnelling or seiches (Bernier and Thompson 2006). This paper will show there is a need to understand the variability of combined, coupled tide-surge boundary conditions to enable accurate representation of total water levels (prescribed here as a mean sea level, astronomical tidal curve, representative surge curve and freshwater input) for warning and flood hazard mitigation (Wadey et al., 2013; Knight et al., 2015; Wainwright et al., 2015).

Hydrodynamic, numerical models can be used to assess the variability of coupled physical processes controlling estuarine water levels to minimize uncertainty in forecasting systems for flood hazard

assessments (Erikson et al., 2018; Hallegatte et al., 2013). Hydrodynamic models, some of which solve the shallow water, Navier-Stokes equations, are often used as a tool to simulate extreme water levels and assess uncertainty of storm surge elevation due to tide-surge interaction (Bernier and Thompson 2007), bottom friction (Garzon and Ferreira 2016), land cover (Ferreira, Irish, and Olivera 2014) and wave setup (Bastidas et al., 2016). Sensitivity analyses allow input parameters to be varied one factor at a time to help distinguish which sources of uncertainty have most impact on an output total water level (Saltelli 1999).

Uncertainty related to storm surge water level has been investigated by varying elevation of the storm surge, duration of the storm surge and timing of the peak of the storm surge with respect to the peak of the normal high tide (de Moel et al., 2012). The Environment Agency in the UK advises phase shifts in the timing of design surge curves relative to tidal high water for shoreline management planning (McMillan et al., 2011). This methodology captures the full range of potential outcomes of an extreme water level event throughout a model simulation. Detailed analysis of a residual surge improves understanding of tide-surge propagation and identifies where variability in surge elevation occurs through the tidal cycle.

Uncertainty can also be accounted for in an operational context (Lewis et al., 2013). For flood forecasting purposes, an ensemble of predicted storm surge conditions are combined with the predicted tide to determine the range of likely high water level that will be observed (a parameter known as ‘skew surge’) (Flather 2001). ‘Skew surge’, i.e. predicted astronomical high tide – nearest observed high tide, is a key indicator for flood hazard to evaluate absolute water level and understand error or sensitivity to surge timing and estuary morphology (Flather 2001). For flood management planning purposes, design surge curves are used to scale tidal simulations such that an extreme water level representing a required storm severity is generated (e.g., a 0.5 % annual probability event (Prime et al., 2016)). In some studies uncertainty within the shape of the total water level curve is also considered (Quinn et al., 2014) as this also impacts the duration of flooding or flood hazard at a defense. The assessment of coastal resilience to flooding along managed coastlines requires a good understanding of the site-specific flood hazard. Understanding of the uncertainty surrounding potential hazard from extreme water level forecasts issued at nearby locations is critical for monitoring defense performance and making informed decisions surrounding the delivery of shoreline management strategies over planning epochs (typically 0-20, 20-50 and 50-100 years for shoreline management in the UK (Brown et al., 2016)). Variability associated with storm surges in estuaries can be analyzed to minimize uncertainty in forecasting systems and storm impact assessments.

This research simulates the tide-surge propagation in a complex, coastal region, to assess the sensitivity of the surge, including a tide-surge interaction component, to storm timing relative to tidal high water, using the Severn Estuary, south-west England as an example of a hyper-tidal estuary. For the purposes

of this paper the “Severn Estuary” is taken to include the Bristol Channel. This research uses the Severn Estuary as test case as it represents one of the most extreme examples worldwide in terms of tidal range and flood occurrence severity (Pye and Blott 2014). The Severn Estuary region exhibits the second largest mean spring tidal range in the world which increases from 6.2 m in the outer Bristol Channel to 12.20 m at Portbury (Pye and Blott 2010). Approximately 120 km² of the Somerest Levels are at or below sea-level, and these floodplains historically suffer regular inundation (Horsburgh and Horritt 2006). The large tidal range and frequency of storm surges can increase flood hazard on heavily populated and industrialized, low-lying floodplains. The paper aims to assess changes in the storm surge at 5 tide gauge locations along the coast of the Severn Estuary (Hinkley Point, Newport, Portbury, Oldbury and Sharpness) and through the thalweg of the estuary. The modelled surge residual, herein termed the surge, contains a meteorological component and a tide-surge interaction component, and is isolated from the total water level by removing the modelled tidal signal (Pugh 1987). The results (section 3) show there is a need to capture uncertainties associated with storm surge elevation and shape in representative surge curves for flood risk assessments or forecast surge residuals when applied up-estuary of the tide gauge at which they are generated. Therefore the methodology and results could be applied to other hyper- and macro-tidal estuaries worldwide, but these are not explicitly tested herein.

3.3. Methods

3.3.1. Delft3D and model domain

Delft3D-FLOW, a hydrodynamic, numerical model (Lesser et al., 2004), is used in this study to simulate barotropic tide-surge-river propagation across a two-dimensional horizontal, curvilinear grid, in the Severn Estuary (Figure 3.1). Gridded bathymetry data at 50 m resolution (EDINA Marine Digimap Service n.d.) were interpolated onto the model grid, and a uniform Manning friction co-efficient of 0.025 is applied to the grid. The sensitivity of the model to the Manning friction co-efficient was tested by running a 99th percentile water level event (3 January 2014), at varying friction values (0.015, 0.02, 0.025, 0.03, 0.035, 0.04) over a 5 day period. These 6 values were selected based on previous works studying tide-surge propagation in coastal and estuarine systems (Chow 1959; Lewis et al., 2013; Martyr et al., 2012; Shen et al., 2006). A value of 0.025 produced best validation with observational tide gauge data and was selected (Figure 3.2 and Figure 3.3). The final mesh was chosen following an iterative process of refining the grid to resolve the channel-bank system and the tidal propagation up estuary. A domain of this size will experience limited internal surge, generated by local meteorological forcing (Brown et al., 2013), so the extent of the domain was located where observations were available to provide an external tide-surge forcing. The model domain has an open boundary to the west, from Rhosilli, Gower Peninsula to Woolacombe, Devon which is forced using 15 minute tide gauge water level data from Ilfracombe and The Mumbles. A river boundary at Gloucester to the east is forced by 15 minute river gauge water level data from Sandhurst. Boundary forcing excludes meteorological or

wave forcing, to allow tide and surge propagation from the open boundary to be assessed up-estuary with consideration for the local interaction.

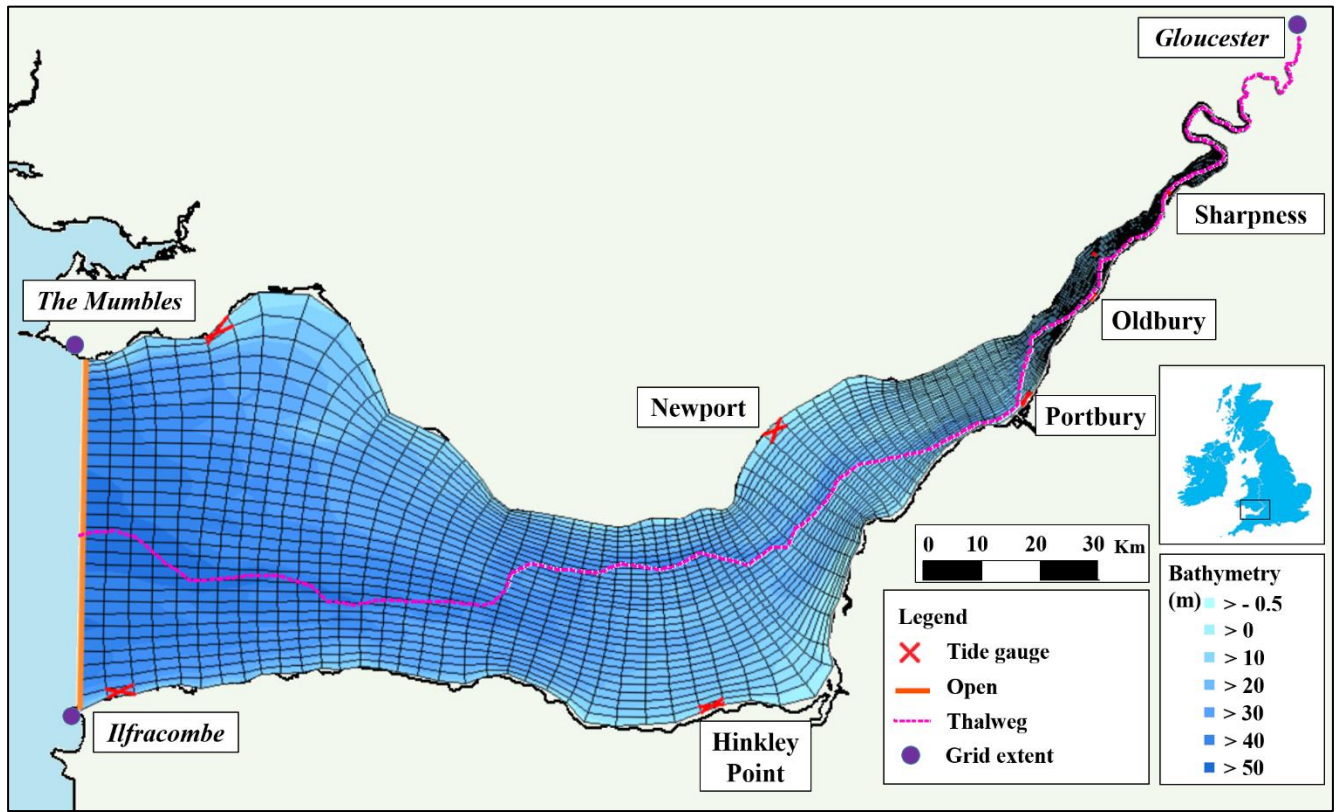


Figure 3.1: Severn Estuary model domain extending from Ilfracome ($51^{\circ}12.668'N$, $4^{\circ}6.743'W$) and The Mumbles ($51^{\circ}34.203'N$, $3^{\circ}58.534'W$) in the west, to Gloucester ($52^{\circ}89.3020'N$, $-2^{\circ}2.6361'W$) in the east. The bathymetry is relative to chart datum (CD).

3.3.2. Long-term tide gauge records

The 15-minute frequency, long-term tide gauge records, collected by the UK Tidal Network (https://www.bodc.ac.uk/data/online_delivery/ntslf/), from Ilfracombe and The Mumbles are used to force the water levels in a series of model setups. Four extreme water level events in the tide gauge record exceeding the 99th, 95th and 90th percentile water level values are identified. The storm tide peak of each extreme water level event is isolated, and the water level time series extracted from the record 3 days prior to and 2 days after the storm tide peak.

3.3.3. Tested tide-surge configurations

The surge component provided within the tide gauge record is separated from the 5-day total water level time series (observed total water level – predicted tide). The predicted, harmonic tidal signal is based on 114 constituents (Hibbert et al., 2015) and is removed from observed total water level at tide gauge locations to estimate the residual and ensure any tide-surge interaction remains within this residual surge component (Proudman 1955b). A Chebyshev type II, low-pass filter is applied to the residual

surge component to remove all energy at tidal frequencies, using a stop-band of 26-h and a pass-band of 30-h (cf.(Brown et al., 2014)). The method separates out the time-varying meteorological residual and the tide-surge interactions, which will have been removed by the filter since it is frequency-dependent (Brown et al., 2014), to leave only the long period surge component. Atmospheric forcing is not included to restrict the sensitivity analysis to tide-surge propagation, without the complication of a locally generated surge contribution.

The filtered surge component is recombined with the predicted tide in a range of time-shifted configurations. The peak of the filtered surge changes relative to the peak of tidal high water to investigate the influence of the timing of the peak of the surge on tide-surge propagation, total water level and surge elevation. The first time series represents the realistic timing of the peak of the surge relative to tidal high water for each of the 4 extreme water level events. A ‘tide-only model’ run is completed to provide the baseline water level which other model runs can be compared to. An additional 13 model time series are created in the time-shift analysis, so the peak of the filtered surge occurs 6 hours before tidal high water and advances incrementally to tidal high water and then continue to 6 hours after, to cover a 12-hour tidal cycle.

3.3.4. Model validation

Model results from the 99th percentile water level event, 3 January 2014, are isolated from the model outputs and standard protocol is followed (Bernier and Thompson 2015; Ferrarin et al., 2013; Quinn et al., 2012) to validate these outputs at the coast with observed data from tide gauges at Hinkley Point, Newport, Portbury, Oldbury and Sharpness. Model outputs for the realistic timing of total water level model run and a tide only run, which provides a baseline, are compared to observation data from the UK Tidal Network, Environment Agency and Magnox. These tide gauge locations are spaced throughout the estuary, and data are freely available to download from the British Oceanography Data Centre, with uninterrupted observational records available for the extreme water level events selected. Widely used error metrics (R^2 (Roberts et al., 2015), NRMSE (Quinn et al., 2012; Brown et al., 2016), Bias of the maximum value (Brown et al., 2016; Kim et al., 2008)) are calculated at tide gauge locations up-estuary. These metrics confirm that the model can reproduce observational tide gauge data without the inclusion of meteorological forcing and waves and can be used to assess the error introduced by this methodology.

Figure 3.2 illustrates validation model runs and observational tide gauge data from Hinkley Point, on the south shoreline of the outer estuary. There is good graphical and statistical agreement between the model output (dashed line) and observational tide gauge data (solid line). Tidal phase is successfully reproduced by the model. The total water level model run is able to reproduce the tide gauge data at Hinkley Point well, with an R^2 value of 0.996 and NRMSE is 1.59 % of observed tidal range. It can be seen high water levels are overestimated by 15-20 cm for the total water level run on the largest tide of

3rd January 2014. This is confirmed with a bias value of 0.242, however with a tidal range of 12.29 m, this over-estimate represents just 1.5% of the overall tidal range. The tide only model run does not resolve the high water peaks, indicating the importance of the inclusion of a meteorological surge component in total water level estimations.

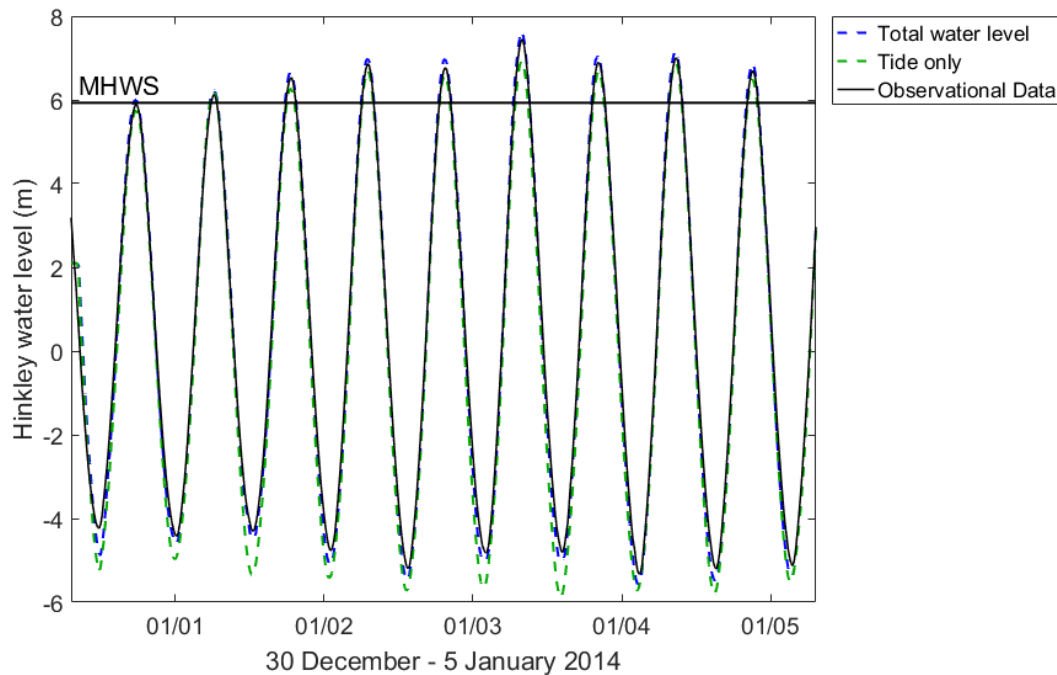


Figure 3.2: Model output validation for realistic timing of total water level and tide only model runs compared to observational data at Hinkley Point tide gauge, Severn Estuary, southwest England.

Figure 3.3 shows model validation at Sharpness river gauge further up-estuary. There is a notable asymmetry in the tidal phase due to shallow water impacts, which are accurately simulated by the model. The total water level model run is able to reproduce the tide gauge data at Sharpness well, with an R^2 value of 0.985 and NRMSE is 1.63% of observed tidal range. The results of the validation indicate that model is in good agreement for the size and resolution of this model domain (see Figure 3.1), and is able to reproduce extreme water levels without the inclusion of meteorological forcing and waves.

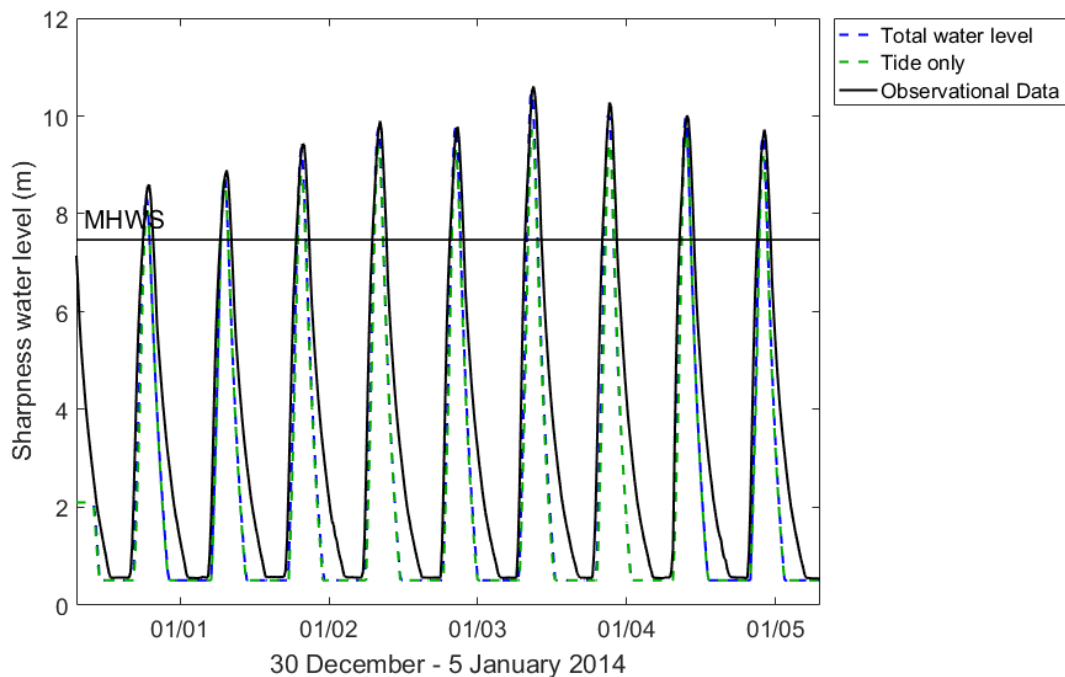


Figure 3.3: Model output validation for realistic timing of total water level and tide only model runs compared to observational data at Sharpness tide gauge, Severn Estuary, southwest England.

The following modelled variables have been analyzed: surge, which is modelled total water level – modelled tide; maximum surge elevation; tidal range, which is modelled mean high water – mean low water; surge range, which is maximum modelled surge elevation – minimum modelled surge elevation; variability in surge elevation, bound by the maximum and minimum surge elevation; and variability in skew surge elevation, bound by the maximum and minimum skew surge elevation.

3.4. Results

Results identify uncertainty in the surge at tide gauge locations in the Severn Estuary. In the first part of the results, the surge is isolated at tide gauge locations and is presented relative to the tide and filtered surge for the 99th percentile water level event, 3 January 2014. In the second part of the results, the tidal range, surge range, and variability in surge and skew surge elevations for time shift configurations is presented along the thalweg of the estuary for each of the four extreme water level events.

3.4.1. Surge elevation on 3 January 2014

The surge is presented over the 5-day model simulation for 99th percentile water level event, 3 January 2014, at tide-gauge locations up-estuary (Figure 3.4). The 5-day, shaded time series (seen in blue in Figure 3.4) captures the full range of potential surge elevations as the filtered surge is moved in time around tidal high water at the open boundary.

Figure 3.4 shows that the maximum elevation of the surge increases at tide gauge locations up-estuary. The maximum elevation of the surge is 0.84 m at Hinkley Point at 05:00. The maximum elevation of the surge increases to 0.88 m at Newport and occurs at the earlier time of 04:30. The maximum elevation of the surge increases further to 0.99 m at Portbury at 05:30 and 1.2 m at 07:00 at Oldbury. The surge reaches maximum elevation, 1.96 m, at Sharpness at 08:00. The maximum elevation of the surge at each tide gauge location consistently occurs on 3 January 2014.

Figure 3.4 shows maximum surge elevation consistently occurs on the flood tide, regardless of the phase shift of the filtered surge at the boundary around tidal high water. Maximum surge elevation at Hinkley Point occurs at 05:00 time on 3 January 2014, which is 2.5 hours before modelled tidal high water. Maximum surge at Sharpness occurs closer to high water at 08:00 time on 3 January 2014, which is 45 minutes before modelled tidal high water.

The shape of the surge curve exhibits noticeable changes as it propagates up-estuary. At Hinkley Point and Newport the surge residual displays long duration, low magnitude elevations. At Portbury, Oldbury and Sharpness the surge curve has short duration, high magnitude elevations and exhibits an M2 tidal signal. This may be caused by the funnelling effect, due to channel convergence (Dyer 1995), which amplifies surges from the deeper part of the outer estuary, through the increasingly narrow, shallow channel towards Portbury (Pye and Blott 2010). The funnelling effect, which amplifies the surge up-estuary, is thus likely to be the driver for an increased positive surge contribution to the total water level up-estuary.

The red line on Figure 3.4 highlights modelled surge elevation for the observed (realistic) timing of the surge on 3 January 2014. The peak of the surge occurs 3 hours after tidal high water at the open boundary, and shows variability in its positioning within the blue band. This demonstrates that each time shift does not cause a consistent surge response over the duration of the modelled event. The dotted orange line on Figure 3.4 shows the filtered modelled residual (modelled total water level – modelled tide). The filtered residual shows a reduction in amplitude up-estuary. This may be due to the influence of quadratic bottom friction as the channel becomes shallower (Proudman 1955b). Frictional influences cause loss of energy in the movement of water to dampen the surges' amplitude as it propagates up-estuary (Garzon and Ferreira 2016). The reduction in filtered surge indicates the increase in total surge is likely to be a consequence of increasing locally generated tide-surge interaction up-estuary to a point where this interaction dominates the shape of the surge curve.

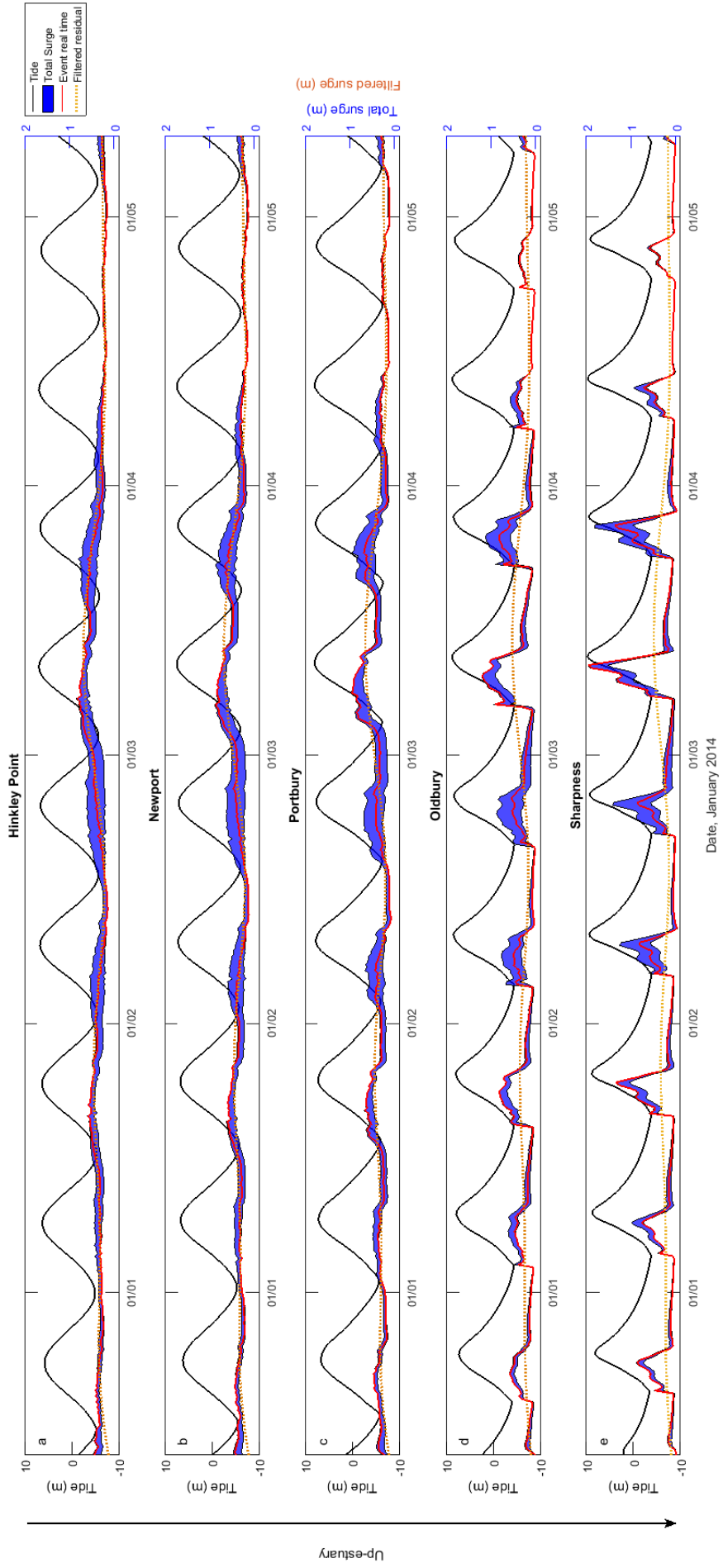


Figure 3.4: Modelled tidal time series (black); modelled surge elevation for the realistic surge timing (red line); range of surge elevations for time shifted configurations shaded (blue band); observed filtered surge (orange line) at a) Hinkley; b) Newport; c) Portbury; d) Oldbury; e) Sharpness for the 3rd January 2014 event.

Table 3.1 shows the contribution of the surge to total water level (prescribed here as a mean sea level, astronomical tidal curve, representative surge curve and freshwater input) (1) when the surge reaches a maximum, (2) at the time of tidal low water and (3) at the time high water at each location.

The surge contributes 11.34% to total water level at Hinkley Point and 12.92% at Newport when it reaches a maximum elevation on 3 January 2014. The contribution of the surge to total water level reaches a peak of 17.49% at Portbury, and then decreases up-estuary to 12.14% at Sharpness. The contribution of the surge to total water level at the time of the surge maxima declines up-estuary despite generating the greatest overall surge elevation. The peak of the surge at locations up-estuary occurs closer to tidal high water than at the down-estuary locations. This larger tidal elevation acts to mask the contribution of the surge.

The surge contributes a greater proportion to total water level at tidal low water. The surge contributes a maximum of 94.39% to total water level at Portbury at the time of tidal low water. The contribution of the surge to total water declines further up-estuary at Oldbury and Sharpness at tidal low water. The contribution of the surge to total water level at the time of tidal high water is small in comparison to tidal low water, and reaches a maximum at Oldbury. The variability in the high and low water contributions is partly due to the phase of the surge peak relative to these times, which is why the skew surge parameter becomes important. These results show the largest contributions occur approximately where the tidal range is also at its largest (Uncles 1984) due to the funnelling influence of the estuary.

Table 3.1: Contribution of surge to total water level at the time of maximum surge (total water level – predicted tidal level), tidal low water and tidal high water.

Contribution of surge to total water level at changing times (%)			
	Maximum surge	Tidal low water	Tidal high water
Hinkley Point	11.34	88.57	5.14
Newport	12.92	92.03	5.02
Portbury	17.49	94.39	4.57
Oldbury	15.50	40.3	7.09
Sharpness	12.14	27.91	5.37

3.4.2. Surge elevation along thalweg

It has been seen in Figure 3.4 that maximum surge elevation increases and occurs closer to tidal high water as it propagates up-estuary, and there is greater influence of tidal harmonics on the surge up-estuary. A change in the surge as it propagates through the estuary therefore influences flood hazard up-estuary. Tidal range, surge range, and variability in the surge and skew surge elevations along the

entire estuary, and through the deepest channel (thalweg) for four extreme water level events are presented in Figure 3.5.

Figure 3.5a shows tidal range increases linearly in the lower estuary, from the open model (sea) boundary to Portbury. The tide is funnelled through the estuary to a maximum range of 13.85 m at Portbury (cf. (Pye and Blott 2010)). A further increase in tidal range is stopped at Portbury and then exponentially decreases beyond Sharpness, potentially due to frictional influences. The range in surge elevations (maximum surge elevation – minimum surge elevation) (Figure 3.5b) and variability in elevation due to the timing of the peak of the surge relative to tidal high water (Figure 3.5c) remain constant from the model boundary to Newport. Both display an exponential increase from Portbury beyond Sharpness. The rate of increase is seen to be greater for a more severe storm. This indicates the system becomes more sensitive to the surge up-estuary. It is noticeable that the 99th percentile water level event (3rd January 2014) produces the greatest variability in surge elevations beyond Portbury, with a maximum elevation of 3.58 m beyond Sharpness.

The variability in skew surge elevations due to the time-shifted configurations (Figure 3.5d) is constant down-estuary for all extreme water level events, similar to the trend seen in the range and variability of surge elevations and tidal range. Skew surge values increase more rapidly than the surge, beyond Portbury, due to the tidal range starting to become damped by friction and the surge starting to increase due to enhanced interaction. The skew surge values decay up-estuary where there is a dominant asymmetrical signal in the tide and surge. This trend is similar for all extreme water level events, for all time shifts. The 99th percentile water level event (3 January 2014) and 90th percentile water level event (18 December 2013) show greatest sensitivity to timing, with greater variability in skew surge values. The 99th percentile water level event (3 January 2014) consistently displays the greatest skew surge values along the channel of the estuary, reaching a maximum of 0.88 m at 112 km up-estuary.

Portbury presents a tipping point in the balance between funnelling and frictional influences, and a change in the dominant contribution to total water level. The funnelling effect acts to increase tidal range up to Portbury, the tide is also the dominant influence on total water level down-estuary. Frictional influences dominate beyond Portbury to dampen the tidal range, which is most noticeable beyond Sharpness. It is suggested that while frictional influence dampens the tidal range it also acts on both tide and surge to enhance asymmetry in the time series, causing the surge range to increase up-estuary in response to tide-surge interaction (Fig 3.4). The relative contribution of the surge to the total water level thus increases past this point.

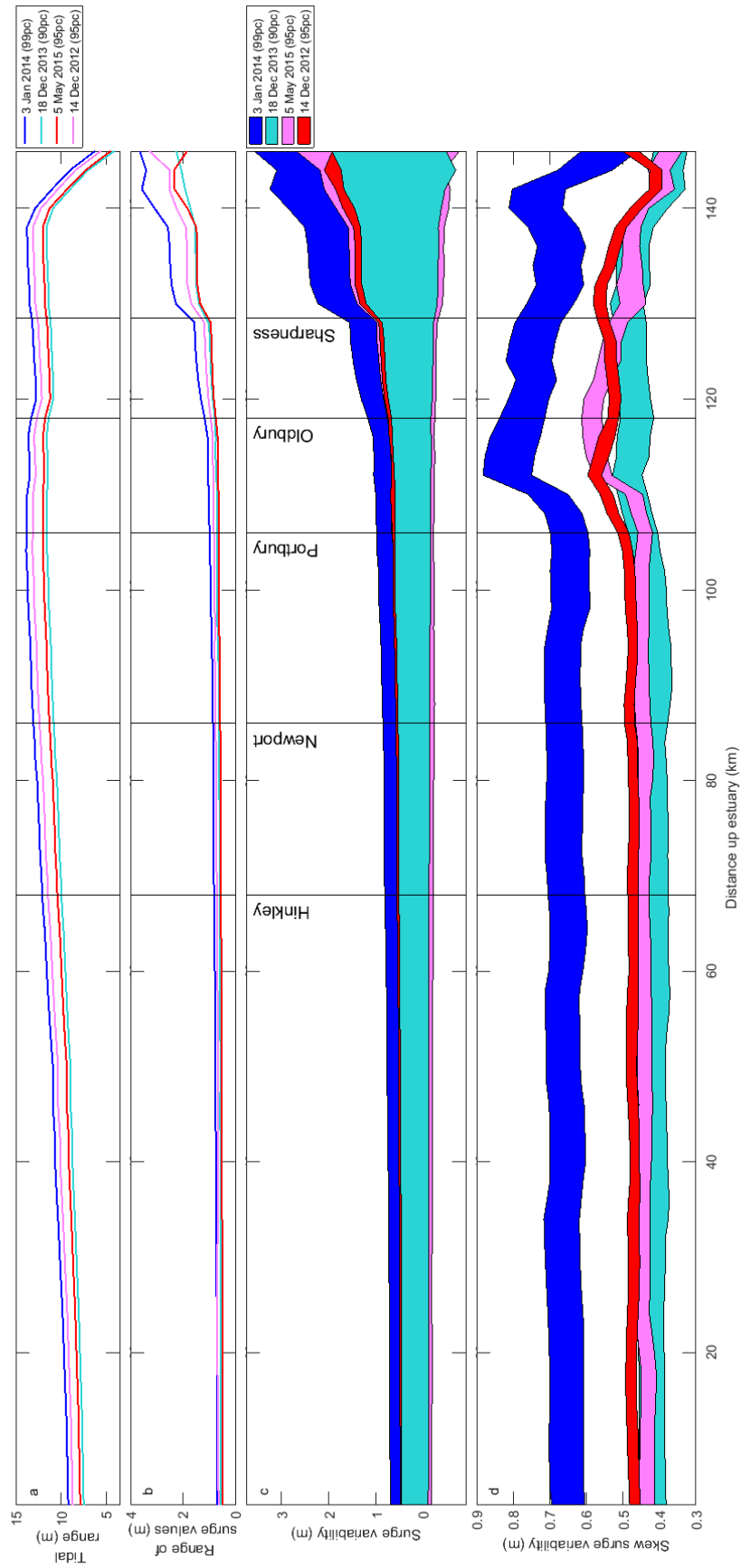


Figure 3.5: a) Tidal range; b) Surge elevation range for observed event timing; c) Variability in surge values; d) Variability in skew surge values for time shift configurations along thalweg of the Severn Estuary.

3.5. Discussion

Variability in the total surge and tide-surge interaction can cause large uncertainties in flood-hazard assessment, which can be a significant concern for coastal asset managers who rely on accurate predictions of total water level for storm hazard mitigation. Here, the barotropic tide-surge-river propagation and interaction across a hyper-tidal estuary has been investigated using the Severn Estuary as test case, and the numerical model Delft3D-FLOW.

The model highlights the influence of the timing of the peak of the surge relative to tidal high water on the surge elevation for 4 historical events in a hyper-tidal estuary, where small changes in surge timing and magnitude can have significant implications for total water levels (Horsburgh and Wilson 2007). A shift in the timing of the peak of a storm surge nearer to the time of tidal high water can elevate water levels and increase the risk of overwashing or overtopping of coastal defenses (Desplanque and Mossman 1999; Lyddon et al., 2018a). The surge contains a meteorological component and a tide-surge interaction component, and is calculated by removing the modelled tide from the total modelled water level. Surge elevation, surge range, variability in surge and skew surge elevation along the channel, and at gauge stations throughout the estuary are presented.

The model confirms the magnitude, duration and shape of the surge (including filtered external surge and local tide-surge interaction) changes up-estuary. On the 99th percentile water level event, the surge component amplifies up to 255% up-estuary as it becomes increasingly asymmetrical and peak water levels occur when the surge is closer to high water. The model clearly illustrates how estuary morphology amplifies tidal wave and surge propagation up-estuary due to topographic features or changing bathymetry (Batstone et al., 2013; Dronkers 1986). The model confirms the importance of shallow water interactions in amplifying tides and storm surges through an increasingly shallow, narrow estuary, which can act to elevate flood hazard (Uncles 1984). The Thames Estuary shows similar behavior as shallow water interactions have a time-displacement effect on tidal propagation (Rossiter 1961). A positive surge can increase phase speed of tidal propagation to alter the timing of tidal high water which is critical for flood hazard during the time of a spring tide and large, positive surge (Prandle and Wolf 1978). Analysis of residuals from tide gauges in the North Sea show that advancement of the surge at tidal high water is of the greatest practical significance for operational forecasts of sea-level (Horsburgh and Wilson 2007). It is of critical importance for surge predictions to consider more than a linear super-position of predicted tide and forecast meteorological surge in shallow water regions, as tide-surge interactions amplify surge elevation and alter the timing of tidal high water (Bobanović et al., 2006).

In shallow water areas dynamic processes such as the effect of bottom friction can cause the tidal and surge components to interact, and become increasingly distorted and asymmetrical (Aubrey 1985; Dixon and Tawn 1994). This is a common phenomenon in the Meghna Delta, Bangladesh, where tidal

range exceeds 4.5 m and bottom friction effects influence the timing and magnitude of high water (As-Salek 1998). The rate of rise of the water level is more rapid than the rate of fall due to decreasing depth of the channel, giving rise to asymmetrical surges (As-Salek and Yasuda 2001). Surges are amplified up-estuary and become more asymmetrical in shape, controlled by channel convergence and contribute more to total water levels, until a tipping point where bottom friction becomes a more important control on surge attenuation (Dyer, 1995). Channel convergence and shallow water effects could modify the shape of the curve prior to tidal high water to alter the duration of high water, and lead to uncertainty in duration and volume of water affecting a region. Modification of the shape of the surge curve up-estuary due to shallow water effects must be captured in surge predictions to avoid incorrect total water level forecasts, which in turn could lead to an increased risk of loss of life and damage to property.

The effect of shallow water on amplifying surge elevation and increasing total water level is well documented in other narrow, hyper- and macro-tidal estuaries worldwide. In the Taiwan Strait, where tidal range exceeds 4 m, nonlinear bottom friction and channel convergence intensifies tide-surge interaction to enhance tidal elevation (Zhang et al., 2010). The influence of tide-surge interaction on peak water levels is also dependent the path of typhoons generating the surge and wind direction (Kates et al., 2006). Local conditions e.g. shallow bathymetry (Bernier and Thompson 2007), storm characteristics (Rego and Li 2010) and tide-river flow interactions (Maskell et al., 2014) may also contribute to changes in surge elevation in shallow water areas, complicating surge predictions. The model highlights the importance of physical processes on total water levels which occur in coastal zones worldwide, not just in estuaries. Simulations of storm surges induced by Hurricane Rita on the Louisiana-Texas coastline present bottom friction as the most important term for surge amplification in nearshore areas (Rego and Li 2010). The importance of considering tide-surge as combined, coupled, physical processes in total water level predictions is shown on the North Queensland coast, where bottom friction can lower total water levels (Tang et al., 1996). It is shown that the addition astronomical tide and meteorological storm surge can overestimate total water level, causing errors in early warnings (Tang et al., 1996). It is clear that local channel morphology, bathymetry and storm event characteristics have strong controls on surge variability and behavior in estuaries which must be captured in storm surge forecasts for accurate predictions of total water level.

The maximum surge elevation consistently occurs on the rising tide, regardless of the phase shift of the filtered surge relative to tidal high water. This effect has been noted in other shallow water regions and estuaries. It has been shown in the North Sea that maximum skew surges are more likely to occur 3-5 hours before tidal high water which can amplify surge magnitude as the shallow water wave travels through deeper water (Horsburgh and Wilson 2007). Noticeable surge influence on the rising tide should be incorporated in the surge curve shape used for flood risk analysis and considered as a source of uncertainty in surge forecasts when applied for up-estuary locations.

The results show noticeable changes in the range of surge elevations through the channel, when the realistic timing of the extreme water level event is analyzed. The range of surge elevations across all four extreme water level events is constant down-estuary, increases slowly beyond Newport and continues to increase exponentially beyond Portbury across all four extreme water level events. The greater range of potential surge elevations that could occur up-estuary may be due to the greater contribution from tide-surge interaction to total water level in these shallow regions. In the Bay of Fundy, Canada, mean spring tidal range can exceed 15 m, which makes it the largest in the world (Desplanque and Mossman 2004). Storm surges gain elevation up-estuary due to near-resonance with North Atlantic tides and strong frictional effects due to shallow water depths (Desplanque and Mossman 1999). Analysis of sea level observations shows that tide-surge interaction, due to bottom friction, can elevate total water level up to 20 cm in the Northumberland Strait during severe storm events (Bernier and Thompson 2006, 2007). The contribution of tide-surge interactions to total water level is of practical significance in terms of water level forecasts and flood hazard assessment. Uncertainty in a storm tide time series, especially when the peak of the surge occurs close to tidal high water (when exceedance of critical thresholds, e.g. defenses, is likely to occur) could influence overflow volume and defense overtopping (Hallegatte et al., 2013). Therefore the shape of surge curves which form basis of flood hazard assessment up-estuary could be wrong for the inner estuary regions if increased variability in maximum surge elevation up-estuary is not accounted for. Incorrect predictions of potential flood hazard will have significant practical implications for communities and critical infrastructure located on low-lying land, with the potential for damage to property and people. At sites of high value (in this case in terms of energy infrastructure) valid modelling tools are required to evaluate coastal resilience. Using a validated model this study quantifies uncertainty surrounding extreme water level forecasts due to tide-surge interaction. Better understanding of this uncertainty informs decisions made by policymakers who set and plan coastal flood response strategies.

Communities and industries developed on low-lying land near tide dominated estuaries (hyper-tidal in this case) require accurate storm surge prediction systems for effective flood hazard mitigation plans and flood warning. Early flood warning in the UK is based on a forecasting system which combines predicted tides and forecasted surges at tide gauge locations in the UK, from the CS3X storm surge model (Flowerdew et al., 2013). An error in flood hazard assessment could occur for tide gauge locations where forecasts are made available due to increased variability in maximum surge elevations and greater magnitude, shorter duration of surge curves, most notably in locations where flood hazard assessments are based on the surge forecast for down-estuary locations. A total water level prediction using down-estuary tide gauge data for a location up-estuary could lead to total water level being under-predicted, and will have consequence for the duration flood water may be able to inundate a site (Hallegatte et al., 2013). Very often the surge forecast is used to forecast a skew surge value relative to

the predicted tide: it is this parameter that provides an indicator for the likelihood of flooding, although it does not indicate the timing or the duration.

The UK Met Office and National Oceanography Centre provide sea-level forecasts, including skew surge predictions, for tide-gauge locations within the Severn Estuary using tidal prediction and surge forecasts (Byrne et al., 2017). The results (Figure 3.5d) show that beyond Portbury there is greater variability in maximum skew surge elevations, indicating sensitivity to the timing of the surge relative to tidal high water. The up-estuary response of skew surge does not follow that of the surge: skew surge values decline beyond Oldbury as tide and surge become increasingly asymmetrical. Therefore surge elevation is low at the time of tidal high water and large when the rising tide is close mean water level. The consequence is a low surge contribution during elevated tidal levels and thus a reduced skew surge up-estuary. Local forecasters should take into consideration both the variability and uncertainties in surge forecast and skew surge forecast when issuing early warning (O'Neill et al., 2016).

3.6. Conclusion

Variability in the storm surge component of total water level thus needs to be captured accurately to reduce uncertainty in site specific hazard assessment. This is especially the case in hyper-tidal estuaries, where tidal range exceeds 6 m and surges can be amplified up-estuary to increase flood hazard, due to reduced hydraulic drag caused by greater mean depths and channel convergence

This research has shown that maximum surge elevations increase up-estuary, with surge curves displaying greater magnitude and shorter duration. A total water level prediction using down-estuary tide gauge data for a location up-estuary could lead to total water level being under-predicted, and will have consequence for the duration that flood water may be able to overwash coastal defenses. Local forecasting systems, which rely on accurate estimations of storm surge, should consider changes in surge elevation and shape with distance up-estuary from nearby tide gauge sites to minimize errors in flood hazard assessment.

3.7. Acknowledgements and Data

The authors thank colleagues at the British Oceanographic Data Centre (BODC) for providing tidal data; Magnox for providing tidal data; Environment Agency for providing tidal data and river gauge data; Gloucester Harbour Trustees for providing tidal data; and EDINA for bathymetric data; Andy Saulter at the Met Office for constructive comments on the analysis in terms of operational model assessment requirements.

4. Increased coastal wave hazard generated by differential wind and wave direction in hyper-tidal estuaries

Chapter 4 progresses the research to look beyond just astronomical tides and meteorological storm surges as key drivers of flood hazard in the Severn Estuary, and consider the effect of wind and wave properties on up-estuary wave propagation and wave hazard. Delft3D-WAVE, based on third-generation spectral wave model SWAN, is used to numerically investigate the sensitivity of significant wave height to uncertainty in representative values for wind and wave characteristics along the shoreline of the estuary. Variability in maximum significant wave height is presented in the estuary for high amplitude shorter period waves and low amplitude, long period, to further understanding of the compound interaction between wind and waves, and identify critical conditions maximizing the hazard and hazard variability along the shoreline. The results can be used to can be applied to the design of coastal infrastructure and facilitation of emergency response planning.

4.1. Abstract

Wave overtopping and subsequent coastal flood hazard is strongly controlled by wind and water levels, and is especially critical in hyper-tidal estuaries where even small changes in wave heights can be catastrophic if they are concurrent with high spring tide. Wave hazard in estuaries is largely attributed to high amplitude shorter period, locally generated wind waves; while low amplitude longer period waves rarely impact low-lying coastal zones up-estuary. Here, the effect of wind and wave properties on up-estuary wave propagation and the sensitivity of significant wave height are investigated numerically along the shoreline of the Severn Estuary, southwest England, as an example. Representative values for wind speed and direction, wave height, period and direction are used to identify key combinations of factors that define the wave hazard generation. High amplitude, short period wind waves are sensitive to opposing winds, with a steepening effect that varies along the estuary shoreline, highlighting the effect of estuarine geometry on wave hazard. Low amplitude, long period wind waves respond with maximum variability in significant wave height to strong winds resulting in their propagation further up-estuary. Our results advance current understanding of the compound interaction between wind and waves, and identify critical conditions maximizing the hazard and hazard variability along the shoreline. The outcomes from this research can help to avoid economic losses from operational downtime in ports and harbours, inform sustainable coastal sea defense design and understand how wave hazard may vary under future climate due to changing storm tracks. Results can also be applied to the design of coastal infrastructure and facilitation of emergency response planning.

4.2. Introduction

4.2.1. Wave hazard impacts

The coincidence of waves with spring high tide and strong winds with a long fetch can be catastrophic in heavily populated and industrialized hyper-tidal estuaries (Desplanque and Mossman 2004; Wolf 2009). The highest waves superimposed on high water levels can cause an instantaneous uprush of water at the coast and push large volumes of water over seawalls or dikes in a short period of time (Hoeke et al., 2015; EurOtop, 2016). This has implications for run-up, wave overtopping, spray and subsequent coastal flooding, which is critical for users and property along the coastline (Allsop et al., 2008; Wolf, 2008; Bastidas et al., 2016; Thompson et al., 2017). Mean overtopping discharges exceeding 0.03 l/s per m, as a function of wave height, wave steepness and water depth (Allsop et al., 2005; Burcharth and Hughes 2011) can pose a hazard to public safety (EurOtop 2016). Despite many seawalls designed to withstand this threshold, 4-8 people are killed each year in the UK through the direct effects of waves on seawalls (Allsop et al., 2005) and approximately 60 killed in Italy over the last 20 years (Allsop et al., 2003).

Wave overtopping imposes serious hazard in heavily populated and industrialized estuaries, where infrastructure, transport networks and natural resources may be located (Geeraerts et al., 2007). Coastal harbours located in hyper-tidal estuaries are economic hubs in terms of trade, communication and tourism. For instance, the Royal Portbury Docks in the Severn Estuary are important for shipping and distribution, and supports 10,000 jobs (Bristol Port Company, 2018). The Port of Shanghai on the Yangtze Estuary is the busiest container port in the world facilitating one of the fastest growing coastal economies (Yap and Lam, 2013). Liverpool Docks in the Mersey Estuary, northwest England, support cruise ships, ferries and vessels which maintain and develop a large network of offshore windfarms (Peel Ports, 2018). Coastal ports and harbours must maintain operating conditions throughout the year, even during extreme conditions, to minimize economic risks and risks to humans and their property (Santana-Ceballos et al., 2017).

Ports and critical infrastructure are often located in estuaries because they are sheltered by land from the impacts of high-energy waves and wind conditions (Phillips 2008; Uncles 2010). It is assumed that up-estuary locations are subject only to the effects of high amplitude, shorter period, locally generated wind waves (Lesser 2009), tides, river flow and storm surges (Monbaliu et al., 2014). However it cannot be assumed that large, hyper-tidal estuaries display a uniform response to forcing factors to provide shelter at all times (Allen and Duffy 1998), and in some instances estuary orientation can act to amplify wave hazard up-estuary (Grady and McInnes 2010). Longer period waves could generate a significant and underestimated hazard up-estuary if exacerbated by local wind-wave effects (Talke and Stacey 2003), due to their relatively high run-up compared to higher amplitude waves (Palmer et al., 2014). The largest overtopping waves, generated under stronger winds on younger sea states in the estuary, can plunge into water in the lee of seawalls, harbours walls and breakwaters and cause new waves to be formed (EurOtop 2016). New waves in ports and harbours, known as transmission waves, can excite harbour seiching and cause unnecessary back-and-forth motions of vessels and subsequent risk for safety thresholds, including avoiding vessels coming loose from moorings (Dongeren et al., 2016).

Run-up will increase with increasing wavelength and wave period (EurOtop 2016), therefore assuming the influence of longer period waves is negligible in estuaries can present a hazard if defenses are not designed to protect against them. This paper will explore how coastal wave hazard changes through a large, hyper-tidal estuary under varying wind wave conditions, to provide an understanding of the frequency, pattern and severity of wave overtopping events. Better understanding of the sensitivity of coastal wave hazard to the interaction of local wind and waves enables more informed decisions by managers of critical coastal infrastructure responsible for operational flood risk management and implementation of policies, which may vary in time, over a 100-year management horizon.

4.2.2. Wave hazard in hyper-tidal estuaries

Coastal zones worldwide are subject to local changes in water level due to the combined effect of astronomical high tides, waves and wind (Allsop et al., 2008; Letchford and Zachry, 2009; Bastidas et al., 2016). Strong winds blowing over the surface of shallow water generate waves which propagate towards the coast at a speed and amplitude dependent on water depth (Wolf 2009). Coastal wave hazard can cause danger to life and property when coinciding with stronger wind speeds or around the time of high water. This is of particular significance in hyper-tidal estuaries where the tidal range exceeds 6 m and where even small changes in total water levels and wave setup can be catastrophic if occurring during high tide (Davies 1964; Robins et al., 2016).

Large tidal ranges occur as a consequence of the orientation, geometry and bathymetry of the estuary funnelling and amplifying tidal wave propagation (Pye and Blott 2014). Extreme water depths, due to a large tidal range, allow waves to propagate far up-estuary, with the impact of waves felt along large stretches of coastline (Brown and Davies, 2010; Brown et al., 2010). The Bay of Fundy, Canada, which has a tidal range over 16 m (Desplanque and Mossman 1999), could in some respects be described as a wave-dominated coast due to the long fetch creating locally-generated waves (Davis and Hayes 1984). High amplitude storm waves can also develop in the Bay due to strong, prevailing southeasterly to southwesterly winds (Desplanque and Mossman 2004). Severe flood conditions are “virtually guaranteed” in the Bay of Fundy when strong winds and adverse weather conditions coincide with high water of large, astronomical tides (Desplanque and Mossman 2004). Measurements of significant wave height in the lower Bay at Tyner Point show that waves exceed 1 m from November to April 25% of the time, and are characterized as swell waves with a period longer than 9 s and locally-generated waves with a 5 s period (Greenberg 1984). Severe storms, such as the “Groundhog Day” storm of 1976 can produce longer period waves (Greenberg et al., 2012). The Severn Estuary, south-west England, is a long shallow, narrow estuary which creates mean spring tidal range up to 12.2 m at Avonmouth (Pye and Blott 2010). The incidence and strength of incoming southwesterly-westerly storms from the Atlantic, tidal modulation and current fields have a strong control on wave evolution up-estuary (Allen and Duffy 1998). A combination of strong winds and a tidal bore caused wave overtopping in Minsterworth, Maisemore, Elmore and Newnham in the Severn Estuary on 3-4 January 2014, causing flooding of roads and houses (BBC, 2014; Haigh et al., 2015). Waves approaching the estuary from 200 – 250° (Sibley et al., 2015) were followed by maximum 25 m/s (55 mph) wind from 230° (CEDA, 2018). Sea defenses were overtopped by water levels up to 0.8 m above crest height, with £2.8 million damage to Welsh sea defenses (as documented in SurgeWatch (Haigh et al., 2015)). Under certain conditions, wind-waves could propagate up-estuary and potentially overtop sea defenses at Barry (7.39 m AOD / 12.89 m CD) or Penarth (8.53 m AOD / 14.3 m CD) (Welsh Office, 1999). Rougher wind-wave seas are unlikely to overtop concrete sea walls at Hinkley Point as their crest height exceeds 8.5 m AOD (14.4 m CD) (Magnox 2014). However, the Bristol Channel is only affected by a narrow band

of storm tracks, which means there is only a 50% chance of a severe storm, and maximum wave height, coinciding with high water (Dhoop and Mason 2018), which can make waves less significant in terms of flooding (Fairley et al., 2014). The orientation of an estuary can also shelter it from swell waves, as seen in the Mersey Estuary, northwest England which predominantly experiences locally wind-generated waves (Wolf 2008). The largest waves in Liverpool Bay, which can exceed 4 m during 1-5 storm events per year, are generated by westerly-northwesterly winds which have the longest fetch (Brown and Wolf 2009). Locally generated, high amplitude waves can still affect infrastructure and utilities, as seen in the Dee Estuary on 5 December 2013. The railway line was closed from Holyhead to Chester as gale force winds caused damage to the line at Colwyn Bay (Natural Resources Wales 2014). Wave amplitude is critical in overtopping hazard thresholds for setting safety margins for people, property and transport (EurOtop 2016).

Simulations of Tropical Cyclone Agnes, August 25, 1981 and Matsa, July 21, 2005, in Hangzhou Bay, where mean spring tidal range can exceed 8.1 m (Zhang et al., 2012), shows wave overtopping can occur in the estuary regardless of wind direction when wind speed is strong enough. Easterly winds with a wind speed of 40.7 m/s (90 mph) were recorded during Tropical Cyclone Matsa, which affected 31.5 million people in the region (Hu et al., 2007; Zhang et al., 2012). Due to the size and hydrodynamics in hyper-tidal estuaries, it cannot always be assumed that ports and infrastructure located up-estuary are sheltered from the effects of swell wave hazard. Wave overtopping volumes and impacts will be site specific, and closely related to the local bathymetry and topography, size and use of the receiving area (Allsop et al., 2008) and characteristics of sea defense structures (Santana-Ceballos et al., 2017). New observations (Brown et al., 2018) at the mouth of the Mersey, NW England, found wave overtopping alerts need to have an increased consideration for the offshore wave conditions. An event with a NW wind caused overtopping along a seawall frontage 26th October 2017, while no alert was triggered due to the wind direction not being directly onshore and the wave conditions being considered as relatively low amplitude. The duration, fetch and strength of wind, in addition to water depth, sheltering effects due to estuary orientation and geometry are important controls on wave evolution and propagation in an estuary.

Accurate prediction of nearshore waves is essential in heavily populated and industrialized estuaries for coastal wave and flood hazard mitigation. Accurate forecasts of coastal waves and understanding of the potential impact is critical for the accurate provision of conditions at the coastal boundary of flood hazard models (of overtopping or inundation) used to inform management activities (Prime et al., 2016) or within operational flood forecast systems (Bocquet et al., 2009). Such prediction requires an accurate understanding of wave generation and evolution at high water combined with the effect of wind, wave type and fetch. Analysis and prediction of wave hazard can improve understanding of the processes and contributions to maximum significant wave heights and economic impacts of waves at the coast. Modeling approaches are often employed to simulate wave generation and evolution to assess the

potential consequences of wave overtopping at tidal high water, and subsequent coastal flood hazard for people, businesses, and the natural and built environment. A coupled wave circulation model application to Mobile Bay, Alabama during Hurricane Georges (1998) in the Gulf of Mexico (Chen et al., 2007) shows spatial and temporal variability of wave heights and wave periods. The results can be applied to the design of coastal infrastructure and facilitation of hurricane emergency planning. There is a clear economic case for improved prediction of nearshore waves during storm events as the replacement cost of sea defenses around England has been estimated at £6 billion (\$8 billion USD) (Allsop et al., 2005). However, simulation of wave hazard in a hyper-tidal estuary is complex due to the extreme tidal range, complex geometry and bathymetry and random nature of wind-generated waves (Santana-Ceballos et al., 2017). Prediction of maximum significant wave heights at high water can facilitate the management and emergency response of coastal resources, improve the design of sea defenses and coastal infrastructure to reduce economic risks, and inform the public and decision makers to minimize loss of life from extreme wave events.

4.2.3. Case study

This research focuses on the Severn Estuary, south-west England, as a test case of hyper-tidal estuaries worldwide, due to its national significance for nuclear and energy assets and because it has the second largest tidal range in the world. For the purposes of this paper the “Severn Estuary” is taken to include the Bristol Channel. The Severn Estuary has a mean spring tidal range of up to 12.2 m at Avonmouth, due to near-resonance and tidal amplification as a result of the funnelling effect (Dyer 1995; Uncles 2010; Lyddon et al., 2018a). The width of the mouth of the Severn Estuary, up to 41 km between Woolacombe, Devon and Rhossili, Gower Peninsula, and the westerly-southwesterly aspect means the estuary is exposed to prevailing southwesterly winds with a long fetch and ocean waves from the North Atlantic (Pye and Blott 2010). Observational wave data from the directional waverider buoy at Scarweather, 15 km off the coast of Porthcawl, South Wales, between 1 January 2012 and 31 December 2016 show on average waves approach from a WSW to W direction (245.4°) (Figure 4.1). The waves have an average significant wave height of 4.8 m, average wave period of 8.3 s and peak period up to 22.2 s. Swell waves enter the estuary from the Atlantic Ocean and can generate a bimodal wave regime, particularly under stormy conditions (Proctor and Flather 1989). Waves approaching from a SW / W have the longest fetch, indicating wind waves generated along longer local fetches can reach longer periods.

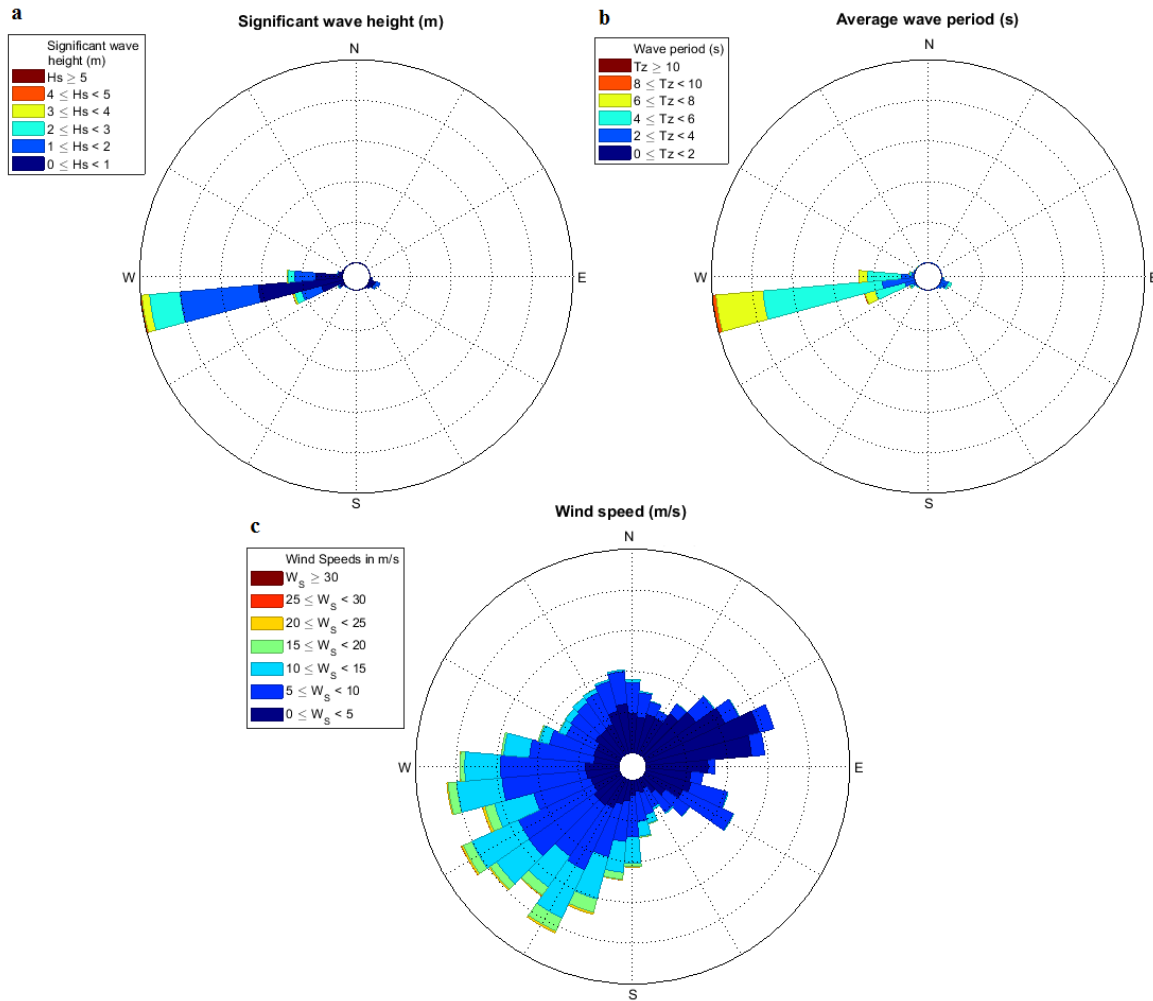


Figure 4.1: 5 years of observational wave buoy data taken from Scarweather (located in Figure 4.2), Severn Estuary, UK showing a) wave direction (deg) and significant wave height (m), b) average wave direction and wave period (s) and c) 5 years of observational wind data taken from Chivenor, Devon (located in Figure 4.2).

This paper describes the effect of wind and wave properties on spatial variability and sensitivity of significant wave height along the shoreline of a hyper-tidal estuary. A sensitivity study is conducted using representative values for wave height, period and direction and wind speed and direction to force the model boundary of Delft3D-WAVE. As explained in the method (section 2), waves are simulated on a spring tide to explore the relative significance of high amplitude, shorter period wind generated waves compared with low amplitude, longer period waves. The results (section 3) identify key combinations of factors which are important for exacerbating wave hazard in ports, harbours and towns and sheltering effects along the shoreline. Before drawing conclusions in section 5 we discuss in section 4 the significance of wave hazard that can be exacerbated by local wind-wave effects in hyper-tidal estuaries, where tide and surge are often considered the primary hazard.

4.3. Methods

4.3.1. Delft3D-WAVE

Delft3D is a modeling suite which is used to simulate flows, waves and morphological developments for coastal, river and estuarine environments (Lesser et al., 2004). Delft3D-WAVE, a third generation spectral wave model, simulates the evolution of wind-generated waves over time and space (Deltares 2014b). Delft3D-WAVE is based on the SWAN model (Simulating WAVes Nearshore(Booij et al., 1999)), which is designed to simulate short-crested waves in shallow, coastal regions dependent on wind forcing, water depth and bottom roughness. The physical processes simulated by Delft3D-WAVE include wave generation by wind, dissipation due to whitecapping, depth-induced wave breaking, bottom friction (using the JONSWAP formulation) and refraction (Deltares 2014b). The modeling system has been successfully applied to many coastal and estuarine regions (Elias et al., 2012; Bastidas et al., 2016).

A 2DH, curvilinear model grid is used to simulate nearshore waves in the Severn Estuary, SW England using Delft3D-WAVE. The model grid extends from Woolacombe, Devon and Rhossili, South Wales in the west to Gloucester in the east and follows the shape of the coastline (Figure 4.2). The model grid resolution has been refined at the coast to improve the accuracy of significant wave height prediction along the shoreline, as this is the area of most interest in this study. Gridded bathymetry data at 50 m resolution (SeaZone Solutions Ltd. 2013) was interpolated over the 2DH curvilinear grid by grid-cell averaging and triangular interpolation. The wave model is forced at one open boundary to the west, with representative water level, significant wave height, wave period and wind speed values.

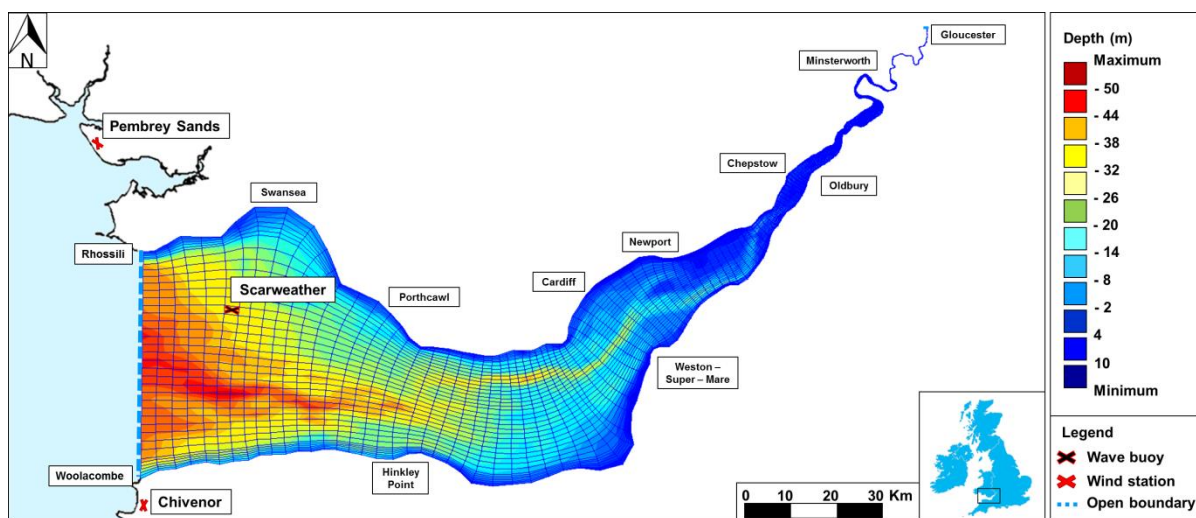


Figure 4.2: Delft3D-WAVE model grid. The bathymetry is relative to chart datum (CD).

4.3.2. Boundary conditions

A schematic diagram of the wave model and forcing data sources used for the model boundary conditions is shown in Figure 4.3.

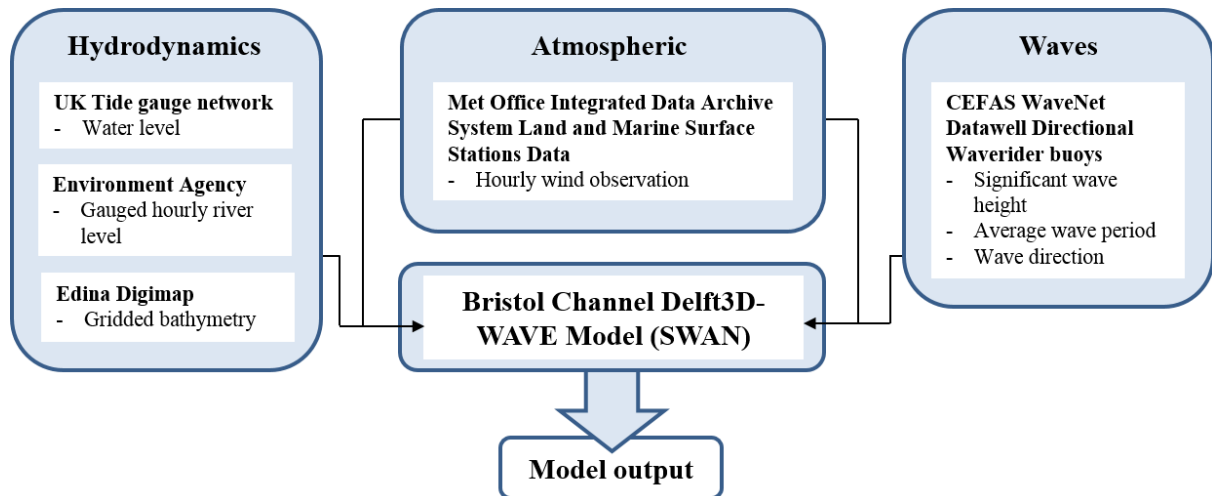


Figure 4.3: Model schematic for the coupled Delft3D hydrodynamic (FLOW) and wave (SWAN) model with forcing data sources.

4.3.2.1. Water level

A large tidal range and strong tidal currents result in tidal modulation of wave conditions in the Severn Estuary (Fairley et al., 2014). For the purpose of this study, which aims to isolate the effect of wind and wave conditions on wave hazard, Delft3D-WAVE is run as a standalone wave model to remove the influence of tidal modulation, wave-current interaction and wind setup on significant wave height. The study aims to build on previous research into tide-surge interaction (Lyddon, et al., 2018a; 2018b), prior to assessing the effect of wave hazard on flood inundation. The model's open sea boundary to the west of the model domain (Figure 4.2) is forced with a constant water level. This water level is the average of mean high water spring tide at Mumbles (4.54 m) and Ilfracombe (4.47 m) (NTSLF, 2018) to produce representative mean high water spring tide (MHWST) value of 4.5 m (relative to chart datum). MHWST was chosen as a representative water level as wave hazard could be increased when wind waves are superimposed on a higher water level.

4.3.2.2. Wave selection

Observational wave data, recorded by the WaveNet directional waverider buoy at Scarweather (51°25'.99N, 003°55'.99W, shown in Figure 4.2) is analyzed to identify representative wave height and period to force the model boundary (CEFAS, 2018). Five years of significant wave height and average wave period, recorded from 1 January 2012 to 31 December 2016 which occurs when the tide is at or above the level of MHWST, is plotted to separate and isolate representative shorter and longer period wind waves (Figure 4.4). The wave record selected provides a series of wave conditions that are representative of conditions which may occur in the estuary, and includes the 2013/2014 winter which

was the stormiest on record (Sibley et al., 2015; Masselink et al., 2016). The record captures low probability, extreme conditions, including the 3 January 2014 storm saw wave heights in excess of 6 m at the Scarweather wave buoy and wave periods up to 20 seconds (Sibley et al., 2015). As seen in Figure 4.4, there is no clear separation between locally generated wind waves and ocean-generated swell waves at or above the level of MHWST. The wave buoy shows a large range of wind waves in response to the range of local fetches NW (fetch limited), W and SW (long fetch open to the Atlantic Ocean). Lower amplitude waves approach from a NW with an average period up to 10 s, and high and low amplitude waves with a range of periods from low to high approach from the W.

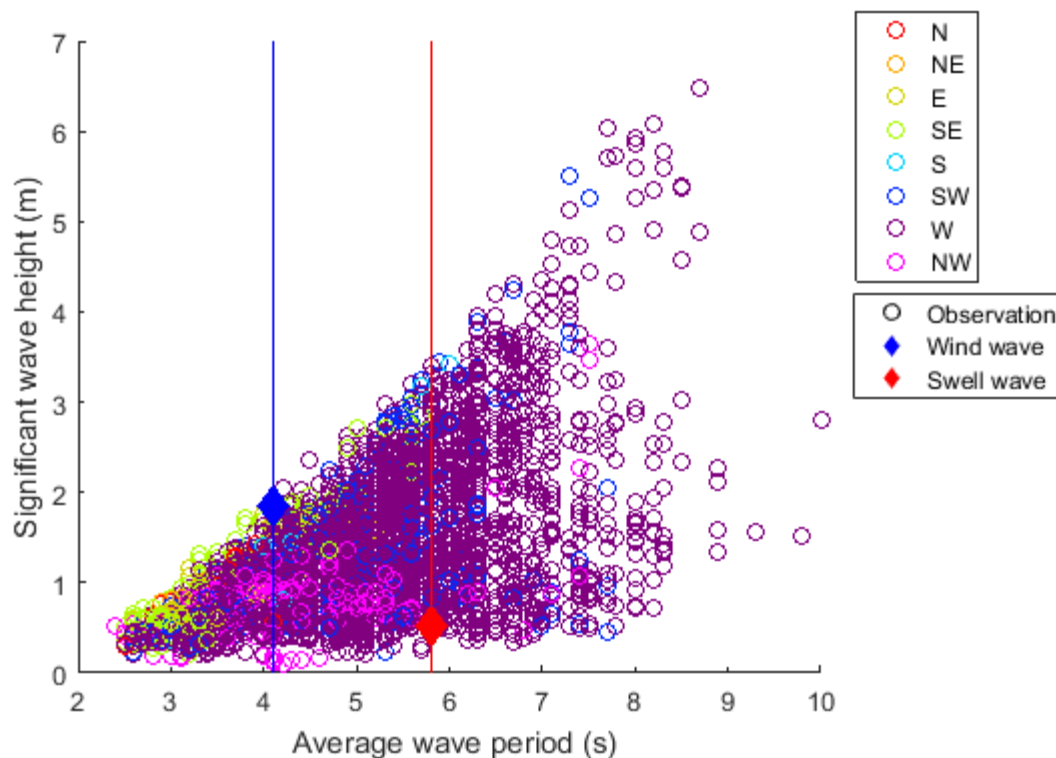


Figure 4.4: Wave selection for H_s and T_z . 25th percentile T_z (blue line) and 75th percentile T_z (red line), color coordinated based on wave direction.

Wave parameters typically used for coastal defense design and coastal flooding strategies are average wave period (T_z) and significant wave height (H_s) (Palmer et al., 2014). To isolate representative wave types from the record to force the model boundary, the 25th and 75th percentile values for average wave period are identified, as this parameter relates to wave power and flood hazard (Prime et al., 2016; Thompson et al., 2017). Equivalent significant wave heights are then identified to represent different wave amplitudes, referred to here after as high and low amplitude waves. A higher significant wave height is selected from the observations based at the 25th percentile value for wave period to represent a higher amplitude wave, which is steeper in shape. A lower significant wave height combined with a 75th percentile value wave period is selected to represent a lower amplitude wave, which is less likely to break at the base which results in water forced upwards and potentially overtopping (Sibley and Cox

2014). These two wave types have been selected to: compare higher and lower amplitude wave propagation up-estuary; represent wave conditions that could occur in the estuary and potentially result in wave overtopping; and, represent waves that have been documented in hyper-tidal estuaries worldwide (Greenberg 1984; Wolf et al., 2011). Modelled results of representative values for wave period and significant wave height (Table 4.1) will show how different waves behave and propagate through the estuary, and the impact of estuary orientation on wave propagation up-estuary. Observations are positioned close to the model boundary and thus the two wave conditions (Table 4.1) are representative of the conditions at the estuary mouth and used to force the open boundary.

Table 4.1: Representative wind wave conditions close to the estuary mouth based on 5 years of observational data from Scarweather Waverider buoy.

	H_s (m)	T_z (s)
High amplitude waves	1.86	4.1
Low amplitude waves	0.53	5.8

The representative wave types presented in Table 4.1 are combined with varying wave direction (SW, W, and NW) to explore the effect of prevailing wind direction on wave propagation into and through the estuary.

4.3.2.3. Wind selection

Observational wind data, taken from the UK Met Office MIDAS Land and Marine Surface Station Data located in coastal locations in the outer Severn Estuary at Chivenor and Pembrey Sands (see Figure 4.2) are used to define representative wind speeds to force the Delft3D-WAVE model (CEDA, 2018). Five years of wind speed data, recorded from 1 January 2012 to 31 December 2016, are analyzed to identify 10th, 50th, and 90th percentile values for wind speed at each station. The average for each percentile wind speed value is calculated from both coastal stations to provide a spread of representative wind speeds within the estuary. The wind direction is also varied and applied to the model domain from 8 points of the compass (N, NE, E, SE, S, SW, W, and NW). The wind speed and direction is uniform in time and space. This will demonstrate how wave behavior responds to changes in wind speed and direction. Delft3D-WAVE is also run with no wind speed (0 m/s) to provide a baseline scenario and to isolate the effect of wind speed and wind direction on wave hazard.

Table 4.2: Representative wind speeds based on 5 years of observational data from Chivenor in Devon (England) and Pembrey Sands in Dyfed (Wales) UK Met Office MIDAS land station data.

	Wind speed (m/s)
10 percentile	1.8
50 percentile	5.18

4.3.3. Model validation and scenarios

Results from model simulation are compared with 5 years of observational data from the Scarweather WaveNet wave buoy in Severn Estuary. The model represents scenario combinations of wave height and wave period combined with varying wave and wind direction. Observational data from the Scarweather waverider buoy, which occurs when the tide is at or above the level of MHWST, are isolated and H_s and T_z plotted (Figure 4). Model simulations at the same location in the model domain as the Scarweather wave buoy are plotted over the observational wave data (Figure 4.5).

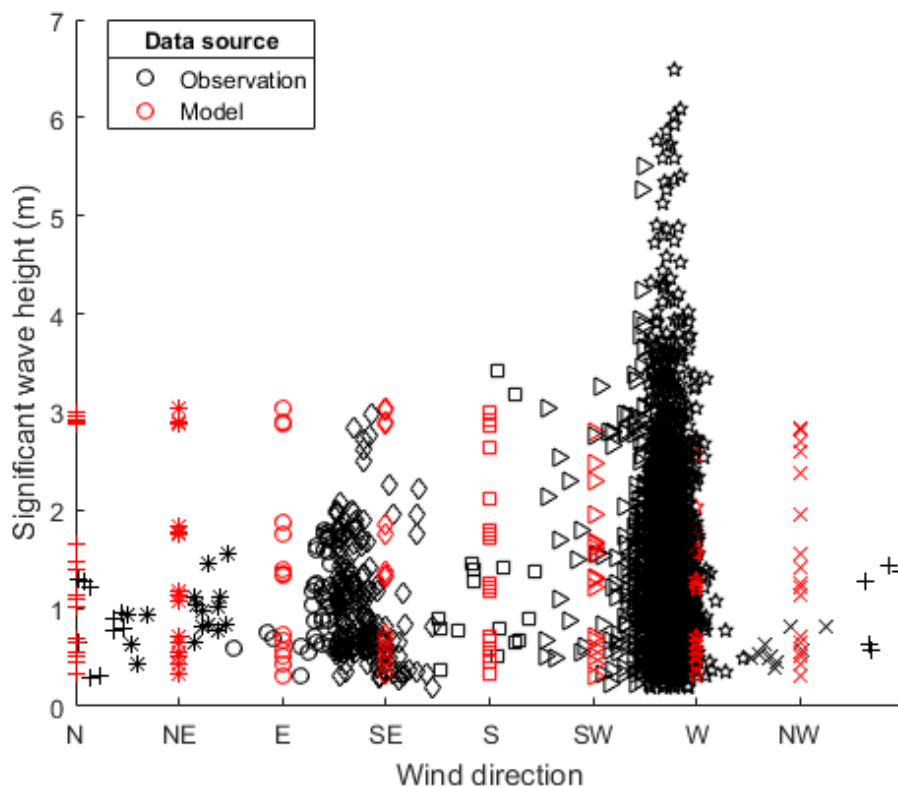


Figure 4.5: Delft3D-WAVE model validation comparing model simulations to 5 years observational data at Scarweather wave buoy. Symbols representing directions over a range of 45 degrees.

Figure 4.5 shows the scenario combinations cover a range of observed conditions. Model simulated waves show good agreement for wind directions from the SE, S and SW. The model overestimates waves approaching from NW, N and NE direction because more extreme winds are not typical for this direction and are causing wave growth over the short fetch (see Figure 4.1c). The wave buoy records lower amplitude waves approaching the estuary from these directions, as seen in Figure 4.1 & 4.4. The scenario combinations simulate cases (NW waves) which are unlikely to occur in reality. The model under-predicts maximum wave conditions from a W direction, from which the highest amplitude waves approach WSW (see Figure 4.5). As seen in Figure 4.4, there is a large number of points that exceed

the 75th percentile value, which are dominated by higher amplitude, longer period wind waves approaching from the W. The scenario combinations do not capture the direction-specific higher amplitude, longer period waves which could occur.

Some 150 wind-wave scenarios are modelled to identify key combinations of factors which are important for wave hazard and wind-wave propagation up-estuary. The model domain is forced using a combination of different representative wind and wave conditions, including a baseline scenario for each wave direction and wave type with no wind forcing.

4.4. Results

Model outputs are analyzed to identify maximum significant wave height every 2 km along the shoreline of the estuary. The difference between the maximum significant wave height along the shoreline and the ‘no wind’ scenario for each wave type and wind direction is presented to quantify the impact of wind on wave hazard. The difference between maximum significant wave height and the baseline scenario is plotted along the shoreline starting at Rhossili, South Wales and moving along the north shoreline of the estuary up to Gloucester, and then along the south shoreline of the estuary to Woolacombe, Devon. Figure 4.6 shows the difference between maximum significant wave height and baseline scenario along the shoreline for representative high amplitude waves, and Figure 4.7 shows representative low amplitude waves along the shoreline of the estuary. Each subplot in Figure 4.6 and 4.7 represents the wave hazard under a different incoming wave direction, line color denotes the different wind direction and line type denotes different wind speed. Results are presented systematically for the two representative wave types selected.

4.4.1. High amplitude waves

4.4.1.1. Maximum significant wave height for high amplitude wind waves

The maximum significant wave height (H_s) produced across all normalized high amplitude wind wave scenarios is 2.04 m, which occurs 20 km up-estuary from the model boundary on the south shoreline. This wave height is produced from a wind wave entering the estuary from a NW direction, with a 90th percentile value wind in an E direction. A 90th percentile value wind speed, 11.06 m/s, represented by the solid lines in Figure 4.6, consistently produces the maximum H_s along each shoreline. As wind speed increases, the friction velocity increases and a steeper, rougher wind sea begins to develop (Lin et al., 2002). There is no consistency along the shoreline as to which wind direction produces the maximum H_s and where this occurs due to the complex orientation of the coastline, however there are a number of general trends which have emerged.

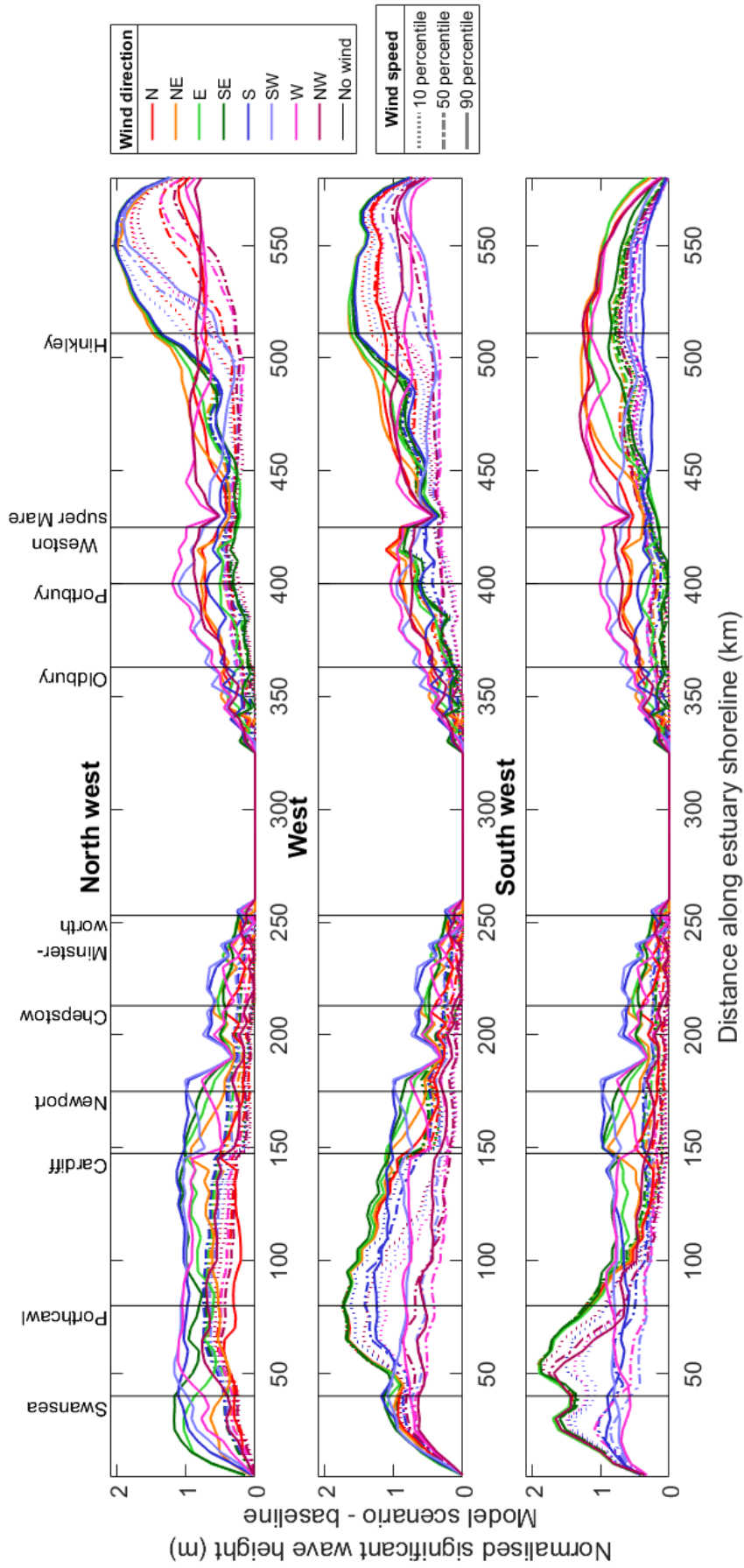


Figure 4.6: Normalized significant wave height (model scenario – no wind baseline scenario) for representative high amplitude, short period waves along the shoreline of Severn Estuary, starting at Swansea to Gloucester and thence down-estuary towards Hinkley Point.

4.4.1.2. Following winds reduce H_s in the outer estuary

A high amplitude wind wave moving towards the shoreline with a 90th percentile value wind speed and following wind does not produce the maximum H_s in the outer estuary. For example a wave traveling from the NW followed by a 90th percentile value wind speed produces normalized maximum H_s of 0.79 m, 30 km up-estuary from the model boundary on the south shoreline. A NW wave followed by a 10th percentile value wind speed value produces a normalized maximum H_s of 1.59 m, at the same point in the model domain. Further to this, a wave moving in a SW direction followed by a 90th percentile value wind speed in a SW direction, produces a normalized maximum H_s of 0.84 m 50 km up-estuary from the model boundary on the north shoreline, between Swansea and Porthcawl. A SW wave followed by a 10th percentile wind speed value produces a normalized maximum H_s of 1.23 m at the same point in the model domain. It is evident that a following wind contributes to wave growth. The addition of wind energy to the rougher sea could cause the wave to feel the effect of bottom friction and break before reaching the shoreline or break due to whitecapping.

4.4.1.3. Opposing, blocking wind acts to steepen waves in the outer estuary

Maximum waves on both south and north shorelines generally occur when wind and wave are propagating in opposite directions. For example, the maximum normalized H_s on the south shoreline, 2.04 m, occurs when NW waves are essentially blocked by 90th percentile value wind speed from a SE / E direction. Likewise, the maximum normalized H_s on the north shoreline, 1.91 m, occurs when the SW waves are blocked by 90th percentile value wind speed from a NE / E direction. Winds block the wave propagation moving in the opposite direction to increase the steepness of waves. Further to this, the younger, rougher wind-wave sea shows increased sensitivity to wind direction. This is particularly the case in the outer estuary where there is greater sensitivity to changing wind direction and wind speed. The range of normalized maximum H_s is 1.47 m between Swansea and Porthcawl on the north shoreline and 1.35 m down-estuary of Hinkley Point on the south shoreline. The blocking effect of wind appears to be a significant contribution to wave hazard along the shoreline of the outer estuary.

There is less sensitivity to wind direction in the upper estuary, beyond Cardiff on the north shoreline and Portbury on the south shoreline as waves begin to attenuate. Following winds from the W and SW produce the maximum normalized H_s in the upper estuary, as fetch may help high amplitude waves to propagate further up-estuary. The effect of bottom friction dissipates wave energy and the lines converge to show H_s decline. H_s is 0 m in the upper estuary at Gloucester as wave energy is not able to propagate this far up-estuary, possibly due to the long, narrow, shallow nature of the Severn Estuary.

4.4.1.4. Effect of estuary geometry on significant wave height

The wind direction produces a different maximum H_s in different locations throughout the estuary, as a function of the local geometry and complex orientation of the coastline. The maximum H_s on the south shoreline occurs with a NW wave direction, and the maximum H_s on the north shoreline occurs with a SW wave direction. It is clear that a shoreline facing an incoming, onshore wave direction will experience increased wave hazard, however the incoming wave direction impacts each shoreline differently. The maximum normalized H_s on the north shoreline occurs further up-estuary, 1.91 m at 55 km away from the model boundary. In contrast, the maximum normalized H_s on the south shoreline, 2.04 m, occurs 30 km up-estuary from the model boundary. The orientation of coast, geometry and bathymetry of the estuary means that the shorelines do not respond in the same way and the maximum is not observed at the same distance up-estuary.

The effect of shoreline geometry on wave hazard is further highlighted by the double peak in maximum significant wave height observed close to Mumbles for a SW wave direction. The headland is smoothed out in the model domain; however complex changes in water depth are reflected in the bathymetry.

4.4.2. Low amplitude waves

4.4.2.1. 90 percentile winds create maximum variability

The 90th percentile value wind speed consistently produces the maximum normalized H_s along the north and south shoreline throughout the estuary for longer period, lower amplitude waves (Figure 4.7). Normalized maximum H_s remains steady along the shoreline from the model boundary to Weston-super-Mare on the south shoreline and Cardiff on the north shoreline for each scenario. This shows the wind has a sustained influence in propagating lower amplitude, longer period waves as far up estuary as Chepstow and Oldbury. Further up-estuary the channel begins to narrow and become increasingly shallow, and waves rapidly decay. There is a varying magnitude of normalized maximum H_s for each scenario with a 90th percentile value wind speed. There is over 1 m variability in normalized maximum H_s between scenarios forced by a 90th percentile value wind speed, as opposed to 0.01 m variability for scenarios forced by a 10th percentile value wind speed.

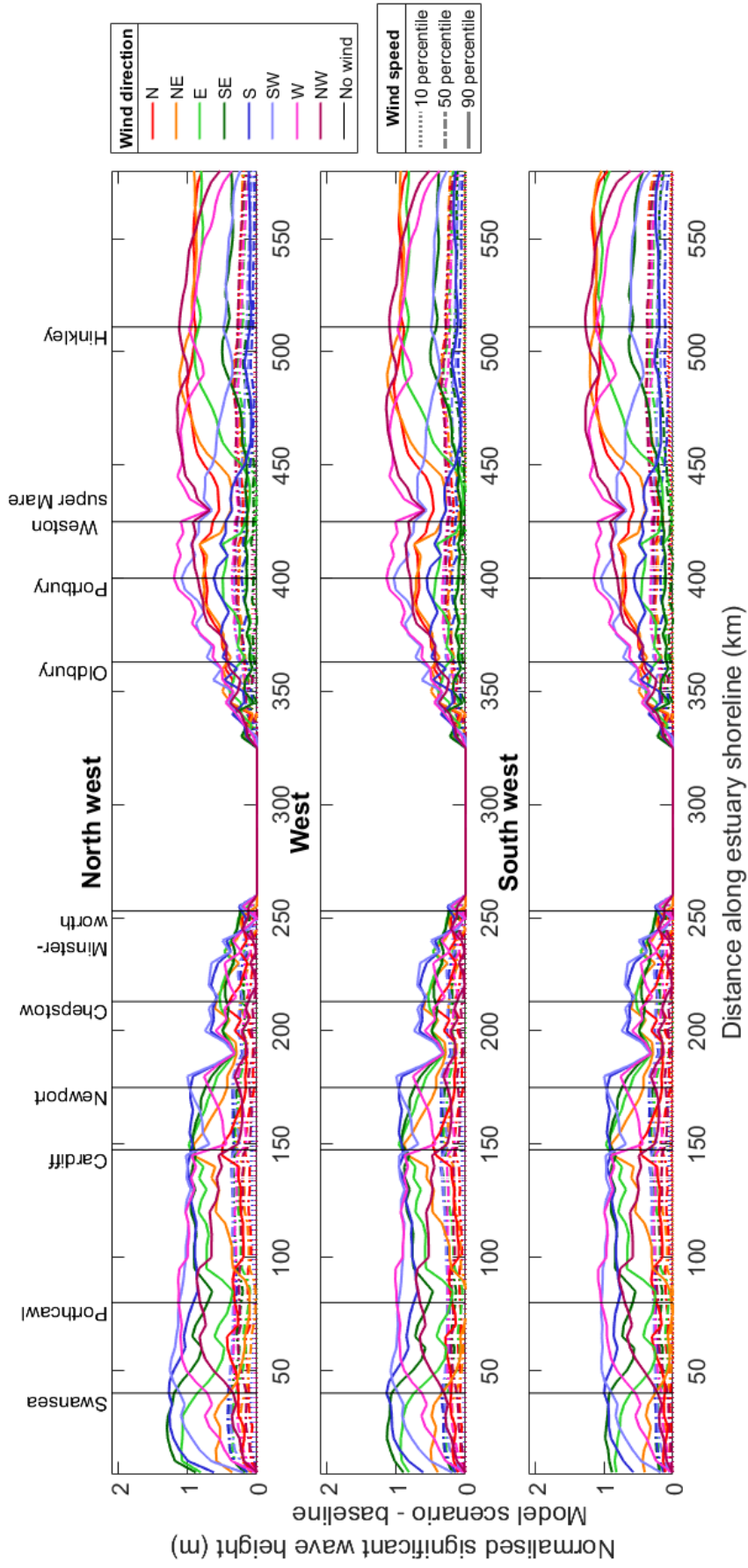


Figure 4.7: Normalized significant wave height (model scenario – no wind baseline scenario) for representative low amplitude, longer period waves along the shoreline of Severn Estuary, starting at Swansea to Gloucester and thence down-estuary towards Hinkley Point.

At Porthcawl, on the north shoreline of the estuary, maximum normalized H_s is 1.13 m with a NW wave and a following 90th percentile value wind speed from a W wind direction. The minimum normalized H_s for a NW wave under a 90th percentile value wind speed is 0.11 m, which occurs with a NE wind. This produces a range of 1.02 m on the north shoreline and shows that lower amplitude, longer period waves can propagate further up-estuary under stronger wind conditions.

In the same location on the north shoreline, normalized maximum H_s under a NW wave direction with a 10th percentile value wind speed is 0.04 m with a SE wind. The lowest normalized H_s produced by a 10th percentile value wind speed is 0 m for a NW wave and E wind. This produces a range of just 0.04 m for H_s at Porthcawl under the 10th percentile value wind speeds. The 0 m normalized H_s at Porthcawl under an E wind shows that the wind is having little effect on significant wave height under this scenario.

The results at Hinkley Point on the south shoreline in the outer estuary follow a similar pattern. The maximum normalized H_s at Hinkley Point is 1.27 m under a SW wave with a 90th percentile value wind speed from the NW. Minimum normalized H_s for a SW wave under a 90th percentile value wind speed is 0.2 m, which occurs with a S wind direction. This produces a range of 1.07 m on the south shoreline of the outer estuary. There is less sensitivity in normalized H_s under 10th percentile value wind speeds. Maximum normalized H_s under a 10th percentile value wind speed for a NW wave is 0.05 m, with a N wind and minimum normalized H_s is 0.01 m, also under a S wind producing a range of 0.04 m. A southerly wind produces the lowest H_s for all percentile value wind speeds, as the orientation of the coastline minimizes the effect of wind to contribute to H_s . Along the north and south shoreline, it is evident that higher period, low amplitude waves show greater sensitivity to wind direction for higher wind speeds.

4.5. Discussion

The results presented here help to identify the contribution of individual factors to variability in coastal wave hazard in a hyper-tidal estuary. Increased wave hazard along the shoreline may influence wave overtopping, which is an important consideration for port and harbour operations, energy infrastructure and residential communities in estuaries when considering direct flood hazard. The results can also help to understand how wave hazard may vary under future climate change, with varying storm tracks and wind conditions.

4.5.1. Younger, rougher seas show more sensitivity to wind direction.

The model highlights that short period, high amplitude waves are sensitive to wind direction, with a stronger, opposing wind increasing significant wave height. There is known to be a strong coupling and transfer of momentum between turbulent atmospheric and oceanic boundary layers. Increasing wind speed acts to increase the drag coefficient on the sea surface (Pugh, 2004), enhancing generation of

wind-waves (Janssen, 1989). The transfer of energy from the atmosphere to sea waves can be affected by sea state (Janssen 1989). Experimental results show that the drag coefficient over a younger, wind-wave sea is up to 50% larger than an older, swell sea (Donelan, 1982). Further to this, a Boussinesq type wave model has been used to show that wind waves are sensitive to changes in wind speed can amplify significant wave height, due to increased energy exchange between the air and sea (Liu et al., 2015). Stronger winds have been shown to be important in amplifying significant wave height in the Dee Estuary. Simulations of the wind-wave climate of the Dee Estuary under a 1 in 100-year storm under 5, 15 and 25 m/s wind speed show an increase in wave height and setup along the coast, which could contribute significantly to flooding (Wolf, 2007). Changes in the wind speed can alter wave conditions, resulting in local-scale changes in sea level at exposed sites.

The sensitivity of waves to wind direction can be site specific. Opposing winds can cause waves to become shorter and higher, and therefore steeper (Wolf et al., 2011). Steeper waves can cause unpredictable and unstable sea conditions, as seen in the mouth of the Colombia River when combined with strong, opposing river outflow which can make the region dangerous for shipping and boats (Elias et al., 2012). Strong, opposing winds blowing against incoming low amplitude waves can generate surface waves and tidal rips in the Bay of Fundy, Canada (Desplanque and Mossman 2004), resulting in dangerous sea conditions. As seen in Figure 4.6, each shoreline can respond differently to prevailing conditions with significant wave height occurring at different distances up-estuary. Simulations of locally wind-generated sea from westerly and northwesterly winds in the Dee Estuary, NW England show that significant wave height varies along the estuary shoreline due to the sheltering effect of West Hoyle Bank and the Welsh coastline and the effect of water depth on refraction (Wolf et al., 2011). Wind direction and speed can act to amplify significant wave height and subsequent wave hazard in hyper-tidal estuaries, and local bathymetry and topography can change influence the response of each shoreline to varying conditions.

4.5.2. Long period, low amplitude waves amplified due to strong winds

The model confirms that stronger wind speeds are important for increasing H_s for higher period, low amplitude waves throughout the estuary. The drag coefficient of air flow, related to shear stress of wind speed on sea surface, low amplitude, longer period waves, does not respond to the influence of shear stress to the same extent as younger, higher frequency wind waves (Brown and Wolf 2009). A fully developed wave field, such as a longer period, low amplitude wave, may receive little momentum from the air (Janssen 1989) and low amplitude waves exhibit less drag than both shoaling and breaking waves (Ancil and Donelan 1996). The drag coefficient in Delft3D-WAVE is linearly related to wind speed (Wu 1982), which may account for some of the effect of surface roughness due to wind. Increased variability in significant wave height for stronger wind speeds may be the effect of increasing wind speed on surface roughness and the drag coefficient, generating local winds on the sea surface

(Letchford and Zachry 2009). Long period waves propagate into the Severn Estuary throughout much of the year (Pye and Blott 2010), and contribute to significant wave heights during low pressure, winter storms (Sibley et al., 2015). Long period waves in the Bay of Fundy, Canada, are exacerbated by strong, southeasterly to southerly winds due to the orientation of the estuary (Desplanque and Mossman 1999). Strong southerly winds during the Saxby Gale, 4 October 1989 resulted in significant damage, as dykes breached, cattle and sheep drowned and railroad beds washed away and only when the wind shifted to a southwesterly direction did the waves cease to cause damage (Desplanque and Mossman 2004). However, certain areas in large estuaries can be sheltered from the effect of swell waves due to sheltering, e.g. in the Dee Estuary, NW England (Brown and Wolf 2009), or shallow water effects which cause extensive dispersion, as seen in San Francisco Bay (Talke and Stacey 2003). The model has shown that low amplitude, long period waves can propagate far up-estuary which disproves the assumption that up-estuary locations are only subject to storm surges and higher amplitude, locally generated wind waves (Lesser 2009; Monbaliu et al., 2014). The effect of low amplitude waves may create similar impacts as an energetic swell wave, which has a longer wavelength and lower frequency, to increase wave hazard along the shoreline (Palmer et al., 2014; Sibley et al., 2015). Further to this, stronger wind speeds superimpose locally generated waves on the sea surface, which can result in dangerous sea conditions for critical infrastructure, ports and harbours. Coastal defenses in hyper-tidal estuaries must be designed to protect against the effect of long period, low amplitude wind-waves as well as tides, storm surges and river flow.

4.5.3. Waves impact on flood hazard and economic activities

The results presented here show the effect of wind and wave properties on variability of significant wave height along the shoreline of the estuary and can be used as an evidence base to inform future coastal management decisions. Increased significant wave height under certain wind-wave conditions can pose a hazard in coastal areas due to wave run-up and defense overtopping (Bastidas et al., 2016) as individual waves exceed the available ‘freeboard’ (height above still water level) of coastal defences (Wolf 2009). The results can be applied to understand the wind-wave condition which could result in maximum significant wave height and subsequent wave overtopping in ports and harbours, which can influence the safety of structures and of people working and traveling immediately behind the defense line (Bouma et al., 2009; Diab et al., 2017). Low amplitudes waves, which can generate rough sea states under stronger winds in the estuary, can propagate into ports and harbours and cause excessive moored ship motions with consequences for operational downtime (Rosa-Santos and Taveira-Pinto 2013). Operational downtime has financial implications, as cargo handling cannot occur and the ship has to leave berth due to unsafe mooring conditions (Van Deyzen et al., 2015). Knowledge of the wind-wave conditions that can cause wave overtopping, transmission or swell wave propagation in the harbour can be used to divert ships away from port during hazardous conditions, to avoid damage to mooring lines or downtime. The hazards of wave overtopping are site specific, especially when people are concerned,

and dependent on estuary orientation, bathymetry and topography (Santana-Ceballos et al., 2017), characteristics of sea walls (Allsop et al., 2005) and the complex nature of wind-generated waves. Increased wavelength and wave period, as seen with swell waves, can also contribute to overtopping hazard as run-up is longer (Thompson et al., 2017), and should also be considered as a hazard in some estuaries. Understanding wave overtopping hazard from combined wind-wave effects can help to reduce economic losses from storm events in estuaries by avoiding operational downtime and damage to vessels and moorings.

The results presented here identify key combinations of wind-wave properties which contribute to wave hazard in a hyper-tidal estuary. While waves contribute towards total coastal water level by means of wave run-up, wave setup and swash (Stockdon et al., 2006; Wolf 2009), the effect of astronomical tides, atmospheric storm surges and river discharges must also be considered. Wave characteristics and propagation in shallow water is partially dependent on tidal elevation. Wave heights may also be related to surge magnitude, and wind has an important role in generating surge and waves (Pye and Blott 2014). Tidal modulation of waves plays a large part of the natural regime of the Severn Estuary (Fairley et al., 2014) and strong currents in the Bay of Fundy can generate tidal rips and hazardous surface waves (Desplanque and Mossman 1999). Future simulations of wind-wave conditions should include tide-surge propagation, evidently important in a hyper-tidal estuary, and the effect of wave hazard sensitivity on morphological response (Phillips et al., 2017), overtopping volumes, and depth and extent of subsequent flood inundation (Prime et al., 2015).

4.5.4. Changing future storm tracks and climate

The model results can also help to understand how wave hazard may develop under future, changing climate patterns, and the impact this may have on future flood inundation and adaptation strategies. It has been seen that maximum significant wave height varies within the estuary dependent on wind speed and wind direction, therefore stronger wind speeds and changing storm tracks under future climate could alter future flood risk from wave overtopping (EurOtop 2016). Changes in the number, frequency and track of mid-latitude (30-60 °) storm tracks would alter wind speed and direction, which would directly influence wave hazard in estuaries (Robins et al., 2016). Simulations of typhoon intensification in the Pearl Estuary has been shown to increase significant wave height, and results have been fed into design of seawalls (Yin et al., 2017). Increasing sea levels and river discharge will allow waves to propagate and impact further up-estuary, and are more likely to overtop sea defenses (Wolf 2007). Increasing frequency and magnitude of storms, or those occurring in clusters, will increase the occurrence of economic damage and potential loss of life across a larger spatial area (Robins et al., 2016). Further to this, changes in storminess have the potential to reduce the effectiveness of existing coastal defenses and result in more extensive and damaging floods (Phillips 2008). Large scale atmospheric changes, such as the North Atlantic and Southern Oscillations, could also result in changes

in wind speed and direction, which will have implications for where maximum significant wave heights will occur, with potential implications in the Severn Estuary and Bay of Fundy (Phillips et al., 2013). However wave hazard under future climate will vary depending on regional- and local-scale processes, strong natural variability and uncertainty in anthropogenic forcing and future wave climate (Woolf and Wolf, 2013; Haigh and Nicholls, 2017). Regional-scale simulations of wind-wave conditions in an estuarine system can identify important processes and interactions which may be effected under future climate. The methodology and results presented here can aid long-term coastal defense and management strategies, as sustainable coastal management requires confidence in the knowledge of any possible future changes to wave hazard.

4.6. Conclusion

There is a need to identify key combinations of wind-wave characteristics which contribute to wave hazard and the relative significance of wind-generated waves compared with swell waves in heavily populated and industrialized hyper-tidal estuaries, where critical infrastructure must be designed to withstand this hazard. Delft3D-WAVE is used to simulate wave evolution in a hyper-tidal estuary to identify key combinations of wind-wave characteristics which contribute to maximum significant wave height, and subsequent wave hazard throughout the estuary. Long-term wind and wave records are used to generate representative wind-wave conditions, and consider the influence of wind speed, wind direction, wave type and wave direction on maximum significant wave height along the shoreline of the Severn Estuary, SW England. Results show that a younger, rougher wind-wave sea, characterized by low period, high amplitude waves, show increased sensitivity to wind direction. Stronger, opposing winds generate maximum significant wave height in the outer estuary. Maximum significant wave height occurs at different locations up-estuary along each shoreline due to estuary orientation and local bathymetric effects. Higher period, low amplitude waves show greatest sensitivity to wind direction under stronger wind speeds, as local wind-generated waves are superimposed. The model highlights how different wind-wave conditions vary in the estuary, and stronger winds amplify and facilitate the propagation of long period, low amplitude further up-estuary under all conditions to impact infrastructure along the shoreline. The research helps to inform sea defense design to withstand wave overtopping under a range of conditions, minimize economic losses from operational downtime in ports and harbours due to wave transmission and inform long-term coastal management of the potential implications of future climate changes on wave hazard in the estuary. Future work needs to consider the effect of tide and surge on wave propagation, and results from fully coupled tide-surge-wind-wave models can force inundation models to explore depth and extent of flooding from severe storm events.

4.7. Acknowledgements and Data

The authors thank colleagues at the British Oceanographic Data Centre (BODC) for providing tidal data; Magnox for providing tidal data; Environment Agency for providing tidal data; Gloucester Harbour Trustees for providing tidal data; UK Met Office for providing observational wind data; CEFAS for providing observational wave buoy data; EDINA for providing bathymetric data; and Judith Wolf at the National Oceanography Centre Liverpool for constructive comments on analysis of the wave buoy record.

5. Quantification of the uncertainty in coastal storm hazard predictions due to wave-current interaction and wind forcing

Chapter 5 progresses the modelling work further to utilize the full functionality of Delft3D by coupling the FLOW with WAVE modules together, and incorporating a time- and space-varying wind and atmospheric pressure field. Maximum significant wave height is statistically validated at four wave buoy locations within the estuary to ensure this model setup can simulate tide-surge-wind-wave-river interaction with confidence. Chapter 5 quantifies uncertainty in maximum significant wave height, total water level and hazard proxy (water level + $\frac{1}{2}$ significant wave height) when interactions between combined hazards or local effects of atmospheric forcing are neglected. The results can help to ensure accurate forecasts to mitigate negative consequences of combined hazards, and ensure flood alerts, warnings and evacuation orders are timely.

5.1. Abstract

Coastal flood warning and design of coastal protection schemes rely on accurate estimations of water level and waves during hurricanes and violent storms. These estimations frequently use numerical models which, for computational reasons, neglect the interaction between the hydrodynamic and wave fields. Here, we show that neglecting such interactions, or local effects of atmospheric forcing, causes large uncertainties, which could have financial and operational consequences because flood warnings are potentially missed or protection schemes under-designed. Using the Severn Estuary, SW England we show that exclusion of locally generated winds underestimates high water significant wave height by up to 90.1%, high water level by 1.5% and hazard proxy (water level + $\frac{1}{2}$ significant wave height) by 9.1%. The uncertainty in water level and waves is quantified using a system to model tide-surge-wave conditions, Delft3D-FLOW-WAVE in a series of eight model simulations for four historic storm events.

5.2. Introduction

Concurrence of astronomical high tides, meteorological storm surge due to hurricanes, cyclones or mid-latitude storms, energetic waves, and strong winds can cause coastal flooding, and subsequent damage to property and loss of life to some of the 600 million people estimated to live in low-lying coastal (<10 m) regions worldwide (Barnard et al., 2019; Wolf 2009). The devastating effects of concurrent coastal hazards are well documented in hyper-tidal regions, where tidal range exceeds 6 m, in the Severn Estuary, UK (Sibley et al., 2015), Bay of Fundy (Greenberg et al., 2012) and Yangtze Estuary (Yin et al., 2017), as combined storm parameters can enhance high water level (HWL) and high water significant wave height (HWH_s), defined as significant wave height at the time of high water, to increase the likelihood of overtopping and subsequent inundation. Increasing coastal population and urbanization, potential future changes in storm tracks and sea-level rise means there is a need to plan for the negative consequences of coastal hazards.

Operational storm surge and wave forecasts are important components of coastal storm hazard mitigation strategies (Tunstall et al., 2004). If operational forecasts exceed pre-defined threshold levels, corresponding to the minimum wave and total water level that represent a potential flood hazard (Del Río et al., 2012), alerts and flood warnings will be issued to detail scale, timing and location of a hazard (Lawless et al., 2016). To prevent negative consequences of forecast extreme storm events, flood warnings issued by local agencies must be accurate and timely. Operational forecasts can make use of measured and modelled meteorological and oceanic data (e.g. O'Neill et al., 2016) and outputs can be used to estimate likelihood of coastal flooding, and the effect of wind, waves and total water level on overtopping and breaching for specific flood events (Quinn et al., 2014). However error can be introduced into operational forecasts due to model, knowledge and data uncertainty (Stephens et al.,

2017). Uncertainty due to a model's ability to accurately represent physical processes or replicate interactions (e.g. Bolaños et al., 2014), lack of knowledge of interactions in a physical system and inaccurate input parameters (e.g. temporally or spatially limited) can be introduced, and propagated through the modelling chain to inundation assessments and flood warnings (Sayers et al., 2003). There is a need to understand and reduce uncertainty in operational forecasts of HWL and HWH_s that contribute to hazard assessments. Uncertainty in operational forecasts could mean flood events are underestimated or missed, which may increase the risk to coastal communities and critical infrastructure.

The accurate definition of HWL and HWH_s is also important for critical storm threshold identification for the design of cost-effective coastal protection strategies. Implementation of hard structures or nature-based solutions, which aim to mitigate the effects of HWL and HWH_s, rely on a thorough understanding of the physical processes and interactions in a region (Conger and Chang 2019). The type and costs of new schemes largely depend on the physical conditions at the site, and sensitivity of the scheme to natural processes and their interaction (Temmerman et al., 2013). Uncertainty in HWL and HWH_s may lead to incorrect hazard thresholds, as defense exceedance is most likely to occur close to the time of high water, or implementation of strategies which are not able to protect hinterlands against normal winter conditions as well as extreme storm tide conditions. Commitment to upgrading engineered structures, such as Canada's recent US\$114 million pledge to upgrade 64 km of dikes and sluices in Nova Scotia (Fairclough 2019), or implementing new strategies, e.g. the new £63 million seawall at Rossall, Lancashire (Environment Agency 2018) are based on multi-disciplinary, cost-benefit analysis in areas with highest potential for protection benefits. Representative, site-specific information of HWL and HWH_s are needed to support decisions to ensure crest level and defense heights are appropriate, for effective storm hazard mitigation and resilience to future change.

5.2.1. Case Study

This research focuses on the Severn Estuary (Figure 5.1a), which borders south Wales and southwest England, as an example of hyper-tidal and funnel shaped estuaries worldwide. The estuary has the third largest mean spring tidal range in the world, up to 12.2 m at Avonmouth due to the funnelling effect (Dyer 1995), which is also known to modulate the local wave climate (Pye and Blott 2010). The orientation of the mouth of the estuary to the Atlantic Ocean means it is exposed to prevailing swell waves, and the large fetch (up to 6000 km) amplifies wave driven hazards in the outer estuary. The south coastline of the estuary is dominated by energy and port infrastructure and large areas of low-lying agricultural land, highlighting the need for accurate operational forecasts in this region.

5.2.2. Outline of the paper

This research quantifies the sensitivity of HWL, HWH_s and high water hazard proxies (HWHP) to model coupling along the Severn Estuary coastline. Hazard proxy (HP) is defined as the $WL + \frac{1}{2} H_s$ and is used to understand the severity of a condition. 32 model simulations are run in total; a series of eight model simulations are run for four events which represent a potential hazard in Delft3D-FLOW-WAVE. The model is applied to consider waves and circulation in isolation (standalone), the influence of circulation on waves (one-way coupled) and the influence of the circulation on the waves and waves on the circulation (two-way coupled). Wind and atmospheric pressure are included on four of the eight model simulations to investigate wind influence on HWL and HWH_s during storms. Water level (WL), significant wave height (H_s) and HP are simulated to explore the sensitivity of each parameter to model coupling (section 2), and the results (section 3) quantify uncertainty introduced into the model due to the coupling and forcing processes. Before concluding in section 5, section 4 discusses the importance of locally generated winds and coupling processes in simulating H_s and HP in hyper-tidal estuaries, and the implications that uncertainty in storm parameters have on flood warnings and management activities.

5.3. Method

5.3.1. Delft3D hindcast of select historic events

The Delft3D modelling system (Lesser et al., 2004) was used to simulate tide-surge-wave propagation across the Severn Estuary for four historic storm events. Delft3D-FLOW simulates hydrodynamic flow under the shallow water assumption, and Delft3D-WAVE simulates the generation and propagation of waves, based on the third-generation spectral wave model Simulating WAVes Nearshore (SWAN), which solves the spectral action balance (Booij et al., 1999). A 2D-horizontal, curvilinear grid of the Severn Estuary extends from Woolacombe, Devon and Rhossili, South Wales in the west, with a maximum resolution of 5 km, to Gloucester in the east with a minimum resolution of 25 m at the coast, to resolve fine-scale processes in shallow water (Figure 5.1a), and has been validated in Lyddon et al., 2018a; 2018b; 2019a. Gridded bathymetry data at 50 m resolution (SeaZone Solutions Ltd. 2013) was interpolated over the 2DH curvilinear grid. Delft3D-FLOW has two open boundaries forced by time-varying, spatially uniform water level, representing the Atlantic Ocean to the west and the River Severn to the east. Delft3D-WAVE was forced with five, space- and time-varying boundary points to the west. Delft3D-WAVE explicitly represents the dissipation of wave energy due to white-capping, bottom friction and depth-induced breaking, and wave generation by wind, and non-linear wave-wave interactions (Deltares 2014b).

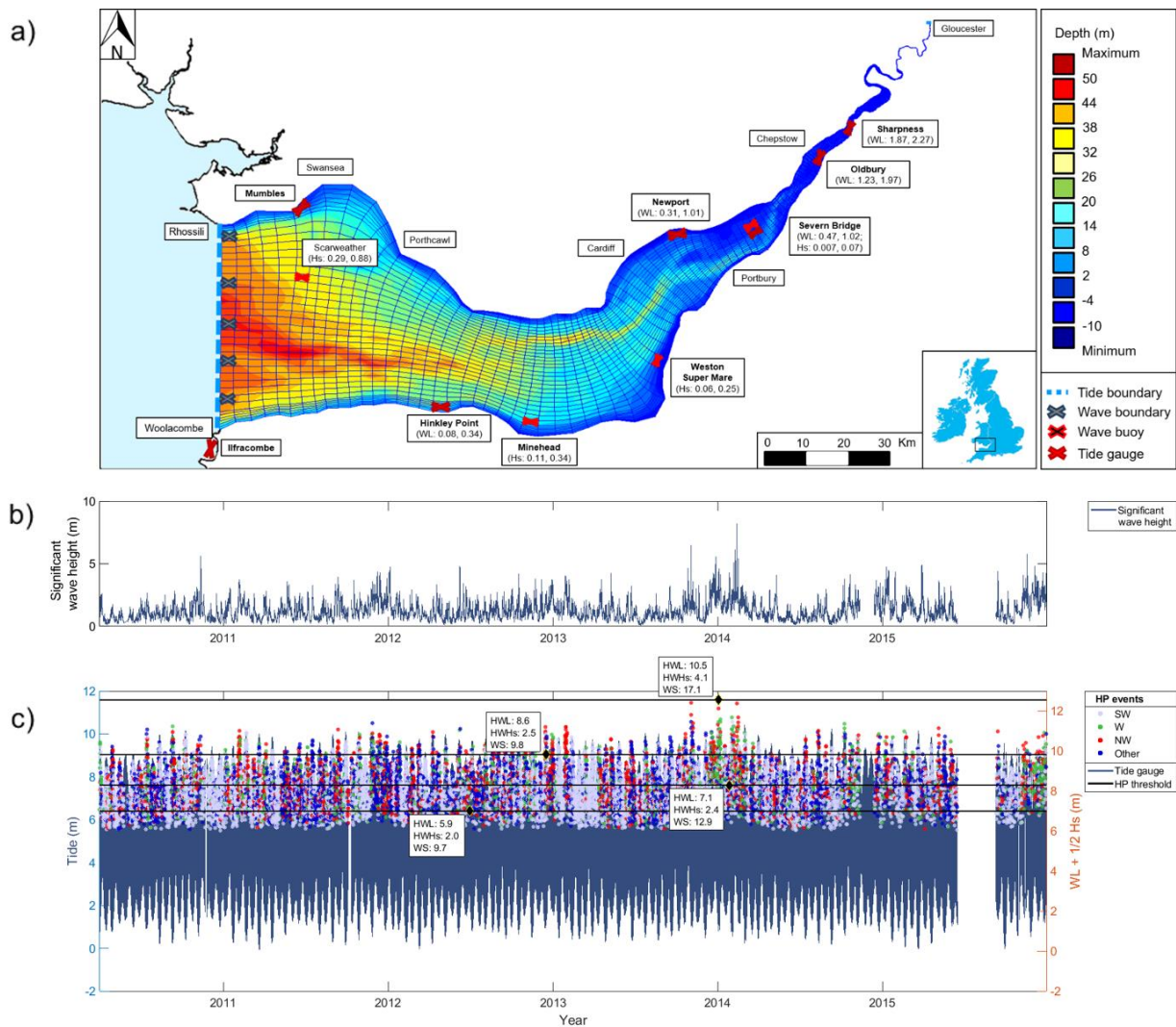


Figure 5.1: a) Delft3D-FLOW-WAVE model domain. Bathymetry relative to CD. Average bias and RMSE (m) of WL and H_s model results for four events to tide gauge and wave buoy observations are shown in brackets; (b) six year H_s record from Scarweather wave buoy; (c) Long-term tide gauge record taken from Ilfracombe, with HWHP grouped based on wind direction at the time of the event. HWL, HWH_s, and wind speed (WS) at the time of the events are shown. Horizontal black lines indicate maximum, 90th, 50th and 10th percentile HP thresholds.

Six years of H_s data from the Scarweather Directional Waverider buoy (Figure 5.1b) (Cefas, 2019) and tide gauge data at Ilfracombe (NTSLF, 2019) were used to identify historical coastal flood and wave hazard events. H_s was isolated when the tide is at or above 5.91 m (the level of lowest high water level in the record), to leave only wave events when overtopping is most likely to have occurred (see Figure 1c). This was used to calculate HP for concurrent water level and wave conditions exceeding this threshold (see colored dots in Figure 5.1c). Each HP event represents a real event with hazard potential, and was grouped according to the concurrent wind direction, using data from the Met Office weather station at Pembrey Sands (CEDA, 2018). Winds from a southwest and west direction have been shown

to generate maximum H_s and contribute to greatest wave hazard in the estuary (Lyddon et al., 2019a). Four events with a southwest and west wind direction were selected, which represent the maximum (3 January 2014, 07:00), 90th (16 December 2012, 19:00), 50th (26 January 2014, 01:00) and 10th percentile (30 June 2012, 12:00) HP thresholds (Figure 5.1c).

The open sea boundary to the west was forced with a time-varying, spatially uniform water level at a 15 minute interval using observation data from Ilfracombe tide gauge (NTSLF, 2018). For WAVE standalone simulations, a constant WL was applied at the open sea boundary, at the level of HWL during the selected event, to eliminate the effect of tidal currents on H_s and variability in WL. Time- and space-varying wave conditions (H_s , wave direction, mean period and directional spread) from the Met Office WAVEWATCH III hindcast (Saulter et al., 2016; Siddorn et al., 2016) were used at five equidistant points along the open sea boundary (see Figure 5.1a), and were linearly interpolated along the boundary to force the model at 15-minute intervals. A time- and space-varying wind and atmospheric pressure field forced the model domain at hourly intervals, using data originating from the Met Office global unified model (Walters et al., 2014) and extracted from the Extended Area Continental Shelf Model CS3X (Williams and Horsburgh 2013). All simulations were forced with 15-minute river gauge data from Sandhurst (Environment Agency, 2016) at an up-estuary open boundary (see Figure 5.1a).

5.3.2. Model validation and scenario test

Model outputs from two-way coupling of Delft3D-FLOW-WAVE, which represents a complete five-way multi-hazard simulation (tide-surge-wind-wave-river), for the four events were validated at five tide gauge locations (Hinkley Point, Newport, Severn Bridge, Oldbury, Sharpness) and four wave buoy locations (Scarweather, Minehead, Weston-super-Mare, Severn Bridge). Average bias and root mean squared error (RMSE) of WL and H_s were calculated at validation locations (see Figure 5.1a). The bias is defined as:

$$Bias = \bar{M} - \bar{O} \quad (1)$$

where M represents the model values, O the observed values and the overbar denotes the mean value of the simulated storm event. A value of 0 indicates an unbiased estimate; a positive value indicates the model is over-predicting; a negative value is under-prediction. The RMSE is defined as:

$$RMSE = \sqrt{(M - O)^2} \quad (2)$$

where a value closer to zero indicates better model performance.

There is good agreement for WL in outer estuary. Hinkley Point has a bias value of 0.08 m and RMSE of 0.34 m, which represents 2.75% of the observed tidal range during the maximum event. Positive bias

and larger RMSE values up-estuary indicate the model overestimates WL at Oldbury and Sharpness. H_s is well reproduced, as bias and RMSE values remain close to zero. Wave data used for validation are available along the southern estuarine coastline, where areas of critical energy infrastructure are located highlighting the importance of accurately representing H_s in this region.

The validated Delft3D-FLOW and WAVE model was run from 48 hours before the event to 12 hours after, in a series of eight standalone, one-way or two-way coupled simulations. Delft3D-FLOW and WAVE can run in ‘standalone’ mode with user-defined properties (Deltares 2014b). Delft3D-WAVE is used in one-way coupled simulations where the FLOW simulation is completed and then input (offline) into the wave simulation, to account for the effect of flow on waves. Two-way coupled simulations allow dynamic (online) interaction of Delft3D-WAVE with FLOW to account for the effect of waves on current, and the effect of current on waves. The FLOW and WAVE modules exchange information at 15-minute intervals, such as wave radiation stresses and water level conditions needed for wave transformation, to represent two-way wave-current interaction, refraction and depth-induced breaking. The influence of wind is considered in both FLOW and WAVE when included, to represent changing forcing processes. Eight model runs were completed for each of the four historical HP events (32 in total) to explore how model coupling and forcing processes contribute to uncertainty in HWL, HWH_s, and HWHP (Table 51).

Table 5.1: Eight model simulations completed in Delft3D-FLOW-WAVE for each historic storm event.

Run	Model	Coupling	Forcing
1	FLOW	Standalone	Water level
2	FLOW	Standalone	Water level + wind
3	WAVE	Standalone	Constant HW water level + Wave
4	WAVE	Standalone	Constant HW water level + Wave + wind
5	FLOW → WAVE	One-way	Water level from 1 + wave
6	FLOW → WAVE	One-way	Water level from 2 + wave + wind
7	FLOW ↔ WAVE	Two-way	Water level + wave
8	FLOW ↔ WAVE	Two-way	Water level + wave + wind

The maximum, mean and median percentage difference in HWL, HWH_s, and HWHP were calculated between each model run and model run 8 as:

$$\text{Percentage difference} = \frac{(\text{Run } 8 - \text{Run } X)}{\text{Run } 8} \times 100 \quad (3)$$

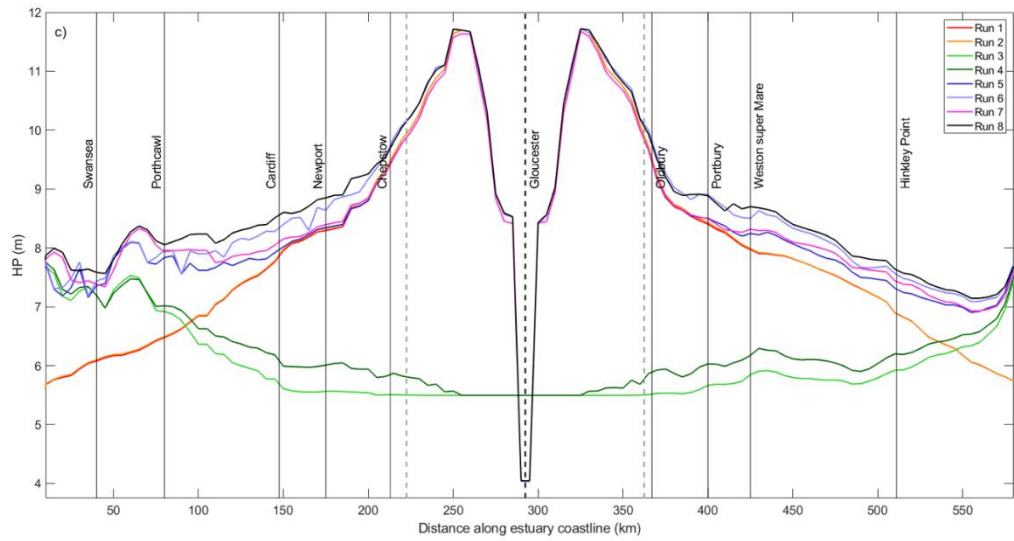
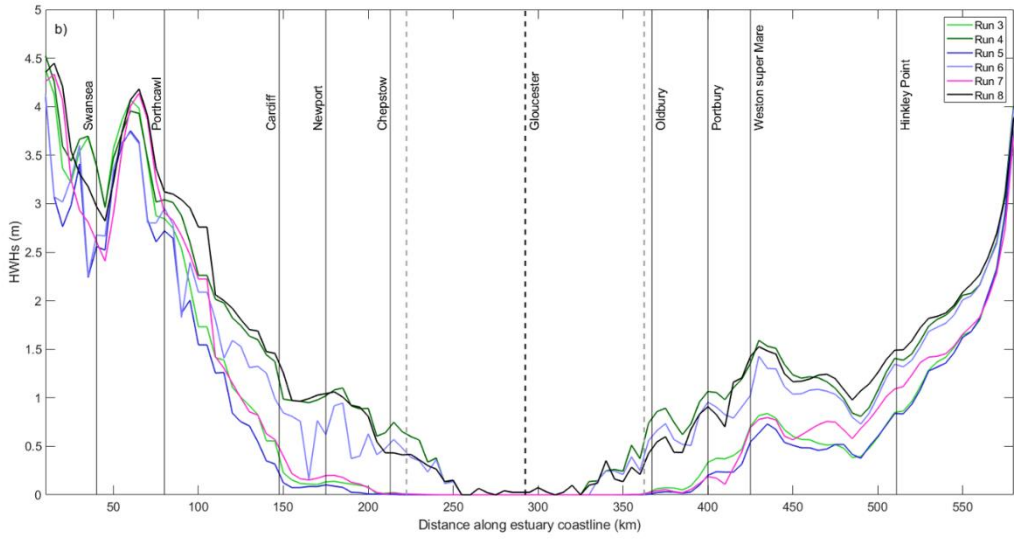
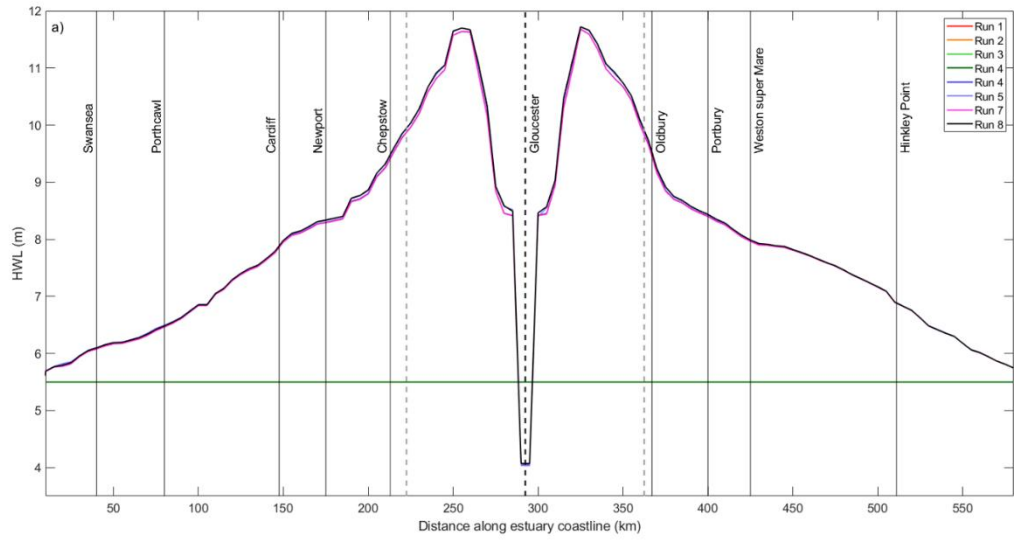
Run 8 is used as the baseline run as it includes all boundary forcing, and has been successfully validated to observational tide and wave data in the estuary. Model results are presented as the % and absolute

difference between each run and the validated run 8 for the north and south coastline to i) identify which coupling HWL, HWH_s and HWHP are most sensitive to and ii) quantify uncertainty introduced into the model due to omitting coupling and forcing processes.

5.4. Results

HWL and HWH_s were extracted from model results every 5 km, from the second row of grid cells in, along the estuary coastline, and HWHP calculated, for each event. Results of the maximum event (3 January 2014) are seen in Figure 5.2a-c. HWL (Figure 5.2a) is amplified to a maximum of 11.7 m up-estuary, beyond Newport and Oldbury, due to the funnelling effect (Uncles 1984). HWH_s (Figure 5.2b) is greatest in the outer estuary near Swansea and Porthcawl. HWH_s dissipates up-estuary but shows greater sensitivity to coupling and forcing processes. HWHP (Figure 5.2c) is greatest up-estuary, and shows greatest sensitivity to model coupling and forcing in the outer estuary.

The cumulative effect of wave dissipation as energy propagates up-estuary, i.e. increased white capping as waves steepen and depth-induced breaking and up-estuary cross-section friction, dampens the hazard, therefore analyses are focused in areas where water level and waves are largest, in the lower- and mid-estuary. Maximum, mean and median percentage difference in HWL, HWH_s and HWHP between each run with run 8 (solid black line in Figure 5.2a-c) is calculated for sections of the estuary coastline up to the point where $H_s < 10$ cm in all simulations, termed the wave limit, to focus on the impact on non-negligible wave conditions (Figure 5.2d-f).



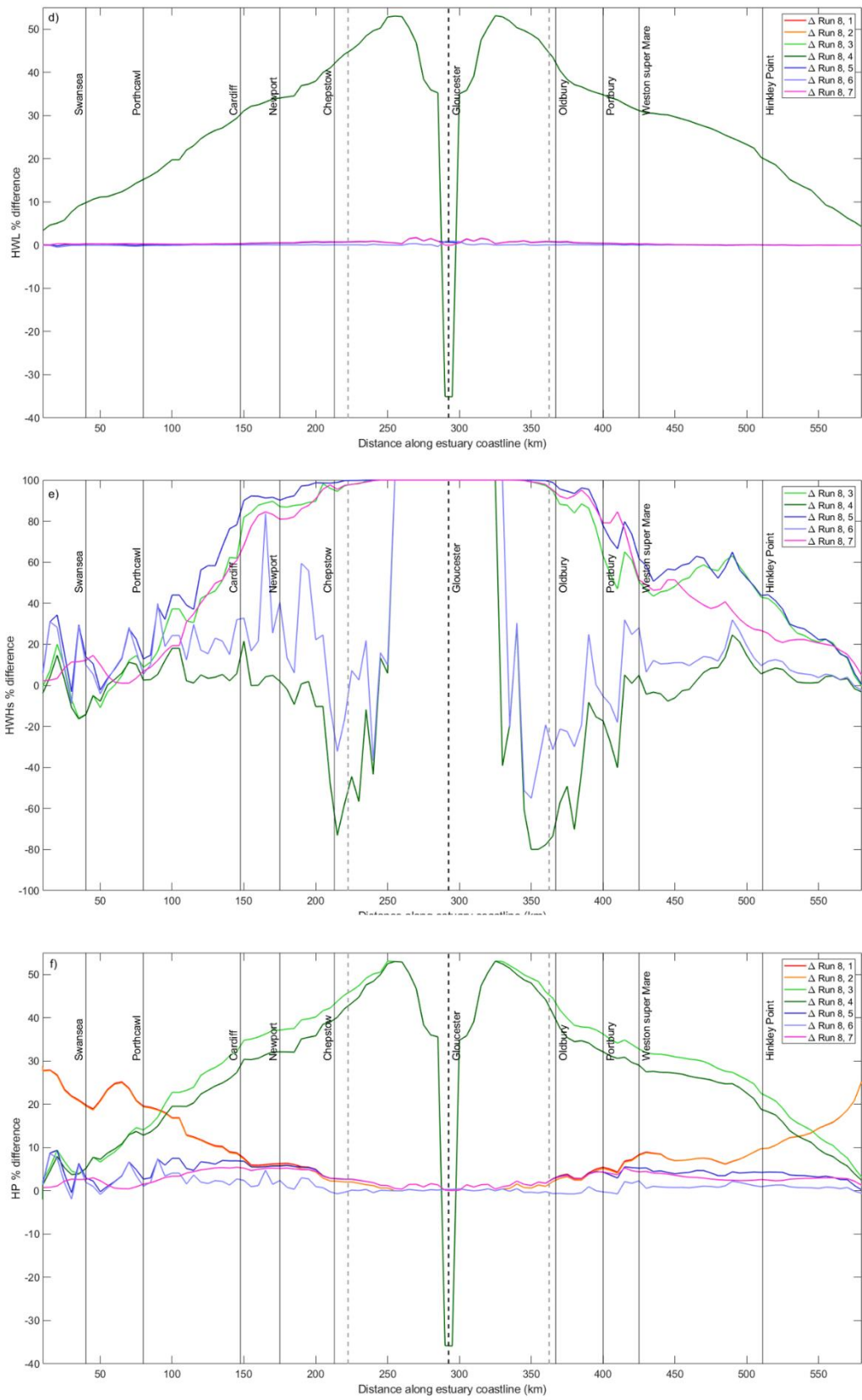


Figure 5.2: Simulated a) HWL; b) HWH_s; c) HWHP along the coastline of Severn Estuary starting at Swansea to Gloucester and thence down-estuary towards Woolacombe for maximum event (3 January

2014 07:00); d-f) % difference between each run and run 8. The divide between north and south coastlines (dashed black vertical line) and wave limit where $H_s < 10$ cm (dashed grey vertical line) is shown. Solid black vertical lines indicate locations of critical infrastructure and coastal towns.

Absolute differences in HWL, HWH_s and HWHP between each run with run 8 along the coastline are shown in Figure 5.3. Run 3 and 4 greatly underestimate HWL as a constant water level at MHWST is applied throughout the model domain, and no funnelling of the tidal wave to amplify tidal range up-estuary occurs. Up to 6.2 m difference in HWL occurs in the upper estuary between runs 4 and 8. Runs 1, 2 and 7 show small changes in absolute HWL occur in outer estuary, and increase up-estuary from Cardiff and Portbury as the estuary begins to narrow. 0.18 m difference occurs 270 km up-estuary, beyond the wave limit, between run 7 and 1. This represents 2% of the tidal range, but could make a substantial difference in coastline response models up-estuary if combined with strong winds, large waves or substantial river discharge.

The largest absolute differences in HWH_s occur in the outer estuary, on the north coastline, from the boundary to Newport. The greatest difference is 1.44 m, which occurs 20 km up-estuary near Swansea, between run 5 and 8. These large differences may indicate that coastlines facing into the direction of prevailing storm conditions are more sensitive to more severe storm events, or may be the effect of the complex geometry of the coastline. Run 7, which includes two-way coupling, shows least variability in the outer estuary. The absolute difference in HWH_s is reduced in the mid- and upper-estuary as the cumulative effect of shallow water processes (whitecapping, bottom friction) dampen wave height. Up to 0.8 m difference can be seen on the south coastline near Weston-super-Mare and Portbury, which could have an impact on inundation, overtopping, erosion. The greatest difference in the mid- and upper-estuary occurs between simulations which do not include local atmospheric forcing.

Runs 1 and 2 underestimate HWHP in the outer estuary, up to a maximum 2.2 m 15 km up-estuary on the north coastline. Wave coupling is excluded from these runs, and highlights the importance of coupling for hazard prediction in the outer estuary. Runs 1 and 2 do not underestimate HWHP to such an extent up-estuary of Cardiff and Weston-super-Mare. Runs 3 and 4 greatly underestimate HWHP, up to 6.2 m up-estuary as the funnelling effect of the tide is excluded.

Similar to HWH_s , HWHP shows greatest difference in the outer estuary on the north coastline for run 5 and 6. Run 7 shows least variability, which includes two-way coupling. The greatest difference is 0.71 m, 20 km up-estuary between run 5 and 8. The greatest difference on the south coastline is smaller compared to the north coastline, at 0.48 m, 165 km up-estuary between Weston-super-Mare and Portbury between run 5 and 8. The difference between run 7 and 8 at this point on the south coastline is similar in magnitude, 0.46 m. This indicates the importance of local atmospheric forcing in coastal

hazard predictions, but also highlights that estuary orientation and sheltering effects on the south coastline can influence hazards.

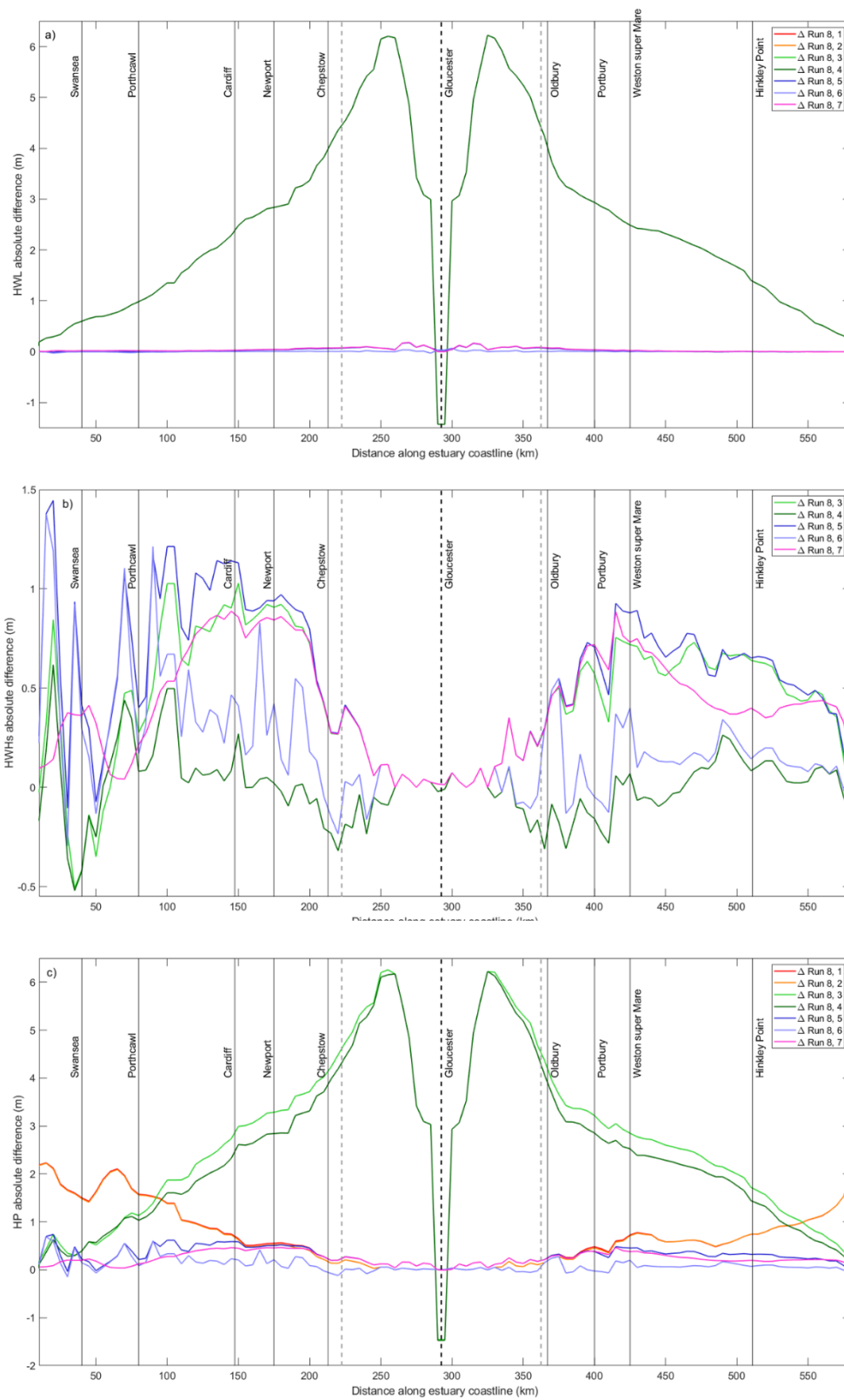


Figure 5.3: Absolute difference for a) HWL; b) HWH_s; c) HWHP between each run and run 8 along the coastline of Severn Estuary starting at Swansea to Gloucester and thence down-estuary towards Hinkley Point for maximum event (3 January 2014 07:00). The divide between north and south coastlines (dashed black vertical line) and wave limit where $H_s < 10$ cm (dashed grey vertical line) is shown. Solid black vertical lines indicate locations of critical infrastructure and towns along the coastline.

Alongshore maximum, mean and median % difference relative to run 8 for HWL, HWH_s and HWHP are presented for the north (Figure 5.4a, left panels) and south (Figure 5.4b, right panels) coastline for each event up to the wave limit ($H_s < 10$ cm), to identify the model's response to coupling processes.

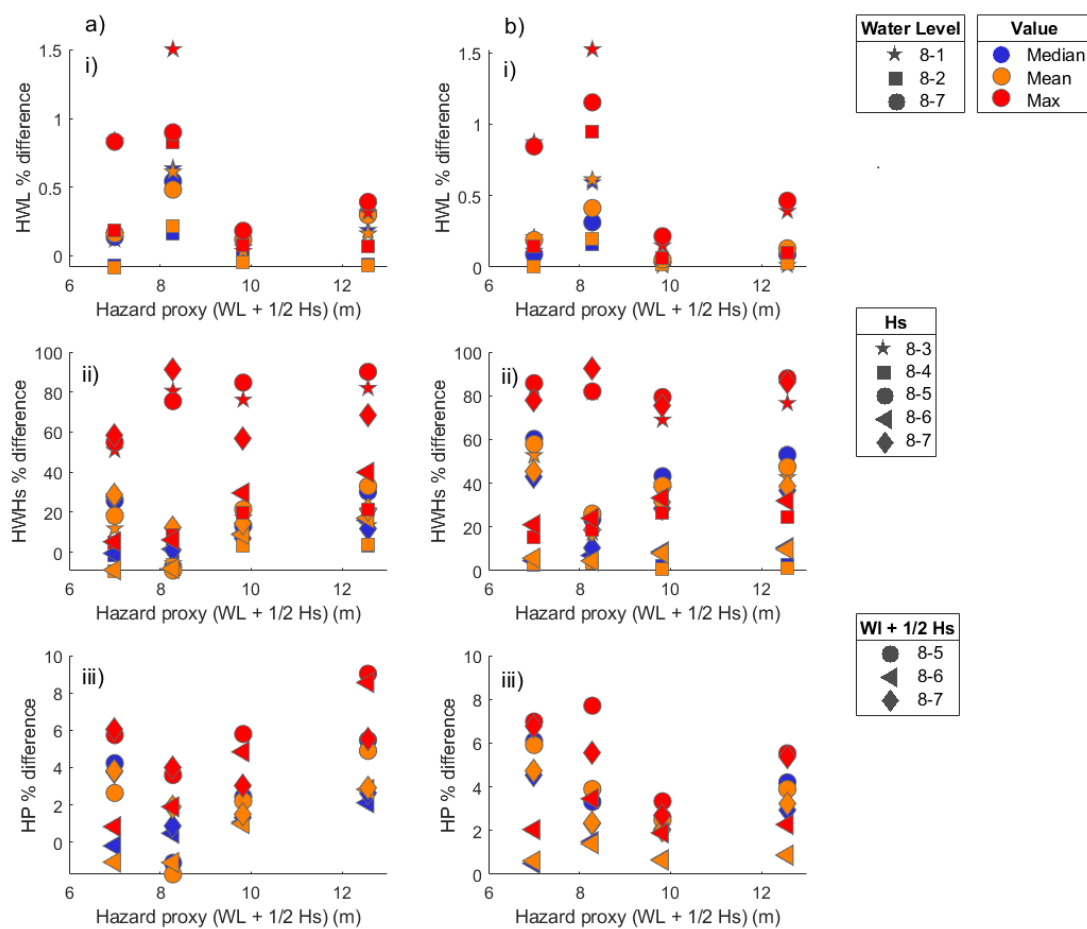


Figure 5.4: For the a) north (left panels) and b) south (right panels) coastlines the alongshore maximum, mean and median percentage difference in i) HWL; ii) HWH_s; iii) HWHP between model simulations is calculated for the four events with hazard potential calculated using the HP parameter.

5.4.1. Uncertainty in High Water Level (HWL)

Run 3 and 4 are simulated with a constant water level at MHWST throughout the model domain, and no funnelling of the tidal wave to amplify tidal range up-estuary occurs (Figure 5.2a). Up-estuary %

difference exceeds 50%, therefore these are excluded from Figure 5.4 and 5.5 to avoid masking other results. Run 5 and 6 use the model outputs from Run 1 and 2, and are excluded to avoid repetition.

The model shows that runs 1 and 7 generate maximum % difference in HWL along the north and south coastline for all events up to the wave limit, regardless of event severity. Maximum % difference in HWL is 1.5% between run 8 and 1 for the 50 percentile event, which also represents maximum absolute difference of 0.046 m (Figure 5.5a). This absolute difference is < 1% of the maximum tidal range. The 90th percentile event shows the least sensitivity to model coupling, where the range in maximum % difference is 0.42% on the north coastline and 0.38% on the south coastline. Run 2 generates the smallest percentage difference in HWL along the north and south coastline for all events, indicating locally generated winds are more important than coupling processes when simulating water level, however the differences remain small.

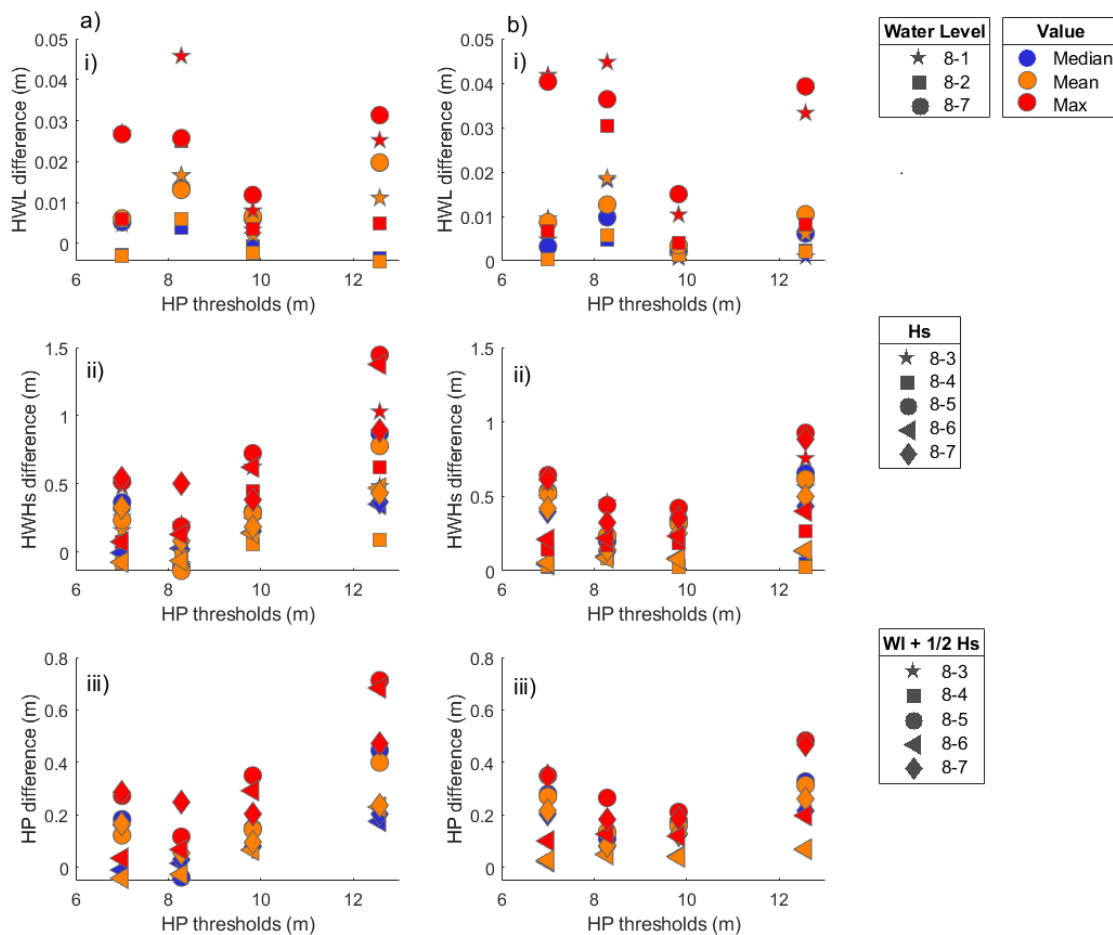


Figure 5.5: For the a) north (left panels) and b) south (right panels) coastlines the alongshore maximum, mean and median absolute difference in i) HWL; ii) HWH_s; iii) HWHP between model simulations is calculated for the four events with hazard potential calculated using the HP parameter.

5.4.2. Uncertainty in High Water Significant Wave Height (HWH_s)

Increasing HP threshold increases the % and absolute difference in HWH_s on the north coastline, but this trend is less clear on the south coastline (Figure 5.4ii). The model highlights up to 90.1% maximum difference in HWH_s 150 km up-estuary, near Cardiff, which represents 1.13 m, between run 5 and 8 for Jan 14.

The maximum absolute difference in HWH_s is 1.45 m between runs 5 and 8, which occurs just 20 km up-estuary west of Swansea, and represents a 34.4% difference for Jan 14. The geometry of the north coastline means some stretches of coastline have a more exposed west facing aspect as waves are generated and propagate towards the coast contributing to increased sensitivity to incoming storms with a west-southwest wind direction.

Runs 4 (standalone) and 6 (one-way) include local atmospheric forcing and generate a closer representation of HWH_s compared to run 8, with a 39.9% maximum difference. Run 4 and 6 generate a range of -9.2 to 17% mean difference for all events. -51.2% % difference occurs between run 8 and 6, which represents 0.48 m, in shallow, sheltered regions (e.g. Swansea Bay and Cardiff Bay) on the north coastline (Figure 5.6b) where the one-way simulation generates larger HWH_s than two-way simulation.

Figure 5.6 shows the % difference in HWH_s across the estuary domain for the 50th percentile event (26 January 2014 01:00). The % difference in HWH_s between run 8 (two-way + wind) and simulation 7 (two-way) (Figure 5.6a) highlights substantial differences in HWH_s up-estuary of the wave limit without locally generated winds. For a domain this size, it is important to continue to add momentum to the system via atmospheric forcing, to accurately simulate up-estuary HWH_s. Figure 5.6b shows difference in HWH_s between simulation 8 (two-way + wind) and 6 (one-way + wind), which represent the two more complex model setups. Each coastline shows a different response to coupling processes; the model shows up to -27% differences in HWH_s in shallow, sheltered regions (e.g. Swansea Bay and Cardiff Bay on the north coastline) and up-estuary of the wave limit, and over 20% difference along the south coastline. The water level does not noticeably change between the simulations; therefore larger HWH_s in the one-way simulation is unlikely to be due to a change in wave breaking. Further to this, wind stress does not change between simulations and so the difference in HWH_s is unlikely to be attributed to whitecapping. Run 6 generates smaller depth-averaged current velocity near Swansea Bay and Cardiff Bay on the north coastline than simulation 8 (Figure 5.6c), with up to 95% maximum difference. The waves, which are approaching from 250-266° during high water for this event, are approaching the north coastline from west-southwest and the one-way simulation is not accurately refracting the waves around the coastline and upper channels. Two-way simulations can help to represent current refraction in shallow regions to ensure accurate HWH_s predictions.

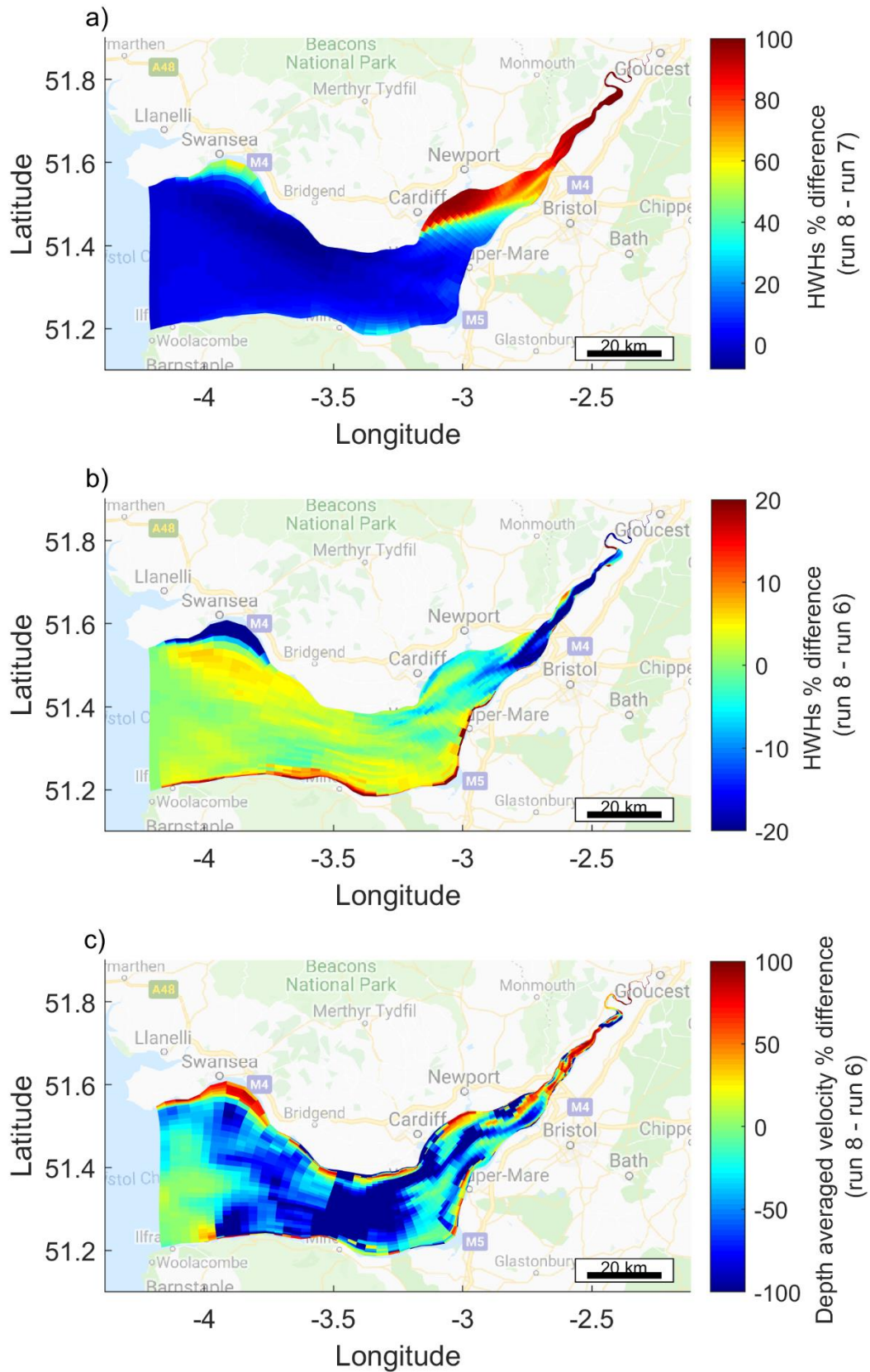


Figure 5.6: % difference across the Severn Estuary model domain in HWHs, for the 50th percentile event between a) run 8 (two-way + wind) – 7 (two-way); b) run 8 (two-way + wind) – 6 (one-way + wind);

and c) % difference depth average velocity run 8 (two-way + wind) – 6 (one-way + wind) Limits are scaled to show the main differences, but the values may exceed these in isolated areas at the coastline.

5.4.3. Uncertainty in High Water Hazard Proxy (HWHP)

Runs 1 and 2 are not included in these comparisons as HP is underestimated in the outer estuary when waves are not included as a physical forcing condition (Figure 5.2f), highlighting the importance of coupling here. Runs 3 and 4 are forced with a constant water level and are not included in these comparisons, as HP is greatly underestimated when tide is not included as a physical forcing condition (Figure 5.2f).

As with HWH_s, increasing HP threshold increases the % and absolute difference in HWHP on the north coastline. Run 5 generates maximum % difference in HWHP of 9.02%, representing 0.71 m, with run 8 at 20 km up-estuary on the north coastline. The difference between runs 5 and 8 generates 8.43% difference, 100 km up-estuary on the south coastline, however this represents just 0.27 m. The south coastline is sheltered from approaching storms simulated here from the southwest, as waves do not propagate directly towards the coastline. Therefore hazard is lower than the north coastline.

5.4.4. Spatial variability of hazard

Each metric is further analyzed up to the wave limit and the entire estuary, indicating the large impact of model coupling and forcing processes on the upper estuary (Table 5.2). A greater maximum, mean and median % difference for HWL and HWH_s occurs when considering the entire estuary coastline. Locally generated winds blow waves into the upper estuary, generating a larger response up-estuary. Conversely, mean and median % difference for HWHP is smaller when including the upper estuary, and maximum % difference in HWHP occurs in the lower estuary shows no difference.

Table 5.2: Overall maximum, mean and median percentage difference in HWL, HWH_s and HWHP in the lower/mid estuary (to wave limit) and the entire estuary coastline.

% difference metric	Hazard percentile event	HWL		HWH _s		HWHP	
		To wave limit	All	To wave limit	All	To wave limit	All
Maximum	10	1.01	2.2	97.5	100	7.9	7.9
	50	1.52	2.1	97.6	100	8.4	8.4
	90	0.33	0.87	97.4	100	5.8	5.8
	Max	0.82	1.78	98.7	100	9.1	9.1
Mean	10	0.33	0.66	52.7	71.3	5.9	5.2
	50	0.69	0.89	32.7	52.7	4	3.4
	90	0.16	0.21	40.2	58.1	2.5	1.9

	Max	0.37	0.53	48.7	65.3	5.1	4
Median	10	0.18	0.55	60.2	77.1	5.5	5.8
	50	0.67	0.83	18.8	62.3	3.8	2.7
	90	0.13	0.16	44.1	77.2	3.1	2.2
	Max	0.33	0.37	53.6	84.2	5.6	3.7

5.5. Discussion

The model highlights that HWL shows least sensitivity to forcing and coupling processes. The 90 percentile event, which showed smallest range of % and absolute difference, has a wind speed of 9.8 m/s from 232 – 247°, representing the most southerly direction of all HP events. This event may be fetch limited, so wind speed is reduced as it approaches from a more southerly direction to reduce setup (Brown et al., 2012), indicating estuary orientation is important when considering uncertainty in simulated HWL at the coastline.

Accurate prediction of HWH_s and HWHP in the outer estuary is important for prediction of wave run-up and wave overtopping, and used to design crest levels of flood defense structures (Sayers et al., 2003). This is particularly important at the time of high tide, when defense exceedance is most likely (Quinn et al., 2014). Largest absolute changes in HWH_s and HWHP occur on sections of the north coastline in the outer estuary with a southwesterly aspect indicating uncertainty, from model and coupling processes, may be sensitive to estuary orientation and coastline geometry in relation to the direction of incoming storm conditions. Accurate model setup for land use planning is critical to avoid under-design, particularly for infrastructure and communities facing the direction of prevailing storms. Defenses could be built too low if the contribution of local winds to sea generated wave hazard is not considered, leading to more regular, low level ‘nuisance flooding’ (Moftakhari et al., 2018). Future flood damages to coastal cities is estimated at over US\$1 trillion damage by the middle of the 21st century (Hallegatte et al., 2013), and this could increase if implementation of new grey or green adaptation strategies are built to inaccurate crest levels and are not able to withstand local storm conditions (Temmerman et al., 2013). At £700-5400 / linear meter for seawalls in the UK (Hudson et al, 2015) and US\$500 million spent annually in the USA on pre-hazard mitigation (Reguero et al., 2018), over design could be a costly use of funding and resources. Further, a high degree of error in forecasts can propagate through the model cascade (Hewston et al., 2010) when used to then force the boundary of shoreline response models. A 1.45 m underestimation of HWH_s in the outer estuary could mean overtopping models (e.g. EurOtop) or inundation depth and extents (e.g. LISFLOOD-FP) do not accurately capture the impacts of extreme events. This could be costly in terms of management activity, or result in financial losses or casualties.

Uncertainty in H_{WH_s} can directly impact on coastal populations up-estuary. H_{WH_s} in run 3,4,5,6 and 7 is consistently smaller than run 8, as wave propagation may have lost momentum up-estuary due to lack of local wind, or be depth limited (Karimpour et al., 2017). Further, one-way and standalone simulations do not account for the effect of waves on current, which may limit wave setup and propagation up-estuary. Increased uncertainty in H_{WH_s} up-estuary of Newport and Weston-super-Mare could underestimate the damaging effects of slopping as a source of coastal flooding (Rego and Li 2010) or simulated critical threshold levels in operational forecasts may not being reached. Flood warnings may be missed and evacuation orders not sent to coastal communities. This is particularly important in low-lying regions near Oldbury Naite, where simulated HWHP of 9.88 m in run 8 for the maximum HP event would breach earthen embankments of 9.0 to 9.5 m OD (Knight et al., 2015). Locally generated winds are an important component of operational forecasts in coastal zones and estuaries to ensure flood warnings are timely and accurate (Marcos et al., 2019).

The importance of locally generated winds in accurate representation of H_s has been shown in coastal and estuarine regions worldwide. Maximum wind speed and surface wind stress is shown to be important in simulating hurricane storm surge with the Sea, Lake, and Overland Surges from Hurricanes (SLOSH) model in northeastern US, and can underestimate hazard by 22% if excluded (Mayo and Lin 2019). The geometry of the mouth of the Mersey Estuary, NW England, at high tide makes it wide enough for substantial local wind-wave generation and for wind setup to elevate the water surface, which should be considered when simulating local flood hazards (Flowerdew et al., 2009). The orientation of hyper-tidal estuaries to prevailing conditions and their large geometries, such as the Bay of Fundy, Canada increase the likelihood that strong winds are coincident with extreme total water levels (Desplanque and Mossman 1999). Simulated H_s during the Patriot's Day storm in the Bay of Fundy show maximum H_s occurs in the outer Gulf of Maine due to long fetch and wind setup (Marsooli & Lin, 2018), indicating the importance of local winds during extreme storm events. Storm surges are often accompanied by large wind-waves in more than half of coastal regions worldwide (Marcos et al., 2019), thus increasing the potential for coastal flooding and highlighting the need for accurate, local boundary conditions when simulating H_{WH_s} .

5.6. Conclusion

Potential future changes in sea level and storm tracks necessitate accurate prediction of HWL and H_{WH_s} in hyper-tidal coastal and estuarine areas for operational forecasts, inundation assessments and cost-effective defence strategies. Delft3D-FLOW-WAVE is used in a series of 32 standalone, one-way or two-way coupled simulations for four historic storm events, to quantify the uncertainty in forecasting HWL and H_{WH_s} due to coupling and forcing processes in the Severn Estuary, SW England, used here as a test case for hyper-tidal and funnel shaped estuaries worldwide. HWL shows least sensitivity to both coupling and forcing processes, with 1.5% difference (0.046 m) between the two-way coupled and

standalone simulation. For a model domain this size, inclusion of local atmospheric forcing is crucial to continue to add momentum to wave generation up-estuary for accurate HWH_s and HWHP prediction. The model shows a 34.4% difference (1.45 m) in HWH_s and 9.02% (0.71 m) in HWHP on the north shoreline in the outer estuary, and up to 90.1% difference (1.13 m) in the upper estuary when local atmospheric forcing is excluded from simulations. Aspect and geometry of the coastline to prevailing storm conditions is also an important consideration for coastal hazard prediction. Results highlight how coastal and estuarine numerical models can be best set up to ensure outputs can be used in confidence to force shoreline response models (e.g. for overtopping or inundation studies), to inform design of new coastal protection schemes or flood warnings.

5.7. Acknowledgments and Data

The authors thank colleagues at the British Oceanographic Data Centre (BODC) for providing tidal data; Magnox for providing tidal data; Environment Agency for providing tidal data; Gloucester Harbour Trustees for providing tidal data; Met Office for providing observational wind data and WAVEWATCH III data; Met Office and NOCL for providing CS3X wind and atmospheric pressure data; CEFAS for providing observational wave buoy data; EDINA for providing bathymetric data. The research is a contribution to the NERC highlight topic “Physical and biological dynamic coastal processes and their role in coastal recovery” (BLUE-coast, NE/N015614/1).

Data used in this research are available from sources stated in the reference list.

6. Uncertainty propagation in flood hazard assessments

Modelled water level and wave height outputs, which are generated in Chapter 5 from the standalone, coupled and uncoupled Delft3D-FLOW-WAVE simulations, are propagated through the model chain to force the model boundary of LISFLOOD-FP, a 2D inundation model, at an up-estuary location. LISFLOOD-FP is used in chapter 6 to quantify sensitivity of flooding to uncertainty in coastal hazard conditions, due to coupling and forcing processes, and method used to force the coastal boundary of the inundation model at Oldbury-on-Seven, southwest England, used as an example of a low-lying floodplain where sites of critical infrastructure are located. The impacts of uncertainty are quantified by presenting change in volume of inundation, hazard rating (and danger to people) and economic costs of inundation to suburban and arable land for each simulation. The accurate quantification of impacts of uncertainty can inform long-term coastal flood hazard mitigation and adaptation strategies and increase knowledge of how estuaries may response to future change in sea level.

6.1. Abstract

Uncertainty in water level and wave height predictions for violent storms and hurricanes may lead to errors in flood hazard assessments, which is critical in industrialized estuaries. A 2D inundation model, LISFLOOD-FP, was used to quantify sensitivity of flooding to uncertainty in coastal hazard conditions and method used to force the coastal boundary of the inundation model. It is shown that flood inundation is more sensitive to small changes in coastal hazard conditions due to the setup of the regional model, than the approach used to apply these conditions as boundary forcing. Once the threshold for flooding is exceeded, a few centimetres increase in coastal conditions increases both the inundation and consequent damage costs for suburbia. Improved quantification of uncertainty in inundation assessments can aid long-term coastal flood hazard mitigation and adaptation strategies, to increase confidence in knowledge of how estuaries will respond to future changes in sea level.

6.2. Introduction

The combined effect of astronomical high tides, storm surges, wind and waves during hurricanes and violent storms can temporarily increase sea level at the coast to exceed critical hazard thresholds, and lead to flooding, damage to infrastructure and potential loss of life. This is particularly critical in heavily populated, industrialised estuaries and deltas, which are the focal point of coastal megacities and hubs for transport, trade and critical infrastructures (Adikari et al., 2010; Sekovski et al., , 2012; Chen et al., 2018). Estuaries with a macro- and hyper-tidal regime are vulnerable to combined hazard effects, as even small changes in water level can influence wetting and drying, local fetch, wave & surge propagation, wave runup, refraction and dissipation to elevate flood hazards at the coast (Lyddon et al., 2018a).

It is of critical, international importance that we fully understand the sources, pathways and degree of exposure of flood hazard in estuaries (Narayan et al., 2012). Typhoon Hato caused 12 fatalities and up to USD 4.34 billion of flood damage in the city of Macau on the south coastline of the Pearl River Estuary on 23 August 2017, as observed tides were 6.14 m above predicted level and a 2.79 m storm surge was exacerbated by 127.9 km/hour winds (Yang et al., 2019). The combined effect of strong winds, high tides and low atmospheric pressure has caused substantial damage on the coastline of the Bay of Fundy, Canada; 166 km/h winds from a category 2 hurricane caused a 2 m storm surge on a spring tide and subsequent overtopping of dykes by 0.9 m to cause damage to buildings, railroads and livestock during the Saxby Gale on October 4-5, 1869 (Desplanque and Mossman 1999). The Groundhog Day storm on 2 February 1976 saw wind speeds exceed 164 km/h and a 2.1 storm surge caused up to 1.6 m flooding in coastal towns including Saint John, New Brunswick, as towns were left without power for 14 days (Greenberg et al., 2012). A perigee new moon spring tide, combined with a 989 mb low pressure system and 6 m waves at Bristol Channel buoy caused one of the worst winter

storms in the UK; many defences held but some flooding occurred across low-lying agricultural land on the Somerset Levels (Muchan et al., 2015; Sibley et al., 2015).

An understanding of the nature and degrees of exposure to coastal flood hazard from violent storms and hurricanes is important for reducing its impacts on communities, property and infrastructure. There is a need for accurate predictive techniques, visualisation tools, and vulnerability maps, and timely flood alerts and warning systems to mitigate the negative consequences of combined hazards. These mitigation techniques require an accurate understanding of the hydrodynamic processes in estuaries during hurricanes and violent storms, and an understanding of coastal and estuarine response to hydrodynamic forcing (Del Río et al., 2012; Teng et al., 2017). The accurate prediction of sources of flood hazard during storms, water level (WL) and significant wave height (H_s), most notably at the time of high water when defence exceedance is most likely to occur, is an important component of flood hazard management, due to their influence on wave runup, wave overwashing and erosion (Lyddon et al., 2018a; Senechal et al., 2011; Suarez et al., 2015). High water level (HWL) and high water significant wave height (HWH_s) predictions can be used to design crest levels of flood defence structures, or force the model boundary of process-based, shoreline response models to predict the pathway, maximum velocities and extent of floodwater, and timing of peak discharge, (Knight et al., 2015; Prime et al., 2016; Didier et al., 2019), wave overtopping (Thompson et al., 2017), morphological change (Karunaratna et al., 2018) and hazard rating (Defra, 2003) arising from the combined effect of these hazards. However uncertainty can arise in HWL and HWH_s predictions due to model coupling processes, local forcing processes and coastal geometry (Lyddon et al., 2019b). The exclusion of locally generated winds underestimated HWH_s by up to 90.1% in the upper regions of the Severn Estuary, southwest England, during simulations of the 3 January 2014 storm event. There is a need to accurately predict HWL and HWH_s for flood hazard management, and quantify uncertainties in hydrodynamic models due to the parameterisation and interaction of physical processes when used to force shoreline response models.

Inaccurate representation of the complex interactions between atmospheric, meteorological, fluvial and tidal processes in estuaries can result in large uncertainties in the hydrodynamic forcing of shoreline response models (Hewston et al., 2010) and have been shown to cause uncertainties in subsequent model outputs. Excluding the contribution of riverine discharge to total water level during simulations of a storm-tide, using hydrodynamic modeling package Delft3D, underestimates flood extent by 30% (20.5 km^2) in the Shoalhaven Estuary, south-eastern Australia (Kumbier et al., 2018). LISFLOOD-FP, a 2D inundation model, has been used to show that uncertainties in boundary conditions are an important factor in the accurate prediction of inundation of the coastal city of Licata, in the Imera basin, Sicily, as this determines whether or not rivers are in flood and reach bankfull stage and discharge (Savage et al., 2016). LISFLOOD-FP has also been used to show the differential flood risk from different combinations of storm return period, wave overtopping and river discharge in Fleetwood, northwest

England, and quantified economic impact (Prime et al., 2015). Large uncertainties in the hydrodynamic forcing of shoreline response models can have substantial practical and financial impacts, as the outputs from these models are used to understand extent and pathways of floodwater to guide decisions about the design and location of sea defences and coastal development, assess options for flood prevention schemes and prioritise areas which would benefit from adaptation and mitigation strategies (Environment Agency 2019; Mcleod et al., 2010; SEPA 2018). Accurate estimation of still water-level, wave setup and runup is crucial for accurate representation of peak storm tides, and may be important in a coastal inundation model than intra-modeling uncertainties, such as bed roughness coefficients (Lewis et al., 2013). Therefore, there is a pressing need to understand how uncertainties in coastal hydrodynamic models propagate and accumulate through the modeling chain to influence shoreline response models, and the accuracy of their outputs for practical, hazard assessment purposes in large, developed estuaries.

6.2.1. Case study

This research aims to understand how uncertainty in the sources of coastal hazards (HWL and HWH_s) propagates into uncertainty in flood hazard at Oldbury-on-Severn on the south coastline of the Severn Estuary, southwest England (Figure 6.1a). The Severn Estuary can be defined as hyper-tidal and has a tidal range up to 12.2 m at Avonmouth as the tide is funnelled up-estuary. Large local fetch at high tide means southwest-west wind direction can generate and propagate locally generated waves up-estuary to Oldbury (Lyddon et al., 2019a). Historically Oldbury and the low-lying area of Oldbury Naite has been susceptible to coastal flooding due to the combined effect of tide-surge-wind-wave-river hazards (Uncles 2010). Flood hazard occurs here due to the combined effect of HW, H_s and winds resulting in the overwashing of lowered foreshore levels and defences as greenwater (Knight et al., 2015; Pye and Blott 2010), rather than wave overtopping which causes dense, vertical plumes of water to travel over the crest. Further to this, inundation occurs in these low-lying areas of the Seven Estuary occur due to overflow from tidal inlets and channels, breaching of defences and embankments (JBA 2017), and high estuary and sea water levels causing tide locking (South Gloucestershire Council 2014). Low-lying agricultural areas at Oldbury Naite, local transport networks and small towns are afforded a level of protection from coastal hazards by earthen banks along the south coastline of the estuary. A decommissioned nuclear facility at Oldbury is protected by earthen banks and concrete seawall.

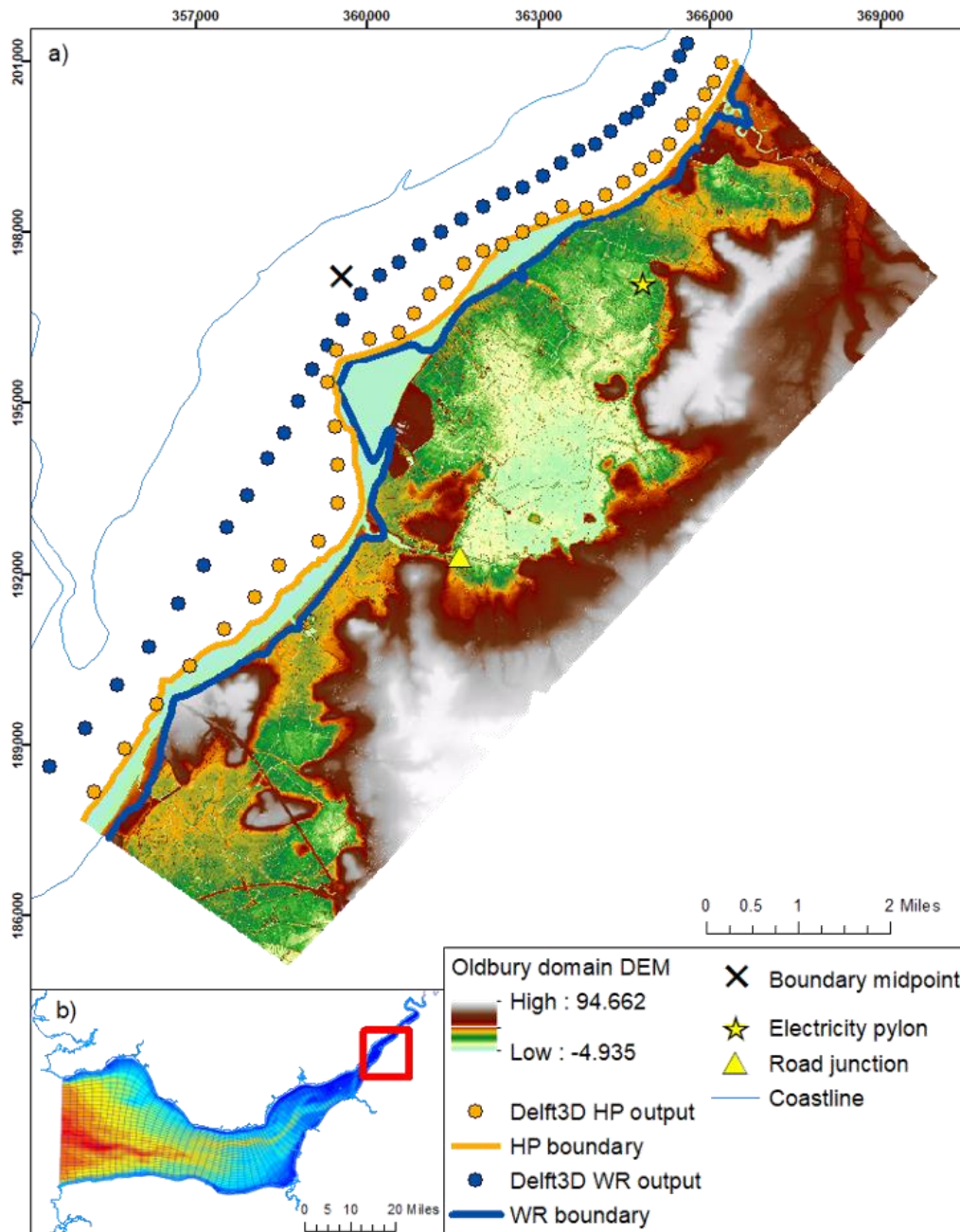


Figure 6.1: a) Oldbury model domain, including the location of Delft3D outputs (coloured dots) used to force the HP and WR boundary approach (coloured lines); boundary midpoint to calculate change in coastal hazard uncertainty (black cross); sites of critical infrastructure (yellow star and triangle); and b) Delft3D-FLOW-WAVE model domain with extent of the up-estuary Oldbury model domain shown.

This paper aims to quantify how coastal hazard uncertainty and approach to forcing the model boundary of LISFLOOD-FP (Bates et al., 2005) influences the impacts of inundation at an up-estuary location. LISFLOOD-FP is a 2D finite difference inundation model based upon the storage cell approach (Bates et al., 2005). The model simulates the movement of water across a grid representing the bathymetry and

land surface, based on LiDAR data, under the influence of gravity. The model has been successfully used in other coastal applications to replicate tidal elevations and simulate inundation during storm events in the Solent (Wadey et al., 2012), Humber Estuary (Skinner et al., 2015), and the Severn Estuary (Smith et al., 2012; Lewis et al., 2013; Quinn et al., 2014). The DEM used for the Oldbury model domain were obtained from EA Geomatics (2019), and the data have a 1 m horizontal resolution and 0.05 m to 0.15 m vertical accuracy. The DEM was resampled to 5 m horizontal resolution to ensure computational efficiency. The model domain extends from the Severn Bridge to the west, up to Sharpness harbour to the east, and includes Oldbury Technical Centre, Oldbury Naite and Oldbury tidal pool. Defences, including earthen banks and sluices, are well represented at 5 m in the model domain. Inland river channels, known locally as rhines, were digitised into the DEM to ensure accurate representation of the floodplain. Topographical features, such as bridges, were removed as these can act as artificial dams. A uniform global Manning friction coefficient of 0.03 m was used, which is a standard value that has previously been applied to study inundation in coastal floodplains (Prime et al., 2016).

Section 2 of this paper will discuss input data and inundation scenarios completed for two historic storm events. Section 3 presents flood maps to systematically show the maximum depth and extent of inundation for each scenario and presents flood hazard ratings at sites of critical infrastructure. The uncertainty in time-integrated volume of inundation and economic cost of damage of each scenario is quantified against uncertainty in regional model predictions of WL and H_s changes flood hazard. Before drawing conclusions in section 5, section 4 will discuss how uncertainty in boundary conditions and position, and local coastal morphology influences depth, extent and volume of inundation across the model domain, and how even small changes in HWL and HWH_s at the boundary have a significant impact on coastal flood hazard.

6.3. Method

Figure 6.2 shows the model inputs and processes followed to derive the impact of each inundation scenario, which are explained through section 2.

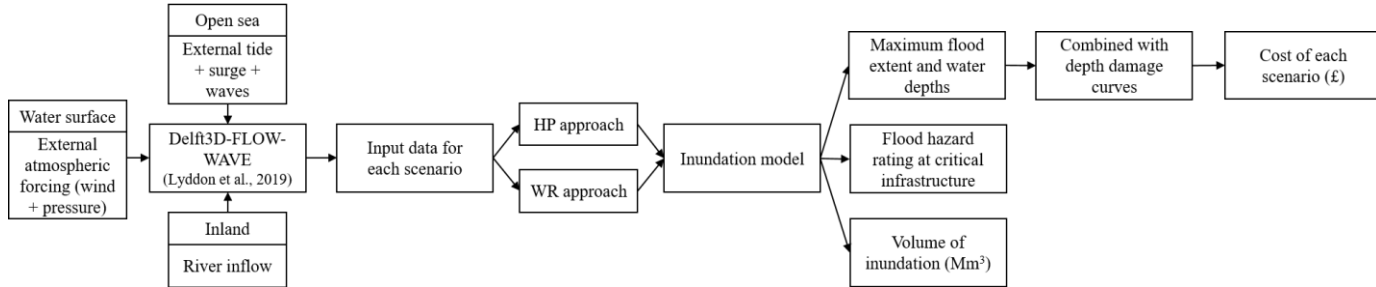


Figure 6.2: Model inputs and the process followed to propagate and quantify uncertainty in flood hazard assessments, and results that are presented in section 3.

6.3.1. Input data

6.3.1.1. Historic storm events

Outputs from previously completed scenarios using Delft3D-FLOW-WAVE, which represent coastal hazard uncertainty in WL and H_s , are used to force the boundary of LISFLOOD-FP. The Delft3D modeling system has been previously validated and successfully used to simulate coastal hazards in the Severn Estuary for two historic storm events; (i) 3 January 2014 (hereafter called Jan 14) which represents the maximum coastal hazard condition; and (ii) 16 December 2012 (hereafter called Dec 12) which represents the 90th percentile coastal hazard condition (Lyddon et al., 2019b). These storm events coincide with winds from a southwest-west direction at the time of high water, as wave hazard is amplified up-estuary with winds from this direction (Lyddon et al., 2019a). Flood warnings were issued along large stretches of the Oldbury coastline for the 3 January 2014 storm event (Chipperfield 2014), and flooding was reported 10 km up-estuary of Oldbury at Minsterworth as defences were overwashed (BBC 2014).

6.3.1.2. Coastal hazard uncertainty

Coastal hazard uncertainty at the boundary of LISFLOOD-FP comes from eight model simulations (Tabl 6.1) completed for the January 2014 and December 2012 events in Delft3D-FLOW-WAVE across the entire Severn Estuary model domain (Figure 6.1b). The Delft3D model for the Severn Estuary has been previously validated and successfully used in Lyddon et al., (2019b). Each model simulation was forced with a combination of time-varying, spatially uniform WL from Ilfracombe tide gauge and time-varying, space-varying H_s from Wavewatch III hindcast at the open sea boundary representing different model coupling setups. Uncoupled model scenarios represent standalone water level simulations in FLOW or wave simulations with a constant mean high water spring tide (MHWST) level in WAVE.

One-way coupled scenarios represent the influence of currents on waves, and two-way scenarios represent the influence of currents on waves, and waves on currents. Simulations were forced with and without local wind conditions, from the UK Met Office Unified Model (Saulter et al., 2016; Siddorn et al., 2016; Met Office, 2019) to represent changing forcing processes. All simulations were forced with river gauge data from the Environment Agency Sandhurst river gauge near Gloucester at the eastern open boundary. Run 8 represents a complete, 5-parameter multi-hazard simulation and outputs were graphically and statistically validated to tide gauges and wave buoys in the estuary (Lyddon et al., 2018a, 2019b). The results of the Delft3D-FLOW-WAVE runs were used to force the boundary of the LISFLOOD-FP Oldbury model domains to represent coastal hazard uncertainty.

Table 6.1: Eight model simulations completed in Delft3D-FLOW-WAVE for each historic storm event, and outputs used to force the boundary of the Oldbury model domain in LISFLOOD-FP from the low water mark and defence crest.

Run	Model	Coupling	Forcing
1	FLOW	Standalone	Water level
2	FLOW	Standalone	Water level + wind
3	WAVE	Standalone	Constant HW water level + Wave
4	WAVE	Standalone	Constant HW water level + Wave + wind
5	FLOW → WAVE	One-way	Water level from 1 + wave
6	FLOW → WAVE	One-way	Water level from 2 + wave + wind
7	FLOW ↔ WAVE	Two-way	Water level + wave
8	FLOW ↔ WAVE	Two-way	Water level + wave + wind

6.3.2. Inundation model boundary conditions

LISFLOOD-FP can be forced with a water level or discharge at its open boundaries. We tested two approaches to forcing the model boundary (as indicated in Figure 1a) to represent different pathways of flood hazard (described in section 2.2.1 and 2.2.2).

1. HP is calculated from Delft3D-FLOW-WAVE outputs and imposed at the low water mark, to resolve wetting and drying in the inundation model.
2. WL and H_s from further offshore are used to calculate wave runup using Stockdon et al., (2006), and provide runup level at the crest.

For both approaches to forcing the model boundary the time- and space-varying predicted WL and H_s from the eight Delft3D-FLOW-WAVE model simulations (see Table 6.1), representing coastal hazard uncertainty, were used.

6.3.2.1. Hazard proxy approach

The first approach to forcing the LISFLOOD-FP model boundary uses a Hazard Proxy ($HP = WL + \frac{1}{2} H_s$) imposed at the low water mark. This method considers if the combined WL and H_s exceeds the defence crest level if waves do not break before the defence crest.

WL and H_s outputs from the Delft3D Severn Estuary model domain were extracted from the Delft3D grid cell closest to the low water mark boundary of the Oldbury model domain (see Figure 6.3). LISFLOOD was forced with WL only from the Delft3D outputs of run 1 and 2, constant HWL + H_s from run 3 and 4, and HP was calculated for run 5-8 along the boundary of the Oldbury model domain.

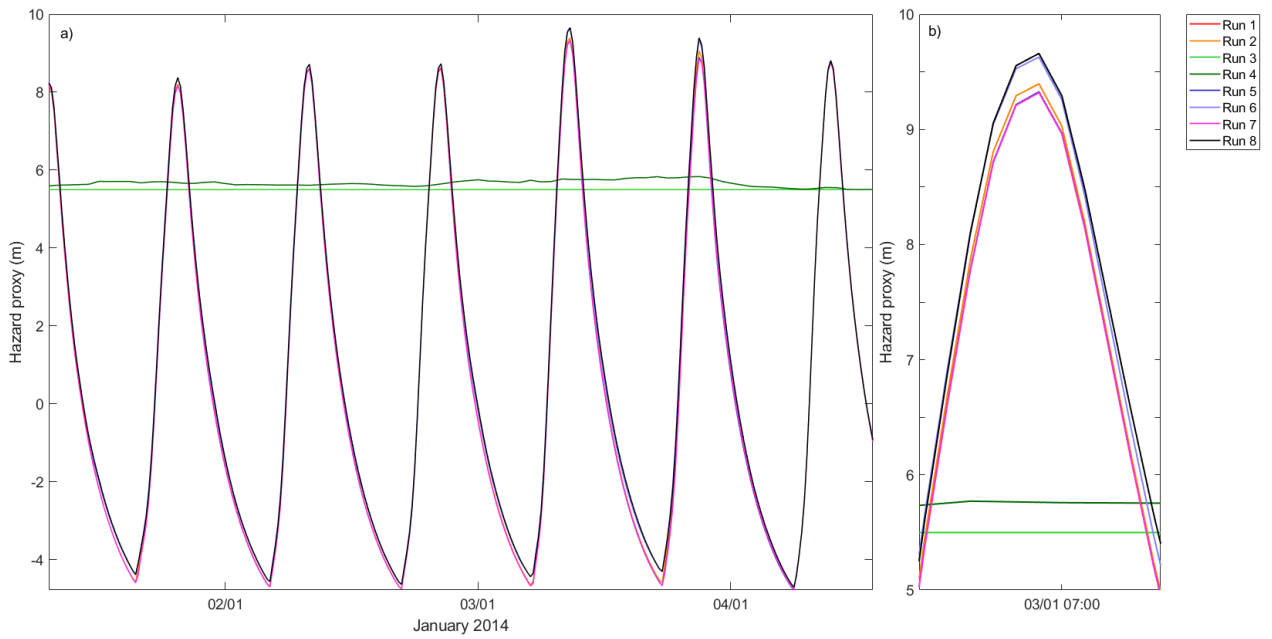


Figure 6.3: a) Coastal hazard uncertainty time series from Delft3D-FLOW-WAVE used to force LISFLOOD-FP, for Jan 14 event using the HP approach, shown here as an example; b) zoom of peak of the Jan 14 event to show coastal hazard uncertainty.

6.3.2.2. Wave runup approach

The second approach to forcing the boundary combines maximum wave runup (WR), which determines the extent of which waves act (Melby et al., 2006), with water level to determine flood inundation from the effect of overwashing at the defence. The 2% exceedance runup level was calculated from Stockdon et al., (2006) equation (Leaman 2019);

$$R_2 = 1.1 \left(0.35\beta(H_s L_p)^{0.5} + \frac{H_s L_p (0.563\beta^2 + 0.004)^{0.5}}{2} \right) \quad (1)$$

where β represents the slope angle at of earthen embankments along the coastline, calculated in ArcMap from the DEM, H_s represents significant wave height in the thalweg of the estuary, and L represents wave length, calculated using peak wave period. H and L were extracted from the Delft3D domain from the deepest part on the Severn Estuary channel. WR was calculated and added to Delft3D water level outputs at the coastline, extracted from the second grid cell into the domain along the coastline. As seen in Figure 6.1, LISFLOOD-FP is forced from the defence crest of the earthen embankments along the south coastline of the Severn Estuary, to represent flood hazard due overwashing of greenwater from waves and water level.

6.3.3. Flood inundation scenarios

LISFLOOD is run for 32 simulations in total (eight coastal hazard uncertainty scenarios, for two approaches to forcing the model boundary, for two historic events). The model was run from 2 days before the selected storm event to allow spin up, to 12 hours after the event. Inundation maps showing maximum depth and extent of inundation are analysed systematically for all scenarios. Results are then presented from low water to low water over the tidal cycle of each extreme event

Flood hazard rating (Bates et al., 2013) is calculated for to two locations of critical infrastructure within the Oldbury model domain to show degree of flooding at a road junction on Oldbury Naite rhine (51.63° N, -2.56° W) and an electricity pylon between Oldbury Technical Centre and Berkeley (51.64° N, -2.55° W). Flood hazard rating is calculated at each location as:

$$\begin{aligned} \text{Flood hazard rating} & \\ &= \text{water depth} \times (\text{flood velocity} + 0.5) \end{aligned} \quad (2)$$

where 0.5 represents a constant value (Defra, 2003). Flood hazard rating is presented at each site of critical infrastructure relative to thresholds to hazard to people. A flood hazard rating of 0.75 -1.25 indicates hazard to some (e.g. children), 1.25 – 2.0 represents hazard to most, and over 2.0 represents hazard to all, including emergency responders (Defra 2003).

The volume of inundation (Mm^3) in the model domain is presented, and then absolute difference in time-integrated volume of inundation (m^3) and economic cost of inundation to suburban and arable land is calculated. This is presented against absolute difference in HP at the boundary midpoint at the time of HW for each run to show how an increase in regional model WL and H_s changes flood hazard. Run 8 is used as a baseline to quantify absolute difference; each difference value indicates what the change in HP, time-integrated volume of inundation or economic cost of inundation is from each model run relative to the value simulated for run 8 (i.e. a positive value of 0.2 m difference in HP indicates run 8 is 0.2m larger than the model run). Absolute difference from each model run to model run 8 is calculated as:

$$\text{Absolute difference} = \text{Run 8} - \text{Run } X \quad (3)$$

where X indicates results from simulations shown in Table 1.

6.3.4. Depth damage curves

The depth and extent of floodwater at the time of maximum inundation in model cells with depth greater than 0.05 m are combined with saltwater depth damage curves (Penning-Rowsell et al., 2013) to place an economic value on each scenario. Water depths less than 0.05 m are considered not damaging and are below the vertical accuracy of the LiDAR data (Prime et al., 2015). Land-use was classified using the 25 m UK Land Cover 2015 dataset (Rowland et al., 2017), and combined with depth damage curves depending on the land use. The impact of inundation on arable (including costs for grassland and horticulture areas) and suburban land uses (classified using a saltwater depth damage curve for housing) was calculated for each scenario and is presented as percent difference compared to run 8.

6.4. Results

The outputs from each simulation, detailed in Table 6.1, have been displayed over Ordnance Survey 1:250,000 (Ordnance Survey, 2019) scale map to highlight infrastructure and communities impacted by inundation. Figure 6.4 to Figure 6.7 shows the flood at its maximum extent during the four simulations. The flood maps shows water depths above 0.05 m, which is the depth saltwater inundation is considered damaging, and is standardised up to the average 99th percentile water depth for run 8 of each coastal hazard conditions (2.7 m for Jan 14, and 1.6 m for Dec 12) to more clearly present shallow water inundation. The 90th, 50th and 10th percentile water depths are quoted in the text as indicators of the extent of shallow water inundation which could cause impacts within the model domain.

6.4.1. Depth and extent of inundation

6.4.1.1. Jan 14 HP

Figure 6.4 shows the maximum depth and extent of flood inundation for Jan 14 using the HP approach. Run 3 and 4 flood only the tidal inlets at Oldury Naite and Berkeley, as constant water level at MHWST + H_s does not exceed the bank crest and floodwater does not breach channels. Excluding run 3 and 4, as the model scenarios become more realistic (from run 1 to run 8), inundation becomes increasingly widespread in the southwest of the model domain, near Oldbury-on-Severn and Littleton-upon-Severn, and is focused around tidal inlets and rhines which have been exceeded. Low-lying agricultural areas in the centre of the model domain, at Shepperdine and Bevington, see increasing extent of inundation from run 2, 6 to 8, up to 1 m deep. Runs which do not include locally generated winds in the boundary condition for LISFLOOD-FP (run 1, 5 and 7) do not cause inundation in these central areas of the model domain because peak HP at the time of HW is lower. Berkeley, to the northeast of the model domain,

is inundated as Berkeley Pill is exceeded in all scenarios, and water depths of over 1 m occur to the east of the channel.

Run 8 represents the greatest extent of inundation, with a 90th percentile water depth of 1.29 m, which shows 10% of the area of inundation exceeds this depth, notably away from full or deep channels e.g. rhines and pills. Run 6 shows a similar extent of inundation, and 90th percentile water depth of 1.3 m. Run 8 and 6 have a 50th percentile water depth of 0.47 and 0.49 m, and a 10th percentile water depth of 0.14 m. The 10th percentile water depth indicates that large areas of shallow water inundation occurs, which may cause saltwater damage to roads, housing and agricultural land. Run 2 also shows similar extent, with a similar 90th percentile water depth of 1.3 m, but lower 50th (0.36 m) and 10th (0.07 m) percentile water depths indicate less shallow water inundation. Run 2, 6 and 8 all include local atmospheric forcing in the boundary condition. Inclusion of locally generated wind causes greater flooding by increases the peak HP value, and makes the HP peak wider to allow higher inflow for longer. Run 1, 5 and 7 show smaller extent of flood inundation than run 2, 6 and 8, and also lower 50th water depth percentiles between 0.35 – 0.37 m, indicating the majority of floodwater is shallower. The results presented here signify that coastal hazard uncertainty influences the depth and extent of inundation.

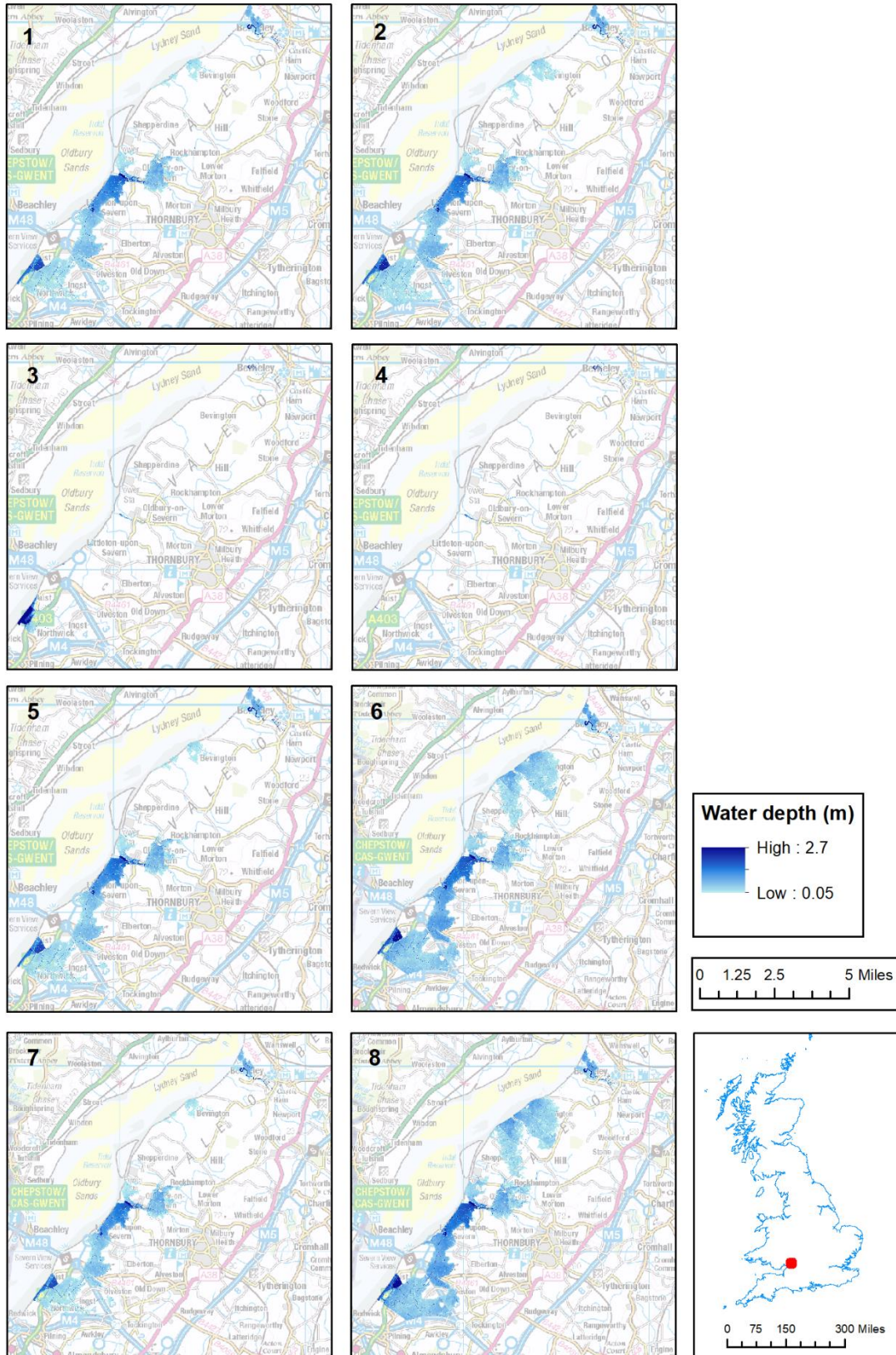


Figure 6.4: Depth and extent of flooding at Oldbury-on-Severn for HP approach to forcing the model boundary where maps 1-8 represent coastal hazard uncertainty (see Table 6.1) for Jan 14.

6.4.1.2. Jan 14 WR

Figure 6.5 shows the maximum depth and extent of flood inundation for Jan 14 using the WR approach. Inundation is widespread in the northeast of the model domain for all runs, at Berkeley, Rockhampton and Shepperdine (excluding run 3 and 4, which show no inundation when using the WR approach). Steeper earthen embankments along the coastline in the northeast of the model domain and large HWH_s during the Jan 14 event means overwashing occurs at multiple locations. Inundation in the southwest of the model domain, near Littleton-upon-Severn and Severn Beach, becomes increasingly widespread from run 1 to run 8. Less inundation is seen around Oldbury Naite rhine. The pattern of inundation seen here can be described as being opposite what occurs when using the HP approach.

Run 8 shows the greatest extent and depth of inundation, with a 90th percentile water depth up to 1.38 m, and a 50th percentile water depth up to 0.7 m, which is up to 0.23 m larger than the HP approach. Run 6 shows a similar extent and a 50th percentile water depth of 0.62 m. The 10th percentile water depth is 0.21 m, indicating greater depth of shallow water inundation across the model domain and is larger than the HP approach. Run 1, 5 and 7 show smaller extent and depths than run 6 and 8, with 50th percentile water depths of 0.45 m, and 10th percentile water depths of 0.1 m.

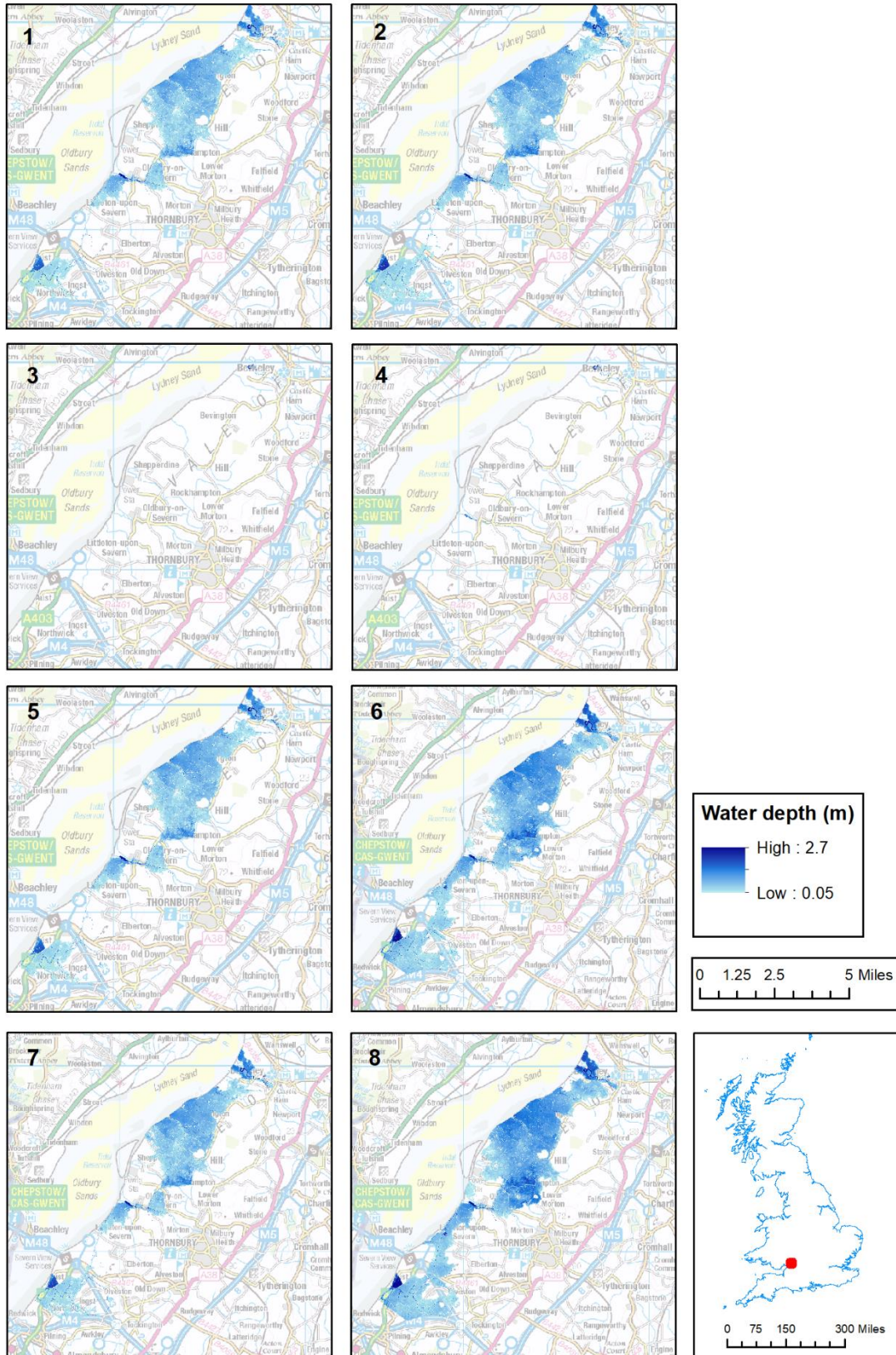


Figure 6.5: Depth and extent of flooding at Oldbury-on-Severn for WR approach to forcing the model boundary where maps 1-8 represent coastal hazard uncertainty (see Table 6.1) for Jan 14.

6.4.1.3. Dec 12 HP

Figure 6.6 shows the maximum depth and extent of flood inundation for Dec 12 using the HP approach. Inundation is substantially less for the Dec 12 event, compared to the Jan 14 event. Inundation occurs on tidal flats at Severn beach only for run 3 and 4 and is focused around Oldbury Naite rhine for all other runs. Run 8 shows greatest extent of inundation, as the rhine exceeds the bank crest to flood Chapel Road and Church Lane in Oldbury-on-Severn, and agricultural areas to the west surrounded by Cowhill rhine. The 50th percentile water depth for run 8 is 0.34 m and 0.06 m for 10th percentile water depth, which shows that the majority of floodwater is shallow.

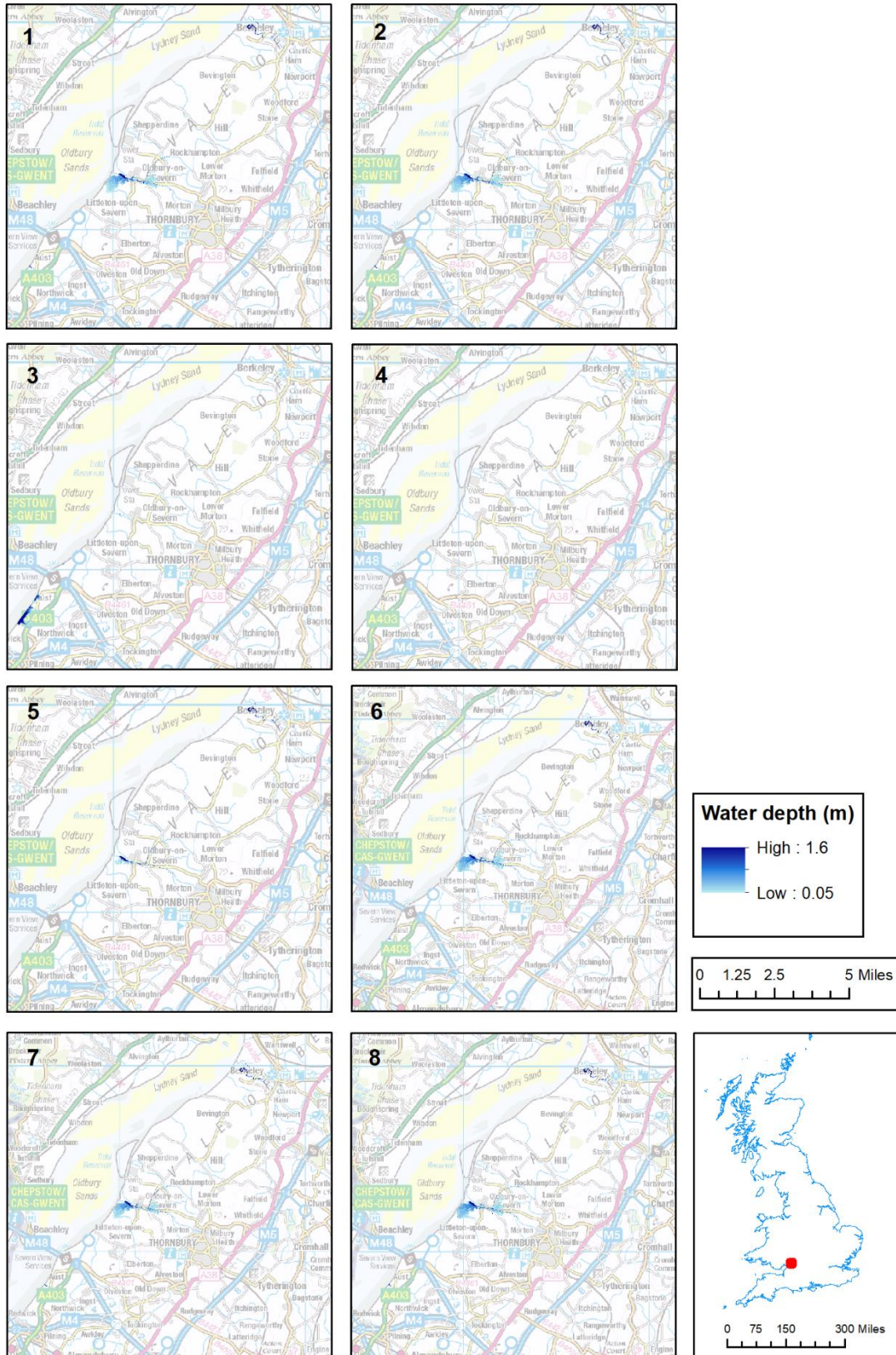


Figure 6.6: Depth and extent of flooding at Oldbury-on-Severn for HP approach to forcing the model boundary where maps 1-8 represent coastal hazard uncertainty (see Table 6.1) for Dec 12.

6.4.1.4. Dec 12 WR

Figure 6.7 shows the maximum depth and extent of flood inundation for Dec 12 using the WR approach. No inundation occurs for run 3 and 4. Inundation in run 1, 2, 5 and 7 is focused around Oldbury Naite rhine, with some inundation occurring at Oldbury-on-Severn and on agricultural land to the south of the rhine. WR for runs 1, 5 and 7, with no local atmospheric forcing, does not reach a limit to cause overwashing along the coastline. Run 4, 6 and 8 also shows inundation at Oldbury Naite rhine, which is deeper, in addition to some inundation of agricultural land directly behind the earthen embankments along the coastline, between Shepperdine and Bevington. The 50th percentile water depth for run 8 is 0.25 m and 0.03 m for 10th percentile water depth, which shows that the majority of floodwater is shallow. Berkeley Pill is filled in all model runs, but the bank crest is not exceeded and no inundation occurs in the northeast of the domain.

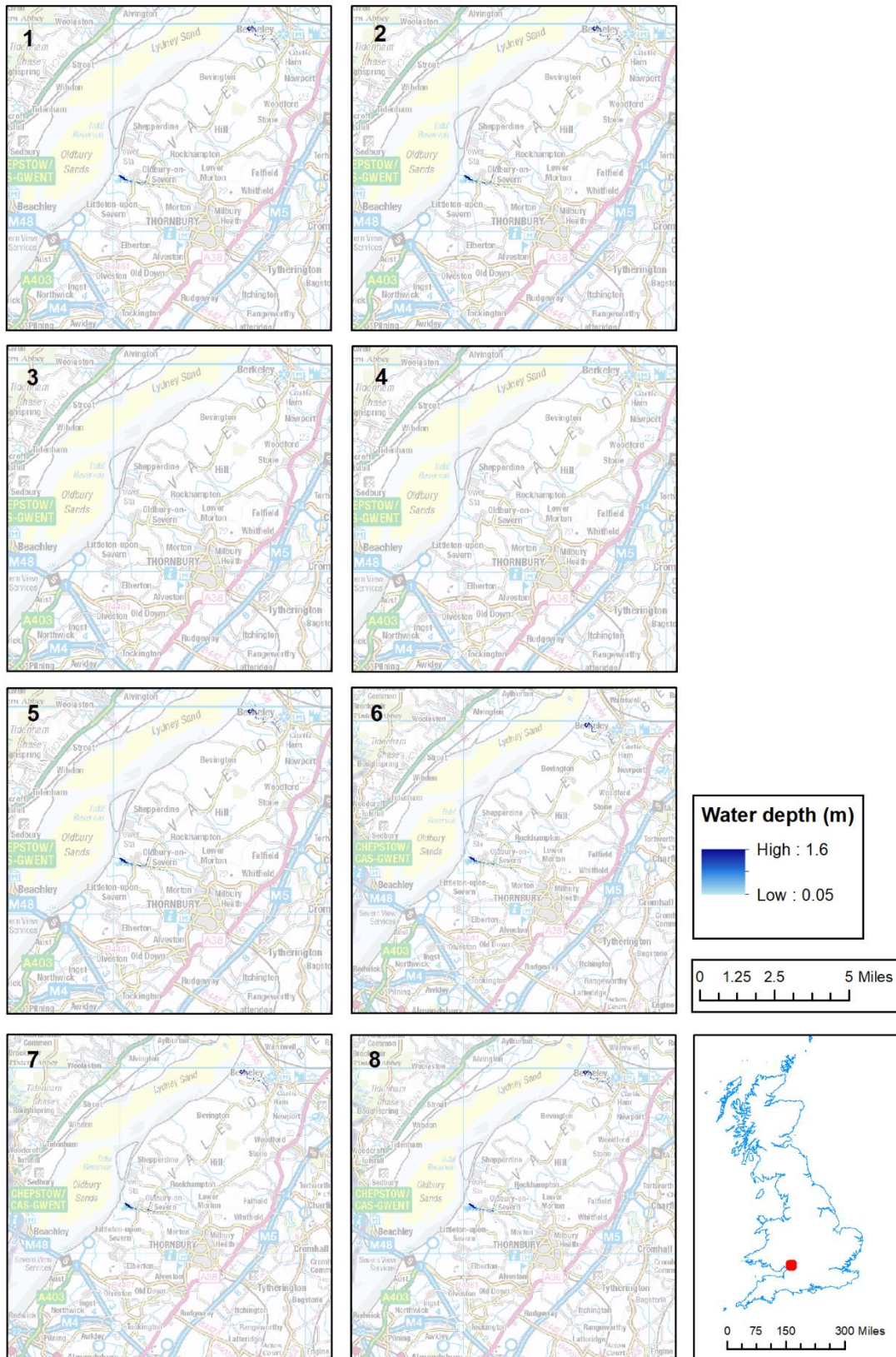


Figure 6.7: Depth and extent of flooding at Oldbury-on-Severn for WR approach to forcing the model boundary where maps 1-8 represent coastal hazard uncertainty (see Table 6.1) for Dec 12.

Figure 6.4 to Figure 6.7 illustrate that the Jan 14 event causes the greatest extent of inundation overall compared to the Dec 12 event. Inundation from the low water mark occurs in the southwest and northeast of the model domain where rhines and pills are exceeded. Inundation from the defence crest occurs where defences are steeper and lower, increasing peak WR to cause overwashing at multiple locations along the central coastline of the domain. Inundation is sensitive to coastal hazard conditions, as inundation is more widespread and deeper for simulations which include local atmospheric forcing. Inundation also shows sensitivity to approach to forcing the model boundary and event severity; Jan 14 shows greater depth of shallow water inundation using WR approach, and Dec 12 shows greater depths of shallow water inundation when using the HP approach. Run 3 and 4 show minimal inundation as they are forced with a constant water level, and inundation is focused around rhines and mudflats when it does occur.

6.4.2. Flood hazard rating at operational sites

Flood hazard rating, calculated using equation 2, is shown at two sites of critical infrastructure at Oldbury; a road junction on Oldbury Naite rhine and an electricity pylon between Oldbury Technical Centre and Berkeley (locations shown in Figure 6.1a). Thresholds for flood hazard rating, which are related to hazard to people, are shown (moderate, significant, extreme), to indicate the extent and duration of exceedance, and timing relative to HW, which is crucial information for emergency response planning.

Figure 6.8a shows flood hazard rating for Jan 14 at the road junction, where the greatest hazard occurs for run 8 from the HP approach, due to the combined effect of deeper water depths and increased floodwater velocities. Run 8, 7, 6, 5 and 2 show a rapid increase in hazard which exceeds the moderate threshold, indicating danger to some (i.e. children) 30 minutes before HW. The extreme threshold, which indicates a flood zone with deep or fast flowing water and danger to all, is exceeded 25 minutes before HW, and peaks 23 minutes after HW at 09:05am. Run 8 exceeds the extreme threshold for 1 hour 39 minutes, and exceeds the moderate threshold for 2 hour 13 minutes in total. The junction, at Pickedmoor Lane, Kington Road, Chapel Road and The Naite provide access routes from the M5 to Oldbury Technical Centre and Oldbury-on-Severn. Access routes for emergency services would be shut for the duration of exceedance of the moderate threshold, and represents hazard to all, which may include children and vulnerable adults living nearby. Uncertainty in the hazard time series curves shows that for the same event there may be a danger to none or to all. Footpaths, conveniences (pub, shop, hotel) and a primary school located within a 750 m radius of the road junction may or may not be at risk of flooding and damage during the event, making it difficult to know if or when to issue warnings or evacuation notices. Uncertainty in hazard time series curves is also seen on the Dec 12, however there is a narrower spread of results, as run 8 and 6 exceed the extreme threshold for just 4 minutes, and

the moderate threshold is exceeded for 23 minutes. There is a smaller danger to all during the less extreme event.

Run 8 and 6 (Figure 6.8b) exceed all thresholds when using the WR approach, representing a danger to some and to all. The moderate threshold is exceeded for up to 1 hour 53 minutes, and the extreme threshold is exceeded for 1 hour 4 minutes. When using the WR approach, run 8 and 6 represents 1 hour 53 minutes that the pylon would not be accessible, however the moderate threshold is not exceeded when using the HP approach, indicating that the pylon would be accessible. Sensitivity in the hazard time series curves for run 8 and 6 covers all thresholds, meaning emergency planning is difficult; a flood event could mean the pylon is or is not accessible.

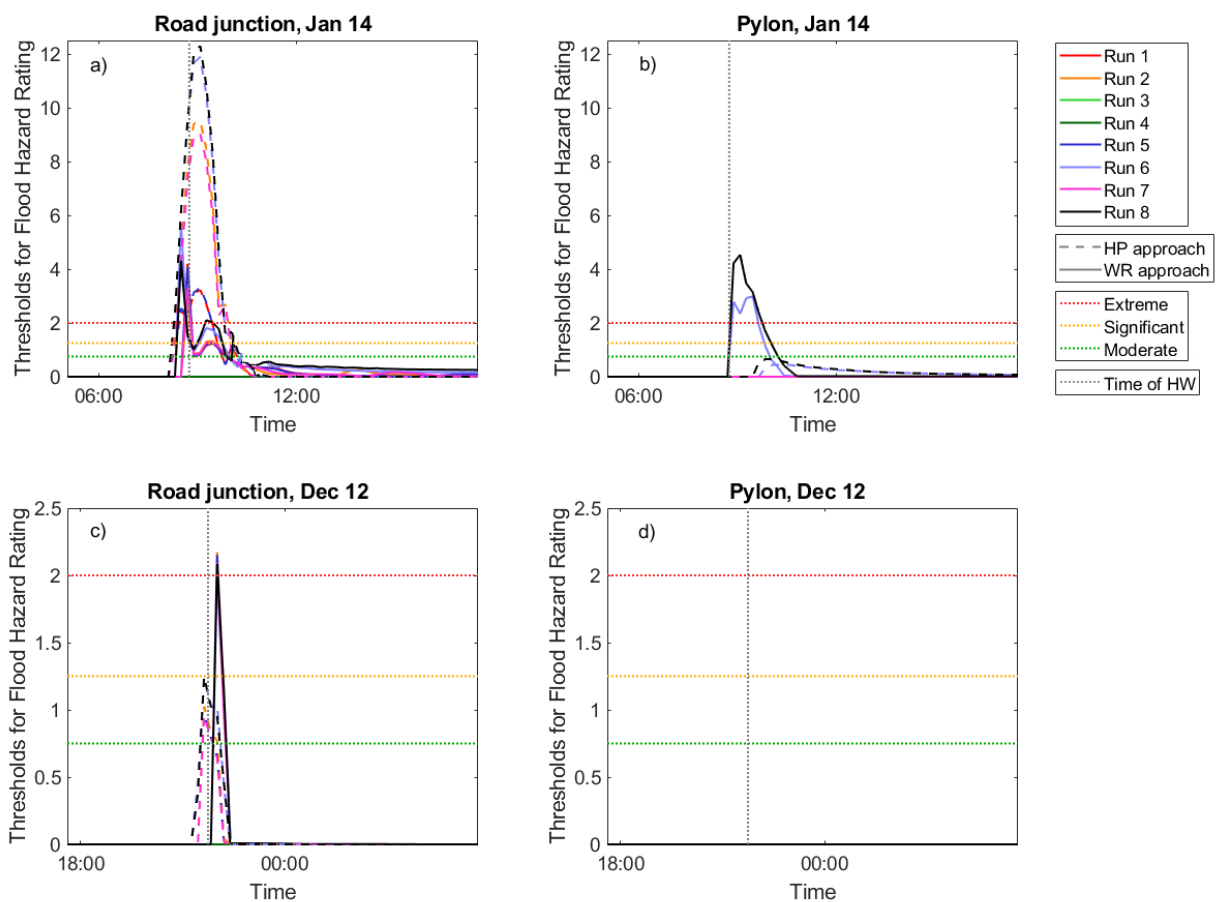


Figure 6.8: Flood hazard rating during the Jan 14 event at a) road junction; b) pylon; and during Dec 12 event at c) road junction; and d) pylon using the HP (dashed black line) and WR approach (solid black line). Modelled tidal signal at the boundary midpoint (vertical dotted black line) and extreme (red, horizontal dotted line), significant (amber, horizontal dotted line) and moderate (green, horizontal dotted line) thresholds for hazard to people (Defra 2003).

6.4.3. Volume of inundation in the model domain

Figure 6.9 shows the change in volume of inland inundation from LW to LW for the Jan 14 and Dec 12 event. The largest volume of flood water for Jan 14 is generated by run 8 using the WR approach, which is 12.5 Mm³. Conversely, the largest volume of flood water for the Dec 12 event is generated by run 6 using the HP approach (see Figure 6.9), which is 5.6 Mm³. The more extreme coastal hazard condition generates a greater volume of flood water, as WL and H_s increase height and duration of peak HP and WR at the boundary.

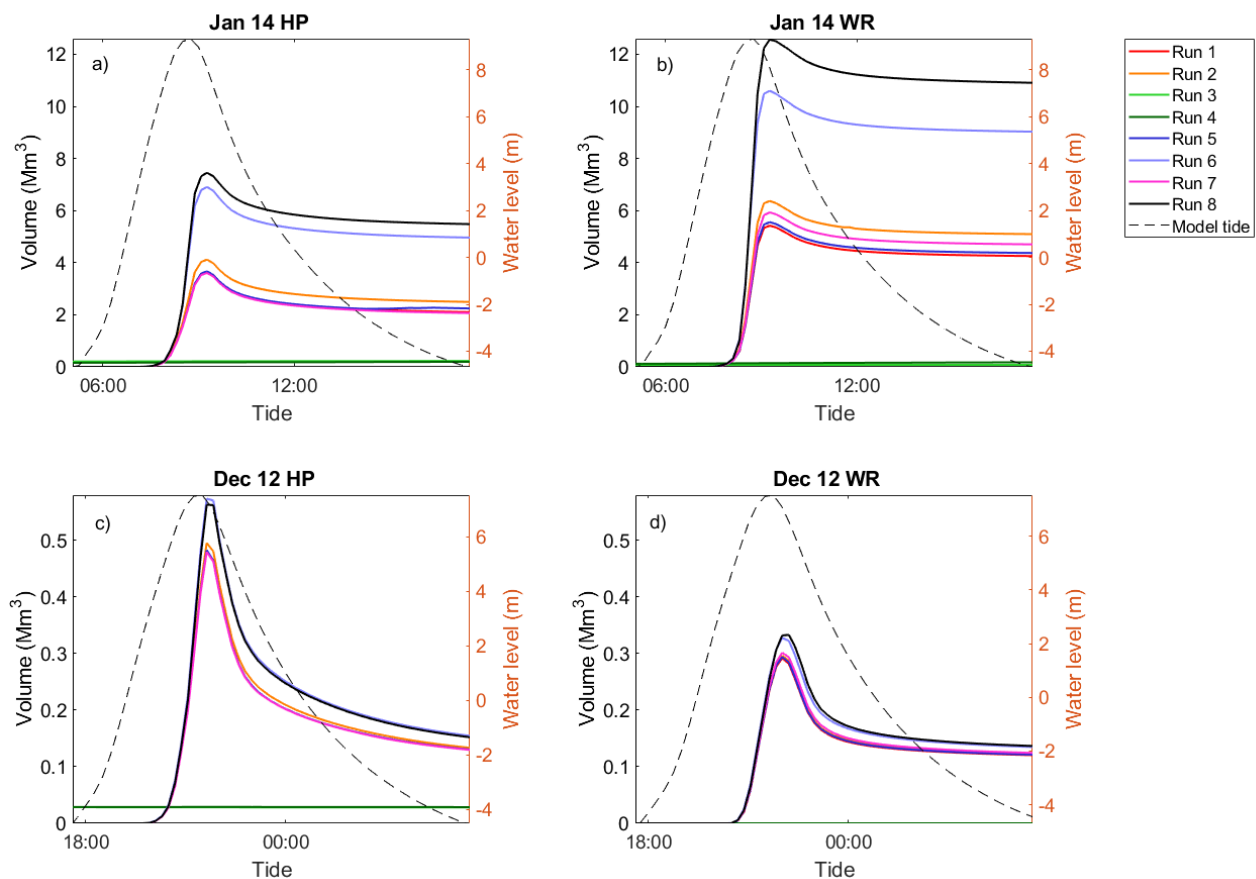


Figure 6.9: Change in volume of inundation (Mm³) in the Oldbury model domain for Jan 14 forced by a) HP and c) WR; and Dec 12 forced by c) HP and d) WR. Modelled high tide from low water to low water is also shown (dashed line).

The Jan 14 event shows greater sensitivity to coastal hazard uncertainty. Run 8 and 6 show greatest volumes of flood water, and then run 1, 2, 7 and 5 are grouped together, with run 1 generating 7.1 Mm³ less flood water than run 8 using the WR approach. Run 3 and 4 show minimal volumes of flood water in the model domains. The results of the Dec 12 event are similarly grouped, but show smaller differences between them, with run 1 generating just 0.05 Mm³ less flood water than run 8 when using the WR approach.

Both events show rapid inundation, and maximum volume of flood water occurs at the same time for each event, with a lag of 8 minutes after tidal high water, which may also be a function of the time step selected for the model simulation. Both events show asymmetric drainage from the model domain. Drainage of floodwater after the time of high water is most rapid for the Dec 12 event using the HP approach, and volume of inundation continues to fall for the duration of the ebb tide. Drainage is slower when using the WR approach, and plateaus on the ebb tide indicating floodwater drains more slowly through this model domain.

6.4.4. Quantification of flood hazard due to coastal hazard uncertainty

Figure 6.10 shows sensitivity in flood hazard (represented by volume of floodwater inundation in the model domain) due to coastal hazard uncertainty. The difference in HP at the boundary midpoint (black cross in Figure 6.1a) is presented against difference in time-integrated volume of inundation in each model domain. The difference in HP is calculated as the change in $WL + \frac{1}{2} H_s$ at the time of high water between each run and run 8, which is used here as a baseline, at a point mid-domain alongshore to show how an increase in regional model WL and H_s changes flood hazard. The difference in time-integrated volume is calculated as the change in integrated area under the curve (Figure 6.10) between each run and run 8. All results present positive difference; this signifies an increase in value presented from each run to run 8. The change in symbol colour in Figure 6.10 indicates a different run; change in symbol shape indicates coastal hazard condition (Jan 14 or Dec 12 event); unfilled symbols represent the WR approach to forcing the model boundary and filled symbols represent the HP approach. Lines connect same runs for each approach to forcing the model boundary for each coastal hazard condition.

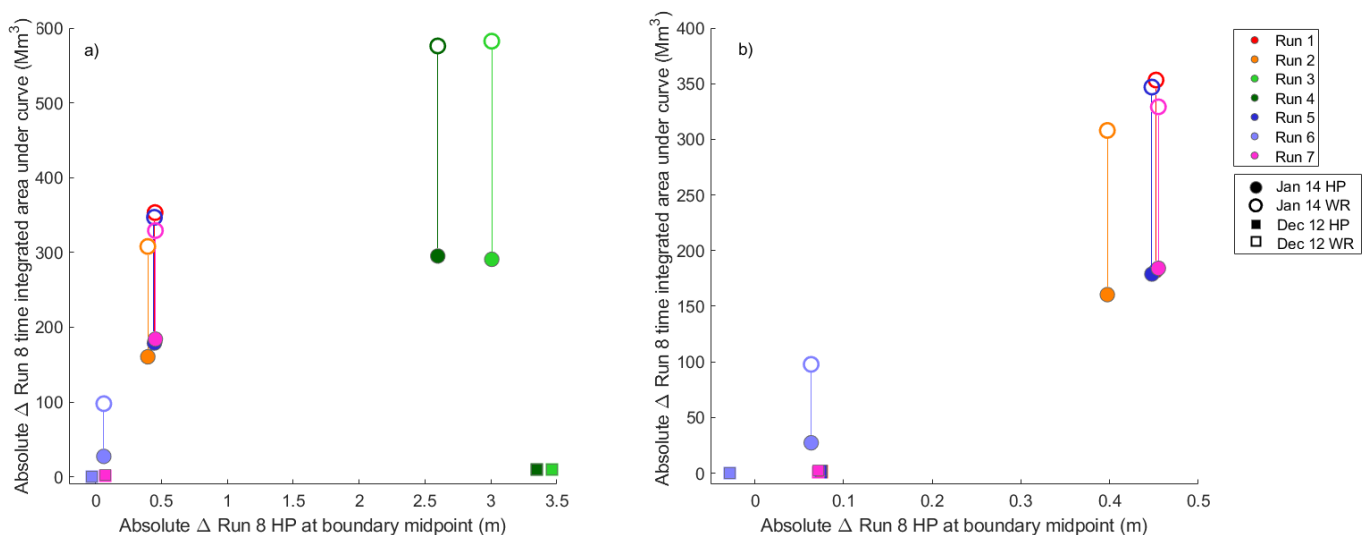


Figure 6.10: Absolute difference in HP at the boundary midpoint (shown in Figure 6.1a) against absolute difference in time-integrated volume for a) all runs compared to baseline run 8; and b) zoomed into run 1, 2, 5, and 7.

Figure 6.10a shows that there is substantial difference in HP at the boundary midpoint (location shown in Figure 1a) and time-integrated volume of inundation between run 3 and 4 with run 8 for the Jan 14 (green circles). Coastal hazard uncertainty generates up to 3.46 m difference in HP at the boundary midpoint between run 3 and 8 for Dec 12, and 3 m for Jan 14. The difference between run 3 and 8 generates up to 582.4 Mm³ difference in inundation. Jan 14 also shows greater sensitivity to approach to boundary forcing, and run 3 generates 280.9 Mm³ difference between WR and HP approaches. Dec 12 generates just 9.9 Mm³ differences in volume of inundation between run 3 and 8, and shows smaller sensitivity to approach to boundary forcing with a difference of 0.8 Mm³ between WR and HP. Runs 3 and 4 are outliers, and not realistic as they are forced with a constant water level; total water level is greatly underestimated when tide is not included as a physical forcing process at the boundary.

Figure 6.10b shows results for realistic runs 1, 2, 5, 6 and 7, compared to run 8. Run 1, 5 and 7 are clustered together for the Jan 14 event, and sensitivity to approach to forcing the model boundary. The Jan 14 event shows up to 353.3 Mm³ difference in volume of inundation with 5.3% (0.45 m) difference in HP at the boundary midpoint, when forced using WR for run 1. The Dec 12 event shows substantially smaller difference in volume of inundation. Run 7 generates 1.16 Mm³ difference in inundation with 0.07 m difference in HP, when forced using HP for run 7. The large difference in volumes of inundation generated between the Jan 14 and Dec 12 event indicates sensitivity to coastal hazard condition. Run 1, 5 and 7 exclude local atmospheric forcing in the boundary condition, which means peak HP and WR values are lower and less overwashing of defences and embankments occurs in the Oldbury model domain. This indicates that the inclusion of local atmospheric forcing in boundary conditions is more important to reduce uncertainty in simulated inundation, than model coupling processes.

Run 2 (orange) is positioned on its own in Figure 6.10b for the Jan 14 event, and shows smaller uncertainty in HP at the boundary midpoint. Run 2 includes local atmospheric forcing, which contributes towards to the peak of WR and HP but excludes wave contribution. This indicates model coupling processes are important to help to improve accuracy of prediction of coastal hazard conditions, but not as important as local atmospheric forcing.

Run 6 for Jan 14 shows smaller uncertainty in HP at the boundary midpoint, but sensitivity to approach to forcing the model boundary remains. For the maximum event, 0.06 m difference in HP at the boundary midpoint generates up to 97.8 Mm³ difference in time-integrated volume (purple, unfilled circle) using the WR approach. Smaller uncertainty in HP is due to the inclusion of local atmospheric forcing and one-way coupling in the coastal hazard from Delft3D, which generates higher WR peak to result in more overwashing at more locations along the crest line. Even a small change in HP at the boundary midpoint can mean hazard thresholds are exceeded to have a substantial impact on volume of inundation.

Overall, the more extreme coastal hazard condition (Jan 14) generates a steeper trend. Jan 14 shows increased uncertainty in flood hazard with increased uncertainty in coastal hazard uncertainty and sensitivity to approach to forcing the model boundary. Dec 12 generates small volumes of inundation as thresholds for flooding are not exceeded.

6.4.5. Economic cost of inundation for arable and suburban land uses

Table 2 and 3 show economic cost of inundation at the time of maximum inundation for arable and suburban land uses. Run 8 for Jan 14 using the WR approach generates greatest cost to arable land (£4.3 M) and to suburban land uses (£60.9 M). Runs 3 and 4 generate smallest economic cost at the time of maximum inundation, for both events across both model domains.

Table 6.2: Simulated economic cost of inundation for arable land cover

		Arable land cost (£ M)							
		1	2	3	4	5	6	7	8
Maximum	HP	1.55	1.91	0.07	0.01	1.56	2.96	1.51	3.06
	WR	2.80	3.09	0.00	0.01	2.84	4.00	2.95	4.31
90 th pc	HP	0.07	0.07	0.01	0.01	0.07	0.10	0.07	0.10
	WR	0.02	0.02	0.00	0.00	0.02	0.03	0.02	0.04

Table 6.3: Simulated economic cost of inundation for suburban land cover

		Suburban land cost (£ M)							
		1	2	3	4	5	6	7	8
Maximum	HP	44.85	46.48	6.13	2.46	44.89	53.10	44.71	54.35
	WR	33.01	36.06	0.62	2.45	33.48	48.55	34.73	60.91
90 th pc	HP	17.61	17.99	1.82	1.80	17.61	19.89	17.56	19.75
	WR	8.49	8.78	0.00	0.00	8.66	10.16	9.05	10.41

Figure 6.11 shows the absolute difference in HP at the boundary midpoint against absolute difference in economic cost to (i) arable land and (ii) suburban land at time of maximum inundation against between each run and run 8. The economic cost of flood events is important information for shoreline management planning. The change in symbol colour in Figure 6.11 indicates a different run; change in symbol shape indicates coastal hazard condition (Jan 14 or Dec 12 event); unfilled symbols represent the WR approach to forcing the model boundary and filled symbols represent the HP approach. Lines connect same runs for each approach to forcing the model boundary for each coastal hazard condition. In the text absolute changes are shown below in brackets for context. Run 3 and 4 are not shown in the following analysis, as they are outliers and not realistic.

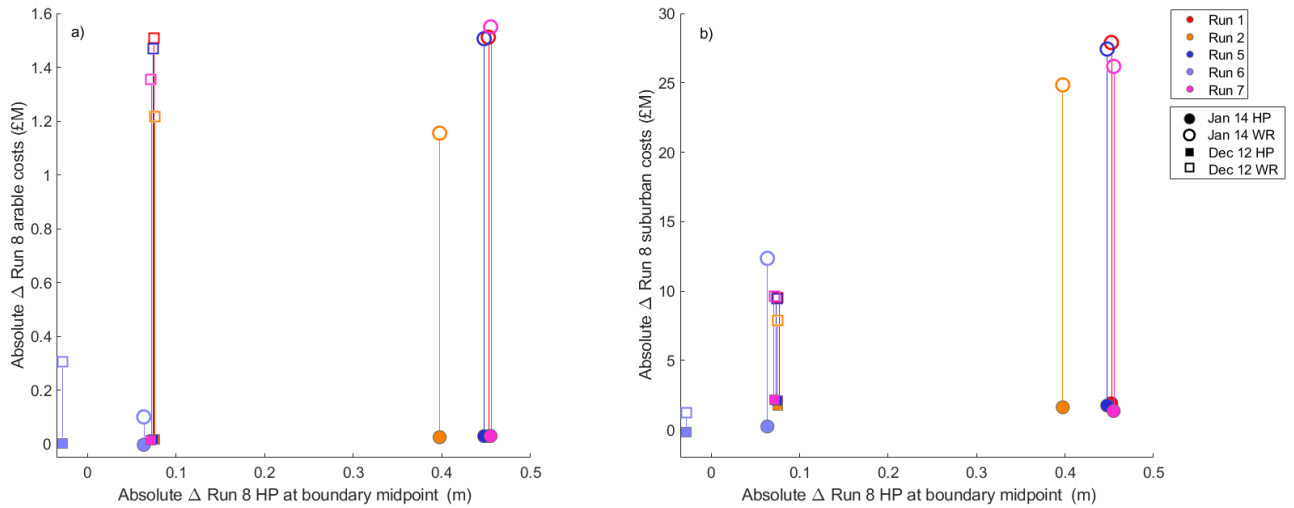


Figure 6.11: Absolute difference in HP at the boundary midpoint (shown in Figure 6.1a) against absolute difference in a) arable land costs and b) suburban land cost for runs 1,2,5,6 and 7 compared to baseline run 8.

Figure 6.11a shows absolute difference HP at the boundary midpoint and arable costs compared to run 8. As also seen in Figure 6.10 for the Jan 14 event, run 1, 5 and 7 are grouped for each event, and then run 2 is positioned on its own, with run 6 showing smallest uncertainty in HP and arable costs. Run 7 for the Jan 14 event with WR approach (unfilled, pink circle) generates up to £1.5M difference in arable costs, against 0.45 m difference in HP at the boundary midpoint, whereas the HP approach (filled, pink circle) generates £30.4k difference. The HP approach generates smaller absolute differences in arable costs for all coastal hazard uncertainty conditions. Both events show steep trends indicating increased uncertainty in boundary condition increases uncertainty in arable costs. Both events also show sensitivity to approach to forcing the model boundary, indicated by the large differences between WR and HP symbols. Sensitivity to approach to forcing the model boundary may also be caused by the land types that are inundated close to flood pathways.

Figure 6.11b shows absolute difference in suburban costs compared to run 8. Wider spacing between the WR and HP symbols for the more extreme Jan 14 event indicates greater sensitivity to boundary forcing approach. For run 1 using the WR approach £27.9 M difference in suburban costs is generated, whereas the HP approach generates £1.9 M difference; sensitivity to boundary forcing approach generates up to £25.9 M uncertainty in suburban costs. Run 6 generates a 0.06 m difference in HP at the boundary for Jan 14, and still generates up to £12.4 M cost to suburbia. It is crucial for shoreline management, infrastructure or residential planning to consider uncertainty in flood costs for long term assessments. For both events WR generates greater difference in suburban costs, which may be due to suburban areas being more closely located to overwash and breach locations along the coastal defences and embankments. The WR approach leads to greater impact as it is more realistic, in considering

surfzone and shoaling processes, compared to the HP approach imposed at the LW mark. Overall, there is a steeper gradient in response to coastal hazard uncertainty for the Jan 14, compared to Dec 12.

The results show that optimal model setup should include local atmospheric forcing and two-way coupling; run 8 has been validated in Delft3D-FLOW-WAVE and generates largest impacts of inundation compared to all other runs. Excluding local atmospheric forcing could cost up to £26.2 M in cost-benefit analysis when considering flooding for long-term hazard assessments and emergency response planning. Excluding two-way coupling processes could cost £12.4M in a flood damage assessments, and exclusion of both forcing and coupling processes could cost up to £60.9M.

6.5. Discussion

Coastal hazard uncertainty, due to coupling and forcing processes in WL and H_s prediction from Delft3D-FLOW-WAVE, was propagated through the LISFLOOD-FP Oldbury model domain using the hazard proxy ($WL + \frac{1}{2} H_s$) and wave runup (Stockdon et al., 2006) approach to the force the model boundary for two historic storm events, to determine the impact on inundation. On the basis of this case study, it has been shown that flood hazard is sensitive to event severity, as the Jan 14 event consistently generated greatest impact of inundation, presented here as flood hazard rating, volume of floodwater and economic cost. Flood hazard is also sensitive to coastal hazard uncertainty as the source of flood hazard; forcing and coupling processes in boundary conditions generates a spread in results in the impacts of inundation. Flood hazard is also sensitive to approach to forcing the model boundary as this influences floodwater pathways, spatial pattern of inundation and drainage of floodwater.

LISFLOOD-FP confirms that run 8 (two-way coupling + local atmospheric forcing) generates the largest volume of inundation, 12.5 Mm^3 and greatest economic cost to arable (£4.31 M) and suburban (£60.91 M) land using the wave runup approach for Jan 14 event. For this event HWH_s is 0.94 m, superimposed on HWL of 9.4 m. Larger waves during the more extreme coastal hazard condition have a greater impact on wave runup, and contribute more directly as a source of flood hazard. Steeper embankments in the northeast of the domain generate larger wave runup, which is a pathway for flood hazard to increase inundation in Shepperdine and Bevington. The Dec 12 event generates substantially smaller time-integrated volume of inundation using both the hazard proxy and wave runup approach, as this event has a HWH_s of 0.31 m on a HWL of 8.09 m. Smaller waves for Dec 12 event means that smaller wave runup is generated and no flood pathway over the earthen embankments is created for the wave runup approach, and hazard thresholds are not exceeded for the hazard proxy approach. Event severity has been shown to be an important control on flood hazard in hyper-tidal estuaries (Lyddon et al., 2018a), as higher water levels during extreme events can propagate wave energy shoreward (Gallien et al., 2018).

Larger wave runup superimposed on a large spring tide, exacerbated in the northwest of the domain due to steeper embankments, creates a compound flood pathway (Gallien et al., 2014). The wave runup approach generates more inundation behind steep earthen embankments due to overwash of greenwater, in addition to inundation in the towns of Berkeley and Oldbury-on-Severn (see Figure 6.5). Once hazard thresholds have been exceeded, the wave runup approach further exacerbates flood hazard because the boundary is located on the defence crest, and the model domain has less floodwater accommodation so floodwater is 'locked in'; there is no intertidal space in the model domain for floodwater to gravity drain into through the rhines and channels after HW. High 'tail water' conditions from a flood tide or storm surge have been shown to prevent drainage, and can exacerbate other flooding source-receptor pathways (e.g. flooding due to wave overwashing and defence breaching) (Gallien et al., 2011; Wahl et al., 2015). Here we show that more extreme storm events and local, site-specific morphology of the coastline generates larger wave runup and more overwashing, to increase flood hazard. The wave runup approach increases the volume of inundation as floodwater enters the domain at multiple locations, and is retained in the model domain which generates an additional compound flooding pathway. Different sources of uncertainty can combine with each to increase uncertainty in flood hazard inundation, and make important contributions to compound flooding pathways at different times during the flood simulation (e.g. event severity during the flood stage, boundary forcing approach during the ebb stage).

Flood hazard is also sensitive to event severity and local morphology of the coastline using the hazard proxy approach. Run 8, used throughout as the baseline, for the 3 January 2014 event generates 311.8 Mm³ time-integrated volume of inundation using the hazard proxy approach for run 8, compared to 589.7 Mm³ generated from the wave runup approach. The position of the boundary using the hazard proxy approach means there is greater floodwater accommodation to provide space for floodwater to drain into in the intertidal areas, unlike the wave runup approach. This shows that boundary position is also able to reduce compound flood hazard, by providing floodwater accommodation and easier drainage pathways on the ebb tide. The influence and importance of uncertainty of input factors on flood hazard sensitivity can change over the course of a flood event; it has been shown that the rising limb of an inflow hydrograph is most important during the flood stage of inundation in the coastal city of Licata, Sicily, then the channel friction parameter is most important during peak inundation and floodplain friction parameter during drying phase of the flood (Savage et al., 2016).

The results presented here show the combined effect of extra- and intra-model uncertainties (Lewis et al., 2013) on flood hazard. Extra-model uncertainties relate to the data and approaches used to force the model boundary. Accurate total water level and wave predictions are important for assessing flood risk in coastal areas with high tidal ranges, or subject to large storm surges (Hawkes et al., 2002). However, model sensitivities vary across space and the contribution of each physical process to a compound flooding pathway is site specific. For example, larger water levels are more important than wave height for inundation for storm events with a 0.5% probability in Dungeness, UK, as 5.28 m WL + 0.92 m H_s

will cause more inundation than 1.8 m WL and 5.72 m H_s (Prime et al., 2016). Intra-model uncertainties, such as boundary position or model domain size, influences floodwater pathways and controls the simulated spatial pattern of inundation and retention of flood water. This research shows changing the approach to boundary forcing influences the flooding pathways and drainage of floodwater at a local scale. The wave runup approach is the more sophisticated approach, as it considers how surfzone and shoaling effects transform deep water waves to the coastline, and generates £11.8 M less subsequent damage costs for suburbia when comparing run 1 for each approach. Structures within the model domain, e.g. the position of bridges, can influence the amount of backwater held in a modelled region to influence flood hazard (Pappenberger et al., 2006), in addition to uncertainty in upstream boundary conditions. The spatial resolution of the DEM may contribute to uncertainty, but is not influential during the wetting phase of large storm events as the rapid rising limb indicates floodwaters are deep enough to move across small fluctuations in topography, but may be more influential during the recession of floodwaters or for less severe events (Savage et al., 2016). The causes of sensitivity in inundation models interact with each other (Perini et al., 2016), and each input factor will require more or less consideration dependent on the decisions or assessments the inundation model is being used to support, or the scale of the area being considered.

The model illustrates that flood hazard is sensitive to coastal hazard uncertainty, as the inclusion of local atmospheric forcing or coupling processes influences the impacts of flooding. Sensitivity of inundation to boundary conditions has been shown in studies worldwide. Uncertainty in boundary forcing, due to interpolation of boundary conditions in data poor regions, has been shown to generate greater uncertainty within an inundation model compared to DEM uncertainty when simulating future storm tide conditions in the Bay of Bengal (Lewis et al., 2013). Different approaches to generating boundary conditions for LISFLOOD-FP (e.g. based on linear interpolation of extreme values, or spatial characteristics of observed storm tides) caused up to 90 cm difference in storm tide peak along the North Somerset coastline, UK when simulating inundation from the December 13 1981, and subsequently up to 8.9 km² difference in overall inundation (Lewis et al., 2011). Uncertainty in coastal water levels and defence failures have been shown to generate greatest sensitivity in coastal flooding of Canvey Island, UK, as opposed to model terrain and bottom friction (Brown et al., 2007). Flood inundation simulations are sensitive to the choice and design of boundary conditions, and it is important to accurately capture the hydrodynamic and atmospheric conditions occurring during extreme events (Pasquier et al., 2019) for storm hazard mitigation, adaptation and resilience planning.

The model shows that for all runs, once conditions exceed hazard thresholds to cause coastal flooding then even small changes coastal hazard uncertainty matter in terms of the cost of flood damages. A 0.45 cm difference in coastal hazard uncertainty at the boundary using the wave runup approach for the Jan 14 event can cause 353.3 Mm³ difference in time-integrated volume of inundation and £27.9 M difference in economic cost to suburban land. Even as small a change in hazard proxy at the boundary

as 0.06 m can generate up to 97.7 Mm³ difference in time-integrated volume of inundation, and £12.4 M difference in cost to suburban land. A water level elevation error of 2-3 cm, due to error in observation of tidal level or lack of wave forcing, has been shown to generate 3-25% variation in flood area in Newport Beach, California, dependent on location and hydraulic connectivity (Gallien et al., 2011). The changes in coastal hazard uncertainty, due to forcing and coupling processes in the boundary conditions, can be used to infer how changes in future sea level could impact inundation in coastal and estuarine areas.

The changes in total water level at the coastline presented here are within the range of the Intergovernmental Panel on Climate Change (IPCC) global projections of SLR, which range from 28 to 98 cm by 2100 (Church et al., 2013) and the UKCP18 projections in Cardiff range from 0.27 to 1.31 m by 2100 (Lowe et al., 2018). Even a small change in sea-level rise will have a large impact on flood hazard as tidal amplitudes and estuarine morphologies change (Leuven et al., 2019), and compound flood pathways may be exacerbated (Moftakhari et al., 2017). As the baseline on which storm surges and waves act is raised, wave energy propagates further shoreward exposing communities and infrastructure to the increased probability of defence failure (Le Cozannet et al., 2015; Marcos et al., 2019). Many low-lying areas that are sensitive to coastal flooding during storm events will be overwhelmed with just 25 cm of sea-level rise along the California coastline; in combination with a 1:100 year storm event this could cause substantial flooding that would impact 150,000 residents and cause up to \$30 billion damage (Barnard et al., 2019). Future sea-level rise will increase ‘tail waters’ and reduce the rate at which low-lying coastal and estuarine areas are able to drain floodwater, increasing the likelihood of further inundation from subsequent storm or rainfall events (Amante 2019). Extreme events can cause initial damage from flooding, but lack of drainage, potentially exacerbated by subsequent events, can cause ripple effects to impact economic sectors in relation to closure of ports and harbours or disruption of transport of goods and services, and critical services (e.g. power, water, and communications), essential for public safety. However the response of estuarine areas to sea-level rise threats may be dependent on their size, as large estuaries may experience increased channel volume due to sediment starvation, and subsequently flood hazard may be reduced (Leuven et al., 2019). Flood hazard assessments should, of course, be site-specific and targeted at understanding local or regional conditions under changing climate conditions, which can provide information on impacts in local areas of high flood risk. Inundation studies can support targeted adaptation strategies allow coastal authorities to warn people living in high risk areas, and reduce risk by implementing resilience measures to minimise flood depths or improve drainage.

6.6. Conclusion

The combined effect of astronomical tides, meteorological storm surges, wind and waves can increase flood hazard in heavily populated and industrialised estuaries, which are the focal point of coastal

megacities, critical infrastructure and economic activity. Accurate predictions of high water level and high water significant wave height are required to develop hazard maps or warning systems to mitigate the negative effects of combined flood hazards. However uncertainties in high water level and high water significant wave height predictions can propagate through the modeling chain to cause uncertainties in shoreline response models, which are used to support decisions for storm hazard mitigation. Coastal hazard uncertainty is increased by an order of magnitude when assessing the uncertainty in resulting inundation.

Time- and space-varying predicted water level and significant wave height at the coast from eight Delft3D-FLOW-WAVE model simulations, each representing uncertainty due to coupling and forcing processes, force LISFLOOD-FP, a 2D inundation model, at Oldbury-on-Severn, southwest England. Two approaches to forcing the model boundary were used; hazard proxy was imposed at the low water mark, and wave runup combined with water level at the defence crest. Simulations were completed for 3 January 2014 event, representing the most extreme coastal hazard condition on record, and 16 December 2012 representing the 90th percentile coastal hazard condition. Inundation is sensitive to sources of flood hazard, notably coastal hazard condition and coastal hazard uncertainty. The 3 January 2014 event generates the greatest impact of inundation, as larger high water level and high water significant wave height increases the peak and width of wave runup and hazard proxy. Run 8 generates up to 12.5 Mm³ of flood water and £60.9 M cost of damage to suburban land using the wave runup approach, caused by overwashing of greenwater at the defence. Once the conditions in run 8 exceed the hazard thresholds to cause coastal flooding, then small changes in the condition matter in terms of the cost of flood damages. The inclusion of local atmospheric forcing and coupling processes are important for reducing uncertainty in inundation. This is confirmed by results from run 6, which simulates inundation most closely with run 8 (used here as the baseline), and generates smallest changes in flood hazard rating, time-integrated volume of inundation and economic costs compared to run 8. Further to this, run 3 and 4 generate up to 582.4 Mm³ difference in time-integrated volume of inundation run 8, as they are forced with a constant water level; total water level is unrealistic and greatly underestimated when tide is not included as a physical forcing process at the boundary. The exclusion of local atmospheric forcing could cost up to £26.2 M in flood damage assessments when considering flooding for long-term, shoreline management plans. Coastal hazard uncertainty also has implications for emergency response planning, as events can present a danger to all or to none.

Impacts of inundation are also sensitive to approach to forcing the model boundary, which interacts with coastal hazard condition to alter the pathway of flood hazard. Once the threshold for flooding is exceeded compound flood pathways can be exacerbated due to coastal hazard condition and approach used to force the model boundary during the flood phase, as site-specific morphology of the coastline increases peak wave runup and location of overwash, and floodwater accommodation in the model domain influences drainage after the peak of the flood. The results show that even a small change in

coastal hazard uncertainty of 0.06 m can influence peak hazard proxy and wave runup and locations of overwash to cause up to 97.7 Mm³ difference in time-integrated volume of inundation and £12.4 M difference in cost of damage to suburban land. These small changes in total water level at the boundary can be used to infer how small changes in future sea level could have a large impact on coastal inundation. Contributions to uncertainty in inundation models should be considered when developing local scale studies of storm events under present and future sea-level scenarios for storm hazard mitigation and adaptation or resilience planning.

6.7. Acknowledgments and Data

The authors thank colleagues at the British Oceanographic Data Centre (BODC) for providing tidal data; Magnox for providing tidal data; Environment Agency for providing tidal and river gauge data; Gloucester Harbour Trustees for providing tidal data; Met Office for providing observational wind data and WAVEWATCH III data; Met Office and NOCL for providing CS3X wind and atmospheric pressure data; CEFAS for providing observational wave buoy data; EDINA for providing bathymetric and LiDAR data, and Ordnance Survey basemaps. The research is a contribution to the NERC highlight topic “Physical and biological dynamic coastal processes and their role in coastal recovery” (BLUE-coast, NE/N015614/1).

Data used in this research are available from sources stated in the reference list.

7. Conclusions and Implications

The results presented in this thesis answer the three main research questions (listed again below) to contribute to local-scale, long-term flood hazard management, particularly when viewed in the context of the source-pathway-receptor-consequence model (Narayan et al., 2012).

- i. Which key sources of coastal hazard uncertainty should be considered when predicting coastal flood and wave hazard?
- ii. What is the relative importance of each source of uncertainty in coastal flood hazard assessments?
- iii. How does coastal hazard uncertainty influence the physical and economic impacts of flooding?

7.1. Uncertainty in sources and pathways of flood and wave hazard

The numerical modelling system Delft3D-FLOW and -WAVE was used in chapters 2, 3, 4 and 5, and LISFLOOD-FP in chapter 6, to understand the sensitivity of coastal hazard predictions to intra- and extra-model uncertainties (Lewis et al., 2013). The Severn Estuary, which borders southwest England and south Wales, is used here as an extreme example of a hyper-tidal estuary. Its length, shape and size is unique in that it generates a tidal range up to 12.2 m, so the Severn Estuary is used here to show how severe flood and wave hazard can be when large tides are combined with storm surge, strong winds or waves. Numerical modelling systems are used here to quantify epistemic uncertainty, which arises due to limited data or knowledge about a physical process, in predictions of water level and wave heights through sensitivity tests to improve confidence in flood hazard assessments. This research has focused on the sensitivity of coastal hazards due to tide, surge, waves, and wind. This could be extended further as future research to study sensitivities in the river flow.

7.1.1. Extra-model uncertainties

Extra-model uncertainties relate to data and approaches used to force the model boundary and its influence on water level and wave height prediction is captured here through the use of sensitivity tests representing variability in forcing and coupling processes. Chapter 2 identifies the combined effect of tide + storm surge as a key source of flood hazard in a hyper-tidal estuary, and the spatial and temporal variability of flood hazard due to different sources of uncertainty. **Event severity** is a key source of uncertainty, and shown to be the most important control on flood hazard at a local scale. A more severe event, generated by the concurrence of a severe, low atmospheric pressure system with equinoctial spring tides or the nodal cycle (as occurred in January 2014 in the Severn Estuary (Sibley et al., 2014)), will increase peak observed water levels above the predicted level, to potentially exceed critical flooding thresholds. Event severity causes variability in flood hazard at tide gauge locations so should be

accurately forecast at a local scale to ensure warnings can be issued to appropriate authorities and the public, so negative consequences can be avoided. **Timing of the storm surge** is another important control on flood hazard and source of uncertainty; tide + surge concurrence increases maximum total water levels by up to 10.2 %, as the peak of two coastal hazard parameters combine at the same time to generate greater magnitude of total water levels. It is important to accurately simulate tide + surge concurrence as this is a source of uncertainty which influences whether critical storm thresholds are exceeded at the time of concurrence. The **shape of the storm surge** component with time (termed surge skewness in chapter 2) generates variability in total water level as it controls the water volume and surge inflow into the estuary and influences the duration of high water peaks so is considered a source of uncertainty. Further to this, chapter 3 highlights that tide + concurrence and surge skewness generates uncertainty in surge amplitude up-estuary, with increases up to 255% at Sharpness due surge-tide interaction from funnelling effects. If surge skewness and timing of a storm surge can be precisely forecast or detected early, then locations in the upper estuary can be warned of consequential amplification of the flood hazard.

Wave hazard in estuaries is largely attributed to high amplitude shorter period, locally generated wind waves; while low amplitude longer period waves rarely impact low-lying coastal zones up-estuary. Representative values for wind speed and direction, wave height, period and direction are used in Delft3D-WAVE in chapter 4 to identify key combinations of factors that define the wave hazard generation along the shoreline of the Severn Estuary. **Wave height** and **wave period** is an important overall control on maximum wave hazard and influences the response of the wave to other forcing factors. Opposing **wind direction** acts to steepen higher amplitude, shorter period waves and generate maximum wave hazard in the outer estuary. In contrast a following wind enhances propagation of lower amplitude longer period waves further up-estuary. Higher **wind speed** contributes momentum to the estuarine system and amplifies the responses to changing wind direction. This is particularly critical for sites of infrastructure up-estuary, as longer period waves could generate a significant and underestimated hazard up-estuary if exacerbated by local wind-wave effects. Accurate representation of critical wind-wave conditions is important for the prediction of wave hazard, and results can inform sea defence design and reduce losses from operational downtime. The results show how wave hazard in hyper-tidal estuaries could be exacerbated if changing future storm tracks alter wind speed and direction.

Chapter 5 identifies that the accurate prediction of flood and wave hazard depends on combined effect of all coastal hazard parameters: tide + surge + wind + wave + river. Local atmospheric forcing is most important when simulating coastal hazard parameters, to ensure momentum is continually added to the estuarine system, for wave propagation and generation. The exclusion of **local atmospheric forcing** from boundary forcing acts a source of uncertainty, and underestimates high water significant wave height by up to 90.1%, high water level by 1.5%, and hazard proxy (water level + $\frac{1}{2}$ significant wave

height) by 9.1%. **Coupling processes**, which represent the physical interaction between waves and circulation in the numerical modelling system, are identified as an additional source of uncertainty when predicting coastal hazards. Two-way coupling represents important shallow water processes to control wave hazard along the coastline, including refraction around headlands and wave breaking. Identifying and quantifying the uncertainty associated with these sources of flood hazard can support the development of intervention strategies and risk management processes. It has been shown that the exclusion of locally generated winds underestimates high water significant wave height by up to 1.45 m. Coastal sea defences, which are critical to protecting communities and infrastructure from flooding, could be built too low if the contribution of local winds to wave hazard is not considered when designing appropriate crest levels. This could lead to overwashing at the time of high water, and increased nuisance flooding and economic costs.

The data used to simulate coastal hazard parameters in chapter 2, 3, 4, and 5 and drive the model boundary utilises observation and model hindcast data, which should also be considered a source of uncertainty. Observation water level and storm surge time series used to force the model boundary in chapter 2, 3 and 5 is taken from two of the UK's national A-Class tide gauge database from the British Oceanographic Data Centre (BODC, www.bodc.ac.uk). Water level measurements are available as 15-minute average values, which is considered high temporal resolution, but could still introduce uncertainty into the model as the exact time or magnitude of high water may be smoothed from the record. Levelling and determining the absolute datum of the tide gauge can also contribute to uncertainty in tide gauge data (Pytharouli et al., 2018). It has been shown that variability in a storm tide time series can influence total water level and subsequent overflow volumes, which can have implications for flood risk assessments (Quinn et al., 2014). All archived tide gauge data from BODC has undergone rigorous quality control, and erroneous or modelled data is clearly flagged. In this study, all modelled and erroneous data in the tide gauge record from Ilfracombe and the Mumbles is removed, to ensure confidence in the data used to force the model boundary. River gauge data is also used from an Environment Agency measuring station near Gloucester which is available at an hourly resolution. This has proven to be an acceptable resolution in this study as the model is well validated in the upper regions of the estuary, and river contribution does not appear significant during extreme coastal events. However, sensitivity of coastal flood hazard to fluvial discharge may require finer temporal resolution of the hydrograph to force up estuary model boundaries in smaller, steeper catchments which are subject to flash floods, such as the Dyfi, Wales (Robins et al., 2018) to capture variability in river levels. Larger catchments, such as the Humber Estuary, England, can be forced with daily river gauge levels as the catchment shows less sensitivity to the shape of the flood hydrograph (Robins et al., 2018). The accuracy of a model is largely dependent on data availability, and often modellers must make the most of what is available. Sensitivity tests can be used to test the suitability of data used to force the model boundary and identify key sources of uncertainty.

Chapters 2, 3, 4 and 5 identify that it is not just coastal hazard parameters (tide, surge, wind, wave, river) that contribute as sources of flood and wave hazard, but estuarine morphology and local bathymetry also act as a source of flood hazard and pathway, which conveys the hazard to people. Chapters 2 and 3 show that estuarine morphology amplifies maximum tide and surge elevations up-estuary; funnelling effects influence magnitude, timing and duration of peak water level. This highlights the importance of accurate boundary conditions to capture initial water level conditions at the mouth of the estuary, to ensure accurate representation of funnelling up-estuary which influences surge predictions away from tide gauge sites. A tipping point occurs up-estuary between funnelling and shallow water effects where friction effects control magnitude of total water levels as energy dissipation minimises tide and surge elevations. This highlights the importance of accurate bathymetry to capture shallow water effects at up-estuary locations. Measured bathymetry, which represents water depth, bed features and the coastline, influences tide, surge and wave propagation as height of these long period waves is controlled by water depth. Bathymetry contains two independent measurements, in the horizontal position (x-y) and the vertical position (z), and is subject to independent uncertainty as a function of the methods used to collect the data, using acoustic technologies from boats or planes (Lucieer et al., 2016). Uncertainty in bathymetry is also dependent on how recently data has been collected due to the nature of river and coastal systems, whereby erosion/deposition processes can alter bathymetry (Byrnes et al., 2002). Therefore, bathymetry may only be accurate for a short period of time, and assumptions must be made about the validity and usefulness of the data available by the user. Quality control and assurance procedures are in place to ensure that uncertainty in bathymetric surveys is reduced, and data availability often leaves modellers with little other choice than to use what is available when setting up model domains and communicate uncertainty and assumptions to the end-user.

7.1.2. Intra-model uncertainties

The choice of model and individual model parameter values can also contribute to uncertainty in modelled water level and wave heights, termed intra-model uncertainties. The modelling systems used here represent a simplification of actual physical processes in estuarine and coastal environments, through mathematical equations including the shallow water equations. Complex hydraulics are represented by a depth-averaged, hydrodynamic model meaning that velocities are averaged over the water column. The structure of Delft3D introduces uncertainty so that processes that occur on a vertical scale, such as turbulent mixing, salinity gradients and heat fluxes not accounted for (Hu et al., 2009; Xia et al., 2010; Iglesias et al., 2019). The selection of a specific solver in LISFLOOD-FP means that certain aspects of the shallow water equations are ignored, so sensitivity tests can be used to compare input parameters. LISFLOOD-FP is not able to capture details of supercritical to subcritical flow, which may be important in areas close to a dam or embankment breach (Néelz and Pender, 2013). The

numerical scheme used by the model has an influence on how well it can capture details of the flow field and could generate uncertainty in results. A model should be selected based on the aims and site-specific conditions of the research to minimise uncertainty.

The representation of the geometry of the estuary and coastline in the model grid also means that processes that occur on a sub-grid scale are not explicitly accounted for, and can introduce uncertainty (Fringer et al., 2019). The curvilinear grid used here in Delft3D was developed over time using a trial and error processes and aims to achieve the best representation of the Severn Estuary. The model grid used in LISFLOOD-FP has a regular grid size, so selecting the correct resolution is critical as it has been shown that flood extent is dominated by topography as opposed to the physics of flood propagation (Maskell et al., 2014). However, computational time increases as the resolution of the grid becomes finer, and the size of output files increases as there are more grid cells and nodes, making files harder to store. There is a balance between accuracy of the model grid and computational efficiency, so that increasing the number of grid cells further will not create better results than achieved with the current mesh, whilst maintaining computational efficiency (Kärnä et al., 2015).

Model parameters are derived over time through calibration and trial and error, as described in section 1.7.1.3 and 1.7.1.4, and it is the job of the modeller to identify which parameters contribute greatest uncertainty, and work to minimise the uncertainty or ensure that the implications of uncertainty are communicated to the end-user. The Manning's coefficient is used to represent the amount of bed friction (bed shear stress from bottom roughness) that is applied to the flow, and provides some control on the flow velocity and direction (Garzon and Ferreira, 2016). The Manning's coefficient is influenced by geometric and hydraulic changes, including depth of flow, channel width, bed slope and sinuosity however it cannot be measured directly (Ding et al., 2004). Incorrect selection of the Manning's coefficient can lead to uncertainty in model results, as model terrain largely determines flow and flood patterns (Brown et al., 2007). Inaccurate flood friction parameters in an inundation model can also lead to errors when modelling floodwater propagation and drainage (Kumbier et al., 2018). Values are determined through a calibration process so that modelled water level outputs match observed water level outputs to the highest degree possible. Monte Carlo sampling techniques can also be used to draw random samples from random, probabilistic values and then evaluate them (Bellos et al., 2017). The calibration process can reduce the level of uncertainty in the Manning's values, and a uniform parameter was selected in this research based on the runs with the best R^2 correlation, and smallest bias and RMSE. A uniform parameter represents a simplification of bottom roughness and represents a common approach in coastal and estuarine modelling studies (Condon and Veeramony, 2012). A spatially varying coefficient can be based on land use data and may be preferred as it is able to represent changes in surface roughness, channel bedforms and vegetation (Mattocks and Forbes 2008). A spatially varying coefficient may be particularly valuable in the upper reaches of an estuary, where energy dissipation and wave breaking is largely controlled by bottom friction due to the shallow nature of channels

(Pascolo et al., 2018). Land cover datasets can be used to represent these spatial changes in bed roughness, and have been used to incorporate bottom friction information into hurricane storm surge models (Liu et al., 2013). It has been shown that bottom friction formulation can have little impact on tidal signal accuracy in the Gulf of Mexico (Kerr et al., 2013), but can cause up to 1 m errors in surge prediction in shelf regions of the Texas coast (Ferreira et al., 2014). A temporal varying Manning's coefficient could also be incorporated to capture changes in erosion/ deposition processes and changing bedforms during the model simulation. It has been shown that the Manning's coefficient varies in time with changes in river inflow rates and tend to decrease with increasing discharge and water depth before reaching a threshold and remaining constant (Kim et al., 2010). Studies which utilise a time-varying Manning's coefficient simulate phenomena on a small temporal scale, such as single meandering channels, small saltmarshes and drainage furrows (e.g. Mailapalli et al., 2008) and may not be appropriate on a large scale. Land use data is not readily available worldwide to develop complex varying Manning's coefficients, and studies have shown that estimation and calibration methods can be sufficient and efficient when deciding on a uniform Manning coefficient (Condon and Veeramony, 2012; Boulomytis et al., 2017).

Chapters 2, 3, 4 and 5 identify key sources of coastal hazard uncertainty (e.g. event severity, local forcing processes and estuarine morphology) which should be considered when predicting coastal flood and wave hazard, and the relative importance of each source of uncertainty in coastal flood hazard assessments. Chapter 5 and 6, as summarized below, discuss the impacts of the uncertainty on flood inundation.

7.2. Impacts of coastal hazard uncertainty on receptors and consequences of flood and wave hazard

Chapters 5 and 6 quantify coastal hazard uncertainty and subsequent variability in the receptors and consequences of flood hazard (e.g. people, businesses and the built environment) occurring due to uncertainties in regional model setup, as well as the approach to forcing the boundary of an inundation model. Chapter 5 highlights the primary importance of local forcing processes and, secondarily, model coupling processes for accurate prediction of coastal hazards. The exclusion of local atmospheric forcing can substantially underestimate significant wave height, high water level and hazard proxy. Chapter 6 shows that the physical impacts of inundation are strongly controlled by coastal hazard uncertainty. Coastal hazard uncertainty will influence whether overwashing and subsequent breaching of defences occurs and where this will occur, which impacts the location and duration that receptors may be affected by flood and wave hazard. Coastal hazard uncertainty also generates a large spread of results in hazard threshold curves. This is highlighted at sites of critical infrastructure, notably a road junction which acts as a primary access route for residents of Oldbury-on-Severn. At this location, flooding presents a hazard to everyone at the road junction for 90 to 135 minutes, for the same event.

Similarly, the same event generates no hazard or up to 113 minutes hazard to everyone for the same event at an electricity pylon located between Oldbury Technical Centre and Berkeley. This spread of results can make emergency response challenging, as it will be difficult to know when to implement evacuation orders for local residents or when to send in divers to stabilise electricity pylons which are flooded.

Chapter 6 quantifies the impacts of coastal uncertainty hazard and **approach to forcing the model boundary** on volume of inundation, hazard to people (including thresholds for hazard with “traffic light rating” to young people, the elderly and to all), and the economic costs of saltwater inundation for arable and suburban land uses at an up-estuary location. The results show that the inundation model is more sensitive to changes in the coastal hazard parameter, due to the regional model setup shown in chapter 4. Once critical thresholds for flooding are exceeded then even small changes in coastal hazard parameter (as small as a few centimetres) can increase inundation and costs. A 0.06 m change in coastal hazard condition can cause up to 97.7 Mm³ difference in time-integrated volume of inundation and £12.4 M in economic costs to suburbia at Oldbury-on-Severn and surrounding low-lying floodplains. These small changes in coastal hazard condition can be used to infer the consequences and impacts of flood hazard under future sea level change.

7.3. Applicability of results to other estuaries

This research has shown that estuary orientation can alter and influence exposure to coastal hazard parameters, and estuarine morphology has a strong control on the propagation of flood and wave hazard. The shape and size of the Severn Estuary amplifies tidal range and surge propagation up-estuary. It is a tide-dominant estuary and an extreme example of how coastal hazard parameters combine to cause overwashing and flooding in a hyper-tidal estuary. The key sources of coastal hazard uncertainty and their relative importance in coastal flood hazard assessments in the Severn Estuary is largely a function of its shape, size, orientation and exposure to prevailing storm conditions. The relative importance of marine and terrestrial drivers which can occur in any combination to amplify hazards will vary worldwide, as the shape and size of an estuary has a strong control on the marine drivers of coastal hazards, and catchment size, geology and topography can influence the terrestrial drivers.

The importance of event severity and the timing of combined hazards (the impacts of which are larger together than individual contribution) would stand as important processes to consider in estuaries worldwide. The winter storms of 2013/2014 caused significant impacts along the UK coastline, predominantly driven by marine and atmospheric processes (Sibley et al., 2015). The 3 January 2014 storm caused a 0.5 – 1 m skew surge in the Irish Sea (Haigh et al., 2015; SurgeWatch 2018), which caused a large tidal bore and flooding due to overwashing in the Severn Estuary (Sibley et al., 2015). The same event caused wave overtopping and flooded 30 homes at Barmouth, on the mouth of the Mawddach Estuary and flooded the town centre and golf course at Aberdyfi, on the Dyfi Estuary in

Wales (BBC 2014; Dugan et al., 2014). These smaller estuaries on the west coast of Wales are substantially smaller in length than the Severn Estuary, with a meso-tidal range (up to 4 m), but the impacts of a severe event remain significant for coastal towns. The severity of an event, which largely controls total water levels and the extent of flooding, depends on the storm characteristics. The prevailing storm conditions and geographical location will also control the relative importance of drivers of flood and wave hazard. Atlantic storms will driver increased rainfall, winds and storm surges on the west coast of the UK, however, storm surges will be the main driver of flood on the east coast of the UK (Hendry et al., 2019). Regardless of estuary shape or size, greater magnitude storms will control extent of flooding and total water levels to cause greatest impacts in estuaries. Other drivers of change, such as land use, ecosystem degradation, pollution and human intervention can also influence the relative importance of drivers of flood hazard in estuaries (Rogers and Woodroffe 2016).

The importance of accurate model setup and accurate bathymetry is also important in estuaries worldwide, irrespective of shape, size or hydrodynamics. Simulation of floodwater propagation and inundation extent in the Shoalhaven Estuary, south-eastern Australia, demonstrates the importance of accurately representing the unique characteristics of an estuary for accurate model simulations (Kumbier et al., 2018). This estuary is characterised as a wave dominated barrier estuary and simulating one or two open boundaries influences tidal range, exposure to storm-tide flooding and wave action (Kumbier et al., 2018). Simulation of wind waves in a wide, shallow estuary, Mobile Bay, Alabama, demonstrates the importance of sufficient spatial resolution to represent bathymetric gradients and ambient currents to ensure accurate prediction of wave heights (Chen et al., 2005). The key sources of coastal hazard uncertainty presented here that would hold for other estuaries worldwide are not dependent on the shape and size of the estuary, but external factors (event severity and model setup) that control magnitude and representation of total water levels and wave heights.

The research presented here highlights the importance of local forcing processes to accurately simulate total water levels and wave heights in a large, hyper-tidal estuary. Local atmospheric forcing is an important control on wave hazard in the Severn Estuary because the wide estuary mouth increases local fetch to enhance wind wave generation. It has been shown that channel size is an important control on wind wave generation in Manukau Harbour, a shallow macro-tidal estuary in New Zealand. Spatial variation in wind speed is important over a short fetch in narrow stretches of the estuary for wave generation but tidally varying depth is important over a longer fetch (Smith et al., 2001). Hilly terrain up-estuary also controls wind speed over water and subsequent wind forcing of waves (Smith et al., 2001). The importance of local atmospheric forcing in estuaries with a large local fetch (as a function of estuary size) for accurate simulation of wind-waves has been shown in other large, coastal plain estuaries including the Ems-Dollard, Germany (Hein et al., 2011), Delaware Bay, USA (Pareja-Roman et al., 2019) and Chesapeake Bay, USA (Fisher et al., 2015). Larger estuaries, with increased local fetch, generally drain larger catchments, and the occurrence of East Coast Lows on the east coast of Australia

have highlighted estuaries with a larger catchment and tidal range will experience increased flood hazard due to increased exposure (Rogers and Woodroffe, 2016). High rainfall increase floodwaters in the upper catchments, and the interaction between winds and storm surges in the lower catchments increase overwash and flooding e.g. Shoalhaven River and Bega River (Rogers and Woodroffe 2016). However, there were exceptions as the sensitivity of estuaries to flood hazard on the east coast of Australia is a function of the site-specific geomorphology of individual estuaries, as opposed to physical processes controlled by estuarine shape. Lake Illawarra has a small catchment and tidal range, but is vulnerable to flooding as the estuary bedrock valley is broad and alluvial infill has created huge expanses of low-lying floodplains vulnerable to inundation (Sloss et al., 2006; Rogers and Woodroffe 2016). Further to this, the barrier integrity controls conditions at the mouth of intermittently open-closed estuaries; tidal conditions were experienced just 9% of the time over a 14-year period at micro-tidal East Kleinemonde Estuary, South Africa, and fluvial outflow conditions <1 % (Whitfield et al., 2008). Large river events in combination with large wave events are most important for natural barrier breaching on wave dominated coastlines such as those seen on the California coastline (Harvey et al., 2020) and Victoria coastline, Australia (McSweeney et al., 2018). In turn, this is important for floodwater drainage, water quality and fish spawning in intermittently closed estuaries (Gillanders et al., 2011). Fluvial outflow conditions have been shown to be more important in smaller, steeper catchments which transport river discharge more rapidly to the coast (Hendry et al., 2019). The Dyfi Estuary, Wales, experiences flash flood regime and displays sensitivity to rainfall at a sub-daily scale (Robins et al., 2016), which should be accounted for in flood hazard estimations. The sensitivity of coastal flood hazard was not considered in this research, as it is considered a smaller contribution to total water levels in the Severn Estuary. However it would be an important consideration in estuaries with smaller and steeper catchments. Human intervention can also control the relative importance of physical processes controlling flood hazard; the construction of Wolwedans Dam in the Great Brak Estuary catchment has reduced fluvial outflow to the estuary by 56%, reducing the volume and duration of a flood event in this small, micro-tidal estuary and causing the estuary mouth to breach less often (Human et al., 2016). No two estuaries are the same, and there are no generic rules to allow for direct comparison between key sources of coastal hazard uncertainty in estuaries. Site-specific consideration should be given to the relative importance of coastal hazard parameters in flood hazard assessments based on local morphological conditions, prevailing storms, and human intervention.

7.4. Practical application of thesis results

The results presented in this thesis can be used to inform local flood hazard assessments, and the results can support the work of coastal modellers and planners which aims to minimise the negative consequences of flood events. The results contribute to knowledge to numerical modellers, by identifying an optimal model setup which can be used to accurately simulate flood and wave hazard.

The primary recommendation is that coastal hazard modelling should include time- and space-varying atmospheric forcing; this is successfully represented by data from the Met Office Unified Model in this research. Simulations should utilise model coupling processes which accurately represent the influence of the circulation on the waves and waves on the circulation (two-way coupled). The results presented here also identify that estuarine morphology is an important control on coastal hazard uncertainty. Numerical modelling systems should use computational grids which accurately represent complex coastlines. The land boundary of model grids should represent headlands and bays to ensure that the influence of wave refraction in shallow water regions on significant wave height is accurate, and narrowing of channels to represent funnelling effects. Funnelling effects are also controlled by shallower channels, as represented by bathymetry. Bathymetry is a key control on the accurate representation of total water level and significant wave height in all estuarine and shelf sea modelling studies (Williams and Esteves 2017). Bathymetric variations control volume and cross-section along the channel, and subsequently influence water level and current variations, sediment transport, and shallow water processes (e.g. energy dissipation and wave attenuation). Accurate numerical modelling outputs are a product of the quality of bathymetry data used. Local atmospheric forcing is an important control on significant wave height prediction; adding momentum to the estuarine system is particularly important as it has been shown that stronger, opposing wind can steepen high amplitude shorter period waves, or enhance propagation of low amplitude longer period waves up-estuary. Inaccuracies in wind speed or direction may underestimate wave hazard up-estuary, which may cause overwashing and subsequent flood hazard for communities on low-lying coastal plains. Modellers should utilise accurate bathymetry and boundary forcing when developing regional models, to minimise uncertainty in total water level and wave predictions.

Outputs from this research has been shared with Principal Hazard Consultant, David Anderson, at Magnox Oldbury Technical Centre, responsible for managing the decommissioning strategy at Oldbury Nuclear Power Station. The work has been useful to the team so far as providing insight into the level of complexity and detailed required in site specific hydrodynamic and inundation models. It was beyond the scope of this research project to consider erosion hazard and morphological development under extreme events, but this is considered to be a crucial future consideration in the Severn Estuary, given the soft, muddy nature of the sediments which move easily in fast tidal currents (Manning et al., 2010). The importance of event severity and locally generated winds is not only likely to generate uncertainty in flood and wave hazard, but also short term, storm-related variations in morphology. This is significant as erosion-deposition cycles in estuaries can modify the tidal prism, alter shipping channels or contribute to loss of coastal wetlands (Yin et al., 2019). Delft3D-FLOW-WAVE could be coupled to the sediment transport module Delft3D-MOR (Lesser et al., 2001) to understand how coastal hazard uncertainty influences net sediment transport pathways and development of sandbanks during extreme events. Further to this, key questions from Oldbury Technical Centre include determining whether the

estuary will be static or stable over the next 5,700 years and how long-term evolution may influence erosion, deposition and sediment transport and subsequently alter currents. A timeframe of 5,700 years is suggested by Oldbury Technical Centre as it is the half-life of carbon-14, a radionuclide produced from reactions in a nuclear reactor primary system. Understanding and predicting tidally induced morphological variations and sea-level change under future climate scenarios over the next 5,700 years will inform whether decommissioned nuclear energy structures should be kept or removed (D Anderson, 2018 personal communication 10 July). Process-based morphodynamic models, such as the sediment transport module Delf3D-MOR, could be coupled to Delft3D-FLOW-WAVE to analyse physical processes and mechanisms which underlie the evolution of the estuary.

The results also highlight how uncertainties in coastal hazard parameters can generate substantial or no hazard to people or infrastructure at the same time and location for the same hazard condition, making emergency response planning more challenging, and can substantially increase inundation and cost of damage once critical thresholds for flooding are exceeded. Large uncertainties in coastal hazard parameters, of the order of 0.5 – 1 m, may be influential in causing initial breaches but once this threshold has been exceeded, then increases of just centimetres can substantially increase inundation and the cost of flood damage. Small changes in coastal hazard condition contribute up to £60.91 M increase in economic costs of flooding events. These small changes should be accounted for when conducting comparative flood risk analysis, which quantifies different hazards within a community, and financial appraisals of flood events to calculate expected annual damages (Merz et al., 2010).

7.5. Coastal hazard uncertainty: implications for long-term planning (up to 2105) with sea level rise

This thesis has quantified coastal hazard uncertainty due to external factors including event severity, timing of the storm surge relative to tidal high water, local forcing and coupling processes, and quantified the range of impacts these uncertainties have on receptors and consequences of flood hazard. Coastal hazard predictions are used to inform hazard management strategies, including shoreline management plans, adaptation and flood alleviation schemes to understand physical processes and systems, and the impacts that intervention schemes may have on inundation and cost of damage (Sayers et al., 2003). These strategies aim to reduce the threat of flooding and erosion to people and their property, over the short-term (up to 2025) to the long-term (up to 2105) (Environment Agency 2010). The design, and subsequent success, of such long-term management plans can hinge critically on accurate flood hazard projection (Ruckert et al., 2019) however, as shown here, predictions of total water level and maximum significant wave height can differ drastically. Uncertainties in physical processes, which generate a large spread of results for just one event, represents a key area of risk within long-term strategy planning (Hutter and Schanze 2008; Robins et al., 2016). Adopting a single hazard projection neglects key uncertainties in physical processes, and can lead to over- or under-estimation of

hazards, and inappropriate design scenarios for the lifetime of coastal structures (Stephens et al., 2017). Further to this, there are great uncertainties associated with future climate scenarios; how much may sea level increase, whether extreme storm surge events intensify in a warming climate, the extent of the Antarctic ice sheet collapse, which will all contribute to future flood hazard projections (Barnard et al., 2019; Leuven et al., 2019; Pasquier et al., 2019; Wong and Keller 2017). These uncertainties may cause more severe consequence for coastal communities from the effects of flooding in the future (Hall et al., 2016; Sriver et al., 2018; Vitousek et al., 2017).

UKCP18 projects that sea level could rise up 1.13 m by 2100 (Lowe et al., 2018), meaning that a particular critical threshold will be exceeded more frequently, as less severe storm conditions are required to exceed that level (Haigh et al., 2016). Research recent states that large, deep estuaries (similar to the Severn Estuary) may not experience significant impacts of future sea-level rise, as sediment starvation will minimise the tidal prism (Leuven et al., 2019). However the results presented here show that coastal hazard uncertainty in hyper-tidal estuaries are sensitive to event severity; this is represented by varying higher water level and wave heights which create large changes in water level at the estuary mouth to increase the possible number of receptors and severity of the consequences of the hazard. Future changes in sea level in hyper-tidal estuaries may act to enhance tide-surge propagation and wave propagation up-estuary, to increase the number of receptors in locations previously unaffected by similar storm conditions, and increase the likelihood that critical thresholds are exceeded. Wave-tide interaction under future climate conditions may lead to increased wave heights at high water, which may be amplified in the long term (Lewis et al., 2019). Uncertainty in coastal hazard predictions and future sea-level changes prove challenging when making decisions for long-term management plans, in particular not knowing how coastlines, policies, and society will develop into the future.

7.5.1. Resilience and flexibility in long-term management plans

Long-term plans should be based on considerable, site-specific technical knowledge which account for future uncertainty to ensure resilience and robustness, and adaptation and flexibility in long-term plans (André et al., 2016). Resilience can be built into long-term management plans by explicitly including considerations on uncertainties in flood hazard modelling and decision making, to understand how intervention schemes will develop under a range of future hazard and sea-level conditions. Robust long-term management plans should utilise optimal model setups which are site-specific and account for natural complexity and evolution of an estuarine system. Numerical models, which fully incorporate and accurately represent local atmospheric wind and pressure systems and represent the influence of the circulation on the waves and waves on the circulation (two-way coupled models), have been shown here to provide a thorough understanding of the sources, pathways, receptors and consequences of a range of hazards. A modelling approach which considers the whole system of physical processes can

be used to understand how intervention schemes can protect communities against local, prevailing conditions (Penning-Rowsell et al., 2000). Flexible long-term plans should acknowledge that hazard conditions, sea level and society may change with time, and soft and hard management options should be able to adapt to uncertainty in the evolution of coastal hazards and sea level changes. The research presented here could be developed further to improve the understanding of the receptor and consequences of site-specific coastal hazards within the Severn Estuary. Changes in volume of floodwater in the Oldbury-on-Severn LISFLOOD-FP model domain are asymmetric; volumes rise rapidly but then drainage from the domain is slower. This asymmetry may occur as a result of the size and number of channels for floodwater to drain into and accommodation for floodwater in the model domain. A lack of drainage means that some areas experience flooding for a longer period. Incorporating storm drainage features into inundation model domains can help to further improve understanding of receptor and consequences at a site-specific level. Subterranean, urban drainage systems could be incorporated into inundation models to consider their influence on economic costs of flooding to suburbia (Gallien et al., 2018). Erosion hazard and morphological change during storm event could also be considered, to understand how the balance of saltmarsh and mudflats will change or be lost. It has been shown that morphological variability has a strong influence on the width of coastal hazard zones which could alter the exceedance of critical thresholds or minimise wave energy dissipation at the coast (Baron et al., 2014). The findings from this thesis have shown the importance of site-specific technical knowledge for accurate model outputs, such as accurate bathymetry and land boundaries in computational grids to represent shallow water processes, or local atmospheric forcing, which can generate up to 90.1% difference in maximum significant wave height if excluded from wave hazard assessments. Utilizing the best data available to setup and force hydrodynamic numerical models will help to minimise uncertainty in water level and significant wave height predictions, which are used to inform long-term intervention and protection strategies for coastal communities and infrastructure.

7.6. Coastal hazard uncertainty: implications for early warning systems

The impacts of uncertainty in coastal hazard modelling also has implications for early warning management, which primarily aims to reduce loss of life, and impacts on livelihoods, health, businesses and communities (Angove et al., 2019). Early warning frameworks have a lead time of 8-11 hours (Bocquet et al., 2009) and aim to avoid fatalities and damage by reducing the occurrence of a hazard (e.g. strategic evacuation), and minimise the consequences of a hazard (e.g. alerts and emergency response planning) (UNISDR 2015). These strategies require rapid access to estimations of when peak total water levels will occur, and when and where flooding is likely to occur during a storm event due to exceeded of critical thresholds (Le Cozannet et al., 2015; Del Río et al., 2012) , which is particularly important at ungauged locations. Uncertainties in predicting the timing and magnitude of a storm event may lead to under-preparation, at the cost of avoidable damage, or over-preparation resulting in

unnecessary evacuation orders and expenses (Jonkman et al., 2013). A balance must be met to ensure that uncertainties do not lead to errors in early warning systems driving alerts and warnings, which can create public doubt and mistrust in early warning systems and emergency responses (Shaw et al., 2005). Uncertainty in offshore conditions for flooding have been shown to cause a range of impacts, and once a critical threshold has been exceeded then even a small change in coastal hazard condition of 0.06 m can increase flood damage costs in suburban areas by £12.4 M. Early warning systems which account for small changes in coastal hazard condition once a threshold has been exceeded can dramatically reduce the number of avoidable and unnecessary deaths and cost of property damage (Doong et al., 2012). This research can help to inform the development of early warning systems by highlighting the extent to which coastal hazard uncertainty influences the negative impacts of storm events; small changes in coastal hazard condition can substantially increase the consequences of events.

8. References

- Adikari, Y., R. Osti, and T. Noro. 2010. "Flood-Related Disaster Vulnerability: An Impending Crisis of Megacities in Asia." *Journal of Flood Risk Management* 3(3):185–91.
- Aerts, Jeroen C. J. H., W. J. Woute. Botzen, Kerry Emanuel, Ning Lin, Hans De Moel, and Erwann O. Michel-Kerjan. 2014. "Climate Adaptation: Evaluating Flood Resilience Strategies for Coastal Megacities." *Science* 344(6183):473–75.
- Allen, J. R. .. and M. .. Duffy. 1998. "Temporal and Spatial Depositional Patterns in the Severn Estuary, Southwestern Britain: Intertidal Studies at Spring–neap and Seasonal Scales, 1991–1993." *Marine Geology* 146(1–4):147–71.
- Allsop, W., T. Bruce, J. Pearson, and P. Besley. 2005. "Wave Overtopping at Vertical and Steep Seawalls." *Maritime Engineering* 158:103–14.
- Allsop, William, T. O. M. Bruce, T. I. M. Pullen, and Jentsje V. A. N. D. E. R. Meer. 2008. "Direct Hazards from Wave Overtopping - the Forgotten Aspect of Coastal Flood Risk Assessment?" Pp. 1–11 in *43rd Defra Flood and Coastal Management Conference*.
- Allsop, William, Tom Bruce, Jonathan Pearson, John Alderson, and Tim Pullen. 2003. "Violent Wave Overtopping at the Coast, When Are We Safe?" Pp. 54–69 in *International Conference on Coastal Management*.
- Amante, Christopher J. 2019. "Uncertain Seas: Probabilistic Modeling of Future Coastal Flood Zones." *International Journal of Geographical Information Science* 33(11):2188–2217.
- Amiruddin, A. M., I. D. Haigh, M. N. Tsimplis, F. M. Calafat, and S. Dangendorf. 2015. "The Seasonal Cycle and Variability of Sea Level in the South China Sea." *Journal of Geophysical Research:Oceans* 120:5490–5513.
- Anctil, F. and M. A. Donelan. 1996. "Air-Water Momentum Flux Observations over Shoaling Waves." *Journal of Physical Oceanography* 26:1344–53.
- André, Camille, Delphine Boulet, Hélène Rey-Valette, and Bénédicte Rulleau. 2016. "Protection by Hard Defence Structures or Relocation of Assets Exposed to Coastal Risks: Contributions and Drawbacks of Cost-Benefit Analysis for Long-Term Adaptation Choices to Climate Change." *Ocean and Coastal Management* 134:173–82.
- Angove, Michael, Diego Arcas, Rick Bailey, Patricio Carrasco, David Coetzee, Bill Fry, Ken Gledhill, Satoshi Harada, Christa von Hillebrandt-Andrade, Laura Kong, Charles McCreery, Sarah Jayne McCurrach, Yuelong Miao, Andi Eka Sakya, and François Schindelé. 2019. "Ocean Observations Required to Minimize Uncertainty in Global Tsunami Forecasts, Warnings, and

- Emergency Response.” *Frontiers in Marine Science* 6(JUN).
- Antony, Charls and A. S. Unnikrishnan. 2013. “Observed Characteristics of Tide-Surge Interaction along the East Coast of India and the Head of Bay of Bengal.” *Estuarine, Coastal and Shelf Science* 131:6–11.
- Arcement Jr, G. .. and V. .. Schneider. 1989. *Guide for Selecting Manning’s Roughness Coefficients for Natural Channels and Flood Plains*.
- Archer, D. R. and H. J. Fowler. 2018. “Characterising Flash Flood Response to Intense Rainfall and Impacts Using Historical Information and Gauged Data in Britain.” *Journal of Flood Risk Management* 11:S121–33.
- As-Salek, J. A. 1998. “Coastal Trapping and Funneling Effects on Storm Surges in the Meghna Estuary in Relation to Cyclones Hitting Noakhali–Cox’s Bazar Coast of Bangladesh.” *Journal of Physical Oceanography* 28(2):227–49.
- As-Salek, Junaid Amin and Takashi Yasuda. 2001. “Tide–Surge Interaction in the Meghna Estuary: Most Severe Conditions.” *Journal of Physical Oceanography* 31(10):3059–72.
- Ashworth, P. J., J. L. Best, and D. R. Parsons. 2015. *Fluvial–Tidal Sedimentology*. Oxford: Elsevier.
- Aubrey, D. G. 1985. “A Study of Non-Linear Shallow Inlet / Estuarine Part I : Observations.” *Estuarine, Coastal and Shelf Science* (5674):185–205.
- Ballinger, R. and T. Stojanovic. 2010. “Policy Development and the Estuary Environment: A Severn Estuary Case Study.” *Marine Pollution Bulletin* 61(1–3):132–45.
- Barker, Lucy, Jamie Hannaford, Katie Muchan, Stephen Turner, and Simon Parry. 2016. “The Winter 2015/2016 Floods in the UK: A Hydrological Appraisal.” *Weather* 71(12):324–33.
- Barnard, Patrick L., Li H. Erikson, Amy C. Foxgrover, Juliette A. Finz. Hart, Patrick Limber, Andrea C. O’Neill, Maarten van Ormondt, Sean Vitousek, Nathan Wood, Maya K. Hayden, and Jeanne M. Jones. 2019. “Dynamic Flood Modeling Essential to Assess the Coastal Impacts of Climate Change.” *Scientific Reports* 9(1):1–13.
- Barnard, Patrick L., Daniel Hoover, David M. Hubbard, Alex Snyder, Bonnie C. Ludka, Jonathan Allan, George M. Kaminsky, Peter Ruggiero, Timu W. Gallien, Laura Gabel, Diana McCandless, Heather M. Weiner, Nicholas Cohn, Dylan L. Anderson, and Katherine A. Serafin. 2017. “Extreme Oceanographic Forcing and Coastal Response Due to the 2015-2016 El Niño.” *Nature Communications* 8:6–13.
- Baron, Heather M., Peter Ruggiero, Nathan J. Wood, Erica L. Harris, Jonathan Allan, Paul D. Komar, and Patrick Corcoran. 2014. “Incorporating Climate Change and Morphological Uncertainty into

- Coastal Change Hazard Assessments.” *Natural Hazards* 75(3):2081–2102.
- Bastidas, Luis A., James Knighton, and Shaun W. Kline. 2016. “Parameter Sensitivity and Uncertainty Analysis for a Storm Surge and Wave Model.” *Natural Hazards and Earth System Science* 16:2195–2210.
- Bates, P. D. and A. P. J. De Roo. 2000. “A Simple Raster-Based Model for Flood Inundation Simulation.” *Journal of Hydrology* 236(1–2):54–77.
- Bates, Paul D., Richard J. Dawson, Jim W. Hall, Matthew S. Horritt, Robert J. Nicholls, Jon Wicks, Mohamed Ahmed, and Ali Mohamed. 2005. “Simplified Two-Dimensional Numerical Modelling of Coastal Flooding and Example Applications.” *Coastal Engineering* 52:793–810.
- Bates, Paul, Mark Trigg, Jeff Neal, and Amy Dabrowa. 2013. “LISFLOOD-FP User Manual: Code Release 5.9.6.”
- Batstone, Crispian, Mark Lawless, Jonathan Tawn, Kevin Horsburgh, David Blackman, Alastair McMillan, David Worth, Stefan Laeger, and Tim Hunt. 2013. “A UK Best-Practice Approach for Extreme Sea-Level Analysis along Complex Topographic Coastlines.” *Ocean Engineering* 71:28–39.
- BBC. 2014. “River Severn Bursts Banks at Minsterworth after Bore.” *BBC News*. Retrieved January 10, 2020 (<https://www.bbc.co.uk/news/uk-england-gloucestershire-25588120>).
- Bernier, N. B. and K. R. Thompson. 2007. “Tide-Surge Interaction off the East Coast of Canada and Northeastern United States.” *Journal of Geophysical Research* 112(January):1–12.
- Bernier, Natacha B. and Keith R. Thompson. 2006. “Predicting the Frequency of Storm Surges and Extreme Sea Levels in the Northwest Atlantic.” *Journal of Geophysical Research: Oceans* 111(10):1–15.
- Bernier, Natacha B. and Keith R. Thompson. 2015. “Deterministic and Ensemble Storm Surge Prediction for Atlantic Canada with Lead Times of Hours to Ten Days.” *Ocean Modelling* 86:114–27.
- Beven, Keith. 2016. “Facets of Uncertainty: Epistemic Uncertainty, Non-Stationarity, Likelihood, Hypothesis Testing, and Communication.” *Hydrological Sciences Journal* 61(9):1652–65.
- Blackburn, Sophie, Mark Pelling, and César Marques. 2019. *Megacities and the Coast: Global Context and Scope for Transformation*. Elsevier Inc.
- Bobanović, Joško, Keith R. Thompson, Serge Desjardins, and Harold Ritchie. 2006. “Forecasting Storm Surges along the East Coast of Canada and the North-Eastern United States: The Storm of 21 January 2000.” *Atmosphere - Ocean* 44(2):151–61.

- Bocquet, Francois, Jonathan Flowerdew, Peter Hawkes, Tim Pullen, and Nigel Tozer. 2009. *Probabilistic Coastal Flood Forecasting: Forecast Demonstration and Evaluation Science Project SC050069/SR2*.
- Bolaños, Rodolfo, Jennifer M. Brown, and Alejandro J. Souza. 2014. “Wave – Current Interactions in a Tide Dominated Estuary.” *Continental Shelf Research* 87:109–23.
- Booij, N., C. Ris, and L. .. Holthuijsen. 1999. “A Third-Generation Wave Model for Coastal Regions.” *Journal of Geophysical Research* 104(C4):7649–66.
- Boon, John D. 2004. *Secrets of the Tide: Tide and Tidal Current Analysis and Applications, Storm Surges and Sea Level Trends*. Philadelphia: Woodhead Publisher.
- Borsje, B. W., P. C. Roos, W. M. Kranenburg, and S. J. M. H. Hulscher. 2013. “Modeling Tidal Sand Wave Formation in a Numerical Shallow Water Model: The Role of Turbulence Formulation.” *Continental Shelf Research* 60:17–27.
- Bouma, Jan Jaap, Delphine François, Albert Schram, and Tom Verbeke. 2009. “Assessing Socio-Economic Impacts of Wave Overtopping: An Institutional Perspective.” *Coastal Engineering* 56(2):203–9.
- Bricheno, Lucy M., Judith Wolf, and Saiful Islam. 2016. “Tidal Intrusion within a Mega Delta: An Unstructured Grid Modelling Approach.” *Estuarine, Coastal and Shelf Science* 182:12–26.
- Brown, J. M. and A. G. Davies. 2010. “Flood/Ebb Tidal Asymmetry in a Shallow Sandy Estuary and the Impact on Net Sand Transport.” *Geomorphology* 114(3):431–39.
- Brown, J. M., M. J. Yelland, R. W. Pascal, T. Pullen, P. S. Bell, C. L. Cardwell, D. S. Jones, N. P. Milliken, T. D. Prime, G. Shannon, J. H. Ludgate, A. Martin, B. Farrington, I. Gold, C. Bird, and T. Mason. 2018. “WireWall: A New Approach to Coastal Wave Hazard Monitoring.” in *3rd International Conference on Protection against Overtopping*.
- Brown, James D., Tom Spencer, and Iris Moeller. 2007. “Modeling Storm Surge Flooding of an Urban Area with Particular Reference to Modeling Uncertainties: A Case Study of Canvey Island, United Kingdom.” *Water Resources Research* 43(6):1–22.
- Brown, Jennifer M., Rodolfo Bolaños, Michael J. Howarth, and Alejandro J. Souza. 2012. “Extracting Sea Level Residual in Tidally Dominated Estuarine Environments.” *Ocean Dynamics* 62(7):969–82.
- Brown, Jennifer M., Rodolfo Bolaños, and Alejandro J. Souza. 2014. “Process Contribution to the Time-Varying Residual Circulation in Tidally Dominated Estuarine Environments.” *Estuaries and Coasts* 37(5):1041–57.

- Brown, Jennifer M., Rodolfo Bolaños, and Judith Wolf. 2013. “The Depth-Varying Response of Coastal Circulation and Water Levels to 2D Radiation Stress When Applied in a Coupled Wave – Tide – Surge Modelling System during an Extreme Storm.” *Coastal Engineering* 82:102–13.
- Brown, Jennifer M., Karyn Morrissey, Philip Knight, Thomas D. Prime, Luis Pedro Almeida, Gerd Masselink, Cai O. Bird, Douglas Dodds, and Andrew J. Plater. 2018. “A Coastal Vulnerability Assessment for Planning Climate Resilient Infrastructure.” *Ocean and Coastal Management* 163(June):101–12.
- Brown, Jennifer M., Danielle L. Norman, Laurent O. Amoudry, and Alejandro J. Souza. 2016. “Impact of Operational Model Nesting Approaches and Inherent Errors for Coastal Simulations.” *Ocean Modelling* 107:48–63.
- Brown, Jennifer M., Jack J. C. Phelps, Andrew Barkwith, Martin D. Hurst, Michael A. Ellis, and Andrew J. Plater. 2016. “The Effectiveness of Beach Mega-Nourishment, Assessed over Three Management Epochs.” *Journal of Environmental Management* 184:400–408.
- Brown, Jennifer M., Thomas Prime, Jack J. C. Phelps, Andrew Barkwith, Martin D. Hurst, Michael A. Ellis, Gerd Masselink, and Andrew J. Plater. 2016. “Spatio-Temporal Variability in the Tipping Points of a Coastal Defense.” *Proceedings of the 14th International Coastal Symposium (SI 75)*:1042–46.
- Brown, Jennifer M., Alejandro J. Souza, and Judith Wolf. 2010. “An 11-Year Validation of Wave-Surge Modelling in the Irish Sea, Using a Nested POLCOMS – WAM Modelling System.” *Ocean Modelling* 33(1–2):118–28.
- Brown, Jennifer M. and Judith Wolf. 2009. “Coupled Wave and Surge Modelling for the Eastern Irish Sea and Implications for Model Wind-Stress.” *Continental Shelf Research* 29:1329–42.
- Brown, Sally, Robert J. Nicholls, Susan Hanson, Geoff Brundrit, John A. Dearing, Mark E. Dickson, Shari L. Gallop, Shu Gao, Ivan D. Haigh, Jochen Hinkel, José A. Jiménez, Richard J. T. Klein, Wolfgang Kron, Attila N. Lázár, Claudio Freitas Neves, Alice Newton, Charitha Pattiaratchi, Andres Payo, Kenneth Pye, Agustín Sánchez-Arcilla, Mark Siddall, Ali Shareef, Emma L. Tompkins, Athanasios T. Vafeidis, Barend Van Maanen, Philip J. Ward, and Colin D. Woodroffe. 2014. “Shifting Perspectives on Coastal Impacts and Adaptation.” *Nature Climate Change* 4(9):752–55.
- Burcharth, H. .. and S. Hughes. 2011. “Part VI, Design of Coastal Project Elements.” P. 378 in *Coastal Engineering Manual*. Vol. 1100, edited by U.S. Army Corps of Engineers.
- Byrne, D., G. Robbins, N. Counsell, A. How, and A. Saulter. 2017. *Improving Sea Level Forecasting at Newport*.

- Cai, Huayang, Hubert H. G. Savenije, Qingshu Yang, Suying Ou, and Yaping Lei. 2012. "Influence of River Discharge and Dredging on Tidal Wave Propagation: Modaomen Estuary Case." *Journal of Hydraulic Engineering VO - 138* 138(10):885.
- Carrasco, A. R., Ó. Ferreira, A. Matias, and P. Freire. 2012. "Flood Hazard Assessment and Management of Fetch-Limited Coastal Environments." *Ocean and Coastal Management* 65:15–25.
- Chen, Qin, Uxia Wang, Haihong Zhao, and Scott L. Douglass. 2007. "Prediction of Storm Surges and Wind Waves on Coastal Highways in Hurricane-Prone Areas." *Journal of Coastal Research* 23(5):1304–17.
- Chen, R., Y. Zhang, D. Xu, and M. Liu. 2018. "Climate Change and Coastal Megacities: Disaster Risk Assessment and Responses in Shanghai City." in *Climate Change, Extreme Events and Disaster Risk Reduction: Sustainable Development Goals Series.*, edited by S. Mal, R. Singh, and C. Huggel. Springer.
- Chen, Yimei, Wenrui Huang, and Sudong Xu. 2014. "Frequency Analysis of Extreme Water Levels Affected by Sea-Level Rise in East and Southeast Coasts of China." *Journal of Coastal Research* 68:105–12.
- Chipperfield, D. 2014. "Flooded Roads Now Impassable as River Severn Bore Overtops Defences." *Gazette*. Retrieved January 10, 2020 (<https://www.gazetteseries.co.uk/news/10912321.flooded-roads-now-impassable-as-river-severn-bore-overtops-defences/>).
- Chow, V. T. 1959. *Open-Channel Hydraulics*. New York: McGraw-Hill.
- Church, John A., Peter U. Clark, Jonathan M. Gregory, Svetlana Jevrejeva, Anders Levermann, Mark A. Merrifield, Glenn A. Milne, R. Steven Nerem, and Patrick D. Nunn. 2013. "Sea-Level Rise by 2100." (December):1445–47.
- Condon, Andrew and Jay Veeramony. 2012. "Development and Validation of a Coastal Surge and Inundation Prediction System." Pp. 1–8 in *Oceans 2012*.
- Conger, Tugce and Stephanie E. Chang. 2019. "Developing Indicators to Identify Coastal Green Infrastructure Potential: The Case of the Salish Sea Region." *Ocean and Coastal Management* 175(February):53–69.
- Cornett, A., J. Cousineau, and I. Nistor. 2013. "Assessment of Hydrodynamic Impacts from Tidal Power Lagoons in the Bay of Fundy." *International Journal of Marine Energy* 1:33–54.
- Le Cozannet, Gonéri, Jeremy Rohmer, Anny Cazenave, Déborah Idier, Roderik van de Wal, Renske de Winter, Rodrigo Pedreros, Yann Balouin, Charlotte Vinchon, and Carlos Oliveros. 2015.

- “Evaluating Uncertainties of Future Marine Flooding Occurrence as Sea-Level Rises.” *Environmental Modelling and Software* 73:44–56.
- Dangendorf, Sönke, Thomas Wahl, Christoph Mudersbach, and Jürgen Jensen. 2013. “The Seasonal Mean Sea Level Cycle in the Southeastern North Sea.” *Journal of Coastal Research* 165(65):1915–20.
- Dastgheib, A., J. A. Roelvink, and Z. B. Wang. 2008. “Long-Term Process-Based Morphological Modeling of the Marsdiep Tidal Basin.” *Marine Geology* 256(1–4):90–100.
- Davies, Gareth and Colin D. Woodroffe. 2010. “Tidal Estuary Width Convergence: Theory and Form in North Australian Estuaries.” *Earth Surface Processes and Landforms* 35(7):737–49.
- Davies, J. 1964. “A Morphogenetic Approach to World Shorelines.” *Zeitschrift Für Geomorphologie* 8:27–42.
- Davis, Richard A. and Miles O. Hayes. 1984. “What Is a Wave-Dominated Coast?” *Marine Geology* 60:313–29.
- Dawson, David, Jon Shaw, and W. Roland Gehrels. 2016. “Sea-Level Rise Impacts on Transport Infrastructure: The Notorious Case of the Coastal Railway Line at Dawlish, England.” *Journal of Transport Geography* 51(February 2014):97–109.
- DEFRA. 2003. “Flood Risks to People (Phase 2).” *Flood Risks to People Phase 2: FD2321 Technical Report 1* 117.
- DEFRA. 2006. *Flood Risks to People: FD2321/TR1 The Flood Risks to People Methodology*.
- Deltares. 2011. *Delft3D-FLOW: Simulation of Multi-Dimensional Hydrodynamic Flows and Transport Phenomena, Including Sediments. User Manual. Version: 3.15 Revision: 14499*. Deltares, 2600 MH Delft, The Netherlands.
- Deltares. 2014a. “Delft3D-QUICKIN: User Manual for the Generation and Manipulation of Grid-Related Parameters Such as Bathymetry, Initial Conditions and Roughness.”
- Deltares. 2014b. *Delft3D-WAVE. Simulations of Short Crested Waves with SWAN Version 3.05, Revision 34160*. Deltares, 2600 MH Delft, The Netherlands.
- Desplanque, Con and David J. Mossman. 1999. “Storm Tides of the Fundy.” *Geographical Review* 89(1):23–33.
- Desplanque, Con and David J. Mossman. 2004. “Tides and Their Seminal Impact on the Geology, Geography, History, and Socio-Economics of the Bay of Fundy, Eastern Canada (Part 1: Preface-Chapter 3).” *Atlantic Geology* 40(1):3–35.

- Van Deyzen, A. F. J., P. B. Beimers, J. C. Van Der Lem, D. Messiter, and J. A. M. De Bont. 2015. "To Improve the Efficiency of Ports Exposed to Swell." in *Australasian Coasts & Ports Conference 2015: 22nd Australasian Coastal and Ocean Engineering Conference and the 15th Australasian Port and Harbour Conference*.
- Dhoop, Thomas and Travis Mason. 2018. "Spatial Characteristics and Duration of Extreme Wave Events around the English Coastline." *Journal of Marine Science and Engineering* 6(14).
- Diab, Hassan, Rafic Younes, and Pascal Lafon. 2017. "Survey of Research on the Optimal Design of Sea Harbours." *International Journal of Naval Architecture and Ocean Engineering* 9:460–72.
- Didier, David, Jérémy Baudry, Pascal Bernatchez, Dany Dumont, Mojtaba Sadegh, Eliott Bismuth, Marion Bandet, Sebastien Dugas, and Caroline Sévigny. 2019. "Multihazard Simulation for Coastal Flood Mapping: Bathtub versus Numerical Modelling in an Open Estuary, Eastern Canada." *Journal of Flood Risk Management* 12(S1):1–19.
- Dissanayake, P., H. Karunarathna, and R. Ranasinge. 2015. "Numerical Modelling of the Impact of Sea Level Rise on Large Tidal Inlet/Basin Systems." (JUNE).
- Dixon, M. .. and J. A. Tawn. 1994. *Extreme Sea-Levels at the UK A-Class Sites: Site-by-Site Analyses*.
- Dongeren, Ap Van, Martijn De Jong, Cock Van Der Lem, Alex Van Deyzen, and Joost den Bieman. 2016. "Review of Long Wave Dynamics over Reefs and into Ports with Implication for Port Operations." *Journal of Marine Science and Engineering* 4(12):1–10.
- Doong, D. J., L. Z. H. Chuang, L. C. Wu, Y. M. Fan, C. C. Kao, and J. H. Wang. 2012. "Development of an Operational Coastal Flooding Early Warning System." *Natural Hazards and Earth System Science* 12(2):379–90.
- Dronkers, J. 1986. "TIDAL ASYMMETRY AND ESTUARINE MORPHOLOGY." *Netherlands Journal of Sea Research* 20(2/3):117–31.
- Dronkers, Job. 2017. "Convergence of Estuarine Channels." *Continental Shelf Research* 144(May):120–33.
- Dyer, K. .. 1995. "Sediment Transport Processes in Estuaries." *Developments in Sedimentology* 53:423–49.
- EDINA Marine Digimap Service. n.d. "33. Gridded Bathymetry: 1 Arcsecond (Ascii), Scale 1:50,000, Tile: NW 55050025, NW 55050030, NW 55050035, NW 55050040, NW 55050045, NW 55100030, NW , 5100035, NW 55100040, NW 55100045, NW 55150025, NW 55150030, NW 55150035, NW 55150040, NW 55150045, Updat."

- Elias, Edwin P. L., Guy Gelfenbaum, and André J. Van Der Westhuysen. 2012. "Validation of a Coupled Wave-Flow Model in a High-Energy Setting : The Mouth of the Columbia River." *Journal of Geophysical Research* 117(C09011):1–21.
- Elliott, Michael, Nicholas D. Cutts, and Anna Trono. 2014. "A Typology of Marine and Estuarine Hazards and Risks as Vectors of Change: A Review for Vulnerable Coasts and Their Management." *Ocean and Coastal Management* 93:88–99.
- Environment Agency. 2010. *Managing the Coast: The Wash Shoreline Management Plan*.
- Environment Agency. 2018. "New £63 Million Defence Scheme Is Turning the Tide against Floods in Rossall." *Gov.Uk*. Retrieved May 9, 2019 (<https://www.gov.uk/government/news/new-63-million-defence-scheme-is-turning-the-tide-against-floods-in-rossall>).
- Environment Agency. 2019. *National Flood and Coastal Erosion Risk Management Strategy for England*.
- Erikson, Li, Patrick Barnard, Andrea O'Neill, Nathan Wood, Jeanne Jones, Juliette Finzi Hart, Sean Vitousek, Patrick Limber, Maya Hayden, Michael Fitzgibbon, Jessica Lovering, and Amy Foxgrover. 2018. "Projected 21st Century Coastal Flooding in the Southern California Bight. Part 2: Tools for Assessing Climate Change-Driven Coastal Hazards and Socio-Economic Impacts." *Journal of Marine Science and Engineering* 6(3):76.
- EurOtop. 2016. *Manual on Wave Overtopping of Sea Defences and Related Structures*.
- Fairclough, I. 2019. "Province, Ottawa Spending \$114m to Reinforce Bay of Fundy Dikes against Rising Seas." *The Chronicle Herald*. Retrieved May 8, 2019 (<https://www.thechronicleherald.ca/news/local/province-ottawa-spending-114m-to-reinforce-bay-of-fundy-dykes-against-rising-seas-302999/>).
- Fairley, I., R. Ahmadian, R. A. Falconer, M. R. Willis, and I. Masters. 2014. "The Effects of a Severn Barrage on Wave Conditions in the Bristol Channel." *Renewable Energy* 68:428–42.
- Familkhalili, R. and S. A. Talke. 2016. "The Effect of Channel Deepening on Tides and Storm Surge: A Case Study of Wilmington, NC." *Geophysical Research Letters* 43(17):9138–47.
- Ferrarin, Christian, Aron Roland, Marco Bajo, Georg Umgiesser, Andrea Cucco, Silvio Davolio, Andrea Buzzi, Piero Malguzzi, and Oxana Drofa. 2013. "Tide-Surge-Wave Modelling and Forecasting in the Mediterranean Sea with Focus on the Italian Coast." *Ocean Modelling* 61:38–48.
- Ferreira, Celso M., Jennifer L. Irish, and F. Olivera. 2014. "Uncertainty in Hurricane Surge Simulation Due to Land Cover Specification." *Journal of Geophysical Research: Oceans*

119(1):1365–82.

Fischhoff, Baruch and Alex L. Davis. 2014. “Communicating Scientific Uncertainty.” *Proceedings of the National Academy of Sciences of the United States of America* 111:13664–71.

Flather, R. A. 2001. “Storm Surges.” Pp. 2882–92 in *Encyclopedia of Ocean Sciences*, edited by J. H. Steele, S. A. Thorpe, and K. K. Turekian. San Diego, California.

Flowerdew, Jonathan, Peter Hawkes, Ken Mylne, Tim Pullen, Andrew Saulter, and Nigel Tozer. 2009. *Coastal Flood Forecasting: Model Development and Evaluation*. Environment Agency.

Flowerdew, Jonathan, Ken Mylne, Caroline Jones, Helen Titley, and Office Published. 2013. “Extending the Forecast Range of the UK Storm Surge Ensemble.” *Quarterly Journal of the Royal Meteorological Society* (139):184–97.

Galland, J. C., N. Goutal, and J. M. Hervouet. 1991. “TELEMAC: A New Numerical Model for Solving Shallow Water Equations.” *Advances in Water Resources* 14(3):138–48.

Gallien, T. W., B. F. Sanders, and R. E. Flick. 2014. “Urban Coastal Flood Prediction: Integrating Wave Overtopping, Flood Defenses and Drainage.” *Coastal Engineering* 91:18–28.

Gallien, T. W., J. E. Schubert, and B. F. Sanders. 2011. “Predicting Tidal Flooding of Urbanized Embayments: A Modeling Framework and Data Requirements.” *Coastal Engineering* 58(6):567–77.

Gallien, Timu W., Nikos Kalligeris, Marie Pierre C. Delisle, Bo Xiang Tang, Joseph T. D. Lucey, and Maria A. Winters. 2018. “Coastal Flood Modeling Challenges in Defended Urban Backshores.” *Geosciences (Switzerland)* 8(12).

Gao, C. and T. Adcock. 2016. “Numerical Investigation of Resonance in the Bristol Channel.” in *Proceedings of the International Offshore and Polar Engineering Conference*.

Garzon, Juan L. and Celso M. Ferreira. 2016. “Storm Surge Modeling in Large Estuaries: Sensitivity Analyses to Parameters and Physical Processes in the Chesapeake Bay.” *Journal of Marine Science and Engineering* 4(45).

Geeraerts, J., P. Troch, J. De Rouck, H. Verhaeghe, and J. J. Bouma. 2007. “Wave Overtopping at Coastal Structures: Prediction Tools and Related Hazard Analysis.” *Journal of Cleaner Production* 15:1514–21.

George, Douglas a., Guy Gelfenbaum, and Andrew W. Stevens. 2012. “Modelling the Hydrodynamic and Morphologic Response of an Estuary Restoration.” *Estuaries and Coasts* 35(6):1510–29.

Gimeno, Vicente, James P. Syvertsen, Inmaculada Simón, Manuel Nieves, Leyanes Díaz-López,

- Vicente Martínez, and Francisco García-Sánchez. 2012. "Physiological and Morphological Responses to Flooding with Fresh or Saline Water in *Jatropha Curcas*." *Environmental and Experimental Botany* 78(3):47–55.
- Godin, Gabriel. 1993. "On Tidal Resonance." *Continental Shelf Research* 13(1):89–107.
- Gouldby, B. P., P. B. Sayers, M. C. Panzeri, and J. E. Lanyon. 2010. "Development and Application of Efficient Methods for the Forward Propagation of Epistemic Uncertainty and Sensitivity Analysis within Complex Broad-Scale Flood Risk System Models." *Canadian Journal of Civil Engineering* 37(7):955–67.
- Grady, Julian G. O. and Kathleen L. McInnes. 2010. "Wind Waves and Their Relationship to Storm Surges in Northeastern Bass Strait." *Australian Meteorological and Oceanographic Journal* 60:265–75.
- Gratiot, N., E. J. Anthony, a. Gardel, C. Gauchere, C. Proisy, and J. T. Wells. 2008. "Significant Contribution of the 18.6 Year Tidal Cycle to Regional Coastal Changes." *Nature Geoscience* 1(3):169–72.
- Greenberg, David A. 1984. "A Review of the Physical Oceanography of the Bay of Fundy." Pp. 9–30 in *Update of the Marine Environmental Consequences of Tidal Power Development in the Upper Reaches of the Bay of Fundy*, edited by D. Gordon and M. Dadswell.
- Greenberg, David A., Wade Blanchard, Bruce Smith, and Elaine Barrow. 2012. "Climate Change, Mean Sea Level and High Tides in the Bay of Fundy." *Atmosphere-Ocean* 50(3):261–76.
- Growneveld, R. .. and G. Meeden. 1984. "Measuring Skewness and Kurtosis." *Journal of the Royal Statistical Society. Series D (The Statistician)* 33(4):391–99.
- Haigh, Ivan D., Matt Eliot, and Charitha Pattiaratchi. 2011. "Global Influences of the 18.61 Year Nodal Cycle and 8.85 Year Cycle of Lunar Perigee on High Tidal Levels." *Journal of Geophysical Research: Oceans* 116(6):1–16.
- Haigh, Ivan D. and Robert J. Nicholls. 2017. "Coastal Flooding." *Marine Climate Change Impacts Partnership: Science Review* 108–14.
- Haigh, Ivan D., Matthew P. Wadey, Shari L. Gallop, Heiko Loehr, Robert J. Nicholls, Kevin Horsburgh, Jennifer M. Brown, and Elizabeth Bradshaw. 2015. "A User-Friendly Database of Coastal Flooding in the United Kingdom from 1915-2014." *Scientific Data* 2:1–13.
- Haigh, Ivan D., Matthew P. Wadey, Thomas Wahl, Ozgun Ozsoy, Robert J. Nicholls, Jennifer M. Brown, Kevin Horsburgh, and Ben Gouldby. 2016. "Analysis : Spatial and Temporal Analysis of Extreme Sea Level and Storm Surge Events around the Coastline of the UK." *Scientific Data*

3:1–14.

- Hall, J. A., S. Gille, J. Obeysekera, W. Sweet, K. Knuuti, and J. Marburger. 2016. *Regional Sea Level Scenarios for Coastal Risk Management: Managing the Uncertainty of Future Sea Level Change and Extreme Water Levels for Department of Defense Coastal Sites Worldwide*.
- Hall, J. W., S. Tarantola, P. D. Bates, and M. S. Horritt. 2005. “Distributed Sensitivity Analysis of Flood Inundation Model Calibration.” *Journal of Hydraulic Engineering* 131(2):97–105.
- Hallegatte, Stéphane, Colin Green, Robert J. Nicholls, and Jan Corfee-Morlot. 2013. “Future Flood Losses in Major Coastal Cities.” *Nature Climate Change* 3(9):802–6.
- Hawkes, Peter J., Ben P. Gouldby, Jonathan A. Tawn, and Michael W. Owen. 2002. “The Joint Probability of Waves and Water Levels in Coastal Engineering Design.” *Journal of Hydraulic Research* 40(3):241–51.
- Heaps, N. .. 1983. “Storm Surges, 1967–1982.” *Geophysical Journal of the Royal Astronomical Society* 74:331–76.
- Hendry, Alistair, Ivan D. Haigh, Robert J. Nicholls, Hugo Winter, Robert Neal, Thomas Wahl, Amelie Joly-Lauge, and Stephen E. Darby. 2019. “Assessing the Characteristics and Drivers of Compound Flooding Events around the UK Coast.” *Hydrology and Earth System Sciences* 23(7):3117–39.
- Hewston, R., Y. Chen, S. Pan, Q. Zou, D. Reeve, and I. D. Cluckie. 2010. “Quantifying Uncertainty in Tide, Surge and Wave Modelling during Extreme Storms.” in *BHS Third International Symposium, Managing Consequences of a Changing Global Environment*.
- Hibbert, Angela, Samantha Jane Royston, Kevin James Horsburgh, Harry Leach, and Alan Hisscott. 2015. “An Empirical Approach to Improving Tidal Predictions Using Recent Real-Time Tide Gauge Data.” *Journal of Operational Oceanography* 8(1):40–51.
- Hinkel, Jochen, Daniel Lincke, Athanasios T. Vafeidis, Mahé Perrette, Robert James, and Richard S. J. Tol. 2014. “Coastal Flood Damage and Adaptation Costs under 21st Century Sea-Level Rise.” *Proceedings of the National Academy of Sciences* 111(9):3292–97.
- Hoeke, Ron Karl, Kathleen L. McInnes, and Julian G. O. Grady. 2015. “Wind and Wave Setup Contributions to Extreme Sea Levels at a Tropical High Island: A Stochastic Cyclone Simulation Study for Apia, Samoa.” *Journal of Marine Science and Engineering* 3:1117–35.
- Hoitink, A. J. F. and D. A. Jay. 2016. “Tidal River Dynamics: Implications for Deltas.” *Reviews of Geophysics* 54(1):240–72.
- Horrillo-Caraballo, Jose M., Dominic E. Reeve, Dave Simmonds, Shunqi Pan, Andrew Fox, Richard

- Thompson, Simon Hoggart, Samuel S. H. Kwan, and Deborah Greaves. 2013. "Application of a Source-Pathway-Receptor-Consequence (S-P-R-C) Methodology to the Teign Estuary, UK." *Journal of Coastal Research* 165:1939–44.
- Horsburgh, K. J. and C. Wilson. 2007. "Tide-Surge Interaction and Its Role in the Distribution of Surge Residuals in the North Sea." *Journal of Geophysical Research: Oceans* 112(8):1–13.
- Horsburgh, Kevin and Matt Horritt. 2006. "The Bristol Channel Floods of 1607 – Reconstruction and Analysis." *Weather* 61(10):272–77.
- Hu, K., P. Ding, and J. Ge. 2007. "Modeling of Storm Surge in the Coastal Waters of Yangtze Estuary and Hangzhou Bay , China." *Journal of Coastal Research* SI50(50):527–33.
- Hudson, Thomas, Kevin Keating, Angus Petit, John Chatterton, and Alan Williams. 2015. *Cost Estimation for Coastal Protection - Summary of Evidence*.
- Hume, Terry M., Ton Snelder, Mark Weatherhead, and Rick Liefing. 2007. "A Controlling Factor Approach to Estuary Classification." *Ocean and Coastal Management* 50(11–12):905–29.
- Van Den Hurk, Bart, Erik Van Meijgaard, Paul De Valk, Klaas Jan Van Heeringen, and Jan Gooijer. 2015. "Analysis of a Compounding Surge and Precipitation Event in the Netherlands." *Environmental Research Letters* 10(3).
- Hutter, Gérard and Jochen Schanze. 2008. "Learning How to Deal with Uncertainty of Flood Risk in Long-term Planning." *International Journal of River Basin Management* 6(2):175–84.
- Idier, D., F. Dumas, and H. Muller. 2012. "Tide-Surge Interaction in the English Channel." *Natural Hazards and Earth System Science* 12(12):3709–18.
- Idier, D., J. Rohmer, T. Bulteau, and E. Delvallée. 2013. "Development of an Inverse Method for Coastal Risk Management." *Natural Hazards and Earth System Science* 13(4):999–1013.
- Idier, Déborah, Xavier Bertin, Philip Thompson, and Mark D. Pickering. 2019. "Interactions Between Mean Sea Level, Tide, Surge, Waves and Flooding: Mechanisms and Contributions to Sea Level Variations at the Coast." *Surveys in Geophysics* 40(6):1603–30.
- Irish, Jennifer L. and Rafael Cañizares. 2009. "Storm-Wave Flow through Tidal Inlets and Its Influence on Bay Flooding." *Journal of Waterway, Port, Coastal, and Ocean Engineering* 135(April):52–60.
- Janssen, P. A. E. M. 1989. "Wave-Induced Stress and the Drag of Air Flow over Sea Waves." *Journal of Physical Oceanography* 19:745–54.
- JBA. 2017. *South Gloucestershire Council Level 2 Strategic Flood Risk Assessment for Oldbury on*

Severn JBA Project Manager.

- Jones, John Eric and Alan Marshall Davies. 2007. "Influence of Non-Linear Effects upon Surge Elevations along the West Coast of Britain." *Ocean Dynamics* 57(4–5):401–16.
- Jonkman, Sebastiaan N., Marten M. Hillen, Robert J. Nicholls, Wim Kanning, and Mathijs van Ledden. 2013. "Costs of Adapting Coastal Defences to Sea-Level Rise— New Estimates and Their Implications." *Journal of Coastal Research* 29(5):1212–26.
- Karimpour, Arash, Qin Chen, and Robert R. Twilley. 2017. "Wind Wave Behavior in Fetch and Depth Limited Estuaries." *Nature Scientific Reports* 7(40654):1–9.
- Karunaratna, Harshinie, Jennifer Brown, Antonia Chatzirodou, Pushpa Dissanayake, and Paul Wisse. 2018. "Multi-Timescale Morphological Modelling of a Dune-Fronted Sandy Beach." *Coastal Engineering* 136(November 2017):161–71.
- Kates, R. W., C. E. Colten, S. Laska, and S. P. Leatherman. 2006. "Reconstruction of New Orleans after Hurricane Katrina: A Research Perspective." *Proceedings of the National Academy of Sciences of the United States of America* 103(40):14653–60.
- Khanal, Sonu, Nina Ridder, Hylke de Vries, Wilco Terink, and Bart van den Hurk. 2019. "Storm Surge and Extreme River Discharge: A Compound Event Analysis Using Ensemble Impact Modeling." *Frontiers in Earth Science* 7(September):1–15.
- Kim, Soo Youl, Tomohiro Yasuda, and Hajime Mase. 2008. "Numerical Analysis of Effects of Tidal Variations on Storm Surges and Waves." *Applied Ocean Research* 30(4):311–22.
- Klerk, W. J., H. C. Winsemius, W. J. Van Verseveld, A. M. R. Bakker, and F. L. M. Diermanse. 2015. "The Co-Incidence of Storm Surges and Extreme Discharges within the Rhine-Meuse Delta." *Environmental Research Letters* 10(3).
- Knight, P. J., T. Prime, J. M. Brown, K. Morrissey, and A. J. Plater. 2015. "Application of Flood Risk Modelling in a Web-Based Geospatial Decision Support Tool for Coastal Adaptation to Climate Change." *Natural Hazards and Earth System Sciences* 15(7):1457–71.
- Kron, W. 2009. "Flood Risk = Hazard · Values · Vulnerability." *Water International* 30(1):58–68.
- Kron, Wolfgang. 2013. "Coasts: The High-Risk Areas of the World." *Natural Hazards* 66(3):1363–82.
- Kumbier, Kristian, Rafael C. Carvalho, Athanasios T. Vafeidis, and Colin D. Woodroffe. 2018. "Investigating Compound Flooding in an Estuary Using Hydrodynamic Modelling: A Case Study from the Shoalhaven River, Australia." *Natural Hazards and Earth System Sciences* 18(2):463–77.

- Lalli, F., A. Bruschi, M. L. Cassese, A. Lotti, and V. Pesarino. 2016. "A Numerical Model for Wave-Current Interaction at the Scale of Marine Engineering." *Journal of Operational Oceanography* 9(sup1):s215–22.
- Lawless, Mark, Matthew Hird, Daniel Rodger, Ben Gouldby, Nigel Tozer, Tim Pullen, Andy Saulter, and Kevin Horsburgh. 2016. "Investigating Coastal Flood Forecasting Good Practice Framework."
- Leaman, C. 2019. "Python Wave Runup v0.1.4."
- Lennon, G. 1963. "The Identification of Weather Conditions Associated with the Generation of Major Storm Surges along the West Coast of the British Isles." *Quarterly Journal of the Royal Meteorological Society* 89:381–94.
- Lennon, Geoffrey William, E. J. Gumbel, N. A. Barricelli, and A. F. Jenkinson. 1963. "A Frequency Investigation of Abnormally High Tidal Levels At Certain West Coast Ports." *ICE Proceedings* 25(4):451–84.
- Leonardi, Nicoletta, Alexander S. Kolker, and Sergio Fagherazzi. 2015. "Interplay between River Discharge and Tides in a Delta Distributary." *Advances in Water Resources* 80:69–78.
- Lesser, G. R. 2009. *An Approach to Medium-Term Coastal Morphological Modelling*.
- Lesser, G. R., J. Van Kester, D. J. R. Walstra, and J. a Roelvink. 2000. "Three-Dimensional Morphological Modelling in Delft3D-FLOW." *SASME Book of Abstracts* 1–5.
- Lesser, G. R., J. A. Roelvink, J. A. T. M. van Kester, and G. S. Stelling. 2004. "Development and Validation of a Three-Dimensional Morphological Model." *Coastal Engineering* 51(8–9):883–915.
- Letchford, C. W. and B. C. Zachry. 2009. "On Wind, Waves, and Surface Drag." in *5th European & African Conferences on Wind Engineering*.
- Leuven, Jasper R. F. W., Harm Jan Pierik, Maarten van der Vegt, Tjeerd J. Bouma, and Maarten G. Kleinhans. 2019. "Sea-Level-Rise-Induced Threats Depend on the Size of Tide-Influenced Estuaries Worldwide." *Nature Climate Change* 9(December).
- Lewis, M., P. Bates, K. Horsburgh, J. Neal, and G. Schumann. 2013. "A Storm Surge Inundation Model of the Northern Bay of Bengal Using Publicly Available Data." *Quarterly Journal of the Royal Meteorological Society* 139(671):358–69.
- Lewis, M., G. Schumann, P. Bates, and K. Horsburgh. 2013. "Understanding the Variability of an Extreme Storm Tide along a Coastline." *Estuarine, Coastal and Shelf Science* 123:19–25.

- Lewis, Matt, Kevin Horsburgh, Paul Bates, and Ros Smith. 2011. "Quantifying the Uncertainty in Future Coastal Flood Risk Estimates for the U . K ." *Journal of Coastal Research* 27(5):870–81.
- Lewis, Matt J., Tamsin Palmer, Resa Hashemi, Peter Robins, Andrew Saulter, Jenny Brown, Huw Lewis, and Simon Neill. 2019. "Wave-Tide Interaction Modulates Nearshore Wave Height." *Ocean Dynamics* 69(3):367–84.
- Liang, Dongfang, Junqiang Xia, Roger A. Falconer, and Jingxin Zhang. 2014. "Study on Tidal Resonance in Severn Estuary and Bristol Channel." *Coastal Engineering Journal* 56(01):1450002.
- Lin, Weiqi, Lawrence P. Sanford, Steven E. Suttles, and R. Valigura. 2002. "Drag Coefficients with Fetch-Limited Wind Waves." *Journal of Physical Oceanography* 32:3058–74.
- Liu, Wen-cheng, Wei-che Huang, and Wei-bo Chen. 2016. "Modeling the Interaction between Tides and Storm Surges for the Taiwan Coast." *Environmental Fluid Mechanics* 16(4):721–45.
- Lowe, J. A. and J. M. Gregory. 2005. "The Effects of Climate Change on Storm Surges around the United Kingdom." *Philosophical Transactions of the Royal Society A: Mathematical, Physical and Engineering Sciences* 363(1831):1313–28.
- Lowe, Jason A., Dan Bernie, Philip Bett, Lucy Bricheno, Simon Brown, Daley Calvert, Robin Clark, Karen Eagle, Tamsin Edwards, Giorgia Fosser, Fai Fung, Laila Gohar, Peter Good, Jonathan Gregory, Glen Harris, Tom Howard, Neil Kaye, Elizabeth Kendon, Justin Krijnen, Paul Maisey, Ruth McDonald, Rachel McInnes, Carol McSweeney, John FB Mitchell, James Murphy, Matthew Palmer, Chris Roberts, Jon Rostron, David Sexton, Hazel Thornton, Jon Tinker, Simon Tucker, Kuniko Yamazaki, and Stephen Belcher. 2018. *UKCP18 Science Overview Report*. Vol. 2.
- Lyddon, Charlotte, Jennifer M. Brown, Nicoletta Leonardi, and Andrew J. Plater. 2018. "Flood Hazard Assessment for a Hyper-Tidal Estuary as a Function of Tide-Surge-Morphology Interaction." *Estuaries and Coasts* 1–22.
- Lyddon, Charlotte, Jenny M. Brown, Nicoletta Leonardi, and Andrew J. Plater. 2018. "Uncertainty in Estuarine Extreme Water Level Predictions Due to Surge-Tide Interaction." *PLoS ONE* 13(10):1–17.
- Lyddon, Charlotte E., Jennifer M. Brown, Nicoletta Leonardi, and Andrew J. Plater. 2019. "Increased Coastal Wave Hazard Generated by Differential Wind and Wave Direction in Hyper-Tidal Estuaries." *Estuarine, Coastal and Shelf Science* 220:131–41.
- Lyddon, Charlotte E., Jennifer M. Brown, Nicoletta Leonardi, and Andrew Saulter. 2019.

- “Quantification of the Uncertainty in Coastal Storm Hazard Predictions Due to Wave - Current Interaction and Wind Forcing.” *Geophysical Research Letters*.
- Magnox. 2014. *Hinkley Point A Site. Strategic Environmental Assessment Site Specific Baseline*.
- Manning, a. J., W. J. Langston, and P. J. C. Jonas. 2010. “A Review of Sediment Dynamics in the Severn Estuary: Influence of Flocculation.” *Marine Pollution Bulletin* 61(1–3):37–51.
- Marcos, Marta, Jérémy Rohmer, Michalis Vousdoukas, Lorenzo Mentaschi, Gonéri Le Cozannet, and Angel Amores. 2019. “Increased Extreme Coastal Water Levels Due to the Combined Action of Storm Surges and Wind-waves.” *Geophysical Research Letters* (1):2019GL082599.
- Marmer, H. A. 1922. “Tides in the Bay of Fundy.” *Geographical Review* 12(2):195–205.
- Marsooli, Reza and Ning Lin. 2018. “Numerical Modeling of Historical Storm Tides and Waves and Their Interactions along the U.S. East and Gulf Coasts.” *Journal of Geophysical Research: Oceans* 123(5):3844–74.
- Martyr, R. C., J. Dietrich, J. Westerink, P. Kerr, C. Dawson, J. Smith, H. Pourtaheri, N. Powell, M. van Ledden, and S. Tanaka. 2012. “Simulating Hurricane Storm Surge in the Lower Mississippi River under Varying FLOW Conditions.” *Journal of Hydraulic Engineering* 139:492–501.
- Marvin, Jeffrey T. and Alexander T. Wilson. 2016. “One Dimensional , Two Dimensional and Three Dimensional Hydrodynamic Modeling of a Dyked Coastal River in the Bay of Fundy.” *Journal of Water Management Modeling* 25(C404):1–13.
- Maskell, J., K. Horsburgh, M. Lewis, and P. Bates. 2014. “Investigating River-Surge Interaction in Idealised Estuaries.” *Journal of Coastal Research* 30(2):248–59.
- Mason, D. C., P. D. Bates, and J. T. Dall’ Amico. 2009. “Calibration of Uncertain Flood Inundation Models Using Remotely Sensed Water Levels.” *Journal of Hydrology* 368(1–4):224–36.
- Masselink, Gerd, Bruno Castelle, Tim Scott, Guillaume Dodet, Serge Suanez, Derek Jackson, and France Flocc. 2016. “Extreme Wave Activity during 2013/2014 Winter and Morphological Impacts along the Atlantic Coast of Europe.” *Geophysical Research Letters* 43:2135–43.
- Mayo, Talea and Ning Lin. 2019. “The Effect of the Surface Wind Field Representation in the Operational Storm Surge Model of the National Hurricane Center.” *Atmosphere* 10(4):193.
- McGranahan, G., D. Balk, and B. Anderson. 2007. “The Rising Tide: Assessing the Risks of Climate Change and Human Settlements in Low Elevation Coastal Zones.” *Environment and Urbanization* 19(1):17–37.
- Mcleod, Elizabeth, Benjamin Poulter, Jochen Hinkel, Enrique Reyes, and Rodney Salm. 2010. “Sea-

- Level Rise Impact Models and Environmental Conservation: A Review of Models and Their Applications.” *Ocean and Coastal Management* 53(9):507–17.
- McMillan, Alastair, Crispian Baststone, David Worth, Jonathan Tawn, Kevin Horsburgh, and Mark Lawless. 2011. *Coastal Flood Boundary Conditions for UK Mainland and Islands Project: SC060064/TR2: Design Sea Levels*.
- McMillan, Alastair, David Worth, and Dr Mark Lawless. 2011. *Coastal Flood Boundary Conditions for UK Mainland and Islands. Project SC060064 TR4. Practical Guidance Design Sea Levels*.
- Melby, J. A., N. C. Nadal-Caraballo, and N. Kobayashi. 2006. “Wave Runup Predictions for Flood Mapping.” Pp. 1–15 in *Proceedings of 33rd Conference on Coastal Engineering, Santander, Spain, 2012*.
- Menéndez, Melisa and Philip L. Woodworth. 2010. “Changes in Extreme High Water Levels Based on a Quasi-Global Tide-Gauge Data Set.” *Journal of Geophysical Research: Oceans* 115(10):1–15.
- Merz, B., H. Kreibich, R. Schwarze, and A. Thieken. 2010. “Assessment of Economic Flood Damage.” *Natural Hazards and Earth System Science* 10(8):1697–1724.
- de Moel, H. and J. C. J. H. Aerts. 2011. “Effect of Uncertainty in Land Use, Damage Models and Inundation Depth on Flood Damage Estimates.” *Natural Hazards* 58(1):407–25.
- de Moel, H., N. E. M. Asselman, and J. C. J. H. Aerts. 2012. “Uncertainty and Sensitivity Analysis of Coastal Flood Damage Estimates in the West of the Netherlands.” *Natural Hazards and Earth System Science* 12(4):1045–58.
- Moftakhari, Hamed R., Amir AghaKouchak, Brett F. Sanders, Maura Allaire, and Richard A. Matthew. 2018. “What Is Nuisance Flooding? Defining and Monitoring an Emerging Challenge.” *Water Resources Research* 54(7):4218–27.
- Moftakhari, Hamed R., Gianfausto Salvadori, Amir AghaKouchak, Brett F. Sanders, and Richard A. Matthew. 2017. “Compounding Effects of Sea Level Rise and Fluvial Flooding.” *Proceedings of the National Academy of Sciences of the United States of America* 114(37):9785–90.
- Monbaliu, Jaak, Zhongyuan Chen, Didier Felts, Jianzhong Ge, Francois Hissel, Jens Kappenberg, Siddharth Narayan, Robert J. Nicholls, Nino Ohle, Dagmar Schuster, Janina Sothmann, and Patrick Willems. 2014. “Risk Assessment of Estuaries under Climate Change: Lessons from Western Europe.” *Coastal Engineering* 87:32–49.
- Muchan, Katie, Melinda Lewis, Jamie Hannaford, and Simon Parry. 2015. “The Winter Storms of 2013/2014 in the UK: Hydrological Responses and Impacts.” *Weather* 70(2):55–61.

- Narayan, S., S. Hanson, R. J. Nicholls, D. Clarke, P. Willems, V. Ntegeka, and J. Monbaliu. 2012. "A Holistic Model for Coastal Flooding Using System Diagrams and the Source-Pathway-Receptor (SPR) Concept." *Natural Hazards and Earth System Sciences* 12:1431–39.
- Natural Resources Wales. 2014. *Wales Coastal Flooding Review Phase 1 Report –Assessment of Impacts*.
- Nicholls, Robert J., Susan E. Hanson, Jason A. Lowe, Richard A. Warrick, Xianfu Lu, and Antony J. Long. 2014. "Sea-Level Scenarios for Evaluating Coastal Impacts." *Wiley Interdisciplinary Reviews: Climate Change* 5(1):129–50.
- Nicholls, Robert J., Susan E. Hanson, Jason A. Lowe, Richard A. Warrick, Xianfu Lu, and Antony J. Long. 2014. "Sea-Level Scenarios for Evaluating Coastal Impacts." *WIREs Climate Change* 5(1):129–50.
- O'Neill, C., A. Saulter, J. Williams, and K. Horsburgh. 2016. *NEMO-Surge: Application of Atmospheric Forcing and Surge Evaluation. Technical Report 619*.
- Olbert, Agnieszka I., Joanne Comer, Stephen Nash, and Michael Hartnett. 2017. "High-Resolution Multi-Scale Modelling of Coastal Flooding Due to Tides, Storm Surges and Rivers Inflows. A Cork City Example." *Coastal Engineering* 121(January):278–96.
- Olbert, Agnieszka Indiana, Stephen Nash, Conleth Cunnane, and Michael Hartnett. 2013. "Tide-Surge Interactions and Their Effects on Total Sea Levels in Irish Coastal Waters." *Ocean Dynamics* 63(6):599–614.
- Ordnance Survey. 2013. "Strategi: User Guide and Technical Specification." Retrieved June 8, 2020 (https://digimap.edina.ac.uk/webhelp/os/data_files/os_manuals/strategi-user-guide_9.pdf).
- Palmer, T., R. J. Nicholls, N. C. Wells, A. Saulter, and T. Mason. 2014. "Identification of 'Energetic' Swell Waves in a Tidal Strait." *Continental Shelf Research* 88:203–15.
- Pan, Cun-Hong, Bing-Yao Lin, and Xian-Zhong Mao. 2007. "Case Study: Numerical Modeling of the Tidal Bore on the Qiantang River, China." *Journal of Hydraulic Engineering* 133(2):130–38.
- Pappenberger, Florian, Patrick Matgen, Keith J. Beven, Jean Baptiste Henry, Laurent Pfister, and Paul Fraipont. 2006. "Influence of Uncertain Boundary Conditions and Model Structure on Flood Inundation Predictions." *Advances in Water Resources* 29(10):1430–49.
- Pasquier, Ulysse, Yi He, Simon Hooton, Marisa Goulden, and Kevin M. Hiscock. 2019. "An Integrated 1D–2D Hydraulic Modelling Approach to Assess the Sensitivity of a Coastal Region to Compound Flooding Hazard under Climate Change." *Natural Hazards* 98(3):915–37.
- Pender, Gareth and Sylvain Néelz. 2007. "Use of Computer Models of Flood Inundation to Facilitate

- Communication in Flood Risk Management.” *Environmental Hazards* 7(2):106–14.
- Penning-Rowsell, E. C., S. M. Tunstall, S. M. Tapsell, and D. J. Parker. 2000. “The Benefits of Flood Warnings: Real but Elusive, and Politically Significant.” *Water and Environment Journal* 14(1):7–14.
- Penning-Rowsell, E., S. Priest, D. Parker, and J. Morris. 2013. *Flood and Coastal Erosion Risk Management*. Routledge.
- Perini, L., L. Calabrese, G. Salerno, P. Ciavola, and C. Armaroli. 2016. “Evaluation of Coastal Vulnerability to Flooding: Comparison of Two Different Methodologies Adopted by the Emilia-Romagna Region (Italy).” *Natural Hazards and Earth System Sciences* 16(1):181–94.
- Phillips, Benjamin T., Jennifer M. Brown, Jean-raymond Bidlot, and Andrew J. Plater. 2017. “Role of Beach Morphology in Wave Overtopping Hazard Assessment.” *Journal of Marine Science and Engineering* 5(1):1–18.
- Phillips, M. R. 2008. “Consequences of Short-Term Changes in Coastal Processes : A Case Study.” *Earth Surface Processes and Landforms* 2107(September 1998):2094–2107.
- Phillips, M. R., E. F. Rees, and T. Thomas. 2013. “Winds, Sea Levels and North Atlantic Oscillation (NAO) Influences: An Evaluation.” *Global and Planetary Change* 100:145–52.
- Pollard, J. A., T. Spencer, and S. M. Brooks. 2019. “The Interactive Relationship between Coastal Erosion and Flood Risk.” *Progress in Physical Geography* 43(4):574–85.
- Pottier, N., E. C. Penning-Rowsell, S. Tunstall, and G. Hubbert. 2005. “Land Use and Flood Protection: Contrasting Approaches and Outcomes in France and in England and Wales.” *Applied Geomorphology* 25(1):1–27.
- Prandle, D. 1985. “Classification of Tidal Response in Estuaries from Channel Geometry.” *Geophysical Journal of the Royal Astronomical Society* 80(1):209–21.
- Prandle, D. 2009. *Estuaries: Dynamics, Mixing, Sedimentation, and Morphology*. Cambridge: University Press.
- Prandle, D. and J. Wolf. 1978. “The Interaction of Surge and Tide in the North Sea and River Thames.” *Geophysical Journal International* 55(1):203–16.
- Prandle, David and Andrew Lane. 2015. “Sensitivity of Estuaries to Sea Level Rise: Vulnerability Indices.” *Estuarine, Coastal and Shelf Science* 160:60–68.
- Prime, Thomas, Jennifer M. Brown, and Andrew J. Plater. 2015. “Physical and Economic Impacts of Sea-Level Rise and Low Probability Flooding Events on Coastal Communities.” *PLoS ONE*

10(2):1–28.

- Prime, Thomas, Jennifer M. Brown, and Andrew J. Plater. 2016. “Flood Inundation Uncertainty: The Case of a 0.5% Annual Probability Flood Event.” *Environmental Science and Policy* 59:1–9.
- Proctor, R. and R. A. Flather. 1989. “Storm Surge Prediction in the Bristol Channel - the Floods of 13 December 1981.” *Continental Shelf Research* 9(10):889–918.
- Proudman, J. 1955a. “The Effect of Friction on a Progressive Wave of Tide and Surge in an Estuary.” *Proceedings of the Royal Society of London. Series A, Mathematical and Physical Sciences* 233(1194):407–18.
- Proudman, J. 1955b. “The Propagation of Tide and Surge in an Estuary.” *Proceedings of the Royal Society of London, Series A, Mathematical and Physical Sciences* 231(1184):8–24.
- Pugh, D. .. 1987. *Tides, Surges and Mean Sea-Level*. John Wiley & Sons Ltd, London.
- Pye, Kenneth and Simon J. Blott. 2010. “A Consideration of ‘Extreme Events’ at Hinkley Point.” *Technical Report Series 2010* (109).
- Pye, Kenneth and Simon J. Blott. 2014. “The Geomorphology of UK Estuaries: The Role of Geological Controls, Antecedent Conditions and Human Activities.” *Estuarine, Coastal and Shelf Science* 150:196–214.
- Quinn, Niall, Peter M. Atkinson, and Neil C. Wells. 2012. “Modelling of Tide and Surge Elevations in the Solent and Surrounding Waters: The Importance of Tide–surge Interactions.” *Estuarine, Coastal and Shelf Science* 112:162–72.
- Quinn, Niall, M. Lewis, Matthew P. Wadey, and Ivan D. Haigh. 2014. “Assessing the Temporal Variability in Extreme Storm-Tide Time Series for Coastal Flood Risk Assessment.” *Journal of Geophysical Research: Oceans* 119:2227–2237.
- Ranasinghe, Roshanka. 2020. “On the Need for a New Generation of Coastal Change Models for the 21st Century.” *Scientific Reports* 10(1):1–6.
- Rego, João L. and Chunyan Li. 2010. “Nonlinear Terms in Storm Surge Predictions: Effect of Tide and Shelf Geometry with Case Study from Hurricane Rita.” *Journal of Geophysical Research: Oceans* 115(6):1–19.
- Reguero, Borja G., Michael W. Beck, David N. Bresch, Juliano Calil, and Imen Meliane. 2018. “Comparing the Cost Effectiveness of Nature-Based and Coastal Adaptation: A Case Study from the Gulf Coast of the United States.” *PLoS ONE* 13(4):1–24.
- Reynolds, C. .. and J. .. West. 1988. *Stratification in the Severn Estuary- Physical Aspects and*

Biological Consequences. Ambleside: Freshwater Biological Association.

- Del Río, Laura, Theocharis A. Plomaritis, Javier Benavente, María Valladares, and Pedro Ribera. 2012. "Establishing Storm Thresholds for the Spanish Gulf of Cádiz Coast." *Geomorphology* 143–144:13–23.
- Roberts, Keith J., Brian A. Colle, Nickitas Georgas, and Stephan B. Munch. 2015. "A Regression-Based Approach for Cool-Season Storm Surge Predictions along the New York-New Jersey Coast." *Journal of Applied Meteorology and Climatology* 54(8):1773–91.
- Robins, Peter E., Matt J. Lewis, Jim Freer, David M. Cooper, Christopher J. Skinner, and Tom J. Coulthard. 2018. "Improving Estuary Models by Reducing Uncertainties Associated with River Flows." *Estuarine, Coastal and Shelf Science* 207:63–73.
- Robins, Peter E., Martin W. Skov, Matt J. Lewis, Luis Giménez, Alan G. Davies, Shelagh K. Malham, Simon P. Neill, James E. McDonald, Timothy A. Whitton, Suzanna E. Jackson, and Colin F. Jago. 2016. "Impact of Climate Change on UK Estuaries: A Review of Past Trends and Potential Projections." *Estuarine, Coastal and Shelf Science* 169:119–35.
- Roebeling, P. C., C. D. Coelho, and E. M. Reis. 2011. "Coastal Erosion and Coastal Defense Interventions: A Cost-Benefit Analysis." *Journal of Coastal Research* 64:1415–19.
- Roelvink, D. and G. K. F. .. Van Banning. 1994. "Design and Development of DELFT3D and Application to Coastal Morphodynamics." Pp. 451–56 in *Hydroinformatics '94*. International Association for Hydraulic Research.
- Roelvink, Dano, Ad Reniers, Ap van Dongeren, Jaap van Thiel de Vries, Robert McCall, and Jamie Lescinski. 2009. "Modelling Storm Impacts on Beaches, Dunes and Barrier Islands." *Coastal Engineering* 56(11–12):1133–52.
- Rosa-Santos, Paulo Jorge and Francisco Taveira-Pinto. 2013. "Experimental Study of Solutions to Reduce Downtime Problems in Ocean Facing Ports: The Port of Leixões, Portugal, Case Study." *Journal of Applied Water Engineering and Research* 1(1):80–90.
- Rossiter, J. R. 1961. "Interaction Between Tide and Surge in the Thames." *Geophysical Journal International* 6(1):29–53.
- Rowland, C. S., R. D. Morton, L. Carrasco, G. McShane, A. W. O'Neil, and C. M. Wood. 2017. "Land Cover Map 2015 (25m Raster, GB)." *NERC Environmental Information Data Centre*. Retrieved (<https://doi.org/10.5285/bb15e200-9349-403c-bda9-b430093807c7>).
- Ruckert, Kelsey L., Vivek Srikrishnan, and Klaus Keller. 2019. "Characterizing the Deep Uncertainties Surrounding Coastal Flood Hazard Projections: A Case Study for Norfolk, VA."

Scientific Reports 9(1):1–12.

- De Ruiter, Peter J., Julia C. Mullarney, Karin R. Bryan, and Christian Winter. 2017. “The Influence of Entrance Constriction on Hydrodynamics and Intertidal Morphology within Estuarine Basins.” Pp. 378–84 in *Australasian Coasts and Ports 2017 Conference*.
- Saltelli, A. 1999. “Sensitivity Analysis: Could Better Methods Be Used?” *Journal of Geophysical Research: Atmosphere* 104:3789–3793.
- Santana-Ceballos, J., C. .. Fortres, M. .. Reis, and G. Rodriguez. 2017. “Wave Overtopping and Flood Risk Assessment in Harbours: A Case Study of the Port of Las Nieves, Gran Canaria.” *WIT Transactions on The Built Environment: Coastal Cities and Their Sustainable Future II* 170:1–10.
- Sassi, M. .. and A. J. .. Hoitink. 2013. “River Flow Controls on Tides and Tide-Mean Water Level Profiles in a Tidal Freshwater River.” *Journal of Geophysical Research Letters* 118:4139–51.
- Saulter, Andy, Chris Bunney, and Jian-guo Li. 2016. *Application of a Refined Grid Global Model for Operational Wave Forecasting*.
- Savage, James Thomas Steven, Francesca Pianosi, Paul Bates, Jim Freer, and Thorsten Wagener. 2016. “Quantifying the Importance of Spatial Resolution and Other Factors through Global Sensitivity Analysis of a Flood Inundation Model.” *Water Resources Research* 52(11):9146–63.
- Sayers, P., B. Gouldby, J. Simm, I. Meadowcroft, and J. Hall. 2003. “Risk, Performance and Uncertainty in Flood and Coastal Defence – A Review.” *R&D Technical Report FD2302/TR1. HR Wallingford* 115.
- Sayers, P., J. Hall, and I. Meadowcroft. 2002. “Towards Risk-Based Flood Hazard Management in the UK.” *Civil Engineering* 150:36–42.
- Sekovski, Ivan, Alice Newton, and William C. Dennison. 2012. “Megacities in the Coastal Zone: Using a Driver-Pressure-State-Impact-Response Framework to Address Complex Environmental Problems.” *Estuarine, Coastal and Shelf Science* 96(1):48–59.
- Senechal, Nadia, Giovanni Coco, Karin R. Bryan, and Rob A. Holman. 2011. “Wave Runup during Extreme Storm Conditions.” *Journal of Geophysical Research: Oceans* 116(7):1–13.
- SEPA. 2018. “Flood Modelling Guidance for Responsible Authorities.” 166.
- Shanze, J. 2006. “Flood Risk Management – A Basic Framework.” Pp. 1–20 in *Flood Risk Management: Hazards, Vulnerability and Mitigation Measures*, edited by J. Shanze, E. Zeman, and K. Marsalek. The Netherlands: Springer.

- Shaw, J., S. Cudmore, D. Turner, and D. Collier. 2005. *Improving Flood Warning Awareness in Low Probability and Medium-High Consequence Flood Zones a Qualitative Study*.
- Shen, J., H. Wang, M. Sisson, and W. Gong. 2006. "Storm Tide Simulation in the Chesapeake Bay Using an Unstructured Mesh Model." *Estuarine, Coastal and Shelf Science* 68:1–16.
- Shepard, Christine C., Vera N. Agostini, Ben Gilmer, Tashya Allen, Jeff Stone, William Brooks, and Michael W. Beck. 2012. "Assessing Future Risk: Quantifying the Effects of Sea Level Rise on Storm Surge Risk for the Southern Shores of Long Island, New York." *Natural Hazards* 60(2):727–45.
- Sibley, Andrew, D. Cox, and Helen Titley. 2015. "Coastal Flooding in England and Wales from Atlantic and North Sea Storms during the 2013 / 2014 Winter." *Weather* 70(2):62–70.
- Sibley, Andrew and Dave Cox. 2014. "Flooding along English Channel Coast Due to Long-Period Swell Waves." *Weather* 69(3):59–66.
- Siddorn, J. R., S. A. Good, C. M. Harris, H. W. Lewis, J. Maksymczuk, M. J. Martin, and A. Saulter. 2016. "Research Priorities in Support of Ocean Monitoring and Forecasting at the Met Office." *Ocean Science* 12(1):217–31.
- Sinha, P. C., I. Jain, N. Bhardwaj, A. D. Rao, and S. K. Dube. 2008. "Numerical Modeling of Tide-Surge Interaction along Orissa Coast of India." *Natural Hazards* 45(3):413–27.
- Skinner, Christopher J., Thomas J. Coulthard, Daniel R. Parsons, Jorge A. Ramirez, Liam Mullen, and Susan Manson. 2015. "Simulating Tidal and Storm Surge Hydraulics with a Simple 2D Inertia Based Model, in the Humber Estuary, U.K." *Estuarine, Coastal and Shelf Science* 155:126–36.
- Smith, Rosemary A. E., Paul D. Bates, and Christopher Hayes. 2012. "Evaluation of a Coastal Flood Inundation Model Using Hard and Soft Data." *Environmental Modelling and Software* 30:35–46.
- Sosa, Jeison, Christopher Sampson, Andrew Smith, Jeffrey Neal, and Paul Bates. 2020. "A Toolbox to Quickly Prepare Flood Inundation Models for LISFLOOD-FP Simulations." *Environmental Modelling and Software* 123(October 2019):104561.
- South Gloucestershire Council. 2014. *Southampton Local Flood Risk Management Strategy Summary*.
- Spencer, Thomas, Susan M. Brooks, Ben R. Evans, James A. Tempest, and Iris Möller. 2015. "Southern North Sea Storm Surge Event of 5 December 2013: Water Levels, Waves and Coastal Impacts." *Earth-Science Reviews* 146(December 2013):120–45.
- Sraj, Ihab, Kyle T. Mandli, Omar M. Knio, Clint N. Dawson, and Ibrahim Hoteit. 2014. "Uncertainty Quantification and Inference of Manning's Friction Coefficients Using DART Buoy Data during

- the Tōhoku Tsunami.” *Ocean Modelling* 83:82–97.
- Sliver, Ryan L., Robert J. Lempert, Per Wikman-Svahn, and Klaus Keller. 2018. *Characterizing Uncertain Sea-Level Rise Projections to Support Investment Decisions*. Vol. 13.
- Stephens, Scott, Robert Bell, and Judy Lawrence. 2017. “Applying Principles of Uncertainty within Coastal Hazard Assessments to Better Support Coastal Adaptation.” *Journal of Marine Science and Engineering* 5(3):40.
- Stockdon, Hilary F., Rob A. Holman, Peter A. Howd, and Asbury H. Sallenger Jr. 2006. “Empirical Parameterization of Setup, Swash, and Runup.” *Coastal Engineering* 53:573–88.
- Suanez, Serge, Romain Cancouët, France Floc’h, Emmanuel Blaise, Fabrice Ardhuin, Jean François Filipot, Jean Marie Cariolet, and Christophe Delacourt. 2015. “Observations and Predictions of Wave Runup, Extreme Water Levels, and Medium-Term Dune Erosion during Storm Conditions.” *Journal of Marine Science and Engineering* 3(3):674–98.
- Svensson, C. and D. .. Jones. 2002. “Dependence between Extreme Sea Surge, River Flow and Precipitation in Eastern Britain.” *International Journal of Climatology* 22(10):1149–68.
- Talke, S. A. and M. T. Stacey. 2003. “The Influence of Oceanic Swell on Flows over an Estuarine Intertidal Mudflat in San Francisco Bay.” *Estuarine, Coastal and Shelf Science* 58:541–54.
- Tang, Y. M., R. Grimshaw, B. G. Sanderson, and G. J. Holland. 1996. “A Numerical Study of Storm Surges and Tides, with Application to the North Queensland Coast.” *Journal of Physical Oceanography* 26:2700–2711.
- Temmerman, Stijn, Patrick Meire, Tjeerd J. Bouma, Peter M. J. Herman, Tom Ysebaert, and Huib J. De Vriend. 2013. “Ecosystem-Based Coastal Defence in the Face of Global Change.” *Nature* 504(7478):79–83.
- Teng, J., A. J. Jakeman, J. Vaze, B. F. W. Croke, D. Dutta, and S. Kim. 2017. “Flood Inundation Modelling: A Review of Methods, Recent Advances and Uncertainty Analysis.” *Environmental Modelling and Software* 90:201–16.
- Thompson, Daniel A., Harshinie Karunarathna, and Dominic E. Reeve. 2017. “Modelling Extreme Wave Overtopping at Aberystwyth Promenade.” *Water* 9(9):1–16.
- Tully, Katherine L., Danielle Weissman, W. Jesse Wyner, Jarrod Miller, and Thomas Jordan. 2019. “Soils in Transition: Saltwater Intrusion Alters Soil Chemistry in Agricultural Fields.” *Biogeochemistry* 142(3):339–56.
- Tunstall, Sm, C. L. Johnson, and E. C. Penning Rowsell. 2004. “Flood Hazard Management in England and Wales: From Land Drainage to Flood Risk Management.” Pp. 1–8 in *World*

Congress on Natural Disaster Mitigation.

- Uncles, R. J. 1981. "A Numerical Simulation of the Vertical and Horizontal M2 Tide in the Bristol Channel and Comparisons with Observed Data." *Limnology and Oceanography* 26(3):571–77.
- Uncles, R. J. 1984. "Hydrodynamics of the Bristol Channel." *Marine Pollution Bulletin* 15(2):47–53.
- Uncles, R. J. 2010. "Physical Properties and Processes in the Bristol Channel and Severn Estuary." *Marine Pollution Bulletin* 61(1–3):5–20.
- UNISDR. 2015. *Sendai Framework for Disaster Risk Reduction 2015 - 2030*. Sendai, Japan.
- Unnikrishnan, A. S. and D. Sundar. 2004. "Analysis of Extreme Sea Level along the East Coast of India." *Journal of Geophysical Research* 109(C6):1–7.
- Vitousek, Sean, Patrick L. Barnard, Charles H. Fletcher, Neil Frazer, Li Erikson, and Curt D. Storlazzi. 2017. "Doubling of Coastal Flooding Frequency within Decades Due to Sea-Level Rise." *Scientific Reports* 7(1):1–9.
- de Vries, Hans, Marguerite Breton, Tom de Mulder, Yannis Krestenitis, Jose Ozer, Roger Proctor, Kevin Ruddick, Jean Claude Salomon, and Aart Voorrips. 1995. "A Comparison of 2D Storm Surge Models Applied to Three Shallow European Seas." *Environmental Software* 10(1):23–42.
- Wadey, M. P., J. M. Brown, I. D. Haigh, T. Dolphin, and P. Wisse. 2015. "Assessment and Comparison of Extreme Sea Levels and Waves during the 2013/14 Storm Season in Two UK Coastal Regions." *Natural Hazards and Earth System Sciences* 15(10):2209–25.
- Wadey, Matthew P., Robert J. Nicholls, and Ivan Haigh. 2013. "Understanding a Coastal Flood Event: The 10th March 2008 Storm Surge Event in the Solent, UK." *Natural Hazards* 67(2):829–54.
- Wadey, Matthew P., Robert J. Nicholls, and Craig Hutton. 2012. "Coastal Flooding in the Solent: An Integrated Analysis of Defences and Inundation." *Water (Switzerland)* 4(2):430–59.
- Wahl, Thomas, Shaleen Jain, Jens Bender, Steven D. Meyers, and Mark E. Luther. 2015. "Increasing Risk of Compound Flooding from Storm Surge and Rainfall for Major US Cities." *Nature Climate Change* 5(12):1093–97.
- Wainwright, D. J., R. Ranasinghe, D. P. Callaghan, C. D. Woodroffe, R. Jongejan, A. J. Dougherty, K. Rogers, and P. J. Cowell. 2015. "Moving from Deterministic towards Probabilistic Coastal Hazard and Risk Assessment: Development of a Modelling Framework and Application to Narrabeen Beach, New South Wales, Australia." *Coastal Engineering* 96:92–99.
- Walters, D. N., K. D. Williams, I. A. Boutle, A. C. Bushell, J. M. Edwards, P. R. Field, A. P. Lock, C.

- J. Morcrette, R. A. Stratton, J. M. Wilkinson, M. R. Willett, N. Bellouin, A. Bodas-Salcedo, M. E. Brooks, D. Copsey, P. D. Earnshaw, S. C. Hardiman, C. M. Harris, R. C. Levine, C. Maclachlan, J. C. Manners, G. M. Martin, S. F. Milton, M. D. Palmer, M. J. Roberts, J. M. Rodríguez, W. J. Tennant, and P. L. Vidale. 2014. “The Met Office Unified Model Global Atmosphere 4.0 and JULES Global Land 4.0 Configurations.” *Geoscientific Model Development* 7(1):361–86.
- Wang, J., W. Gao, S. Xu, and L. Yu. 2012. “Evaluation of the Combined Risk of Sea Level Rise, Land Subsidence, and Storm Surges on the Coastal Areas of Shanghai, China.” *Climate Change* 115:537–58.
- Wang, Zheng Bing, Wouter Vandenbruwaene, Marcel Taal, and Han Winterwerp. 2019. “Amplification and Deformation of Tidal Wave in the Upper Scheldt Estuary.” *Ocean Dynamics* 69(7):829–39.
- Ward, Philip J., Anaïs Couasnon, Dirk Eilander, Ivan D. Haigh, Alistair Hendry, Sanne Muis, Ted I. E. Veldkamp, Hessel C. Winsemius, and Thomas Wahl. 2018. “Dependence between High Sea-Level and High River Discharge Increases Flood Hazard in Global Deltas and Estuaries.” *Environmental Research Letters* 13(8).
- Warren, I. .. and H. .. Bach. 1992. “MIKE 21: A Modelling System for Estuaries, Coastal Waters and Seas.” *Environmental Software* 7(4):229–40.
- Webster, Tim, Kevin McGuigan, Kate Collins, and Candace MacDonald. 2014. “Integrated River and Coastal Hydrodynamic Flood Risk Mapping of the Lahave River Estuary and Town of Bridgewater, Nova Scotia, Canada.” *Water* 6(3):517–46.
- Williams, J. A. and K. J. Horsburgh. 2013. “Evaluation and Comparison of the Operational Bristol Channel Model Storm Surge Suite.” *NOC Research and Consultancy Report*.
- Williams, J., K. Horsburgh, J. .. Williams, and R. Proctor. 2016. “Tide and Skew Surge Independence: New Insights for Flood Risk.” *Geophysical Research Letters* 43(12):6410–17.
- Williams, J., C. Wilson, and K. Horsburgh. 2012. *Re-Analysis of the December 1981 Storm Surge Event in the Bristol Channel Using the Current Operational Tide-Surge Model Suite: National Oceanography Centre Research & Consultancy Report No. 26*.
- Williams, Jon J. and Luciana S. Esteves. 2017. “Guidance on Setup, Calibration, and Validation of Hydrodynamic, Wave, and Sediment Models for Shelf Seas and Estuaries.” *Advances in Civil Engineering* 2017.
- Williams, V. J. 2009. “The Ecological Effects of Salt Water Intrusion on the Agriculture Industry

- After Hurricane Katrina.” in *Proceedings of the 2007 National Conference on Environmental Science and Technology*, edited by E. Nzewi. New York, NY: Springer.
- Wilmott, C. .. 1981. “On the Validation of Models.” *Physical Geography* 2(2):184–94.
- Wilmott, C. ..., S. .. Robeson, and K. Matsuura. 2012. “A Refined Index of Model Performance.” *International Journal of Climatology* 32(13):2088–94.
- Wolf, Judith. 2007. *Development of Estuary Morphological Models: Annex A1: SWAN Modelling of Liverpool Bay Including Dee, Mersey and Ribble Estuaries. R&D Project Record FD2107/PR.*
- Wolf, Judith. 2008. “Coupled Wave and Surge Modelling and Implications for Coastal Flooding.” *Advances in Geosciences* 17:19–22.
- Wolf, Judith. 2009. “Coastal Flooding: Impacts of Coupled Wave-Surge-Tide Models.” *Natural Hazards* 49(2):241–60.
- Wolf, Judith, J. M. Brown, R. Bolaños, and Hedges T. S. 2011. *Waves in Coastal and Estuarine Waters*. Vol. 2. Elsevier Inc.
- Wolf, Judith and R. A. Flather. 2005. “Modelling Waves and Surges during the 1953 Storm.” *Philosophical Transactions of the Royal Society A: Mathematical, Physical and Engineering Sciences* 363(1831):1359–75.
- Wong, Jefferson S., Jim E. Freer, Paul D. Bates, David A. Sear, and Elisabeth M. Stephens. 2015. “Sensitivity of a Hydraulic Model to Channel Erosion Uncertainty during Extreme Flooding.” *Hydrological Processes* 29(2):261–79.
- Wong, Tony E. and Klaus Keller. 2017. “Deep Uncertainty Surrounding Coastal Flood Risk Projections: A Case Study for New Orleans.” *Earth’s Future*.
- Woolf, David and Judith Wolf. 2013. *Impacts of Climate Change on Storms and Waves*.
- Woth, Katja, Ralf Weisse, and Hans von Storch. 2006. “Climate Change and North Sea Storm Surge Extremes : An Ensemble Study of Storm Surge Extremes Expected in a Changed Climate Projected by Four Different Regional Climate Models.” *Ocean Dynamics* 56:3–15.
- Wright, A., J. Shipton, B. Carroll, and S. Armstrong. 2011. “Lessons for Designing Managed Realignment Sites along Hyper Tidal Estuaries - a Case Study on the Bristol Port Company’s Steart Habitat Creation Scheme.” in *Proceedings of the ICE Coastal Management 2011*.
- Wu, Jin. 1982. “Wind-Stress Coefficients over Sea Surface from Breeze to Hurricane.” *Journal of Geophysical Research* 87:9704–6.
- Xia, Junqiang, Roger A. Falconer, and Binliang Lin. 2010. “Impact of Different Tidal Renewable

- Energy Projects on the Hydrodynamic Processes in the Severn Estuary, UK.” *Ocean Modelling* 32(1–2):86–104.
- Xie, Dong-mei, Qing-ping Zou, and John W. Cannon. 2016. “Application of SWAN+ADCIRC to Tide-Surge and Wave Simulation in Gulf of Maine during Patriot’s Day Storm.” *Water Science and Engineering* 9(1):33–41.
- Yang, Jie, Linlin Li, Kuifeng Zhao, Peitao Wang, Dong Wang, and In Mei Sou. 2019. “A Comparative Study of Typhoon Hato (2017) and Typhoon Mangkhut (2018) – Their Impacts on Coastal Inundation in Macau.” 1–30.
- Yin, Kai, Sudong Xu, Wenrui Huang, and Yang Xie. 2017. “Effects of Sea Level Rise and Typhoon Intensity on Storm Surge and Waves in Pearl River Estuary.” *Ocean Engineering* 136:80–93.
- Yin, Yunzhu, Harshinie Karunarathna, and Dominic E. Reeve. 2019. “A Computational Investigation of Storm Impacts on Estuary Morphodynamics.” *Journal of Marine Science and Engineering* 7(12).
- Zhang, Jisheng, Chi Zhang, Xiuguang Wu, and Yakun Guo. 2012. “Astronomical Tide and Typhoon-Induced Storm Surge in Hangzhou Bay, China.” in *Hydrodynamics - Natural Water Bodies*, edited by H. E. Schulz, A. L. A. Simoes, and R. J. Lobosco. InTech.
- Zhang, Kejiang and Gopal Achari. 2010. “Uncertainty Propagation in Environmental Decision Making Using Random Sets.” *Procedia Environmental Sciences* 2(5):576–84.
- Zhang, Wen Zhou, Fengyan Shi, Hua Sheng Hong, Shao Ping Shang, and James T. Kirby. 2010. “Tide-Surge Interaction Intensified by the Taiwan Strait.” *Journal of Geophysical Research: Oceans* 115(6):1–17.
- Zheng, Feifei, Seth Westra, and Scott A. Sisson. 2013. “Quantifying the Dependence between Extreme Rainfall and Storm Surge in the Coastal Zone.” *Journal of Hydrology* 505:172–87.

Source of data

CEFAS (2018) WaveNet Data download [online] Available at: <http://wavenet.cefas.co.uk/Map> [Accessed August 2018].

Centre for Environmental Data Analysis (2018) Met Office Integrated Data Archive System (MIDAS) Land and Marine Surface Stations Data [online] Available at: <http://catalogue.ceda.ac.uk/> [Accessed January 2018].

Environment Agency (2016) “River Severn hourly water level data, Sandhurst gauge”, SHWGenquiries@environment-agency.gov.uk.

Environment Agency Geomatics (2019) LiDAR dataset, Tile: SO50se, ST58ne, ST59ne, ST59se, SO60se, SO60sw, ST68ne, ST68nw, ST69sw, , ST69ne, ST69se, ST69nw. Available: <https://www.data.gov.uk/dataset/fba12e80-519f-4be2-806f-41be9e26ab96/lidar-composite-dsm-2m>. Accessed August 2019.

Gloucester Harbour Trustees (2016) “Sharpness 10 minute tidal data” Received fom Mike Johnson [mike.johnson@gloucesterharbourtrustees.org.uk]

Gridded bathymetry: 1 Arcsecond [ascii], Scale 1:50,000, Tile: NW 55050025, NW 55050030, NW 55050035, NW 55050040, NW 55050045, NW 55100030, NW , 5100035, NW 55100040, NW 55100045, NW 55150025, NW 55150030, NW 55150035, NW 55150040, NW 55150045, Updated August 2013, Crown Copyright / SeaZone Solutions Ltd., UK. Using: EDINA Marine Digimap Service, <http://edina.ac.uk/digimap>, [Accessed January 2016].

Magnox (2016) “Oldbury tide gauge record” Received from David Anderson [david.k.anderson@magnoxsites.com]

Met Office (2019) Hindcast WAVEWATCH III model wave data at grid points 51.217 N 4.240 W, 51.927 N 4.243 W, 51.377 N 4.246 W, 51.457 N 4.250 W, 51.537 N 4.252 W.

Ordnance Survey (2019) Ordnance Survey Backdrop mapping data. Tile SO60, SO70, ST47, ST48, ST57, ST58, ST59, ST68, ST69, ST79. Available: <http://digimap.edina.ac.uk/digimap/home>. Accessed December 2019.

National Oceanography Centre Liverpool (2019) CS3X hindcast wind and atmospheric pressure model data.

National Tidal and Sea Level Facility (2018) UK Tide Gauge Network [online] Available at: https://www.bodc.ac.uk/data/hosted_data_systems/sea_level/uk_tide_gauge_network/

Delft3D User Guide

March 2020

Contents

Table of Figures	198
1. How this guide works	199
2. How Delft3D works on the UoL / NOCL system	199
3. Set up Delft3D on Windows	199
4. Set up Delft3D on NOCL Linux.....	199
4.1. Recompile from source code	200
5. Starting off with Delft3D	201
5.1. Getting Help	201
6. Delft3D Input files.....	202
6.1. Working directory	202
6.2. Land boundary file (.ldb).....	202
6.3. Curvilinear grid.....	202
6.4. Bathymetry	204
6.4.1. Courant number.....	205
6.5. Boundary conditions	206
6.5.1. Water level data.....	206
6.5.2. Pressure data	206
6.5.3. Wind data.....	206
6.5.4. River level data	207
6.6. Datums	207
7. Insert the data in Delft-FLOW	208
7.1. .mdf.....	208
7.1.1. Time.....	208
7.1.2. Computational time step	208
7.1.3. Friction coefficient	208
7.1.4. Physical processes	208
7.1.5. Save intervals	208
7.1.6. .grd.....	209
7.1.7. .enc	209
7.1.8. .dep	209
7.1.9. .bnd.....	209
7.1.10. .bct.....	209
7.1.11. .obs	210
8. Decomposed Domain (DD) Boundaries	210

8.1.	Creating 2 grids with different resolution.....	210
8.2.	Add bathymetry to decomposed domain.....	212
9.	Run the model on Windows.....	215
9.1.	Run the model on Windows with decomposed domain.....	215
10.	Run the model on Mobius.....	215
11.	Validation and Calibration.....	216
12.	Obtaining results of model run.....	216
12.1.	GPP.....	216
12.2.	QUICKPLOT.....	216
12.2.1.	Water level time series.....	216
12.2.2.	Cross section.....	217
12.3.	Obtaining results in Matlab.....	217
13.	Post-processing results.....	219
13.1.	Animations and GIFs.....	219
13.2.	Graphs /and plots.....	219
14.	Delft3D-WAVE.....	219
14.1.	WAVE model grid.....	219
14.2.	WAVE boundary conditions.....	220
14.2.1.	Uniform values in the [runID].mdw file.....	220
14.2.2.	Time-varying: wavecon.[runID].....	223
14.2.3.	Time-varying and space-varying: [runID].bcw.....	224
14.2.4.	Some friendly advice.....	226
14.3.	Wind and pressure boundary conditions.....	226
14.3.1.	Uniform.....	226
14.3.2.	Time- and space-varying.....	226
14.4.	Set up .mdw for WAVE standalone.....	227
14.4.1.	Running WAVE standalone.....	227
14.5.	Set up .mdw for one-way FLOW → WAVE.....	228
14.5.1.	Running one-way coupling.....	228
14.6.	Set up .mdw (FLOW) and .mdw (WAVE) for two way FLOW ↔ WAVE online coupling	228
14.6.1.	Description.....	228
14.6.2.	Hydrodynamics.....	228
14.6.3.	Grids.....	228
14.6.4.	Boundaries.....	229
14.6.5.	Physical parameters.....	229

14.6.6. Output parameters	229
14.6.7. Running online coupling.....	229
14.7. Obtaining WAVE results in Matlab	229
15. Appendix	231
Appendix 1 Instructions for ArcMap, QUICKPLOT, RGFGRID and QUICKIN.....	231
ArcMap	231
Create a grid in RGFGRID	232
Bathymetry and LiDAR in ArcMap	233
Combine bathymetry and grid in QUICKIN.....	234

Table of Figures

Figure 1: Example of a land boundary (red) and splines (green) created in RGFGRID.	203
Figure 2: Example of a curvilinear grid created in RGFGRID	203
Figure 3: Example of depth and grid created in QUICKIN	205
Figure 4: (a) Select grid points (b) block delete exterior.	211
Figure 5: Small grid over large grid	211
Figure 6: (a) Select big grid to delete (b) two separate grids of different resolution.....	212
Figure 7: Edit DD boundaries	212
Figure 8: Bathymetry mismatch between big and small grid.....	213
Figure 9: Take a note of the depth where the big and small grid share a grid point (black dots).....	213
Figure 10: Updated grid with refinements at the coast to improve resolution in WAVE.....	220
Figure 11: Delft3D-WAVE uniform boundary conditions setup.....	223
Figure 12: Delft3D-WAVE space-varying boundary setup.....	225
Table 1: Example .bct file for hourly data	209

1. How this guide works

Delft3D is a 2D/3D modelling suite to investigate hydrodynamics, sediment transport, morphology and water quality for fluvial, estuarine and coastal environments. Delft3D is made up of a series of modules, including FLOW (hydrodynamic module), MOR (morphological module) and WAVE (based on 3rd generation spectral wave model, SWAN).

This guide sets out how to set up and operate Delft3D on the UoL / NOCL system.

The guide initially provides a brief overview on how to set up a Delft3D-FLOW model run for hydrodynamic simulations only. The guide then describes how to set up online Delft3D-FLOW / WAVE coupling.

It should be noted that this guide does not replace the Delft3D user manuals which should be referred to throughout your journey with the model.

2. How Delft3D works on the UoL / NOCL system

- Input files compiled on Windows using the Delft Graphical User Interface (GUI). Input files cannot be created on Linux. For Linux, please use the pre-compiled Windows GUI, and transfer the input files to Linux.
- Calibration and test runs can be completed on Windows.
- Batch model runs, larger domains, longer time frame can be run on Mobius.
- Analysis and visualisation of results is then completed in the GUI on Windows.

3. Set up Delft3D on Windows

Register with the Delft3D online;

https://oss.deltares.nl/web/Delft3d/home?p_p_id=58&p_p_lifecycle=1&p_p_state=maximized&p_p_mode=view&saveLastPath=0&_58_struts_action=%2Flogin%2Fcreate_account

You will be emailed your screen name and password for the Delft3D website.

To receive a version of the GUI and a license file valid for one year, fill out the form GUI request form; <https://docs.google.com/forms/d/1CwctKqWAlOtAjFrpj5PmlhcWKw-zGxYGt0BJulXxfQ/viewform> You will need your screen name and password at this stage.

An email link will be sent to you to download the latest pre-compiled version of Delft3D (Installer, GUI, pre- and post-processing tools plus manuals and tutorials): **Delft3D 4.01.01.rc.03** (Delft3d_ohmw_4.01.01.rc.03.zip and other files).

Follow the instructions in the Read Me and install locally on your Windows machine.

4. Set up Delft3D on NOCL Linux

Copy the files from the following folder to you /work area;

- /work/nicleo/Delft_bk

Inside the folder /work/nicleo/Delft_bk there is a file called INSTALLREADME, which lists all used module, and commands necessary to recompile the source code from the beginning.

Copy the following into your \$HOME/.bashrc file;

```
# Cluster environment
HOST=`hostname`
if [[ ( $HOST = "mobius-master1" ) || ( $HOST = "mobius-master2" ) ]] ; then
    echo "This is Mobius cluster, so adding appropriate modules"
    module add shared slurm
fi
"~/bashrc" 53L, 1163C
```

This will load the modules to run jobs on cluster with sbatch.

Instructions on how to run the model on the cluster can be found in section ‘Run the model on Mobius.’

4.1. Recompile from source code

Follow these instructions if you wish to recompile Delft3D from source code yourself;

Register with the Delft3D online;

https://oss.deltares.nl/web/Delft3d/home?p_p_id=58&p_p_lifecycle=1&p_p_state=maximized&p_p_mode=view&saveLastPath=0&_58_struts_action=%2Flogin%2Fcreate_account

Once registered, go to the online Delft3D depository; <https://svn.oss.deltares.nl/>

Choose a directory where you want the source code to be placed and execute the checkout command.

Example (to put the source code in the newly created directory "Delft3d_repository"):

```
svn checkout https://svn.oss.deltares.nl/repos/Delft3d/tags/5656 Delft3d_repository
```

You will now be prompted for your username and password following registration.

The download will start automatically.

Type the commands into the terminal specified inside */work/nicleo/Delft_bk/INSTALLREADME*

If required, contact Dr Nicoletta Leonardi, Department of Geography and Planning, University of Liverpool for further information.

5. Starting off with Delft3D

Read through the Delft3D manuals provided with the Windows download.

Work through the model tutorials for FLOW, RGFGRID, QUICKIN, QUICKPLOT, TIDE, GPP in Windows. The data for each tutorial was in the download along with the GUI and 1 year license. The instructions for each tutorial are in the respective manuals, also downloaded with the GUI and license.

Watch some of the webinars: <http://oss.deltares.nl/web/Delft3d/webinars> and screen casts: <http://oss.deltares.nl/web/Delft3d/screen-casts>

Say hello on the Delft3D Forum. The LinkedIn Delft forum is also active.

- <https://oss.deltares.nl/web/delft3d/forum>
- <https://www.linkedin.com/groups/3745991/profile>

5.1. Getting Help

If you have any error messages or questions, someone else has almost certainly had it and posted it on the Delft3D open source community forum. Search the forum for answers. If you can't find the answer you are looking for then definitely post a question. The Delft3D computer scientists prowl this forum on a daily basis to provide comprehensive, easy to follow answers.

Training courses: <https://www.deltares.nl/en/academy/Delft3d-block-1/> Expensive but maybe worth it. Discounts on course fees are offered to full time, academic members of staff (lecturers, readers, professors). No discounts or funding are available for PhD researchers to attend these courses.

Google! There are so many tutorials, lecture slides, presentations online in respect to most aspects of Delft3D that you should spend time looking through them if you have any problems.

6. Delft3D Input files

See Appendix 1 for detailed instructions on using ArcMap, QUICKPLOT, RGFGRID and QUICKIN for your input files.

6.1. Working directory

Create a working directory where all of your Delft input files and output files will be saved. Set your working directory when you first start up Delft. It is recommended you create a new working directory for each model run you complete.

6.2. Land boundary file (.ldb)

This file defines the boundary of your model and forms the template for your grid.

One method is to create a polyline in ArcMap which follows the boundary/coastline of your required domain. Export your polyline as a shapefile. Convert your shapefile to a .ldb file in DELFT-QUICKPLOT.

6.3. Curvilinear grid

You can create a curvilinear or flexible mesh grid in RGFGRID. The following will give brief details on how to create a curvilinear grid;

Set your co-ordinate system to either Cartesian or spherical. The latter is recommended for larger, regional domains.

Import your .ldb file into RGFGRID. Create splines along your land boundary, through the middle of your domain and along any areas you want higher resolution (Figure 1).

Once your splines are complete, use the 'Generate grid from splines' function (Figure 2). You can change the grid properties to your own preference. You should refer to the Delft-RGFGRID handbook for further directions.

Tips:

- Two splines can only intersect at one point. The programme will crash and close if your splines intersect at 2 or more points.
- Save your splines as you go along; it is recommended you save your splines to a **new** file each time you draw them in. This means you have a backup of your spline creation in stages. If one file crashes, then you do not need to start again.
- Grid cells should follow flow direction.

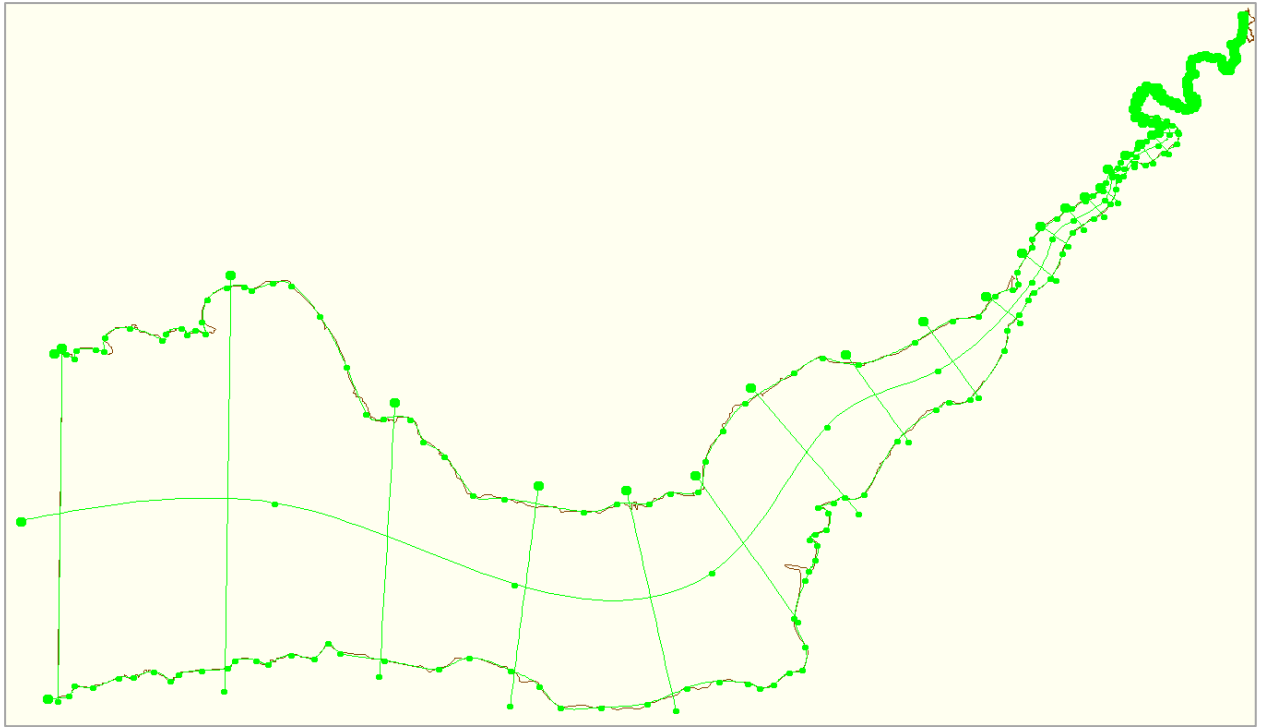


Figure 1: Example of a land boundary (red) and splines (green) created in RGFGRID.

Export your grid to your working directory as a .grid file

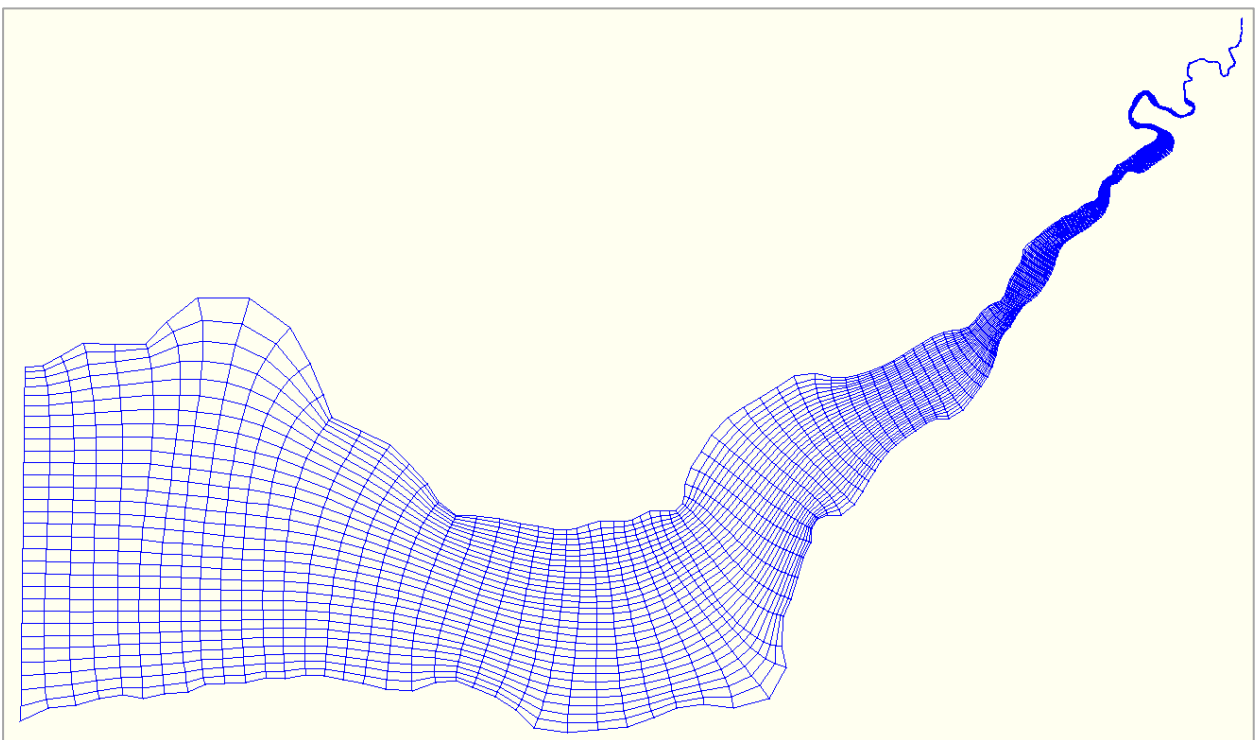


Figure 212: Example of a curvilinear grid created in RGFGRID

6.4. Bathymetry

Obtain bathymetry data for site of interest. If your bathymetry is downloaded as several tiles, then mosaic them together in R Studio or ArcMap. Optional: resample your raw bathymetry data to a resolution of your choice and crop to the desired size. Do not worry if there are gaps in your bathymetry, these can be interpolated at a later data in Delft-QUICKIN.

Ensure each water depth point has an associated latitude and longitude. This can be completed in ArcMap or R Studio.

Delft3D operates with bathymetry values increases from 0, with depth. The shallowest value is 0 and the deepest value is largest positive number. You can multiply your bathymetry values by -1 if they are downloaded as negative numbers.

Make a note of the coordinate system your bathymetry is in. Ensure your .grd file and bathymetry are set to the same coordinate system (Cartesian or Spherical). If your bathymetry is downloaded in WGS84 then it is Spherical. You can convert your data to BNG (Cartesian) in ArcMap or RStudio.

Save your bathymetry file (with X and Y coordinates) as a .txt file and change file extension to .xyz.

Adjust your bathymetry to a datum of choice.

Start Delft3D and set your working directory. Open Delft3D-QUICKIN.

Import your .grd file.

Import your .xyz bathymetry file as a Sample.

Refer to instruction in Delft-QUICKIN handbook for methods of interpolation for any gaps in your data set. The options available include;

- Triangular interpolation
- Grid cell averaging
- Internal diffusion

You will need to undertake one of the first 2 processes, so that you assign depth values to each grid cell.

This is a general rule that you can follow (ftp://ftp.io.usp.br/lampo/19jun2012/Apresentacoes/ic_103_quickin.ppt);

- Triangular interpolation if your grid resolution is greater than your bathymetry resolution.
- Grid cell averaging if you bathymetry resolution is greater than your grid resolution.

Save your bathymetry in your working directory as a .dep file. Reopen the grid and depth file in QUICKIN and the colours of the bathymetry will look clearer and smoother (Figure 3).

Any -999 values in the bathymetry can be smoothed out using Internal Diffusion;

- Draw a polygon around the area to fill in with about 1-2 cell buffer, Operations, Internal Diffusion and the space gets filled.
- Delete the polygon and repeat for all gaps
- If you have lots of little gaps you can draw one big polygon around the whole domain instead, rather than filling them individually.

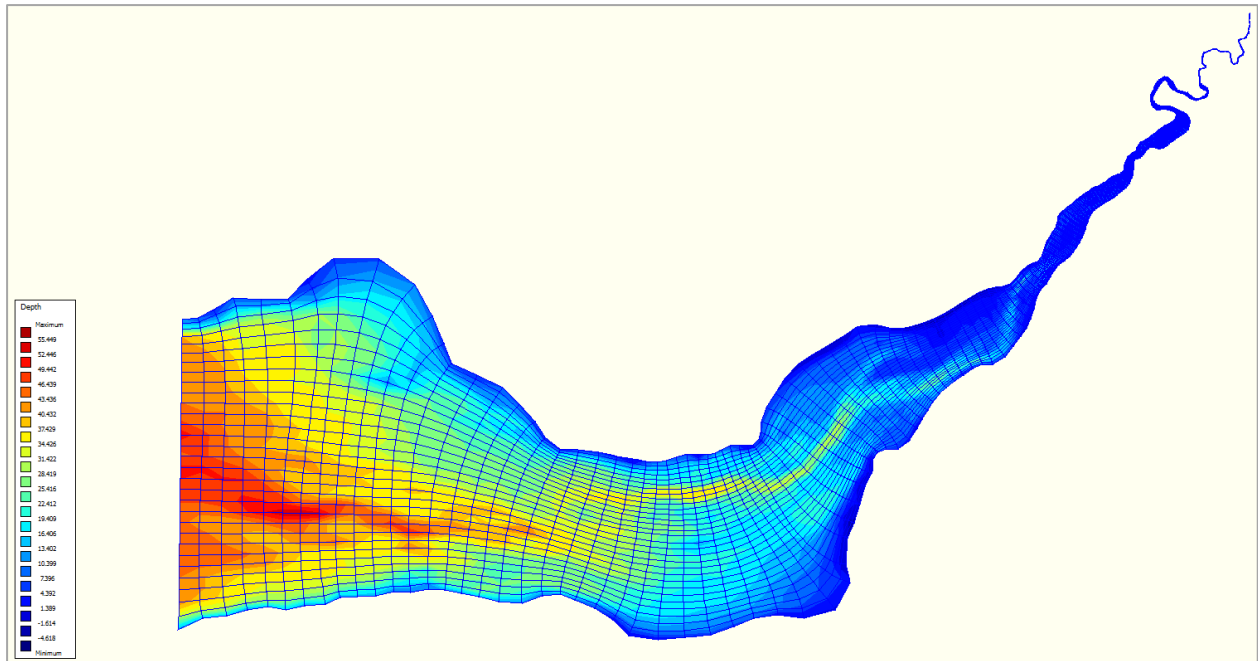


Figure 3: Example of depth and grid created in QUICKIN

6.4.1. Courant number

This is a user defined number which is dependent on the resolution of your grid and is used to define the time step for the model run. The time step (Courant number) must be less than a certain time to allow the calculations to be computed correctly across the grid. If the number is not set correctly then water flows faster through the domain than the calculations can be completed, leading to spurious incomplete results.

As a rule of thumb you Courant number should be less than 10. Your grid may need editing if the Courant number is too high. Refer to the Delft3D-FLOW manual for more information on this.

You can check the Courant number across the domain in the map file once you have completed a model run. Set the time step to 1, run a model run and then open QUICKPLOT. Once in QUICKPLOT do the following;

- Open the trim- map file
- Click 'File Dependent Options' on the bar of icons under the Menu bar
- Check time step

QUICKPLOT will verify the time step restrictions. Look at the 'Spatial variation of maximum allowed time step.' Any errors will likely arise where the grid is a very fine resolution. Set the time step near to the lowest value shown on this map. If the value is smaller than 0.01 then you may need to look at domain decomposition or derefine some areas of your grid.

The following error message is also related to having a time step set too high:

'ERROR Water level change too high'

Water is moving through the domain faster than calculations can be completed. You should re run your model with a lower time step. This is trial and error. It is likely you will need to run 3 or 4 runs until you have got a number which doesn't come back with an error.

6.5. Boundary conditions

6.5.1. Water level data

Create an hourly time series of water elevation. This could be obtained from CS3/CS3X.

Ensure your water level data is to the same datum as your bathymetry.

Save as a .txt file

Ideally you will have 1 set of water level data for at each point of your grid boundary. You can write down the latitude and longitude of your grid point boundaries in RGFGRID to ensure you have corresponding grid values and water level data.

Adding your boundary condition as a time series is only 1 option available within Delft3D-FLOW. You should refer to the manual for other formats.

6.5.2. Pressure data

You will need to obtain time- and space-varying pressure data from your own source. See section 14.3 referring to pressure data in WAVE.

If a time- and space-varying wind and pressure file is used for the simulation then ensure that the following text is included at the end of the .mdf:

```
Commnt =  
Online = #N#  
WaveOL = #Y#  
Fwndgu = #wind.amu#  
Fwndgv = #wind.amv#  
Fwndgp = #pressure.amp#  
Airout = #Y#  
Commnt =
```

6.5.3. Wind data

Go to Processes and tick Wind. Then go to Physical Parameters -> Wind where you can define the uniform wind field.

Alternatively you can select space varying wind and pressure. You will need to obtain time- and space-varying wind data from your own source. See section 14.3 referring to pressure data in WAVE.

If a time- and space-varying wind and pressure file is used for the simulation then ensure that the following text is included at the end of the .mdf:

```
Commnt =  
Online = #N#  
WaveOL = #Y#  
Fwndgu = #wind.amu#  
Fwndgv = #wind.amv#  
Fwndgp = #pressure.amp#  
Airout = #Y#  
Commnt =
```

6.5.4. River level data

You can request hourly / quarter of an hourly river level data from the Environment Agency. You will need to know the river gauging station number first and state this in your email request. Details can be found on the Environment Agency website.

6.6. Datums

Ensure you adjust the bathymetry and boundary conditions to datum of your choice.

7. Insert the data in Delft-FLOW

Use the GUI in Windows to set up your Master Definition File (.mdf) which will be used for the model run in Windows or Linux.

Open Delft3D and set your working directory. Navigate to 'FLOW' → 'FLOW INPUT.'

Tips:

- Give your model run and all associated files a name. It is recommended you call all files for one model run the same thing. E.g. A.mdf, A.bct, A.bnd, A.obs. It is good practice to keep a file directory stating model parameters associated with each model run (e.g. just a .txt file).
- Save All As after every change you make in FLOW.
- Ensure you also refer to instructions in the Delft-FLOW manual for comprehensive instructions.
- It is recommended you begin with a shorter model run and build upwards. If you have a 365 day long data set of hourly water levels at each boundary point, then consider running just 6 hours to start with. You can slowly increase the time as you become more confident in your model set up and the parameters you have set.

7.1. .mdf

Master Definition File.

It's in the name – this is what the model communicates with and all input files are saved to. It defines your model run via the Flow input GUI .

Save All As as soon as you open a new model run. Same as file name e.g. 'A.mdf'

7.1.1. Time

dd mm yy hh mm ss.

Must define the same start and end time throughout the .mdf and in your .bct file.

7.1.2. Computational time step

Your time step can be less than 1. The step time is defined by the Courant number, which is specific to your grid. You can find this out in QUICKPLOT.

7.1.3. Friction coefficient

Can be variable or uniform.

7.1.4. Physical processes

You can select tidal processes, salinity etc to be turned on.

7.1.5. Save intervals

This can be as fine or coarse a time resolution as you wish; 15 minute save intervals matches well with the resolution of tide gauge data making validation simpler.

7.1.6. .grd

Import your .grd file

7.1.7. .enc

An enclosure file will have been saved automatically too when you exported your RGFGRID. Open this.

7.1.8. .dep

Open your bathymetry file.

7.1.9. .bnd

This file defines your open boundary/boundaries.

Go to View → Visualisation. This will open you bathymetry and grid file in a new window.

Go to Edit Mode → Add

Go to Edit → Open Boundaries.

Click, hold, drag along the boundary and then release.

This function will allow you to draw your open boundaries onto your model domain by hand. Once completed you will see that the GUI now shows the coordinates of your boundary points. You can rename the boundary e.g. sea or river. Click save. Save your .bnd in your working directory. Give it the same name as your .mdf file.

Save these.

7.1.10. .bct

As previously mentioned there are a number of options available for your boundary data.

Select water level and time series as your boundary condition for all open boundaries you have drawn if appropriate.

Save the .bct file in your working directory with the same name as your .mdf and .bnd file. Ensure you Save All As at this point.

Open the .bct file using a text editor. E.g. TextPad.

You can now copy and paste your time series data into your .bct, and will ensure you insert your data in the correct format.

Copy your water level series from a .txt file / Excel sheet into the .bct file in the same format shown in Table 1. Time is shown in column 1. Table 1 shows hourly data. Column 2 and 3 show the water level. These can be same at the start and the end. Do not edit anything else in the .bct file. Only paste in your 3 columns of data for each boundary point. Ensure there are no commas in your data. Replace these with “.”, a full stop.

Table 1: Example .bct file for hourly data

Column 1	Column 2	Column 3
Time (mins)	Water level start (m)	Water level end (m)

0.000000e+000	-3.6867000e+000	-3.6867000e+000
6.000000e+001	-2.8166000e+000	-2.8166000e+000
1.200000e+002	-1.2466000e+000	-1.2466000e+000
1.800000e+002	7.2676000e-001	7.2676000e-001
2.400000e+002	2.6101000e+000	2.6101000e+000

If your model run is starting at midnight then column 1 should start at 0.00

If your save interval is set to 15 minutes and your model run is starting at 07:15am (for example) then column one should start at 435 minutes.

Save the .bct file.

Reload your .mdf file in the GUI and your boundary condition data should have updated. Your time series data will now show for each boundary point.

7.1.11. .obs

Every model run requires at least 2 observation points. Observation points will record a water level time series at a specific location on the grid which can be plotted after the model run.

Add these in the visualisation area.

Go to View → Visualisation.

Go to Edit Mode → Add

Go to Edit → Observations

You could place an observation point near a tide gauge or one of your open boundary points in your domain and use this to validate to your results. The observation points appear in the GUI and these can also be renamed to reference the real locations e.g. Avonmouth.

You can also extract water level time series from a specific location on your grid in the .mat you will create once model runs have finished. So you do not actually need to do anything with the observation point data file on completion of the model run.

Once all of your files and parameters have been set, ensure you Save All As



8. Decomposed Domain (DD) Boundaries

If you want to nest finer resolution grids within a coarser resolution grid then you will need to decompose your grid. The 'DD boundary' function will allow you to run a coarse/big grid alongside a fine/small grid within the same domain. I would recommend copying all of your original grid and depth files into a new folder when starting the DD boundaries and edit these. Do not edit your originals, you do not want to lose them or break them!

These instructions will utilize RGFGRID and QUICKIN to achieve this set up for you.

8.1. Creating 2 grids with different resolution

- Open RGFGRID.
- Import your original, big grid (e.g. SevernEstuaryGridbig.grd). Edit, Grid.

- Click the ‘block orthogonalise’ button on the tool bar; . You are not going to block orthogonalise, but this function allows you to select grid points!
- Select 4 points around the area you wish to designate as your small grid (Figure 4a). Click the 4 points, then click ‘Block delete exterior’ button on the tool bar and right click;  (Figure 4b).

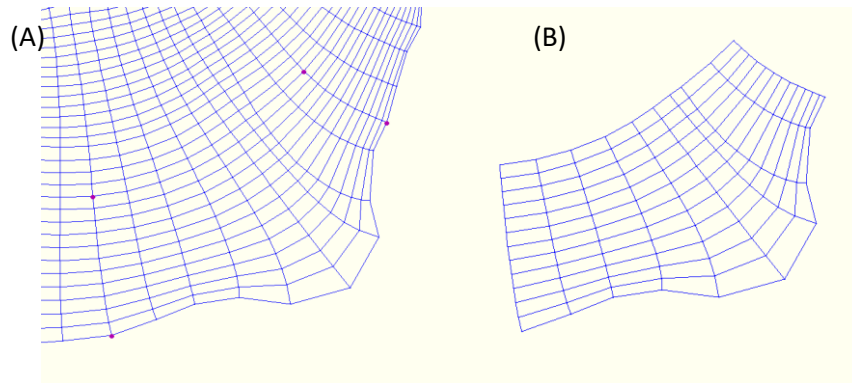


Figure 4: (a) Select grid points (b) block delete exterior.

- Save this as your small grid e.g. SevernEstuaryGridsmall.grd
- Now refine this small grid as desired. Set the M, N refinement values; Settings, General. To refine the grid go to Operations, Refinement, Refine Grid. Export refined grid.
- Create a new project. Import the big grid, then the small grid. It has to be in this order!

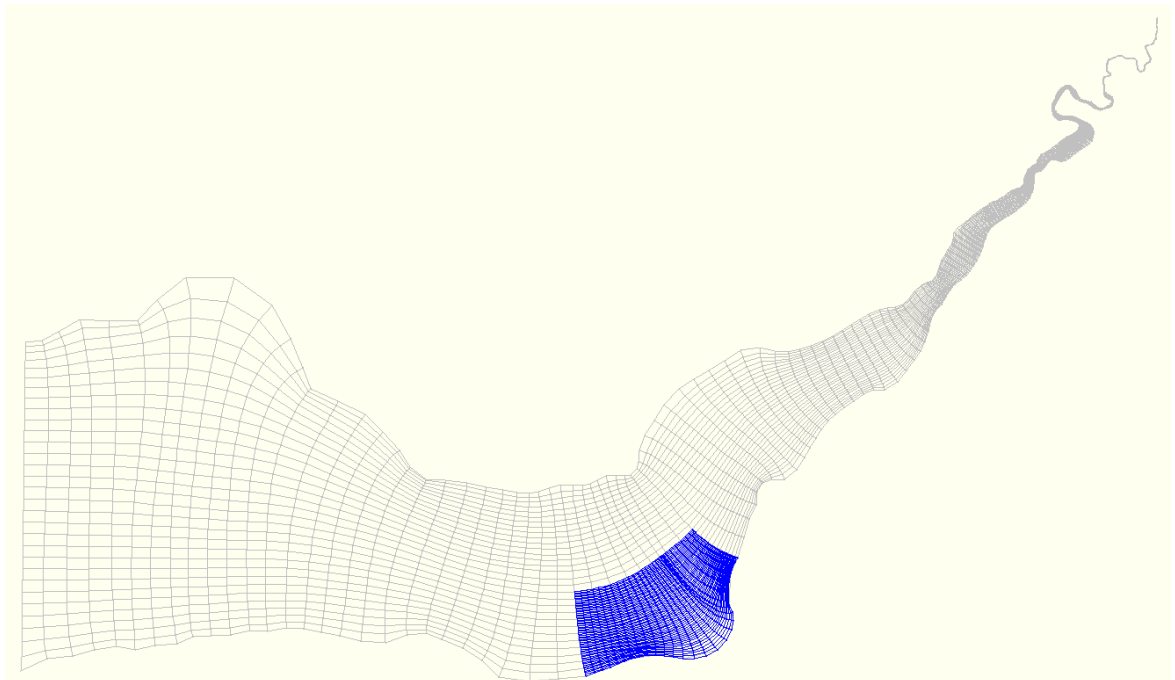



Figure 5: Small grid over large grid

- You can toggle between the big and small grid by clicking the ‘Select Domain’ button on the tool bar; 

- Select the big grid. Click Edit, Polygon, New. Draw a polygon just inside boundary between the big and small grid, which covers the area where the big grid covers the small (Figure 6a). Double click to finish.
- Operations, delete, grid.
- You should now have 2 grids which share a boundary, but do not overlap (Figure 6b).

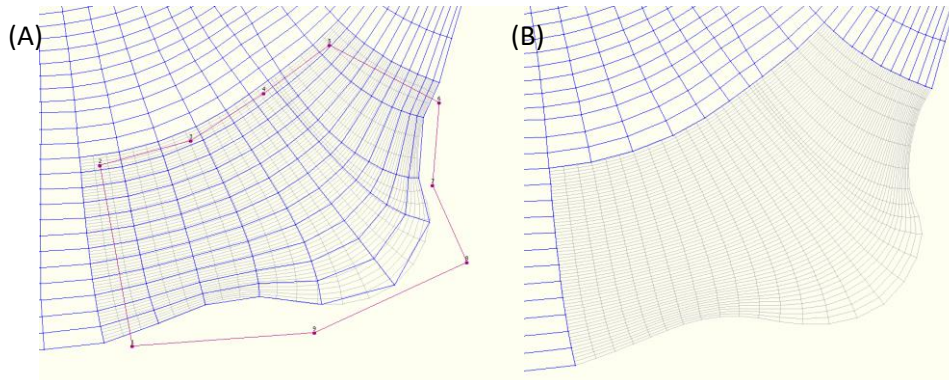


Figure 6: (a) Select big grid to delete (b) two separate grids of different resolution.

If you zoom in closely to the boundary between the 2 grids you will see that the grid cells do not line up exactly. This will throw back errors when you try and run the 2 grids together in the model. They need to be a perfect match!

- Load your 2 grids into RGFGRID. Select your smaller grid, using the ‘Select Domain’ button.
- Edit, DD boundaries, Start Edit.
- Draw a line along each boundary line (Figure 7). You will need to click twice at the end of a boundary, to finish one line and start another one. Once you have your lines along the boundary click Operations, Attach Grid at DD boundaries, Regular Grid. Your boundary should now be perfectly joined together with no gaps.

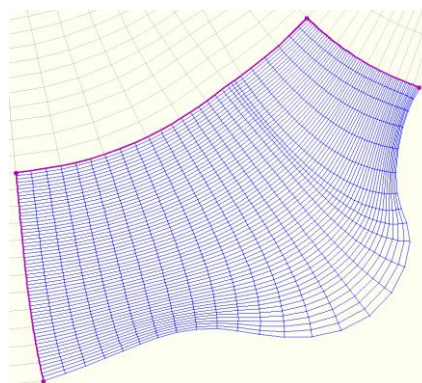


Figure 7: Edit DD boundaries

The proof of a perfect match will become evident when we add in the bathymetry!!

8.2. Add bathymetry to decomposed domain

You will need to add bathymetry to each grid separately. Everything you do not one grid must now be done to another!

- Open QUICKIN.

- Load one of your 2 grids. Repeat the processes described in the Bathymetry section to apply depth values to each grid.

Once you have bathymetry applied to each grid you may notice a jump in the depth across the boundaries (Figure 8). This is because the grids have been refined to a finer resolution. The smaller grid will have more accurate bathymetry due to the finer resolution, so you should apply the depth at each coarse grid point to be the same as the corresponding fine grid point.

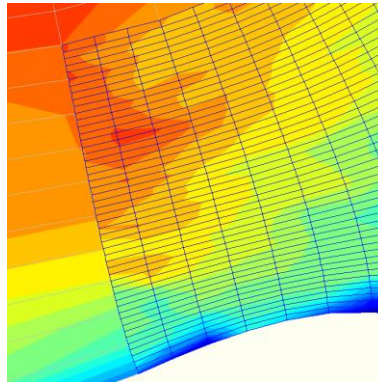


Figure 8: Bathymetry mismatch between big and small grid

- Open QUICKIN.
- Import the big grid, big depth, small grid, small depth to QUICKIN.
- Operations, Edit Depth.
- This is the quickest way we have found to align the bathymetry. Click the Select Domain button. Select the small domain. Get yourself a pen and paper. Operations, Edit Depth. Click on the big grid points which share the boundary with the small grid. Take a note of the small grid depth at each grid point where the big grid points are, as shown by the black dots in Figure 9.

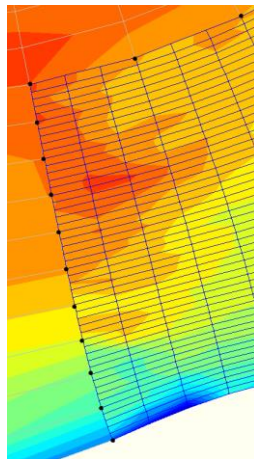


Figure 9: Take a note of the depth where the big and small grid share a grid point (black dots).

- Once you have a note of all of these, Select Domain and chose the big grid. Operations, Edit Depth. Go back over these points and replace the depth with the value from the small grid.
- Export the big grid depth file.

You will then need to compile the 2 grids so that they speak to each other within Delft.

- Open RGFRID.

- Edit, DD boundary, Start.
- Draw 3 lines around the small grid, and double click at each corner.
- Operations, compile DD. Give your .ddb file a name.
- Open the .ddb file in a text editor. Replace .grd with .mdf file extensions. This file is used when running the model to define the decomposed domain boundaries.

See '**Run the model on Windows with demcomposed domain**' for information on what to do next.

9. Run the model on Windows

Set your working directory to the file where all of your input files (.mdf, .bnd, .bct) are saved.

Navigate to 'FLOW → 'START'

Browse and select your .mdf file in the pop up window.

Wait for the model to run. This could take anything from 5 seconds upwards... obviously the larger the domain and the longer the time series, then the more time the model will take to run.

There are now 2 scenarios:

- The model run completes with no errors. Congratulations! Check the diagnostics file for any warning messages and act on these if necessary. Move onto 'Validation and Calibration.'
- The model run does not complete and returns a series of error messages. Read the diagnostics file once the model run has finished. Refer to the Delft forum with any errors. Re-run your scenario.

The output files will be saved into your working directory.

9.1. Run the model on Windows with decomposed domain

You will set up 2 .mdf files. One for the big grid (which will probably include all of your open boundaries) and one for your small domain (unlikely to include open boundaries, unless you have a river running into the domain). Ensure you have the same settings in each .mdf file.

The time step will need to be the same in both .mdf files, and set to the appropriate time step for the small grid. Check the new Courant number for the small grid in QUICKIN as before.

The .mdf files must have the same names as those defined in the .ddb file.

Flow → Start DD. Select the .ddb file.

10. Run the model on Mobius

You can run the model via sbatch submit.sh or just running the executable ./run_flow2d3d.sh on the Desktop.

If you chose the former then queue can be used to double check if your job is submitted. scancel [job number] can be used to cancel the job. Output files will be saved on the cluster and then need to be transferred to your Windows working directory to extract data and visualize. It is not possible to post-process these files on the cluster as the GUI only runs on Windows.

11.Validation and Calibration

If required, validate your output water level to the nearest tide gauge. Double check your time step, datum, bathymetry, friction coefficient or wall roughness (under Roughness in the .mdf input) if you are not happy with the results. Begin calibrating your model run by making small changes to friction etc. continue to validate your results until you are happy.

12.Obtaining results of model run

12.1. GPP

This GUI can be used to extract time series data and velocity data from individual observation points in your domain from the history file.

- FLOW → Tools → GPP
- Datasets, Add, Select File. Delft3D Hydrodynamic History File. Select the trih-[model run].dat file. Ok.
- Parameters, Water Level. Select Observation Point. Create.
- Export. Give File Name e.g. HinkleyDelft.txt in your working directory. Ensure you give the file a .txt extension! Ok.
- Write Timseries to a Text File. Export.
- Repeat for each observation point you want a time series for.
- The text file can then be read into Matlab.

12.2. QUICKPLOT

Quickplot can be used to obtain datasets from your model run e.g. velocity, depth averaged velocity, water depth and water level.

12.2.1. Water level time series

You can extract data across the whole domain (all M, N values in the grid) for every time interval. This will create a 3D matlab file (M, N, time) which can be imported into Matlab. You can then extract a time series at different observation points of interest (M,N).

- FLOW → QUICKPLOT.
- File, Open, trim-[model run].dat file.
- Select the data you want from the dropdown menu e.g. water level. Quickplot automatically selects 'morphological grid.'
- Time Step, Tick 'All.'
- M range and N range, Tick 'All' for both M and N.
- Export data as a mat file (v6)
- Open Matlab. You can use the following code as an example of how to extract a time series at a specific grid cell:

```
run = 1;
delft_output = load([num2str(run), '_water level.mat']);
wl = delft_output.data.Val;
time = delft_output.data.Time;
Hinkley = wl(:, 30, 2); %Hinkley is located a M=30, N=2.
plot(time, Hinkley)
```

```
datetick('x', 'hh:00');
```

12.2.2. Cross section

- FLOW → QUICKPLOT
- File, Open, com-[model run].dat file
- From the dropdown menu (which automatically selects morphological grid) select water level.
- Under Time Step check Show Times. Select the times you want a time series for along your cross section / transect. You can select all times to show the whole model run, or just a few to show a specific event.
- Under M range and N range uncheck All.
- Type in the range of grid cells for your transect. The estuary axis for the domain shown in Figure 2 would be M = 2:527, n = 15. This selects every grid cell in the M direction (going across) from 2 to 527, along the 15th.
- Axes Type: X-Val
- Export file type: Tekal file (time series). Export Data. Change 'Save as Type' to All File. Give the file a name and give it a .txt file extension. It can then be opened in Matlab, TextPad or Excel. Save.
- You will need to open your .txt file in Matlab / Excel and transpose the bottom line to the top of the spreadsheet or file. For some reason, the time series is saved at the end of the file rather than next to the appropriate grid reference.

12.3. Obtaining results in Matlab

QUICKPLOT is written using Matlab, therefore the writers of Delft3D have provided a plethora of Matlab functions which can be utilized to obtain model results without opening the GUI.

The following code will extract water level data across the whole domain (all M values, all N values in the grid), for all time intervals (T, which you can set yourself). You can open the qpread function in more detail in a text editor for options on how to open water level data at specific times (only have 1 value for T), or at a specific location (using M,N coordinates).

Note: file pathways may differ on your machine.

```
clear  
close all
```

```
addpath C:\.....\delft3d_50\delft3d_ohmw_4.01.01.rc.03\delft3d\win32\delft3d_matlab % The folder with the  
matlab functions in for Delft. The underlined will be the same for all users.
```

```
Filename =  
Filename = 'F:\..\myname\myfiles\flow\runA'; % Set this to the folder with your model output files in. You can  
either write this in a loop to go through all of your model runs, or just change the file name each time.
```

```
FILE = qpfopen(Filename); % When the code comes to this command you will need to select the trim.dat file in  
the pop up window.
```

```
times = qpread(FILE,1,'water level','times'); % This will just provide you with a list of time intervals on for your  
model runs. Useful when plotting data and using 'datetick.'
```

```
T = 1:481; % Set this index to the total number of time intervals in your model run.
```



```
WaterLevel = qpread(FILE, 1, 'water level', 'data', T, 0,0) % Read qpread.m for more details on how to set your outputs. This line will output water level data, at time interval 1:481, at all M and all N locations on the grid.
```

```
eval(['save ', ['WaterLevel.mat'] ' WaterLevel']); % Save your outputs as a .mat file
```

You can then use the code shown under ‘Water level time series’, section 12.2.1, on how to extract a time series from a specific location in your grid.

You can replace ‘water level’ as the data type with one of the following; ‘d.a. suspended transport’, ‘depth averaged water velocity.’ This list is not exhaustive.

IMPORTANT NOTE:

When you run the above code for the first time, a series of errors may appear which state some functions are not available e.g. `stack2str`, `qp_gettype`, `qp_file2function`. Do not worry – these are likely saved in this folder instead:

```
C:\.....\delft3d_50\delft3d_ohmw_4.01.01.rc.03\delft3d\win32\delft3d_matlab\private
```

Search for them in this folder, and copy the function/file into the same folder that `qpread` appears in (the one defined when you added a path). If the functions are not in the ‘*private*’ folder, search for the name of the function on Google, followed by Delft3D online. You should be able to copy the code into Matlab and save as a new function, in the same folder as `qpread` appears.

13. Post-processing results

13.1. Animations and GIFs.

These can be created in QUICKPLOT using the communication file.

13.2. Graphs /and plots

You can use GPP and QUICKPLOT to produce graphs from your map or history file, however Matlab provides more control and an easier user experience when it comes to creating your plots.

14. Delft3D-WAVE

It is advised that you work through all of the available WAVE tutorials provided, prior to setting up your own wave model.

WAVE can operate in a number of different modes;

- Standalone
- One-way coupling
- Two-way dynamic coupling with FLOW. There is a feedback of information between both models at a set time step. Values from FLOW will be used to compute wave fields, and WAVE values will influence FLOW. This means wave-current interactions are included.

The manual will demonstrate how WAVE can be setup in each of these modes, including information on how to set a uniform wave and wind boundary, time-varying wave boundary, and time- and space-varying wave boundary. The manual will also explain how to setup a time- and space-varying wind and pressure field.

WAVE is based on the spectral model SWAN (<http://swanmodel.sourceforge.net/>). When WAVE is run in the Delft3D model suite then a series of .tmp files are created. These can be used to force SWAN to compare Delft vs SWAN simulations.

14.1. WAVE model grid

You may want to consider editing your grid resolution at areas of interest in the domain for the WAVE simulations, to ensure accurate results (Figure 10). This can be done in RGFGRID, but do not forget to re-load your bathymetry in the .xyz file (aka Sample) and interpolate this back onto the new grid.

It is possible to interpolate previously edited bathymetry in a .dep onto a new grid (as long as the new grid has the same boundary as the old grid).

- Import the original grid and .dep file into QUICKIN.
- Draw a polygon around the grid.
- Go to Operations → Copy Depth to Samples.
- Go to File → Attribute Files → Save Samples.
- Go to File → New Project.
- Import your new grid, with refinements (File → Import → Grid (RGFGRID))
- Go to File → Attribute Files → Open Samples.
- Follow the instructions in section 6.4 on how to interpolate the samples (.xyz file) onto the new grid using Grid cell averaging, Triangular Interpolation and Internal Diffusion.

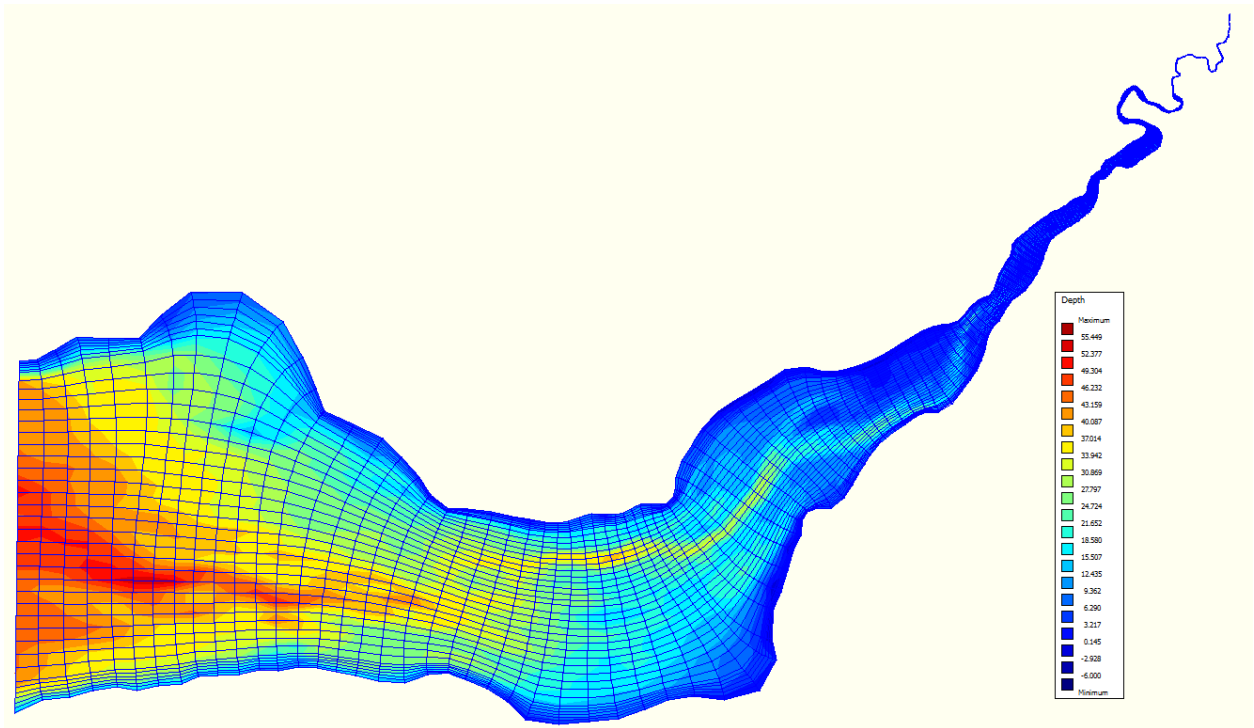


Figure 10: Updated grid with refinements at the coast to improve resolution in WAVE

14.2. WAVE boundary conditions

There are 3 options to force the wave boundary depending on the research aims and setup of the model. The information below shows examples and comments on how you can set up the different options, and there is more information available in the WAVE manual.

14.2.1. Uniform values in the [runID].mdw file

This .mdw file setup is used when WAVE is run in standalone. There will be no .mdf or com-[runID].dat or com-[ID].def files in the project folder to define boundary conditions. You will need to define the time steps and water level at each time step, and the wind and wave parameters. This can be setup in the Delft3D GUI or in text editing software.

The example below shows a 15 minute time step and constant water level (4.59 m), wind speed (5.15 m/s), wind direction (0 deg (north)) (section 14.3.2 will show how to incorporate a time/space varying wind and pressure field if required, which will automatically overwrite wind conditions set here) and wave parameters. The example below also shows a uniform wave boundary, where conditions are applied at every grid cell along the boundary (i.e. not spatially varying).

```
[WaveFileInformation]
  FileVersion      = 02.00
[General]
  ProjectName      = WindWave
  ProjectNr        = 1
  Description       = NW wave direction
  Description       = N wind direction
  Description       = 50 percentile wind
  Description       = Wind wave (high amplitude, low period)
  OnlyInputVerify  = false
```

```

SimMode      = stationary
DirConvention = nautical
ReferenceDate = 2018-01-01
WindSpeed    = 5.1500001e+000
WindDir      = 0.0000000e+000
[TimePoint]
Time         = 0.0000000e+000
WaterLevel   = 4.5939999e+000
XVeloc      = 0.0000000e+000
YVeloc      = 0.0000000e+000
[TimePoint]
Time         = 1.5000000e+001
WaterLevel   = 4.5939999e+000
XVeloc      = 0.0000000e+000
YVeloc      = 0.0000000e+000
[TimePoint]
Time         = 3.0000000e+001
WaterLevel   = 4.5939999e+000
XVeloc      = 0.0000000e+000
YVeloc      = 0.0000000e+000
[TimePoint]
Time         = 4.5000000e+001
WaterLevel   = 4.5939999e+000
XVeloc      = 0.0000000e+000
YVeloc      = 0.0000000e+000
[TimePoint]
Time         = 6.0000000e+001
WaterLevel   = 4.5939999e+000
XVeloc      = 0.0000000e+000
YVeloc      = 0.0000000e+000
[Constants]
WaterLevelCorrection = 0.0000000e+000
Gravity              = 9.8100004e+000
WaterDensity         = 1.0250000e+003
NorthDir             = 9.0000000e+001
MinimumDepth         = 5.0000001e-002
[Processes]
GenModePhys          = 3
Breaking              = true
BreakAlpha            = 1.0000000e+000
BreakGamma            = 7.3000002e-001
Triads                = false
TriadsAlpha           = 1.0000000e-001
TriadsBeta            = 2.2000000e+000
WaveSetup             = false
BedFriction           = jonswap
BedFricCoef           = 6.7000002e-002
Diffraction           = false
DiffracCoef           = 2.0000000e-001
DiffracSteps          = 5
DiffracProp           = true
WindGrowth            = true
WhiteCapping          = Komen
Quadruplets           = true
Refraction            = true
FreqShift             = true
WaveForces            = dissipation 3d
[Numerics]
DirSpaceCDD           = 5.0000000e-001
FreqSpaceCSS          = 5.0000000e-001

```

```

RChHsTm01      = 2.0000000e-002
RChMeanHs      = 2.0000000e-002
RChMeanTm01    = 2.0000000e-002
PercWet        = 9.8000000e+001
MaxIter        = 15
[Output]
TestOutputLevel = 0
TraceCalls      = false
UseHotFile      = false
WriteCOM        = false
[Domain]
Grid            = ..\..\SevernEstuaryGrid3.grd
BedLevel       = ..\..\SevernEstuaryWindStudy4.dep
DirSpace       = circle
NDir           = 36
StartDir       = 0.0000000e+000
EndDir         = 0.0000000e+000
FreqMin        = 5.0000001e-002
FreqMax        = 1.0000000e+000
NFreq          = 24
Output         = true
[Boundary]
Name           = Boundary 1
Definition     = orientation
Orientation    = west
SpectrumSpec   = parametric
SpShapeType    = jonswap
PeriodType     = peak
DirSpreadType  = power
PeakEnhanceFac = 3.3000000e+000
GaussSpread    = 9.9999998e-003
WaveHeight     = 1.8600000e+000
Period         = 4.0999999e+000
Direction      = 3.1500000e+002
DirSpreading   = 4.0000000e+000

```

Uniform boundary conditions can be changed in the GUI by navigating from the start window -> WAVE -> WAVE input -> Boundaries -> Edit Conditions. This is shown in Figure 14.

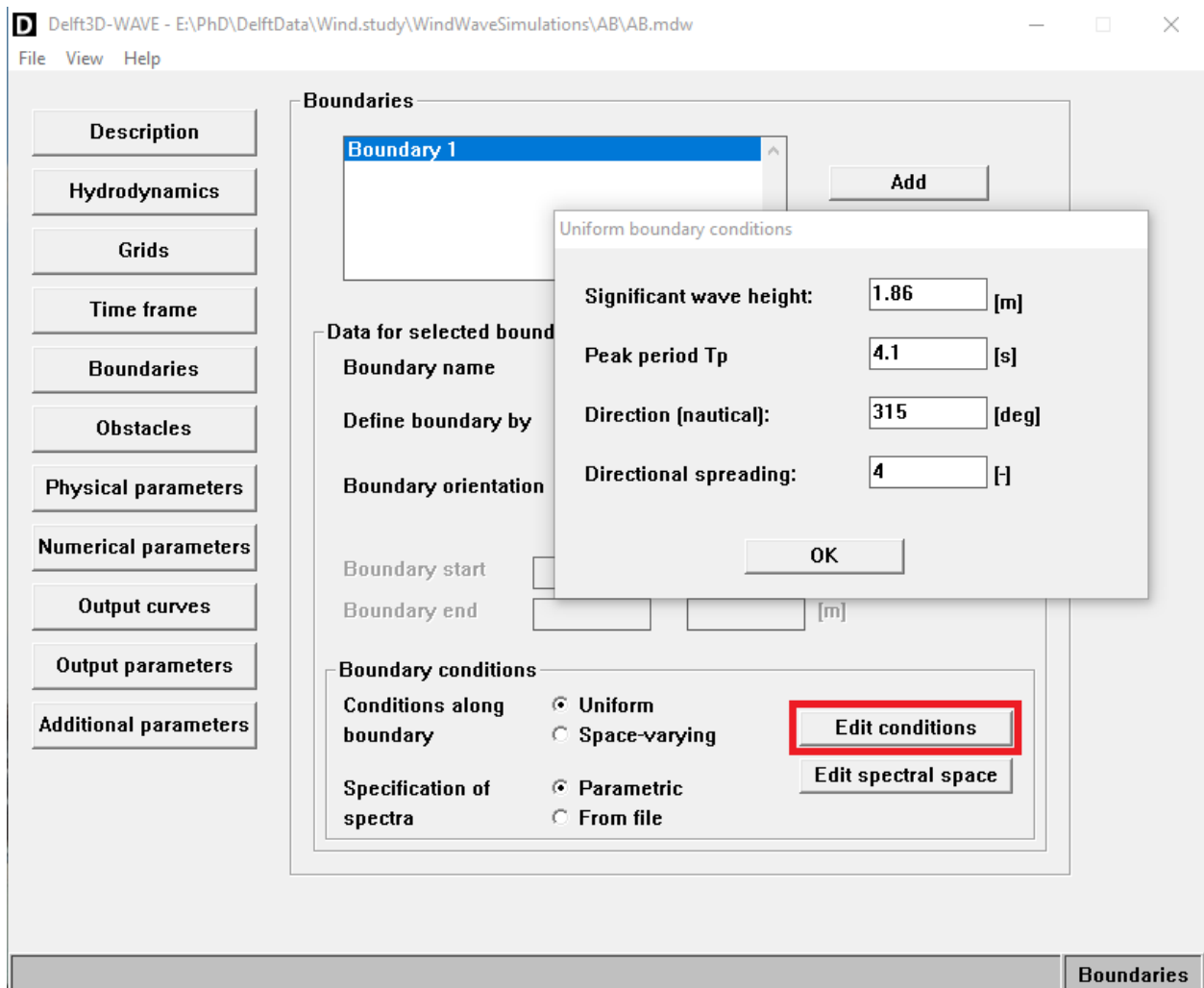


Figure 141: Delft3D-WAVE uniform boundary conditions setup

14.2.2. Time-varying: wavecon.[runID]

A wavecon.[runID] is an additional file that can be referred to in the .mdw file and added to the runID folder to define time-varying WAVE boundary conditions. The file can be created in a text editor.

527 39 refers to the size of the model grid, and each column defines the uniform wave boundary conditions.

*Itdate	Hs	Tm01	Dir(^o N)	ms	wl	windspeed	winddir(^o N)
BL01							
527	39						
420	2.08	11.8	257	4.000	5.731	1.000	250
435	2.08	11.8	257	4.000	5.731	1.000	250
450	2.12	11.8	256	4.000	5.731	1.000	250
.							
.							
2580	5.27	11.8	246	4.000	5.731	1.000	250

The wavecon.[runID] does not need to be referred to in the .mdw file as it will be automatically detected.

14.2.3. Time-varying and space-varying: [runID].bcw

If you want to run time- and space-varying wave conditions then you will need a space varying WAVE boundary first. This can be set in a text editor or the GUI. This is appropriate if you have a number of data points to force the model along a certain boundary e.g. from other model data. You do this by defining 1 boundary and splitting it into sections using **CondSpecAtDist**. You can specify the distance along Boundary 1 that each section begins at. (Note: The example below has very small values for each section as the grid is defined in decimal degrees).

```
[Boundary]
Name          = Boundary 1
Definition    = orientation
Orientation    = west
SpectrumSpec  = parametric
SpShapeType   = jonswap
PeriodType    = mean
DirSpreadType = degrees
PeakEnhanceFac = 3.3000000e+000
GaussSpread   = 9.9999998e-003
DistanceDir   = counter-clockwise
CondSpecAtDist = 2.9999999e-002
WaveHeight    = 0.0000000e+000
Period        = 0.0000000e+000
Direction     = 0.0000000e+000
DirSpreading  = 4.0000000e+000
CondSpecAtDist = 1.0000000e-001
WaveHeight    = 0.0000000e+000
Period        = 0.0000000e+000
Direction     = 0.0000000e+000
DirSpreading  = 4.0000000e+000
CondSpecAtDist = 1.8000001e-001
WaveHeight    = 0.0000000e+000
Period        = 0.0000000e+000
Direction     = 0.0000000e+000
DirSpreading  = 4.0000000e+000
CondSpecAtDist = 2.5999999e-001
WaveHeight    = 0.0000000e+000
Period        = 0.0000000e+000
Direction     = 0.0000000e+000
DirSpreading  = 4.0000000e+000
CondSpecAtDist = 3.4000000e-001
WaveHeight    = 0.0000000e+000
Period        = 0.0000000e+000
Direction     = 0.0000000e+000
DirSpreading  = 4.0000000e+000
```

Each boundary section can be edited in the GUI by navigating to Boundaries -> Edit conditions (see Figure). The values for Hs, Tm etc. below are shown as 0 because a [runID].bcw will be used to define boundary conditions and these values will be overwritten.

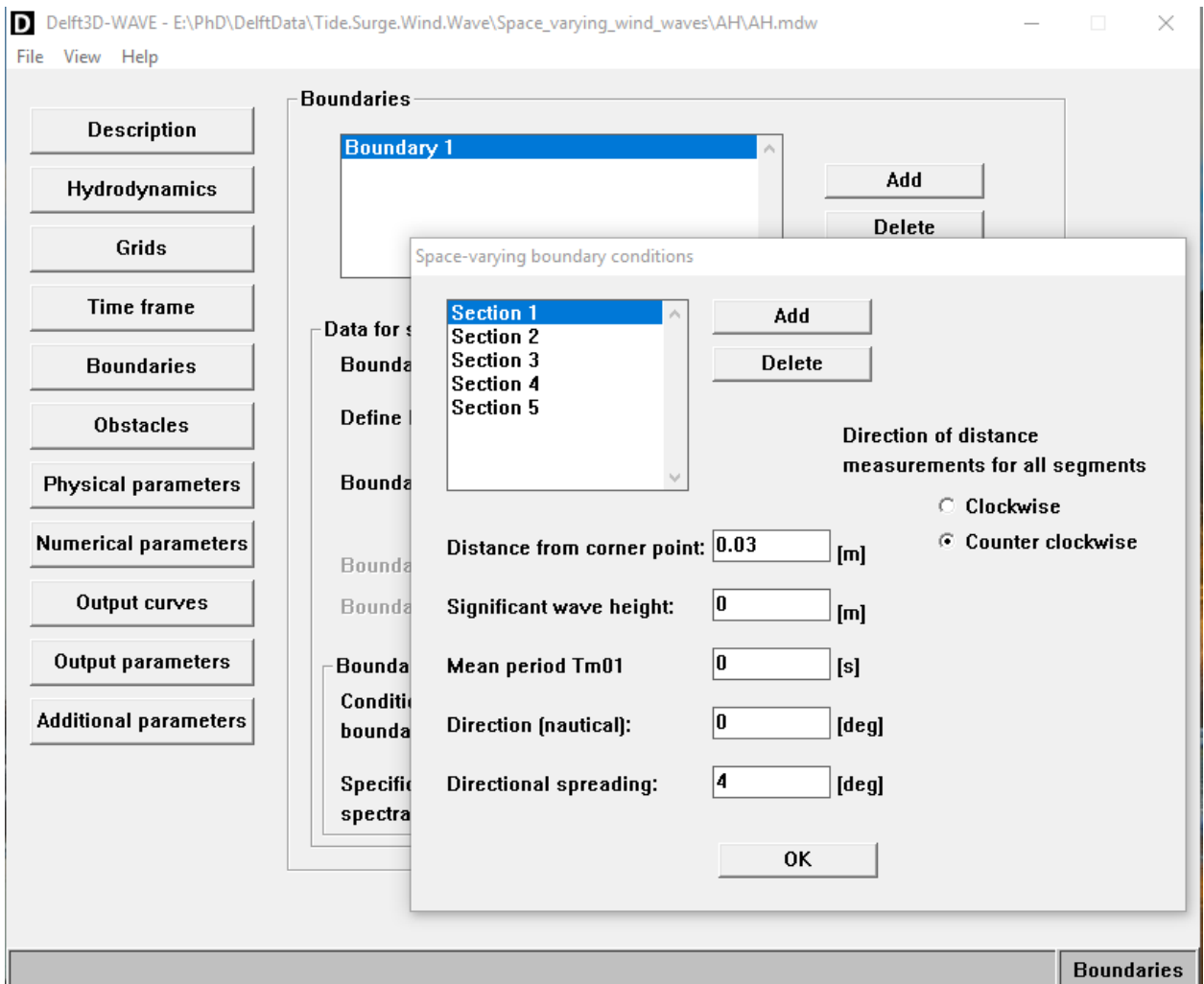


Figure 12: Delft3D-WAVE space-varying boundary setup

Much like a [run-ID].bct file for FLOW, a [run-ID].bcw defines the time- and space-varying boundary conditions to be applied at each boundary section. 5 different boundary sections were defined above, and each section required a specified boundary condition. Wave conditions at each section are defined for each time step. The following text needs to be added to the [General] section of the .mdw file:

TSeriesFile = [run-ID].bcw

```

location      'Boundary 1'
time-function  'non-equidistant'
reference-time 20140101
time-unit     'minutes'
interpolation  'linear'
parameter     'time'      unit '[min]'
parameter     'WaveHeight' unit '[m]'
parameter     'WaveHeight' unit '[m]'
parameter     'WaveHeight' unit '[m]'
parameter     'WaveHeight' unit '[m]'
parameter     'WaveHeight' unit '[m]'
parameter     'Period'    unit '[s]'
parameter     'Period'    unit '[s]'
parameter     'Period'    unit '[s]'
parameter     'Period'    unit '[s]'
parameter     'Period'    unit '[s]'
parameter     'Direction' unit '[[N^o]]'

```


parameter	'Direction'	unit	'[[N^o]]'		
parameter	'Direction'	unit	'[[N^o]]'		
parameter	'Direction'	unit	'[[N^o]]'		
parameter	'Direction'	unit	'[[N^o]]'		
parameter	'DirSpreading'	unit	'[degrees]'		
parameter	'DirSpreading'	unit	'[degrees]'		
parameter	'DirSpreading'	unit	'[degrees]'		
parameter	'DirSpreading'	unit	'[degrees]'		
parameter	'DirSpreading'	unit	'[degrees]'		
0	3.22	3.69	3.62	3.49	3.27
	10.41	10.06	9.39	8.95	9.24
	222.03	222.2	222.35	222.06	221.08
	15.4	16.4	17	17.3	16.2
60	3.23	3.69	3.62	3.49	3.27
	10.46	10.09	9.42	8.97	9.32
	215.33	216.53	217.97	218.91	218.13
	15.5	16.4	16.9	17.2	16.1
120	3.24	3.71	3.64	3.51	3.29
	10.43	10.05	9.37	8.94	9.21
	210.67	210.49	210.78	210.7	210.49
	15.6	16.7	17.2	17.5	16.4

14.2.4. Some friendly advice

These instructions should not be used as standalone guidance. There are many ways to set up your FLOW-WAVE model, and the Delft3D handbooks and forum have been invaluable in working out how to do this. Please do refer to all available literature when setting up the model. You may find you have to run each simulation 100 times until it actually works.

Delft3D is very sensitive to file names, and you must ensure that every input file accurately defines the date, starting time step (make your life easy and always start at 0 minutes which is midnight/12:00am), end time, coordinate system, total number of time steps, grid reference points in model domain.

If the simulation doesn't work then read the Delft diagnosis file and SWAN diagnosis file will give you a good idea as to what has gone wrong. If you can't solve why a certain simulation won't run then have a go at creating the input files again – maybe the date is wrong and you might just miss this. Sometimes it's better for your confidence to just re-create the files rather than keep bashing away at a simulation that won't work.

14.3. Wind and pressure boundary conditions

14.3.1. Uniform

This is only a uniform wind field and set in a .wnd file.

14.3.2. Time- and space-varying

This type of wind and pressure field can be applied in Delft3D-FLOW standalone simulations, WAVE standalone, one way and two way FLOW-WAVE coupling. You will need to obtain the raw data from your own source.

You will need a grid for each wind and pressure file.

Wind should have an x and y file. An **x_wind.wnd/wind.amu** headers are shown below. Replicate for **y_wind.wnd/wind.amv**. The .wnd and .amv are identical files but with different file endings for the .mdf and .mdw files (see below).

```

FileVersion   = 1.03
Filetype      = meteo_on_curvilinear_grid
grid_file     = wind.grd
first_data_value = grid_ulcorner
data_row      = grid_row
NODATA_value  = 999.999
n_quantity    = 1
quantity1     = x_wind
unit1         = m s-1
TIME = 0 minutes since 2014-01-01 00:00:00 +00:00

```

Pressure.amp headers are shown below:

```

FileVersion   = 1.03
Filetype      = meteo_on_curvilinear_grid
grid_file     = pressure.grd
first_data_value = grid_ulcorner
data_row      = grid_row
NODATA_value  = 999.999
n_quantity    = 1
quantity1     = air_pressure
unit1         = mbar
TIME = 0 minutes since 2014-01-01 00:00:00 +00:00

```

The following text should be added to the [General] section of the .mdw file.

```

MeteoFile      = x_wind.wnd
MeteoFile      = y_wind.wnd

```

The following text should be added to the end of the .mdf file.

```

Commnt =
Online = #N#
WaveOL = #Y#
Fwndgu = #wind.amu#
Fwndgv = #wind.amv#
Fwndgp = #pressure.amp#
Airout = #Y#
Commnt =

```

14.4. Set up .mdw for WAVE standalone

A standalone simulation has no interaction with FLOW and will require water level time series to be defined. A standalone wave simulation can use any of the above wave boundary conditions. Standalone mode can be run with a constant water level to eliminate influence of tides (set in the .mdw file), or can be time-varying. The time steps when each WAVE calculation will be completed needs to be defined as a [TimePoint].

In Grids -> Hydrodynamics select Do not Use for all parameters.

14.4.1. Running WAVE standalone

GUI → WAVE → Start

14.5. Set up .mdw for one-way FLOW → WAVE

Ensure that a FLOW simulation has been run in advance that uses the boundary conditions required for your WAVE simulation. Copy the output com-[runID].dat and com-[runID].def file from a pre-existing FLOW run in your selected working directory where WAVE files are stored.

In .mdw, go to Grids -> Hydrodynamics and select Extend and Use for all parameters.

Include wavecon. or .bcw for wave boundary conditions

14.5.1. Running one-way coupling

GUI → WAVE → Start

14.6. Set up .mdw (FLOW) and .mdw (WAVE) for two way FLOW ↔ WAVE online coupling

The .mdf should be set up in the same way as detailed in section 7 of this manual, in your selected working directory. A few additional options must be ticked.

- Processes → Check WIND, WAVE, Online Delft3D – WAVE

Double check your Start time, End time and save Interval for the map and communication file are correct.

Use the GUI in Windows to set up your Master Definition WAVE File (.mdw) which will be used for the coupled FLOW-WAVE model run in Windows or Linux.

If a specific setup option has not been discussed explicitly, then default values have been used.

If a time- and space-varying wind and pressure file is used for the simulation then ensure that the following text is included at the end of the .mdf:

```
Commnt =  
Online = #N#  
WaveOL = #Y#  
Fwndgu = #wind.amu#  
Fwndgv = #wind.amv#  
Fwndgp = #pressure.amp#  
Airout = #Y#  
Commnt =
```

Open Delft3D and set your working directory. Navigate to 'FLOW' → 'WAVE INPUT.'

14.6.1. Description

Specify the project name, project number and Description of your model run.

14.6.2. Hydrodynamics

Check Run WAVE together with FLOW.

Click 'Select FLOW file' and navigate to and select the .mdf for this model run in your working directory. Click Ok.

14.6.3. Grids

Select 'Import' and navigate to the working grid you wish to use. Click Ok.

Click the 'Bathymetry' tab and then click 'Select bathymetry data.' Navigate to your bathymetry file.

Click the 'Hydrodynamics' tab. Select 'Use but do not extend' from the drop down menus for Water level, Current and Bathymetry. You can change Wind depending on the boundary conditions that are being used.

14.6.4. Boundaries

Click 'Add.' You can rename the boundary (e.g. ocean), and define the location of the boundary based on orientation, between 2 grid points on your mesh or latitude and longitude.

Define the boundary conditions along the wave boundary. Click 'Edit conditions' and input values for Hs, Tp, direction and directional spreading.

14.6.5. Physical parameters

Select 'Wind' and input your desired Speed and Direction if using uniform values.

14.6.6. Output parameters

Select the grid you wish outputs to be available on under 'Output for computational grids.'

Save as .mdw file.

14.6.7. Running online coupling

Navigate to 'FLOW' → 'Start.' Select your .mdf and then the .mdw.

As expected, the simulation could take up to 6 or 7 times longer than the FLOW simulation alone.

Tip: For every new model run you start, ensure that only the input files are present in the folder. Delete old diagnosis files, output files, restart files etc or archive them. The model can crash if it's trying to overwrite a lot of files.

14.7. Obtaining WAVE results in Matlab

Results can be quickly viewed in GPP or Quickplot. Results from WAVE can also be obtained in Matlab (as seen in section 12.3). Note: file pathways may differ on your machine.

```
addpath C:\.....\delft3d_50\delft3d_ohmw_4.01.01.rc.03\delft3d\win32\delft3d_matlab
```

```
Filename = 'F:\...\myname\myfiles\waves\runA';
```

```
FILE = qpfopen(Filename); % Select the wavm.dat file
```

```
times = qpread(FILE,1,'water level','times');
```

```
T = 1:481;
```

```
Hs = qpread(FILEwav, 1, 'hsig wave height', 'data', T, 0,0);
```

```
Period = qpread(FILEwav,1,'smoothed peak period','data', T, 0,0);
```

```
eval(['save ', ['Hs.mat'] ' Hs]);
```

```
eval(['save ', ['Period.mat'] ' Period]);
```

Good luck!

15. Appendix

Appendix 1 Instructions for ArcMap, QUICKPLOT, RGFGRID and QUICKIN

ArcMap

ArcMap is available on all University computers, but may not be installed on the specific machine you are using. You can easily install it:

- Login on to a University computer
- Go to Start → All programs → Install University Applications
- Search for 'ArcGIS Desktop 10.3' and Install.
- A series of programmes will be installed including Arc Catalog, Globe, Map and Scene. We will be using Arc Map. Arc Catalog is a file viewer, and can be used to copy, paste and delete files from the geodatabase we will create in ArcMap.
- You will probably need to restart the computer after you have installed it.
- Open ArcMap.

Getting started: Close the pop up menu 'Getting Started' when you open the programme, or select 'Blank map.' You want to be able to see the different layers of data and your data files. So go to Windows (on the top menu bar) → click Table of Contents and Catalog. You can then dock these within the main view window.

Create a new working directory and File Geodatabase: Create a new folder in File Explorer on your hard drive or working directory where are of your files and outputs can be saved. Go to your Arc Catalog window and click the small yellow file with a black plus sign, 'Connect To Folder.' Navigate to your new working directory, Click Ok. Right click your working directory in Arc Catalog. New → File Geodatabase. Give it a name. You should select this geodatabase when creating or saving all files in the future. This is an easy method to keep all of your files in one place.

Set the geographic coordinate system: You need to set the coordinate system for your data so that it is projected in the correct format, and lines up in Delft3D. Right click Layers in the Table of Contents window, select Properties, select Coordinate System. Choose Geographic Coordinate System, World, WGS 1984. Then go to View, Data Frame Properties and set the coordinate system to WGS 84 too.

Add base map; File, Add Data, Add Basemap. Select one. I normally use Streets.

Add bathymetry: Bathymetry data is downloaded from the Digimap as an ascii file, but it needs to be converted to a raster (grid) format before it can be manipulated in ArcMap.

ArcToolBox, Conversion Tools, To Raster, Ascii to Raster. Input the ascii, save the output raster to your File GeoDatabase and give it a name e.g. Bathy1. Save the output data type as Float. Ok. Repeat for all bathymetry files.

Add LiDAR: LiDAR data is downloaded in ascii format too, so you will need to convert this as well.

Create the land boundary; this is the outside line of your domain. ArcToolbox → Data Management Tools → Feature Class → Create Feature Class.

- Feature Class Location: Select your File Geodatabase.
- Give the feature class (line) a name e.g. LandBoundary
- Geometry Type: Polyline
- Ok

Go to Arc Catalog. Right click the polyline feature you have just created. Go to Properties. Set the XY Coordinate System.

- Geographic Coordinate System
- World
- WGS 1984

To draw the land boundary:

- Editor → Start Editing: click LandBoundary. Continue
- Click LandBoundary in Create Features window. The cursor should now become a small cross.
- Draw your boundary line. It doesn't have to meet up or be particularly detailed, but give a good idea of the outline of the area. Each click creates a point, so your line will be made up of a series of points. Double click to finish your line. Click Editor → Stop Editing. Save your Edits.
- You can add, delete and move points in the Editor toolbar once you have drawn the line.

Export the land boundary:

- ArcToolBox → Conversion Tools → To Shapefile → Feature Class to Shapefile
- Input Features: select your polyline from the dropdown menu.
- Select your file geodatabase as the output folder. Ok.
- Ensure your shapefile is in the WGS 84 projection.
- Open Delft
- Select working directory.
- Flow → QUICKPLOT
- File → Open File → Show All Files. Select the .shp file
- Export File Type → landboundaryfile
- Click Export Data. Give the file a name. Save.
- File. Exit.

Create a grid in RGFGGRID

Delft3D menu page → Grid → RGFGGRID.

Co-Ordinate system → Spherical.

File, Attribute Files, Open Land boundary file. Select your land boundary.

Create a minimum of 4 splines, which form the basis of your grid.

Edit, spline, new. Left click to place a new point. Left click to finish a spline. Select your spline, click spline to land boundary to ensure it closely mirrors your boundary.

File, Export Splines. You can export the splines with the points you have created, or save them with additional intermediate points. Give the splines a name e.g. SplinesHinkley1. Each time you edit your splines, save export them as a new file. Do not overwrite them – if they crash / do not work you always want a backup which you know does work, rather than have to start again.

Settings, General. Change the number of grid cells which are created in the M and N direction e.g. 5 and 3. Play about with the number combinations until you find a grid you are happy with.

Operations, Change Splines into Grid.

Operations, Orthogonalise Grid. See the RGFGGRID manual for instructions on how to move, add, delete grid cells.

File, Export Grid (RGFGRID). Save in your working directory.

Bathymetry and LiDAR in ArcMap

Join the 2 bathymetry files into one. ArcToolBox, Data Management Tools, Raster, Raster Dataset, Mosaic.

- Select your 2 input rasters (e.g. Bathy1 and Bathy2).
- Target Raster; select Bathy1. This will add Bathy2 to Bathy1.
- Leave the other fields as they are. Ok.

You can then mosaic LiDAR data onto the bathymetry data using this method too.

You may only want a small area of the bathymetry data downloaded. You can clip it to a specific shape that you want.

- ArcToolBox, Data Management Tools, Create Feature Class.
- Select your File Geodatabase as the location.
- Class Name e.g. BathyClip
- Geometry Type: Polygon
- Ok
- Editor, Start Editing.
- Draw a polygon roughly the shape of your domain / area you want. Save Edits. Stop Editing.
- Data Management Tools, Raster, Raster Processing, Clip.
- Input Raster: Bathy1 (the raster bathymetry file)
- Output extent: BathyClip (the hand drawn polygon)
- Tick 'Use Input Feature for Clipping Geometry'
- Tick 'Maintain Clipping Extent'
- Output your clipped raster to your File Geodatabase and give it a name e.g. BathymetryHinkley.
- Ok

You might want to make the resolution of your bathymetry coarser. This can be done using the resample tool.

- ArcToolBox, Data Management Tools, Raster, Raster Processing, Resample.
- Input Raster: BathymetryHinkley.
- Output: save in your file geodatabase.
- Change the cell size in the X and Y direction. E.g. from 2.77 E-04 to 8.77E-04. Ok.

You now need to export your clipped bathymetry file to a .xyz file so it can be read into Delft QUICKIN.

- ArcToolBox, Spatial Analyst, Extraction, Sample.
- 'Input Raster' and 'Input Location or point features' both as BathymetryHinkley_Resample.
- Save the output table to your File Geodatabase e.g. BathyHinkley.
- Resampling = Nearest.
- Give the table a name. Ok.
- This may take a while. The finer the resolution the longer it will take.
- Right click BathyHinkley table when it is completed. Data, Export. Export all Records. Save in your working directory. Use the dropdown menu to select text file.
- Open in Matlab. Delete column 1 and 2 and the top row of text. You only want column 3, 4, and 5. Export this as a .xyz file to your working directory.

You have created a table with coordinates and bathymetry depths.

Open the .txt or .xyz file in Matlab and multiply the file by -1. This will give you bathymetry data which increases in value from zero as depth increases. This is how Delft handles bathymetry.

Combine bathymetry and grid in QUICKIN

Delft -> Grid -> QUICKIN. Coordinate system, Spherical.

File, Import, Grid.

File, Attribute Files, Samples. Select your .xyz file with deleted columns and top row.

If the grid and bathymetry do not line up then this is because they are not in the same coordinate system. Go back and ensure that everything you are working with has been exported from ArcMap in the WGS84 projection. This includes the land boundary shapefile and the bathymetry. Double check the grid was produced in the spherical coordinate system too. Then need to assign a depth to each grid cell:

- Edit, Polygon New. Draw a polygon around your domain. Left click to place a point, right click to finish it.
- Operations. Select one of the 2 following;
 - Triangular Interpolation: Grid resolution > bathymetry
 - Grid cell averaging: Bathymetry resolution > grid.
- File, Export Depth. Save.
- New, Import Grid and then .dep file.
- If some grid cells are missing depth then draw a new polygon around them, Operations, Internal Diffusion. Save .dep file.

The .grid file and .dep file are now ready to be loaded into a .mdf file.

LISFLOOD User Guide
March 2020

Contents

Table of Figures	237
Table of Tables.....	237
1. How this guide works	238
2. How LISFLOOD-FP works on the UoL system	238
3. Set up LISFLOOD-FP on Windows.....	238
4. Getting started with LISFLOOD-FP.....	238
5. LISFLOOD-FP input files.....	239
5.1. Digital Elevation Model (.asc).....	239
5.2. Start model run DEM	243
5.3. Boundary conditions	243
5.3.1. Forcing data	243
5.3.2. LISFLOOD-FP model boundary.....	244
5.4. Boundary condition type file (.bci)	245
5.5. Time varying boundary conditions file for spin-up (.bdy)	245
5.6. Time varying boundary conditions file for model run (.bdy)	247
5.7. Parameter file for start run (.par)	248
5.8. Parameter file for model run (.par)	250
6. How to run a simulation.....	251
6.1. Troubleshooting	251
6.2. Model run times	251
7. Outputs.....	251
7.1. .max files	252
7.2. .vx and .vy files.....	253
8. Matlab functions.....	253
9. Depth Damage Curves	254
10. Bibliography.....	256

Table of Figures

Figure 1: Raw LiDAR data which has been mosaic-ed to one raster dataset and resampled to 5 m..	240
Figure 2: Polygon from the low water mark to the inland extent of the model domain.	241
Figure 3: Locations where rhines (small river channels), bridges, or missing data are digitized back into the raster.	242
Figure 4: Start model domain for LISFLOOD-FP to generate baseline water level	243
Figure 5: Location of coastal boundary including orange dots (which is the location of boundary condition data) and red dots (which is the location where data from orange dots is propagated into the model domain).	244
Figure 6: Water level time series for start .bdy file	246
Figure 7: BC101 water level time series.....	248
Figure 8: Example start run .par file.....	249
Figure 9: Example .par file	250
Figure 10: Clip .max or .wd files to the inland floodplain in ArcMaph	252
Figure 11: 25 m land cover data used to calculate damage assessments for arable and suburban land uses.	254

Table of Tables

Table 1: Example .bci file.....	245
Table 2: Example of a start .bdy file	246
Table 3: Example .bdy file.....	247
Table 4: Model run times.....	251
Table 5: Arable land costs used in damage assessments (Penning-RowSELL et al., 2013).....	255
Table 6: Suburban land costs used in damage assessments (Penning-RowSELL et al., 2013).	255

1. How this guide works

LISFLOOD-FP is a two-dimensional hydrodynamic model that is used to simulate floodplain inundation (Bates and de Roo, 2000). The model predicts the movement of flood water over a raster grid and computes water depth at each time step, and has been successfully used in fluvial, coastal and estuarine environments.

This guide sets out how to set up and operate LISFLOOD-FP on the University of Liverpool system, complete a simulation and analyse the outputs. It should be noted that this guide does not replace the LISFLOOD-FP user manual (Bates et al., 2013) which should be referred to throughout your journey with the model.

The author would like to acknowledge and thank Dr Thomas Prime for his help and advice in using LISFLOOD-FP.

2. How LISFLOOD-FP works on the UoL system

- Input files can be created in ArcMap / QGIS, and in Matlab.
- LISFLOOD-FP is run from the command line and simulations can be run in batch if required.
- Analysis can be completed in ArcMap or Matlab too.

3. Set up LISFLOOD-FP on Windows

The model files can be downloaded on request from this website:

<http://www.bristol.ac.uk/geography/research/hydrology/models/lisflood/downloads/>

The files downloaded from this link will provide you with all the model files needed – there are no other prerequisites.

4. Getting started with LISFLOOD-FP

Read through the latest update of the model handbook here: <http://www.bristol.ac.uk/media-library/sites/geography/migrated/documents/lisflood-manual-v5.9.6.pdf>

Training materials are provided here:

<http://www.bristol.ac.uk/geography/research/hydrology/models/lisflood/training/>

5. LISFLOOD-FP input files

Every simulation that is completed in LISFLOOD-FP will need a start run and a model run. A start run is completed first to ensure that the model domain is filled with water to a baseline level. The model run can then propagate water into the model domain from this baseline level.

It is advised that you have two working directories: one for start runs and one for model runs. All input files (e.g. .asc, .bci, .bdy, .par which are explained below) can be kept in the same start or model run working directory, and the model is run from the same directory. Outputs can be saved in a separate folder.

LISFLOOD-FP start and model runs requires a series of input files most notably a digital elevation model (DEM), time-varying water level time series (.bdy), specification of boundary location (.bci) and a parameter file (.par).

- This guide will first describe how to set up the DEM, which is used in the model runs and used to generate a DEM for the start runs.
- The guide will then describe how to set up the .bci file used across all model simulations (both start and model runs).
- The guide will then describe how to set up input files (.bdy, .par) for the start runs and then the model runs.

5.1. Digital Elevation Model (.asc)

An accurate DEM is crucial to the success of your LISFLOOD-FP modelling work. It is worth spending some time on the development of your DEM prior to starting to set up the other model inputs, as this will ensure the best results.

- Download LiDAR data in ASCII format for the study site of your choice. Edina Digimap is a good option, which has a user friendly graphical user interface. The LiDAR data will be downloaded as a series of square tiles, which need to be individually loaded into a GIS. ArcMap is used in this guide, but QGIS will also do the job (some of the commands may be different).
- Convert the individual raw LiDAR ASCII files into raster in ArcMap, and then mosaic the individual tiles into one raster file.
- Take a note of the geographic coordinate system used for your DEM – this will need to be used when setting the location of the boundary. British National Grid is used here.

As can be seen in Figure , the LiDAR captures the bathymetry in the Severn Estuary (used as a case study here) well. If it was patchier then it might be necessary to mosaic bathymetry data in. However be careful with step changes at the join where there might be a mismatch in datums. The dataset with a mismatched datum could be loaded into Matlab in ASCII format, and a uniform datum correction applied to the whole dataset. It is at the discretion of the user to identify the correction.

Alternatively, set the coastal open model boundary at a point where there is less of a need for bathymetry e.g. at the low water mark.

- The LiDAR data shown in Figure 1 has been resampled to 5 m for computational efficiency.

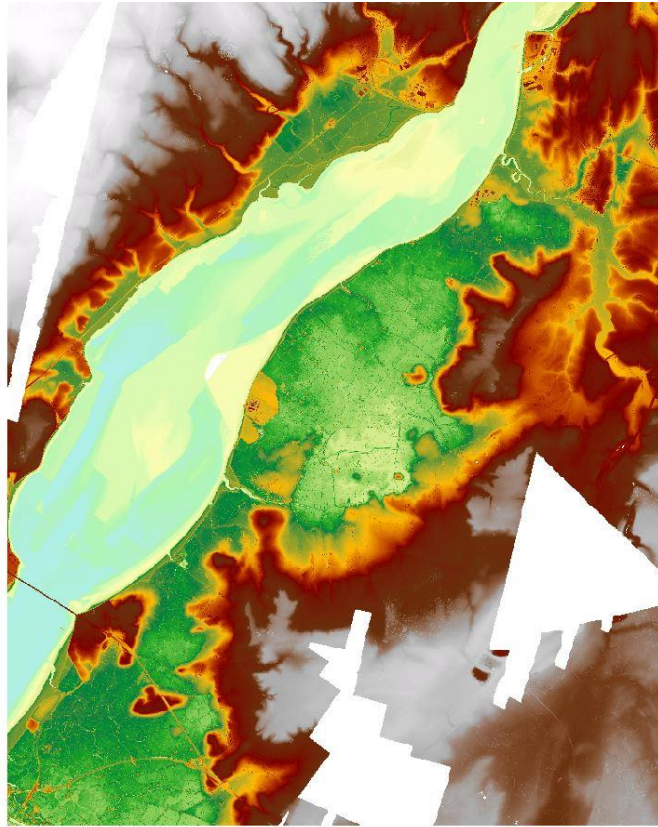


Figure 1: Raw LiDAR data which has been mosaic-ed to one raster dataset and resampled to 5 m.

- Create a polygon in the shape of the model domain you wish to use. Figure shows the model domain from the low water mark to the inland extent of the floodplain, aiming to avoid areas of missing data. Select the open coastal boundary at a location that is suitable for the aims of your study.
- Clip the mosaic-ed raster dataset to this polygon.

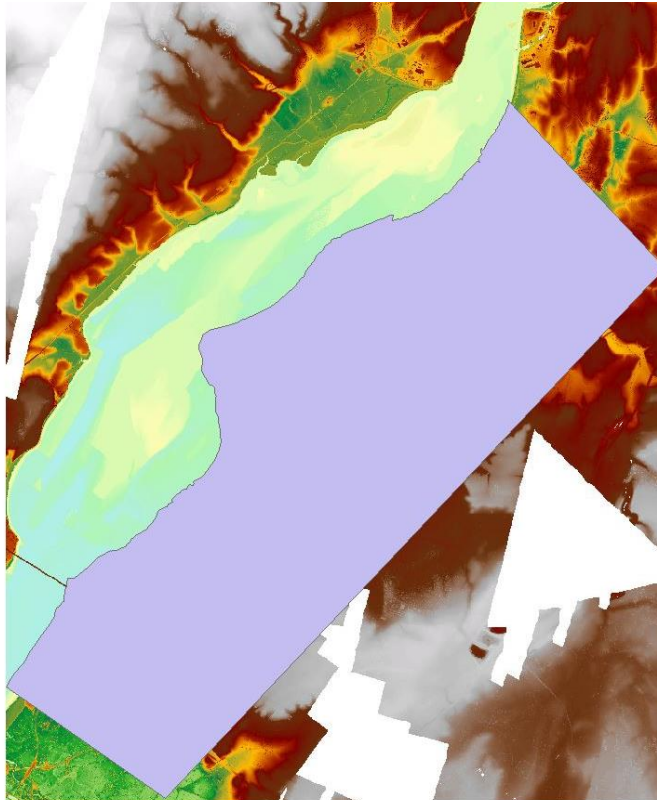


Figure 2: Polygon from the low water mark to the inland extent of the model domain.

- Digitise features that are important to your study which may have been smoothed out when resampling the raster data set. For example, channels and rivers or sea defences can be digitized by hand using polylines. Uniform elevation values can be assigned to these features based on observations, literature or other LiDAR sources.
- In this DEM the tidal pool in front of Oldbury Technical Centre (which can be seen in Figure 1) had an area of data missing. This was filled using a polygon with a uniform elevation value assigned based on nearby values.
- An additional field of data can be created in the attribute table for the polylines and polygons, and a uniform depth value assigned.
- Convert the polylines and polygons to raster. Ensure the conversion carries over their assigned uniform value.
- Mosaic the digitized raster features to the raster elevation data.

Refer to the LISFLOOD-FP handbook on the best approach to handle bridges for your study. The bridges were removed from the rhines (a local name in Somerset for drainage ditches) and channels in this study.

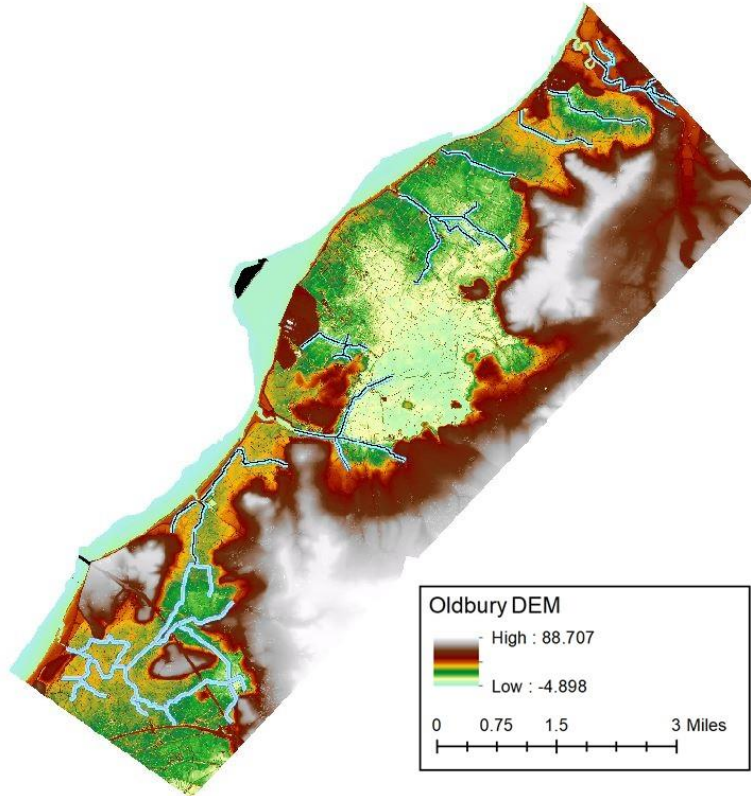


Figure 3: Locations where rhines (small river channels), bridges, or missing data are digitized back into the raster.

- Export your cropped and resampled raster dataset to an ASCII (.asc) format and save in your working directory. This is the .asc file that will be used in the model runs.

5.2. Start model run DEM

Matlab code is available on request from the author which takes the .asc exported from ArcMap and creates a new DEM for the start runs – this generates a DEM which only has data in regions which should be wet from the start, e.g. river channels and coastal areas. Note that the highest elevation in Figure 4 is the lowest elevation shown in Figure 3.

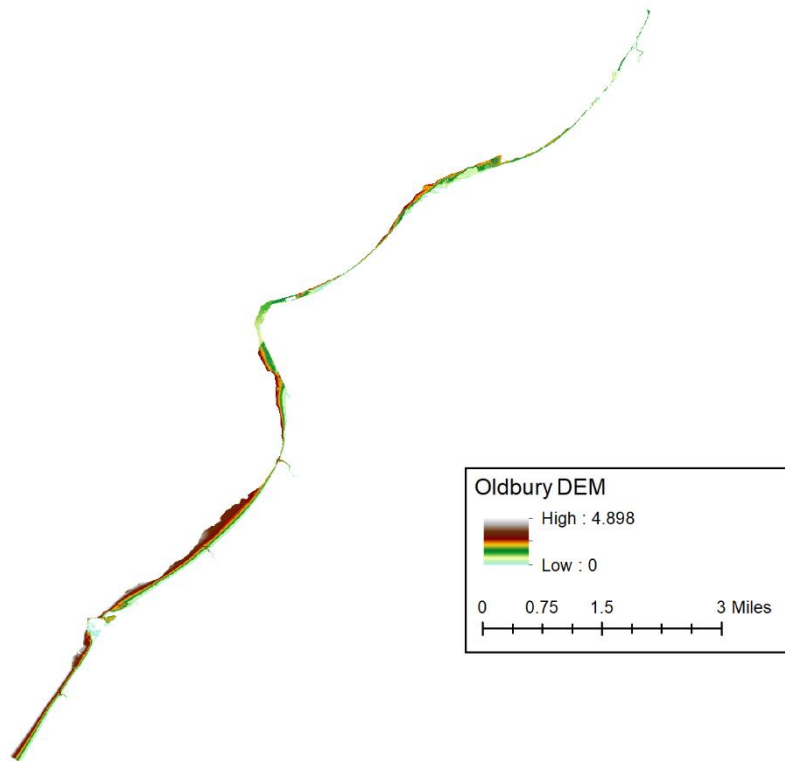


Figure 4: Start model domain for LISFLOOD-FP to generate baseline water level

5.3. Boundary conditions

5.3.1. Forcing data

The following section will explain how to identify the location of the data points used to force the LISFLOOD-FP boundary, and then set the location of the LISFLOOD-FP boundary.

- First of all, it is best to identify the co-ordinates of where your forcing data is coming from, and display this in ArcMap. This forcing data may come from outputs of a hydrodynamic model, observational tide gauge data or tidal predictions.
- The data used to force the LISFLOOD-FP model boundary here came from Delft-3D, with outputs from grid cells along the coastline used. The location of these outputs is shown as orange dots in Figure 5. Ensure the location of the orange dots is in the same geographic coordinate system as the LiDAR data (e.g. BNG for this study).

Data from the orange dots (Figure 5) will be used to force the LISFLOOD-FP model boundary. The data will be represented in the .bdy file for each scenario.

5.3.2. LISFLOOD-FP model boundary

A user-defined LISFLOOD-FP model boundary is required; the user-defined boundary for LISFLOOD-FP forms the basis of the .bci file (section 5.4), which remains the same for all model simulations.

- To create the LISFLOOD-model boundary, first create a polyline along the coastal boundary you wish to use. Then create a points feature and assign points at a regular distance along this coastal boundary line; this study set the points at a distance of 5 m apart.
- Assign XY values to the series of red dots, and export as a .asc file.

This series of red dots (see Figure 5 – the red dots are 5 m apart so merge to look like a line here), which are very close together, will use data from the orange dots and propagates this into the model domain.

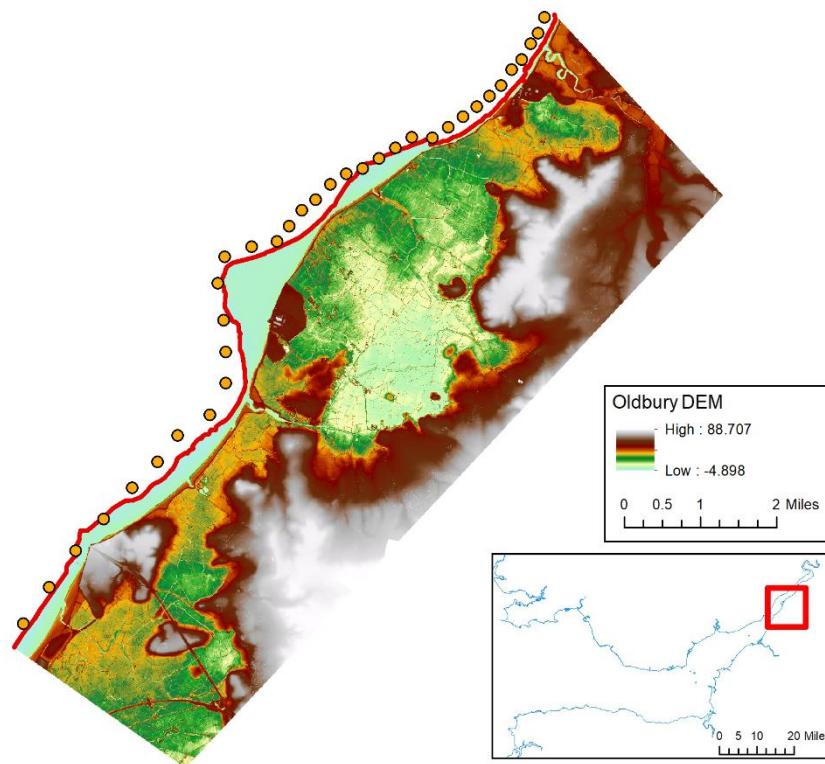


Figure 5: Location of coastal boundary including orange dots (which is the location of boundary condition data) and red dots (which is the location where data from orange dots is propagated into the model domain).

5.4. Boundary condition type file (.bci)

Once you have created the series of red dots along the boundary line and exported these as a .asc file, then they will need to be formatted into a .bci file. A nearest neighbor approach is used to assign each red dot along the user defined LISFLOOD-FP model boundary to an orange dot, which will have the forcing data to drive the inundation model.

An example .bci file is shown in Table 1.

Column 1 in Table 1 defines the boundary as a point (P). The XY coordinates of each individual red dot along the boundary is defined, the .bci file prescribes HVAR (time-varying water level time series) as an input, and then defines which orange dot should be referred to for the actual time series.

HVAR can be substituted for HFIX for a constant water level, and then state the water level value in metres.

Table 1: Example .bci file

P	355001.66	187658.54	HVAR	bc101
P	355004.34	187662.76	HVAR	bc101
P	355007.02	187666.98	HVAR	bc101
P	355009.71	187671.2	HVAR	bc101
P	355012.39	187675.41	HVAR	bc101
P	355015.08	187679.63	HVAR	bc101
P	355017.76	187683.85	HVAR	bc101
P	355020.45	187688.07	HVAR	bc101
P	355023.13	187692.29	HVAR	bc101

The same .bci file will be used for both start runs and model runs.

The .bci file will need to be updated if the position of the open coastal boundary changes.

5.5. Time varying boundary conditions file for spin-up (.bdy)

Once the .bci file has been created which defines which orange dot each red dot takes data from, then the time-varying water level changes needs to be assigned to each orange dot. This is done in the .bdy file.

The spin-up will fill the LISFLOOD-FP model domain from 0 m to the water depth of the first value in each model run. These data are not use in the final analysis of each run. In this study, 50 time steps were assigned to each orange dot to fill the model domain from 0 m to the first water level value in the model run (shown in Table 2 e.g. 0.36 m for bc101).

Table 2 shows that there are 50 time steps for each orange dot, with values from 0 m which will increase up to the first value The length of the start run is at the discretion of the user.

Table 2: Example of a start .bdy file

BDY file Oldbury_start No	1
bc101	
50	seconds
0	0
0.01	900
0.01	1800
0.02	2700
0.03	3600
bc102	
50	seconds
0	0
0.01	900
0.01	1800
0.02	2700
0.03	3600
bc103	
50	seconds
0	0
0.01	900
0.01	1800
0.02	2700
0.03	3600

The 50 time steps, increasing in increments of 900 seconds (15 minutes), from 0 to 0.36 m is shown in Figure 6, showing the model will slowly fill in even increments up to 0.36 m.

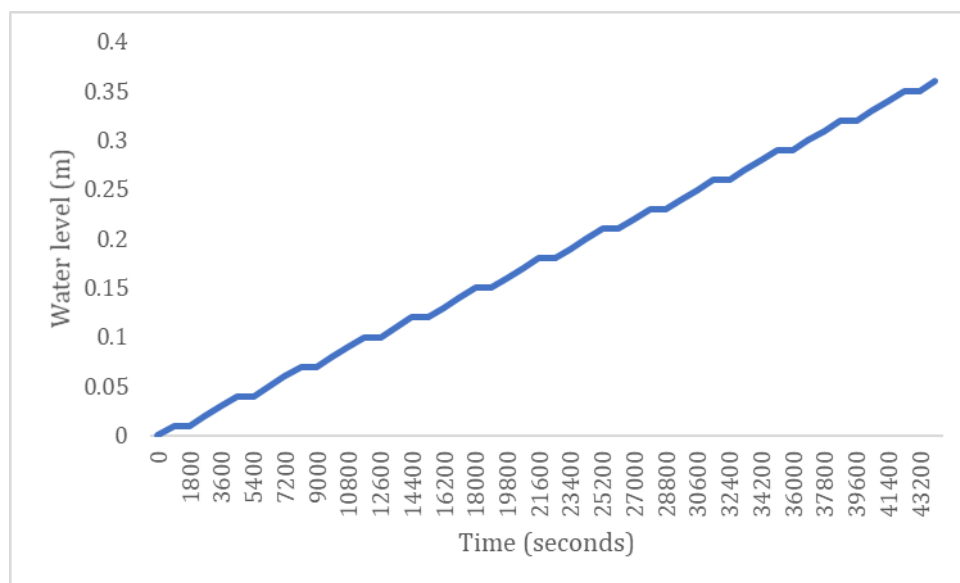


Figure 6: Water level time series for start .bdy file

5.6. Time varying boundary conditions file for model run (.bdy)

Once the spin-up has been completed then the model is ready to run the full simulation, as baseline water depths will have been reached.

Table 3 shows an example of the model run .bdy file.

Row 1 defines the name of the .bdy file. Row 2 starts by defining the name of the first orange dot. Note that this must be identical to the names of the orange dots assigned in the .bci file. Row 3 defines the number of time intervals for each orange dot, and the time step should be defined in seconds. The following rows show the water level changes in column 1, and increasing time interval every 900 seconds (15 minutes) in column 2. The second orange dot is then defined, with the water level time series shown for this point along the boundary. This continues until all orange dots have an assigned water level time series.

Table 3: Example .bdy file

BDY file Oldbury No	1
bc101	
78	seconds
0.36	0
-0.05	900
-0.43	1800
-0.79	2700
-1.13	3600
bc102	
78	seconds
0.36	0
-0.05	900
-0.43	1800
-0.79	2700
-1.13	3600
bc103	
78	seconds
0.36	0
-0.05	900
-0.43	1800
-0.79	2700
-1.13	3600

Figure 7 shows the time-varying water level elevation at orange dot BC101 for one tidal cycle for one simulation. The x-axis shows time changing in seconds. This is the water level that is then propagated into the LISFLOOD-FP model domain from orange dots to red dots (assigned using a nearest neighbor approach).

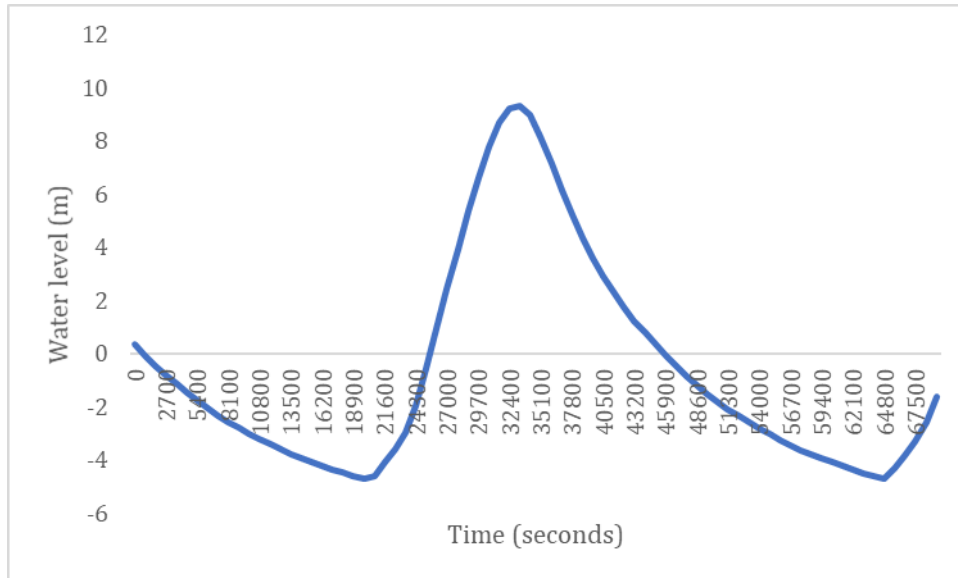


Figure 15: BC101 water level time series.

5.7. Parameter file for start run (.par)

The parameter file defines the inputs for each model run. The creation of .par files can be automated in Matlab, but sometimes it is just easier to do it by hand!

Figure 8 shows an example .par for a start run.

- The DEM file should match the name of the DEM exported from ArcMap and edited in Matlab. This should be located in the same working directory as all other input files.
- Note that the resroot and dirroot should specify that these are start runs.
- sim_time should match the length of the start .bdy file in seconds.
- saveint is set to 9999999.0 so that no output files are saved at certain time steps through the model simulation.
- Note that the .bdy file is specified for the start run.
- The .bci file can be used across all simulations (start and model) and does not change.
- Use the keywords at the end of the .par depending on the outputs you want.
- **The most important output from the start run is the .max file.** This will give maximum water depth across the model domain at the end of each simulation, and should be copied into your model run working directory.

You will need a start run for every separate model simulation that you complete.

```
DEMfile          oldbury_5m_start.asc
resroot          output_start1
dirroot          output_start
sim_time         44100.0
initial_tstep    1.0
massint          44.0
saveint          9999999.0
#manningfile     mann.asc
fpfric           0.03
bdyfile          Oldbury_max_start1.bdy
bcifile          Oldbury.bci
startfile        start_oldbury5m.asc
depthoff
elevoff
voutput
acceleration
theta 0.95
SGC_enable
```

Figure 8: Example start run .par file

5.8. Parameter file for model run (.par)

The keywords shown in Figure 9 (e.g. elevoff, hazard) are explained further in the LISFLOOD-FP handbook.

- The DEMfile should match the name of the DEM exported from ArcMap, and be located in the same working directory as all other input files.
- resroot defines the name of the output files – this can be changed with each simulation you do.
 - Name each simulation with a number; make a note of this in a separate document to keep track of all runs.
- dirroot defines the directory where model outputs will be saved.
- sim_time is the total length of the simulation in seconds. This should match the final time value in the .bdy file for each orange dot.
- massint is at the discretion of the user.
- saveint will specify how often you want output files to be saved e.g. just one file at the end, or every 10 minutes.
- If a space-varying manning friction value is used then name the file here. Or assign a uniform value below.
- Ensure that the name of the .bdy and .bci file is correct.
- State the name of the .max file from the start runs.

```
DEMfile           oldbury_5m.asc
resroot           output1
dirroot           output
sim_time          69300.0
initial_tstep     1.0
massint           69.0
saveint           690.0
#manningfile      mann.asc
fpfric            0.03
bdyfile           oldbury_max1.bdy
bcifile           Oldbury.bci
startfile         output_start1.max
#depthoff
elevoff
voutput
acceleration
theta 0.95
SGC_enable
hazard
```

Figure 9: Example .par file

See the LISFLOOD-FP manual which will describe the key words to include in .par for certain outputs, e.g. for hazard rating, velocity.

6. How to run a simulation

For both start and model runs ensure that all required input files are in each respective working directory; .asc, .par, .bci, .bdy (start.max for model runs).

LISFLOOD-FP model files are available from the author on request.

The model is run from the command line.

- In the command line navigate to your working directory.
- Use the following command to run a simulation:
 - `lisflood -v run_*.par > log*.txt`, where * indicates the identification (name or number) of each simulation
 - the first 'lisflood' command may change depending on the version you are using.
 - refer to the handbook for advice on how commands may change with each version.
 - The logx.txt command will save a log of the model simulation, showing the progress of each run.

6.1. Troubleshooting

It can be quite tricky to figure out what the problem is if a simulation does not run – error messages are not always clear...

- Refer to the log.txt file, this may give some ideas at the end of the document to identify when the simulation stopped.
- Check that the name of each file is correctly spelled in the .par file.
- Do the orange dot values in the .bci match those in the .bdy?
- Is the duration of the simulation correctly stated in the .par?

6.2. Model run times

The table below gives an approximate idea of the time taken to run a simulation on a standalone Windows desktop with an i5 processor, and a Windows laptop with an i7 processor, for a LISFLOOD-FP simulation from low water to low water (approximately 12 hours).

Table 44: Model run times

	Standalone desktop (i5 processor)	Laptop (i7 processor)
12 hour simulation	24 hours	1 hour

It is clearly the case that the more powerful processor substantially speeds up the model run times. It is recommended that if modellers have access to a more powerful processor then this should be used as it will speed things up immeasurably. It seems obvious, but always good to know.

7. Outputs

Output files will depend on what was specified in the .par file, and the save interval that was defined.

7.1. .max files

The .max file will show the maximum depth and extent of inundation in the model domain over the whole course of the simulation. The instructions below can be applied to the .max file, but also .wd which the user may have chosen to save at specific intervals.

The .max or .wd files can be clipped to the inland area only to visualize just inundation across the floodplain.

- Rename the file extension to .asc file.
 - This can be done via the command line:
 - Change directory in the command line and set it to your output file where all .max or .wd files are saved.
 - Use the following command: `ren *.max *.asc`
 - Or `ren *.wd *.asc`
- Convert from .asc to raster in ArcMap.
- Clip the raster file to a polygon which is the shape of just the inland floodplain area (Figure 10).
 - Visualize the water depths in ArcMap and export as an image.
 - Export this file as an ASCII and load into Matlab.
 - See section 8 for more information on analyzing in Matlab.

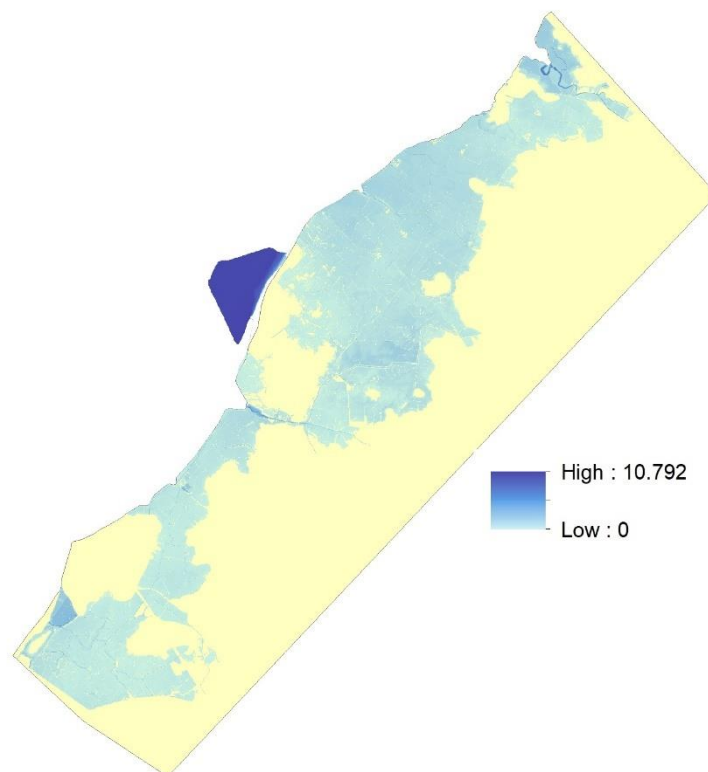


Figure 10: Clip .max or .wd files to the inland floodplain in ArcMap

7.2. .vx and .vy files

Velocity files can also be renamed to ascii, clipped in ArcMap to the inland area and loaded into Matlab to calculate velocity at each grid cell in the model domain.

Matlab code is available on request from the author to load and analyse velocity outputs.

8. Matlab functions

The code on this website was found to be invaluable when analyzing outputs in Matlab:

https://source.ggy.bris.ac.uk/wiki/LISFLOOD-FP_and_MATLAB

9. Depth Damage Curves

To quantify the economic impact of each simulation, water depths of greater than 0.05 m in each grid cell are combined with salt water depth damage curves (Penning-Rowsell et al., 2013).

25 m UK land cover data was downloaded from Edina Digimap and clipped to the floodplain area of the model domain (Figure 11).

- <https://digimap.edina.ac.uk/roam/download/environment>



Figure 11: 25 m land cover data used to calculate damage assessments for arable and suburban land uses.

The land cover raster data set was exported as an .asc file, and imported into Matlab.

Matlab code is available on request from the author to complete depth damage assessments.

Areas of arable land which are covered by water are identified and multiplied by the associated cost. There are four land types used to calculate overall arable damage value for each simulation (Table 5). The damage assessment does not change depending on the depth of the value; a uniform value is applied.

Table 5: Arable land costs used in damage assessments (Penning-RowSELL et al., 2013).

Arable Land costs (£ per grid cell)	
Arable and Horticulture	2.86
Improved Grassland	0.45
Rough Grassland	0.13
Neutral Grassland	0.25

Suburban damage is dependent on water depth and a cost is assigned to each grid cell depending on water depth (Table 6).

Table 5: Suburban land costs used in damage assessments (Penning-RowSELL et al., 2013).

Water depth (m)	Suburban land costs (£ per grid cell)
0	0
0.05	3317
0.1	5334
0.2	9109
0.3	11120
0.6	13525
0.9	14676
1.2	16084
1.5	17383
1.8	18869
2.1	20134
2.4	21325
2.7	24093
3	25308

The arable and suburban costs can be compared between simulations to quantify the impact of flood events.

10. Bibliography

Bates, P., De Roo, A. (2000) A simple raster-based model for flood inundation simulation. *J Hydrol* 236: 54–77.

Bates, P., Trigg, M., Neal, J., Dabrowa, A. (2013) LISFLOOD-FP User manual Code release 5.9.6 [online] Available at: <https://www.bristol.ac.uk/media-library/sites/geography/migrated/documents/lisflood-manual-v5.9.6.pdf> [Accessed 15 August 2019].

Penning-Rowsell, E., Priest, S., Parker, D., Morris, J. (2013) *Flood and Coastal Erosion Risk Management*. 2013th ed. Routledge. <https://doi.org/10.3390/jpm3040288>

Land Cover Dataset 2015 (2015) Available at <https://digimap.edina.ac.uk/roam/download/environment> Accessed 10 January 2020.